Alma Mater Studiorum – Università di Bologna

DOTTORATO DI RICERCA IN

# Nanoscienze per la Medicina e per l'Ambiente

Ciclo XXXIV

**Settore Concorsuale: 03/B1**
**Settore Scientifico Disciplinare: CHIM/03**

## *"Nanoglial Interfaces: Nanostructured Materials, Interfaces and Devices to unveil the role of astrocytes in Brain Function and Dysfunction"*

**Presentata da:** Emanuela Saracino

**Coordinatore Dottorato**

Prof. Dario Braga

**Supervisore**

Dr. Valentina Benfenati

**Co-supervisori**

Prof. Alberto Credi

Prof. Marco Caprini

**Esame finale anno 2022**

## -Abstract-

The role of non-neuronal brain cells, called astrocytes, is emerging as crucial in brain function and dysfunction, encompassing the neurocentric concept that was envisioning glia as passive components. Ion and water channels and calcium signalling, expressed in functional micro and nano domains, underpin astrocytes' homeostatic function, synaptic transmission, neurovascular coupling acting either locally and globally. In this respect, a major issue arises on the mechanism through which astrocytes can control processes across scales. Finally, astrocytes can sense and react to extracellular stimuli such as chemical, physical, mechanical, electrical, photonic ones at the nanoscale. Given their emerging importance and their sensing properties, my PhD research program had the general goal to validate nanomaterials, interfaces and devices approaches that were developed ad-hoc to study astrocytes. The results achieved are reported in the form of collection of papers. Specifically, we demonstrated that i) electrospun nanofibers made of polycaprolactone and polyaniline conductive composites can shape primary astrocytes' morphology, without affecting their function ii) gold coated silicon nanowires devices enable extracellular recording of unprecedented slow wave in primary differentiated astrocytes iii) colloidal hydrotalcites films allow to get insight in cell volume regulation process in differentiated astrocytes and to describe novel cytoskeletal actin dynamics iv) gold nanoclusters represent nanoprobe to trigger astrocytes structure and function v) nanopillars of photoexcitable organic polymer are potential tool to achieve nanoscale photostimulation of astrocytes. The results were achieved by a multidisciplinary team working with national and international collaborators that are listed and acknowledged in the text.

Collectively, the results showed that astrocytes represent a novel opportunity and target for Nanoscience, and that Nanoglial interface might help to unveil clues on brain function or represent novel therapeutic approach to treat brain dysfunctions.

# Index

*...alla Scienza: la MIA Filosofia...*



.

# Introduction

**Nanoneuroscience: an emerging bridge between Nanotechnology and Neuroscience**

*Nanoneuroscience* has been defined as an emerging field that will bridge opportunities and challenges across *Nanoscience* and *Neuroscience*[1]. The focus of such cross disciplinary field is to reply to a major demand of tools needed to study the brain structure and function at the organ scale and, at the same time, to unravel the chemical communications and biomolecular interactions occurring at the nanoscale in the brain[1]. In this respect, neurons have been for centuries, the focus of brain studies and related technological development. However, recent progress, sustained by empirical results demonstrated in humans, have provided a more holistic and articulated perspective on the central nervous system (CNS). The latter is indeed characterized by a sophisticated genetic and molecular and functional heterogeneity of its components: i) billions of neurons with their 100 trillion of synapses, ii) non neuronal cells called glial cells, numerically similar to neurons, with their signalling and complex dynamics that have consolidated regulatory function, and unexpected modulatory capabilities; and finally iii) the vascular system that is providing metabolic and regulatory support to the machine iv) the ependymal secreting intracerebral fluid. All the different components cooperate to the complex activity and fluctuations of the brain network, with dynamics occurring at many spatio-temporal scale (i.e. from nanometers (nm) to meters (mt); from seconds (s) to hours (h)). The function of the whole-network has been associated with behaviour, cognition and its dysfunction is considered as the neural basis alteration. However, fundamental questions remain to be answered: to define mechanism beyond the cross-talk of different components and on the processes that allows integration of information at scales with multiple spatiotemporal resolution. In this view, there is a demand for *Nanotechnologies* that can selectively monitor and control major molecular and cellular targets of the differet brain components, avoiding loss of relevant information in transitions across

scales[2]. Such and high challenge demanded cross-fertilization between neuroscience, cell biology, chemistry, physics and engineering and material science, as well[3].

As a result, the late part of 20$^{th}$ century led to the development of nanoscale materials, devices and nanotools designed to interact with neural and non-neural cells, and provided notable opportunities in neuroscience fundamental investigations and applications. Despite the efforts and the major results achieved, applications of nanotechnology, in basic and clinical neuroscience, are still in an early-stages of development. At the same time the lack of knowledge of specific mechanisms that generate the complexity of the mammalian CNS and underline the brain functions and dysfunctions continue to attract Nanoscientists and to push Neuroscientists to contaminate each other promoting unexplored domains of their respective field[4]. In this respect, the past four decades highlighted the importance of glial cells in brain homeostasis, modulation of cognitive function and systemic functionalities. Frequently neglected or marginally considered as a barrier to be overcome between neural implants and neuronal target, glial cells, and in particular astrocytes, are increasingly considered as an active player in determination of the outcomes of device implantation. Consequently, the almost unexplored domain of **Nanoglial science** is parallel emerging to feed the demand of tools the selective monitoring and control of glial cells.

In this scenario, this PhD thesis analyzed the advantages to generate and explore nanointerfaces and devices to study brain glial cells and their contribution to processes underlying brain function or dysfunction. The **introduction,** reported as **Chapter I,** has the objective to provide an overview on the defined and emerging physiological and pathological role of astrocytes, then to critically discussing the most recent advances on **nanoglial interfaces** and **devices** that enabled to reach unprecedented insights into the role of astroglial cells in brain function and dysfunction. The research activities and methodologies implemented within my PhD, reported in **Chapter IV** and discussed in **Chapter V** had the general objective (**Chapter II**) to propose Nanoglial science and Nanoglial interfaces as multidisciplinary fields that will potentially i) increase

the understanding of the mechanisms underlying the structure and function of astroglial cells ii) enable to extend our knowledge on the role of these cells in brain functions and/or in neuropathologies as Epilepsy and Ischemia, Glioma or Alzheimer. All the activates were performed at CNR-ISOF, under the supervision of Dr. Benfenati and with the Co-supervision of Prof. Alberto Credi, Universityof Bologna, (UNIBO) and of the Prof. Marco Caprini, Universityof Bologna, (UNIBO). All the work presented was developed thanks to a multisciplinary collaborative interaction with colleagues at CNR-ISOF, CNR-IPCB, CNR-IMM, IIT-CNST, University of Bologna, University of Bari, University of Maryland, Air Force Research Laboratory, Army Research Laboratory. All these interactions occurred through secondments and periods spent in different labs, enabling me to be exposed to a variety of approaches, techniques, background and human beings, truly enriching my professional experience. Nonetheless,the participation in a regional project, in collaboration with MISTER SMART INNOVATION helpedme to understand the fundamental step of technology transfer and industrial research. The methodologies learned, adapted and developed to implement the research activities are reportedin **Chapter III**.

The results are reported in the form of collections of paper in **Chapter IV**. Specifically, I tested i) nanostructured materials interfaces made of organic polymers used electrospun nanofibers made of biopolymers and composites developed in collaboration with the group of Prof. Luigi Ambrosio of CNR-IPCB, Naples; ii) gold silicon coated nanowires interfaces and devices developed collaboration with the group of Dr. Annalisa Convertino and Dr. Luca Maiolo of CNR-IMM, Rome; iii) colloidal hydrotalcites films in collaboration with Dr. Tamara Posati and Dr Roberto Zamboni at CNR-ISOF;

iv) gold nano cluster tools in collaboration with Dr. P. Shashi Karna of Army Research Laboratory, Auberdeen, USA; v) semiconducting polymer interfaces based on polythiophene in form of nanopillars in collaboration with Dr. Maria Rosa Antognazza at Italian Institute of Technology, CNST, Milan. The biological, functional characterizations were performed in collaboration with Prof. Marco

Caprini, FABIT, UNIBO, Prof. Grazia Paola Nicchia, UNIBA, Prof. Wolgang Losert, University of Maryland.

Collectively, as discussed in **Chapter V**, the results achieved demonstrate the ability of different nanomaterials and approaches to impact on astrocytes structure and function and the transformative potential of nanomaterials to contribute to the advance and in studying the human brain. The products of dissemination of results and the training activities performed abroad are reported in the **Chapter VI**.

**The Brain Structural and Functional components**

The brain appears as the most complex organ in humans, the systemic difficulty in appreciating and revealing profoundly its architecture, is due to 1) its structural organization, 2) the multitude physiological roles of all its constituents, 3) the complexity of the network and all the connectivity among all the cells needed to guarantee specific behavior. According, to the neurocentric view in neuroscience, the components the brain have been classified into: 1) neurons, also named excitable cells that can generate action potential, that is propagated across neurons through chemical synapses; 2) glial cells, non-excitable cells, as they do not fire action potentials; 3) endothelial cells, forming the walls of the brain blood vessels and 4) ependymal forming the choroid plexus that regulate intracranial fluid in the 4th ventricle. The human brain contains about 100 billion neurons. The architecture of a single neuron is made to maximize the surface area to spread connections to other neurons through branches called dendrites. The elongation of dendrites that departs from the axon depends on the different levels of mammalian evolution. Neurons are embedded in an extracellular environment diffused in a volume of 1.5 lt and 200 trillion contacts enabling the genesis of a higher hierarchical dynamic organization called oscillation. In this regard, while the feature and the code of a single action potential (spike) has been almost fully understood, neuroscientists are still not able to unveil the mechanism at the basis of the complex and synchronized network connectivity forming brain oscillations [5-10]. Neurons in the brain were supposed to be supported by a class of cells, called

glial cells. The term ‘‘glia” was introduced to recall the concept of ‘‘glue”, (Virchow, 1856) and it was thought that glial cells acted just as passive supporters “filling the space” between neurons. The first precise images of glial cells (‘‘round cells with quite long and very fine processes, many of which were directed towards blood vessels”) were drawn in 1870 by Camillo Golgi. His idea about glial cells being not just “connective tissue and passive actors" of the brain was supported by Ramon´ y Cajal (1893); in 1891, both coined the ‘‘neuron doctrine” indicating in the white and grey matter composing the brain of star-shaped glial cells[12]. Glial cells are divided into other two classes: microglial and macroglial cells. Microglial cells are small, round, motile cells, present in all the CNS regions and mediating the “immune response” by phagocytosis of debris in the CNS and apoptotic cells against pathogens elements. Recently their role is emerging in the shaping of synapsis plasticity and in regulating neuronal survival as well[5-12]. Among macroglial cells are astrocytes, one of the four major types of glial cells in the central nervous system (CNS) along with the oligodendrocytes, microglia, and polydendrocytes/NG2 cells[13]. Oligodendrocytes are small cells endowed with processes that envelope axons in a structure of membrane called myelin rich in saturated lipids and proteins. Myelin insulates the neurons’ axons and allows to increase the propagation speed of the action conduction[14-16]. The myelin formation is the most important function of the oligodendrocytes; however, they secrete a series of molecules, called neurotrophin (neurotrophins -3) mediating the neural outgrowth.

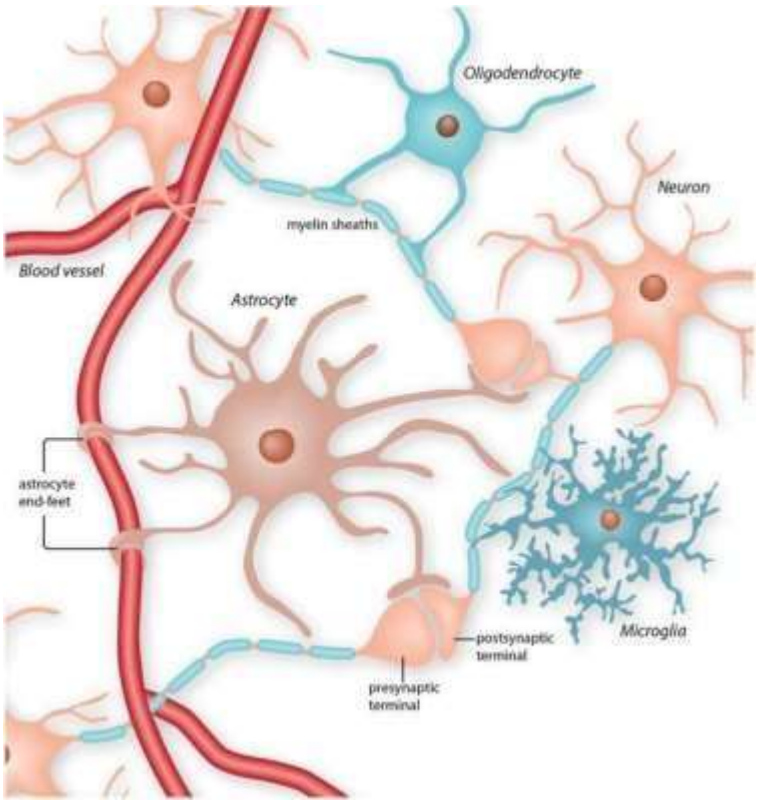


**Fig.1.1: Glia cells' interaction with neurons and blood vessels.** Astrocytes control the homeostasis of the central nervous system (CNS), astrocytes' endfeet around synapses control and modulate the synapses function, while oligodendrocytes form the myelin sheaths around axons. Microglia induce the immune response in the CNS[17]. Permission from: Copyright © 2020 Wiley-VCH GmbH.

The revolution in the definition of the morphology, the structure and the hypothesis on the role of both neurons and glial cells arose with the development of technologies, at the end of the 1970s and early 1980s. This happened, especially, in the microscopy field that offered a more accurate definition in terms of time and space and the possibility to identify alteration in case of brain disease. However, the first proof of astrocytes' involvement in disease was given by Wilder Penfield and Pío del Río-Hortega in the 1920s, when they investigated the role of glial cells in response to injury; while in the early 1960s, the group of Stefen Kuffler (1964) demonstrated, performing patch-clamp experiments, that glial cells show properly biophysical properties. One year later, in 1965, it was described that astrocytes were involved in the uptake of extracellular potassium released by neurons after synapses. Similarly, electrical coupling between glial cells and neurons was first presented in 1966 leading to the hypothesis of potassium spatial buffering mediating synaptogenesis, which was not confirmed in

1969[18]. The strong physical interaction between neurons and astrocytes functions leads to several studies focused on the role of glia in the brain network. Astrocytes cells are the most numerous cells of the CNS, about 10 times more in number with respect to 100 billion neurons are estimated in the human brain[19]. In particular, i) **glia regulates synapse formation:** after neurogenesis, neuronal migration, and axon elongation, neurons start to create synaptic connections; the glial signals induce synaptic stabilisation and maturation[20]; ii) **glia modifies synaptic communication and plasticity:** astrocytes regulate neurotransmitter uptake, via glutamate transporters, which is dynamically regulated, with glutamate transporters receptors for multiple neurotransmitters and neuromodulators. Glio-transmitters include adenosine-triphosphate (ATP), when converted to adenosine, act on presynaptic adenosine receptors to allow neurotransmitter release and short-term plasticity[21-24]; iii) **glia regulates ion homeostasis and affects circuit function:** glia can affect neuronal excitability by regulating ion homeostasis, for example by clearing potassium ($K^+$) ions from the extracellular space, after neurons' action potential[25]. The latter will be better explained in a dedicated paragraph of this chapter; iv) **neuro-glial-vascular coupling provides metabolic support**: brain health depends on the intimate contact of CNS blood vessels and glial cells. Specifically, it is called the astrocytes' coupling. The blood vessels have specialised barrier properties, known as the blood-brain barrier (BBB), which limits the movement of substances between the blood and the brain. However, astrocytes can actively supply neurons with nutrients, thanks to their processes that contact both blood vessels and neurons[26,27]. For example, astrocytes are enriched in lipid synthesis pathways and provide lipids to neurons, including cholesterol, essential for maintaining presynaptic function[28]. Astrocytes are also enriched in glycolytic pathways and make glycogen, which can be converted into lactate and transferred to neighbouring neurons by mono-carboxylate transporters[29](Fig.1.1).

**Homeostatic Role of Astrocytes**

As a basic principle for cell physiology, it should be stated that the differences in ion concentrations across the plasma-membrane determine membrane potential of all the living cells. These differences are the driving force for the electrical activity of cells. In neurons, electrochemical gradients determining neurons' membrane potential, set the so-called excitability properties of the cell at the resting state. The quantitative gap of the neurons' membrane potential from the *voltage threshold*, defined as the voltage at which the action potential process is triggered, determines the ability of the neuron to be "excited", i.e. its ability to generate and propagate action potential.

Accordingly, unbalanced changes in the ions concentration could alter the neuronal excitability and the neuronal network capability to generate action potential and propagate communication signals through synapses[31,32]. The possible variations in ions concentration, essentially $Na^+$, $K^+$, $Ca^{2+}$ and $Cl^-$ occur in a space called "Extracellular Space" (ECS) and that is the interstitial place between the different types of brain cells. This space represents 20% of the brain volume. In this environment, **astrocytes are the cells responsible for the homeostatic regulation of ions and water concentration regulation**, through the transmembrane fluxes allowed by specific ion channels and aquaporins and by specific neurotransmitter transportes and co-transporters[33-34]. Protein channels, receptors and transporters in astrocytes are localized in specific areas called "microdomains", that are the major functional unit, where the homeostatic function of glial cells is exploited. The cytosolic ion concentrations are defined by respective membrane permeability and an equilibrium potential, (Erev): intra-astrocytic concentration of $K^+$ between 140 mM, while $K^+$ concentration in the extracellular compartments such the interstitial fluid (ISF) is ~4 mM, this sets Erev$K^+$ at -98 mV(at 37°C). Concentration of cytosolic $Na^+$ in astrocytes 10 mM, $Na^+$ concentration in the CSF is ~140mM, the corresponding Erev$Na^+$ ranges between 55 and 60 mV. Concentration of ionised $Ca^{2+}$ in thecytoplasm of astrocytes ranges between 100 nM, with the assumption of $Ca^{2+}$ in CSF around 1.5

mM, the Erev$Ca^{2+}$ lies between –120, -140 mV, high concentration of $Cl^-$ 30-60 mM and CSF 120 mMions with Erev$Cl^-$ being set around -35 mV[35] (Tab.1.1).

| Intracellular | Extracellular | Erev |
|---|---|---|
| **$[K^+]_i$ 140mM** | **$[K^+]_0$ 4mM** | **-98 mV** |
| **$[Na^+]_i$ 10 mM** | **$[Na^+]_0$ 140 mM** | **60mV** |
| **$[Ca^{2+}]_i$ 100nM** | **$[Ca2^+]_0$ 1,5 mM** | **140mV** |
| **$[Cl^-]_i$ 30-60mM** | **$[Cl^-]_0$ 120 mM** | **-35mV** |

**Table 1.1:** Intracellular and extracellular major ions' composition and Erev in CNS.

Among different homeostatic processes, the most studied and widely recognized activity of astrocytes is the maintenance of the extracellular concentration of potassium ($[K^+]_{out}$), thought processes known as potassium-uptake and spatial $K^+$ buffering[36].

$[K^+]_{out}$ is indeed majorly involved in the depolarization of neuronal resting membrane potential and in the crucial mechanism of generation of neurons' action potential. $[K^+]_{out}$ continuously changes, because of $K^+$ extrusion occurring after each action potential occurring at each synaptic domain.

The imbalance of this ion leads to an over-excitation of the neuronal network and a series of cascading events, such as uncontrolled synaptic release of neurotransmitters, CNS compromise, damage to neuronal viability. The accumulation of $K^+$ at the perisynaptic space makes the resting membrane potential of astrocytes negative respect to the Nernst equilibrium potential for $K^+$ [37-40]. How astrocytes are able to act in the activity of $K^+$ regulator is explained by the functionality of a pump, known as the "$Na^+/K^+$ ATPase" pump. The correct activity of the pump is restoring the electro-neutrality by the efflux of cations: 3 sodium ($Na^+$) and by the influx of 2 $K^+$. The $Na^+/K^+$ ATPase is expressed bothin neurons and astrocytes, but it is stimulated by elevated $[K^+]$o only in astrocytes[65] (Fig.1.2 and Fig. 1.3).

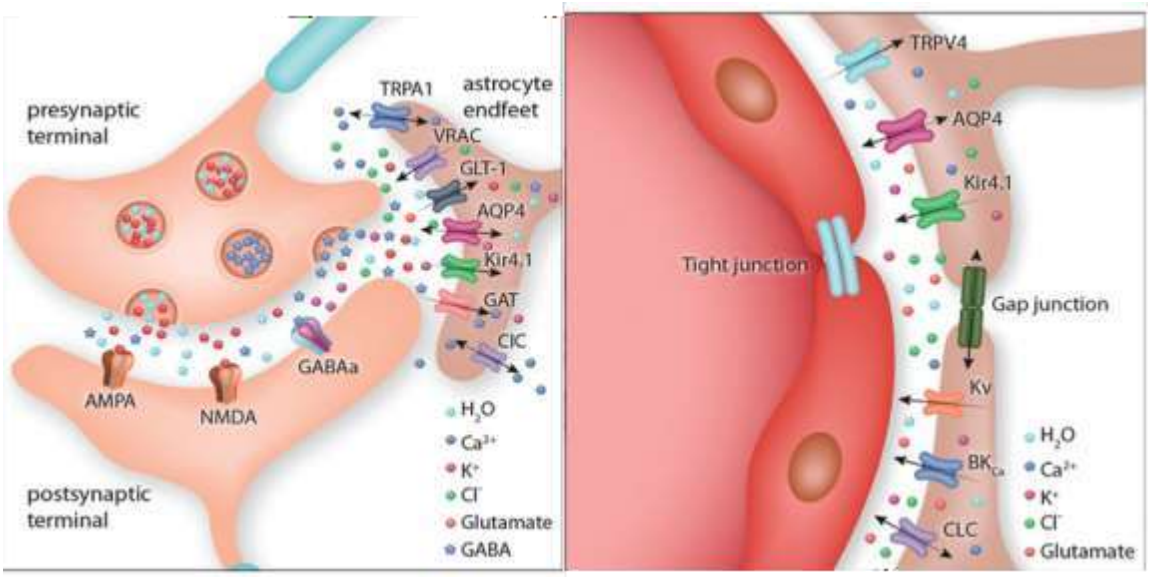


**Fig. 1.2: Scheme of astroglial cells microdomains**: pumps and transporters that contribute to the transmembrane movement of ions and aquaporins, involved in potassium buffering and volume homeostasis of the brain. Right panel represents zoomed-in view of distinct domains in contact with synapses and the glia-vasculature interface[17]. Permission from: Copyright © 2020 Wiley-VCH GmbH.

The $K^+$ uptake could be accompanied by water influx and swelling of the cells. After its uptake, the excess of $K^+$ travels through the astroglial syncytium through gap junctions, and then it is released in the distal compartment of the ECS[41] or to the closest blood vessel. This process, called *potassium spatial buffering*, allows for restoration and maintenance of $[K^+]_{out}$ that is demanded after each action potential.

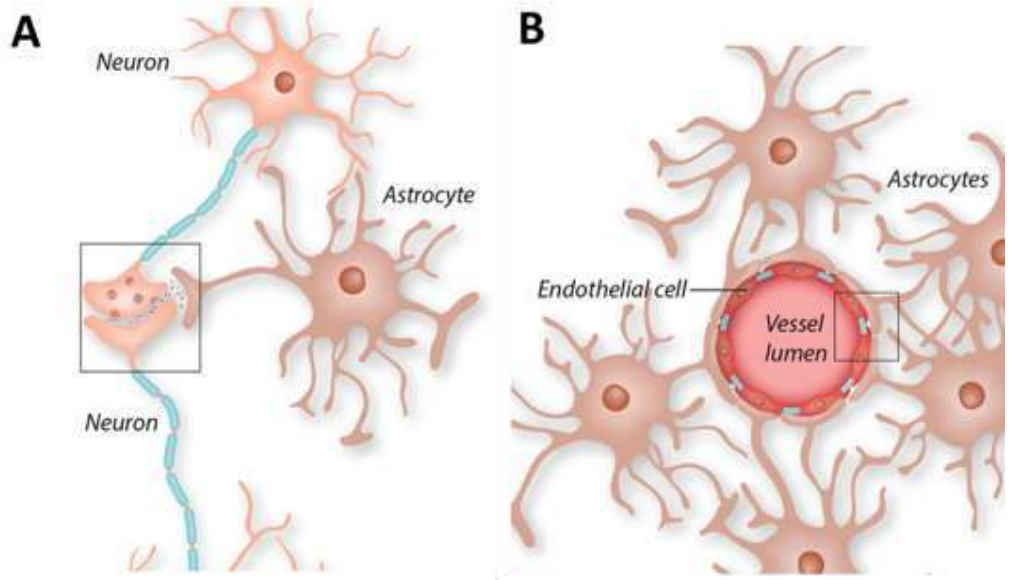

**Fig. 1.3: Scheme representing astrocytes and distinct microdomains.** A) Perysinaptic astrocytic domain implicated in chemical synapse activation, neurotransmitters and $K^+$ released by neurons. B) The gliovascular astrocytic domain: the syncytium to reach the glia- vasculature interface[17]. Permission from: Copyright © 2020 Wiley-VCH GmbH.

*Ion channels in astrocytes*

Astrocytes express a variety of **$K^+$ channels** expressed in their plasma membrane. The most abundant and functionally relevant in potassium homeostasis are the *inward rectifying $K^+$ channels* (Kir). Structurally, Kir channels are divided into 7 families, they are organised into 2 transmembrane domains and 16 subtypes, whose voltage and gating properties are depending by the Erev$K^+$[42]. Among them the Kir 4.1 is the most commonly expressed Kir in astrocytes *in vivo*. It localised in astrocytes endfeet that contact synapses and blood vessels to contribute to the control of brain homeostasis, contributing either to the uptake and to the release of potassium. Actually, $Cs^+$ and $Ba^{2+}$are confirmed to inhibit Kir channels[43-45] (Fig. 1.4). In addition to Kir, potassium channels that are members of Voltage-gated $K^+$ channels (Kv)[46,47], Calcium-dependent potassium channels (KCa) and[48,49] Two Pore-domain potassium channels (K2P), have been identified in astrocytes. As a general statement, potassium channels are involved in determine the membrane potential of astrocytes and in the homeostasis of potassium. However, as described above, such a massive potassium flux across the plasma-membrane might generate variations in the transmembrane potential in the microdomains, **u**nfortunately they cannot be recorded with available technologies. As a consequence, the role of each channel in the brain function or cortical oscillations is far to be determined. Similarly, the role of the **Voltage-gated $Na^+$ channels (Nav)** is still not well known in astrocytes. However, the sodium function is necessary for the activity of the of $Na^+/K^+$-ATPase, meaning for the $K^+$ homeostasis in the CNS and their crucial role for the brain[50,51].

**Chloride ($Cl^-$) channels** have been also identified in astrocytes**.** The $Cl^-$ balance is fundamental in the neuronal communication and the maintenance of electrical equilibrium. The CLC family of channels with its 9 members and 10 to 12 transmembrane domains, localized in the plasma membrane, especially in the hippocampal area and in intracellular organelles[52,53]. The ClC channels, such as ClC-

1, ClC 2 and ClC-3 have been detected in astrocytes processes.

The hypothesis about their role goes around 1) the GABAergic transmission by regulation of [$Cl^-$] efflux in the synaptic space, 2) modulators of the resting potential by variations in cell volume $Cl^-$ release in response to cell swelling[54,55].Differently, the Volume-regulated anion channels (VRACs) need to be activated by a hypotonic stress. VRAC is crucial for RVD and its currents have been characterized *in vitro*[52]. In particular, in our lab, we showed that the leucine-rich repeat-containing protein 8 (LRRC8) forms hexameric complexes in the extracellular membrane of VRAC channels. Other authors demonstrated that VRAC is implicated in the release of excitatory aminoacids like glutamate or taurine and aspartate, while carbenoxolone (CBX) can inhibit the VRAC activity. It has been observed, there are calcium activities dependent by $K^+$ protein channels, evidence demonstrates that VRAC is involved in $Ca^{2+}$ wave propagation as well, through ATP release[56-61]. Through microdomains, osmolytes, ions, water flux as response of physiological or triggering stimuli; astrocytes activate a mechanism called regulatory volume decrease (RVD) to recover the initial cell volume, while the opposite mechanismis called regulatory volume increase (RVI) and it is activated by astrocytes to compensate the cell swelling with cell shrinkage, activating a process of release of osmolytes (Fig. 5).

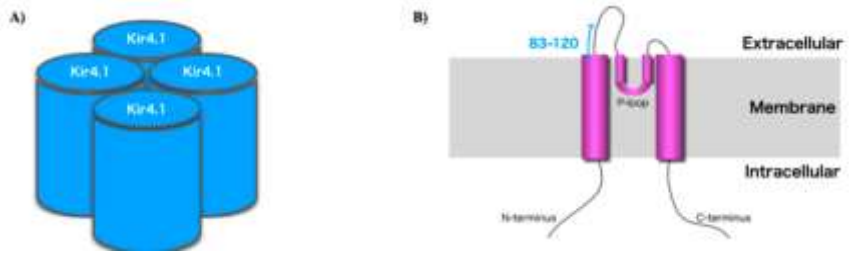


**Fig. 1.4:** A) KIR4.1 is expressed *in vivo* as a homotetramer (four units of KIR4.1) (B) The protein contains two extracellular domains and two transmembrane regions. Kir4.1 channels localize on astrocytes at perisynaptic or perivascular processes, KIR4.1 channels are essential for potassium homeostasis in the brain by maintaining the ionic and osmotic environment in the extracellular space. Permission from: Creative Commons Attribution4.0 International, Int. J. Mol. Sci. 2020, 21(24), 963.

*Ion channels and receptors mediating calcium signaling in astrocytes*

Astrocytes are not silent cells. They express a kind of "excitatory system" of communication with the other cells in the ECS. The signalling established by astrocytes is mediated by oscillations in the intracellular calcium concentration ($[Ca^{2+}]i$). Calcium membrane dynamics processes in astrocytes several functions, in particular energetic delivery, vascular activity, role in regulating homeostatic signalling and water transport and distribution, facilitated by the cooperation with water channel AQP4. Dysfunction in calcium signalling in astrocytes leads to brain swelling, ischemia, epilepsy, and brain tumors[62].

Astrocytes can sense and respond to extracellular modification by oscillations $[Ca^{2+}]_i$. It has recently been highlighted that the dynamics of $[Ca^{2+}]_i$ are spatio-temporally distinct depending on whether they occur at the soma, at their process in the so-called microdomains or through the astroglial syncytia, by means of gap junctional coupling, originating what are known as $Ca^{2+}$ waves. Astroglial $[Ca^{2+}]_i$ signalling occurs at astrocytic domains that enwrap the majority of pre- and post-synaptic cortical neurons in the tripartite synapse. Of note, the speed of $[Ca^{2+}]_i$ propagation and waves increase with the evolution, further suggesting that astrocytic calcium signalling might have a role in computation. These findings led to the intriguing hypothesis that $[Ca^{2+}]_i$ are involved in and can become a therapeutic target for the improvement of cognitive functions. The entry of extracellular $Ca^{2+}$ or the efflux of the $Ca^{2+}$ stored in the endoplasmic reticulum both contribute to $[Ca^{2+}]_i$ oscillations and waves. Among different paths, extracellular $Ca^{2+}$ can flow through the membrane of astrocytes via the ionotropic purinergic receptor P2X7 and through Transient Receptor Potential Vanilloid 4 (TRPV4) and TRP Ankirin 1 (TRPA1) and through Voltage-gated calcium channels (VGCCs)[62].

**Voltage-gated calcium channels (VGCCs)** are complex proteins of 4-5 subunits, encoded by several genes, with different properties and features. $Ca^{2+}$ influx followed by membrane depolarization is the

consequence of their activation L-type current has been identified in cortical astrocytes, Cav 1.2 and Cav 1.3 channels, to be activated the L-type $Ca^{2+}$ channels need a strong depolarization, the latter seems to happen during astrogliosis. Studies showed the upregulation of Cav 1.2 and how the deletion of these channels, by phenylalkylamines, dihydropyridines and benzothiazepines, avoided gliotic response[63-65]. N-type, P/Q-type, and R-type channels need a strong depolarization, and specific polypeptide toxins from snail and spider venoms can block them. T-type $Ca^{2+}$ currents are transient and activated by weak depolarization. Any of the conventional molecules used as antagonists of the activity, can inhibit them[66-67].

The recent Nobel Prize for Physiology and Medicine (2021) to David Julius and Ardem Patapoutian for their discoveries of receptors for temperature and touch, highlights the role of a specific channel belonging to the superfamily of **TRP channels**. In human species there are about 27 members of TRP channels into 6 subfamilies. Structurally, they show 6 transmembrane domains and a TRP domain in the C-terminal region. The pore region is formed between the fifth and sixth transmembrane domains. Our ability to sense heat, cold and touch is essential for survival and underpins our interaction with the world. The discovery of TRP channels contributes to a rapid increase in our understanding of how our nervous system senses heat, cold, and mechanical stimuli. TRP acts on many different physiological functions (thermosensation, nociception, chemoreception and taste). TRP channels are diffuse in the CNS, in particular, vanilloid (TRPV), ankyrin (TRPA), mellastain (TRPM) and canonical (TRPC) family receptors, permeable to ions, such as sodium, calcium and potassium, too[65-70]. The discovery of TRPV1 by David Julius and Ardem Patapoutian was a major breakthrough leading the way to the unravelling of additional temperature-sensing receptors and how differences in temperature can induce electrical signals in the nervous system. Among the TRPV family, TRPV4 has been detected in the cortical and hippocampal regions of astroglial cells *in vitro* and *in situ*, specifically TRPV4 localized in astrocytes' end feet. The TRPV4 protein is made of 6 transmembrane domains that include the pore region, a cytosolic N-terminal and an intracellular C-terminal tail, as

all the components of the same family, The main trigger of TRPV4 activation in primary cortical astrocytes is the cell swelling with the result of an increase in $[Ca^{2+}]i$. Molecules, such as RN-1471 (RR), are specific inhibitors of the calcium signal mediated by TRPV4 in astrocytes *in situ*, while 4α-phorbol 12,13-didecanoate (4αPDD), is used as agonist of the activity of TRPV4 to increase the cationic currents *in vitro* and *in situ*. Interestingly, TRPV4 can act together with channels involved in the water transport, called aquaporin AQP4, to regulate the cell volume, though a mechanism called for the regulatory Volume Decrease, (RVD)[73-77] (Fig. 1.5).

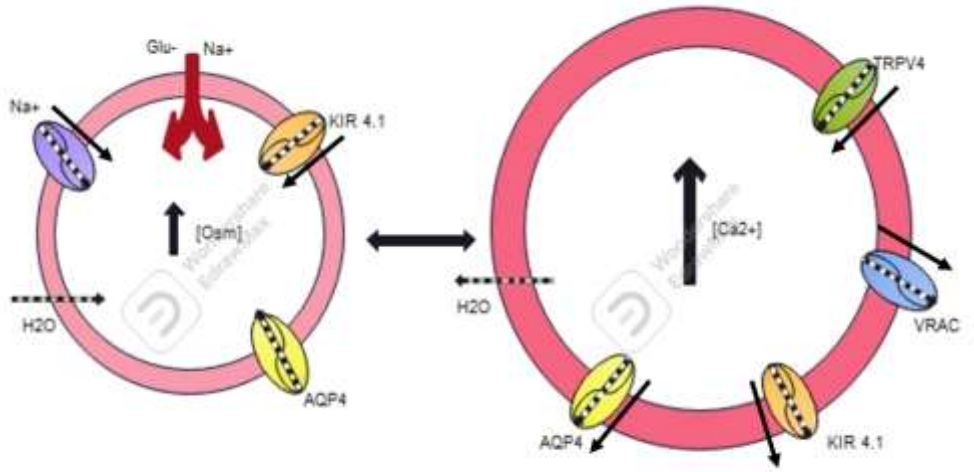


**Figure 1.5: Scheme representing astrocyte swelling and RVD** based on the efflux of intracellular solutes that generate osmotic gradients accompanied by water. $K^+$, $Na^+$ and glutamate uptake occur causing an increase in osmolytes that produce water influx. $Ca^{2+}$ elevation is involved in the sensing and transduction of volume and osmolyte changes (created by EdrawMax ®).

TRPA1 is also expressed in astrocytes, and it is activated by noxious cold stimulus and pungent substances and pro-inflammatory agents[65, 78,79].

The demonstrated role of TRPA1 is to decrease the resting $[Ca^{2+}]_i$ in order to reduce GABA uptake and to regulate inhibitory synapses[80]. Seven members of another family are the TRPC channels (TRPC1-7), which are expressed in astrocytes and activated by phospholipase C (PLC), diacylglycerol (DAG) and mechanical stimulation[69]. TRPCs probably activate $Ca^{2+}$ signals mediated by purinergic, glutamatergic and mechanical stimulation[111], although evidence on their role calcium

induced calcium release in astrocytes are still controversial.

*Aquaporins and Water Transport in astrocytes*

Three members of the aquaporin family are expressed in astrocytes, AQP1, AQP4 and AQP9, the dominant one is the AQP4 made of 8 transmembrane segments and 2 translation initiation sites called Met1 and Met23, localised in astrocytes' endfeet and assembled in orthogonal arrays (OAPs) of particles, still undefined[80-86](Fig. 1.6). AQP structure and plasma membrane organisation were described for the first time by Peter Agree, and its mysterious 28 kDa protein, AQP1 gave him the Nobel Prize 1991. Cloning the AQP4 homolog in brain by Jin Sup Jung led to a major new chapter in the recognition of water transporters at the blood-brain barrier by Søren Nielsen and Ole Petter Ottersen. The structural basis of AQP4 localization resulted from a pivotal observation by John Neely and led to the recognition by Mahmood Amiry-Moghaddam that AQP4 contributes detrimental to the onset of brain edema. The highest expression of AQP4 has been identified in the cerebellum, hippocampus, diencephalons, and cortex[35].

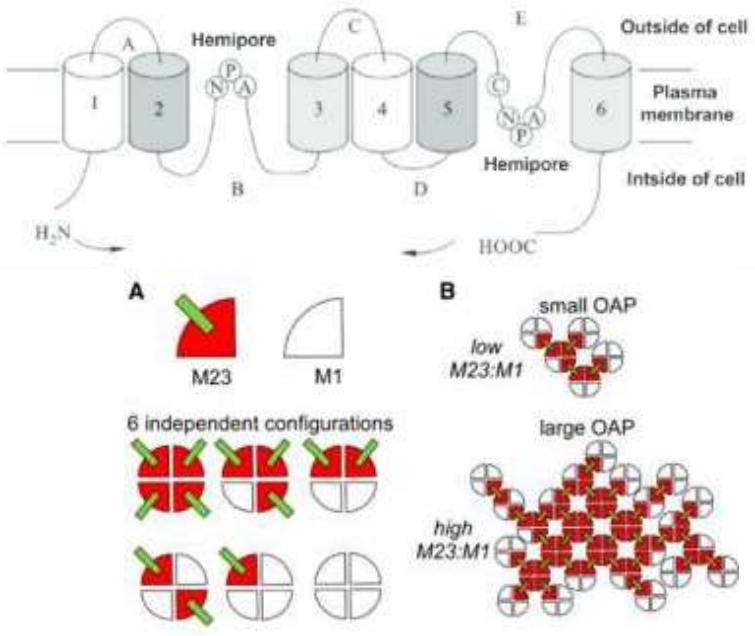


**Fig. 1.6: The structure and distribution of aquaporin-4 (AQP4). (**A) AQP4 has six transmembrane domains (1–6) and five connecting loops (A–E). Loops B and E contain highly conserved " NPA " motifs (hemipores) that overlap midway creating a highly selective water pore. Permission from: Creative Commons Attribution (CC-BY) licence (http://creativecommons.org/licenses/by/4.0/). A, B) Schematic of OAP assembly from AQP4 M1/M23 heterotetramers. M23 and M1 AQP4 monomers. Projection from M23 monomer denotes potential site of M23-M23 intertetrameric interaction. bottom) Six possible independent AQP4 M1/M23 heterotetramers. Four-way rotational variants of each are possible as well. (B) low and high M23:M1 ratios OAPs[88]. Permission from: Creative Commons Attribution (CC-BY) licence (http://creativecommons.org/licenses/by/4.0/) and Elsevier.

Recently, M. A. Moghaddam et al., discovered the AQP4ex, a new isoform of AQP4 abundant in the perivascular astrocytic membrane domains near brain microvessels. His new data suggest that AQP4 is implicated in scar formation[87]. The astrocytic endfeet have been identified as the area of co-localization of AQP4, and Kir 4.1, this means that both of them collaborate to the correct water flux, $K^+$ movement and RVD process[88.]

The volume regulation process involving astrocytes ion channels and aquaporin cooperation can be described as follows: 1) the mechanism of ion homeostasis induces ions' flux by astrocytes at the synaptic site, 2) the latter increase in intracellular concentration of $K^+$induces an increase in therm osmotic gradient that drives and calls water influx, 3) water flux through mainly AQP4 determine cell swelling, 4) cell swelling or alteration in the osmolyte concentration, or alteration in the cell volume is sensed by TRPV4, through an influx of $Ca^{2+}$ that finally initiate the so-called RVD, 5) the activation of volume-regulated anion channels (VRACs) in response to hypotonic challenge, as well as during the cell's swelling[89-90] majorly contributed to the extrusion of anions (inorganic and organicosmolytes) while co-transportes are involved in the extrusion of cations. The protocol is to cause a hypotonic stress by exposing primary cell culture to extracellular hypotonic solution. The RVD process has been shown to be dependent on TRPV4 mediated $[Ca^{2+}]i$ increases. Nonetheless, the cooperation of astrocytic TRPV4 and AQP4, as well as of the function of VRAC are determinant to an efficient RVD process[204]. It is highlighted, however, that while the correlation between TRPV4 and AQP4 or the one between AQP4 and VRAC have been determined, the effect of the synergy among different key elements has never been demonstrated. In this respect, one of the key challenges is the lack of systems where to study cell volume regulation in a controlled manner.

To reach the resolution required for studying dynamics of microdomains in two photon-imaging experiments *in vivo*, higher power exposure is required that can lead to phototoxicity. On the other hand, a major pitfall in the study of astroglial membrane channels involved in volume homeostasis *in*

*vitro* is that, in standard cell culture conditions, their expression pattern does not resemble that observed *in vivo*[88,92]. In a previous work, Posati et al., have demonstrated that plating astrocytes on a nano-structured interface, called hydrotalcite (HTlc), is an efficient method to obtain differentiated astrocytes *in vitro*, in terms of morphology differentiation and both molecular and functional features. In particular, HTlc astrocytes displayed highly branched morphology, accompanied with increased expression of Kir4.1 protein and conductance and overexpression of AQP4, that was paralleled with increased swelling-induced water permeability[88].

Given the peculiarity of this cell culture approach, which allows for the study of astrocytes *in vitro* in a way that recapitulates important features of astrocytes *in vivo*, we sought to study cell volume regulation mechanisms in these differentiated astrocytes. The results of this approach are reported in **Chapter IV.**

*Astrocytes as a functional syncytium*

Astrocytes are not single cells but they work as a functional syncytium. The connections between one astrocyte and the other are made by protein structures called connexons that form the so-called gap junction. **Connexons** are formed by 6 subunits known as **connexins** (Cx), 21 types of connexins with a molecular mass between 26 and 62 kDa. When connexins, forming connexons are not aligned, they may form pores known as hemichannels. The specific activity of gap junctions into a functional syncytium between the cytoplasm of two neighbouring cells, is to maintain the membrane potential of potassium, by two **hemichannels or connexons**, mediating electrical and metabolic coupling by allowing cytoplasmic exchange of ions ($K^+$, $Ca^{2+}$, $Na^+$), second messengers (cAMP, IP3) and metabolic substrates and products; **Connexins**, where firstly described by the group of David Spray. They consist of a four α-helical transmembrane domain connected by 2 extracellular and 1 intracellular loop and having both the C- and N-terminal in the cytosol.

All of them present four transmembrane domains. Astrocytes'homocellular gap junctions are formed mainly by Cx26, Cx30 and Cx43 of which the Cx43 is the most abundant[91]. Connection's pore diameter ranges between 6.5 and 15 Å allows the passage not only of ions but also of hydrophilic molecules up to 1kD[92,93]. On the contrary the panneconnexons are single pores in the CNS, Pannexin 1 (Panx 1) is present in neurons and glial cells*in vivo* and *in vitro*. Panx1 forms hemichannels implicated with ATP release after activation by membrane depolarization or P2X7 stimulation[94]. Panx1 can also form a complex with P2X7 receptorimplicated as well in ATP-release mechanism that helps in the propagation of intercellular $Ca^{2+}$ wavesand D-serine release. Pannexins are proteins belonging to the integrin protein family[13-95-97](Fig. 1.7).

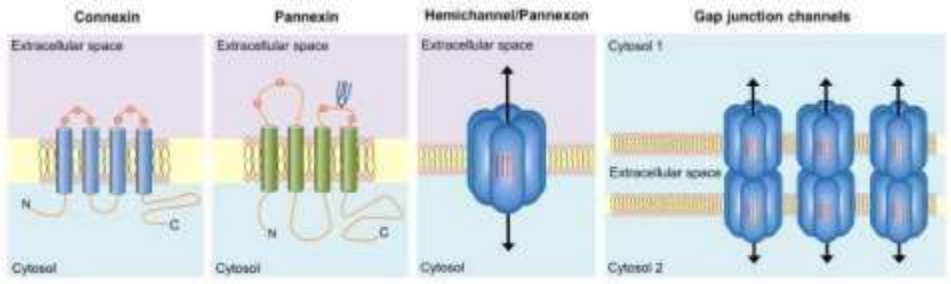


**Figure 1.7:** Scheme of the structure of connexin and pannexin-based channels. Connexins and pannexins present a similar membrane structure with 4 a-helical transmembrane domains connected by 2 extracellular loops and one cytoplasmic loop. The red balls are extracellular loop cysteines, and glycosylated asparagines (blue branches) are also shown. Hemichannels (also known as connexons) are formed by the oligomerization of 6 subunit connexins around a central pore. Pannexons are single membrane channels that are composed of 6 pannexin subunits. Hemichannels dock each other to form functional cell-to-cell channels termed gap junction channels (right panel)[98]. Permission from: Creative Commons Attribution 4.0 International.

*Gliotransmission and the concept of "Tripartite Synapsis"*

The term *gliotransmission* indicates the ability of astrocyte to release molecules, substrates and factors such as excitatory and inhibitory amino acids: glutamate (Glu-), adenosine, D-serine, or $\gamma$-aminobutyric acid (GABA) lactate to neurons, nucleotides and nucleosides (purine nucleotides adenosine triphosphate, ATP), eicosanoids and other lipid mediators (prostaglandins), (neuropeptides (proenkephalin, angiotensinogen, endothelins), neurotrophins (nerve growth factor, neurotrophin-3, brain-derived neurotrophic factor), cytokines (interleukins (IL), interferons (IFN), tumour necrosis factors alpha (TNFα)), structurally associated chemokines and growth factors[99,100,101,]. Several

different mechanisms of release from cultured astroglia have been documented, including (1) volume-sensitive organic anion channels (2) hemichannels (3) P2X7 receptor channels (4) reversed operation of reuptake carriers (5) exchange via the cystine–glutamate antiporter (6) $Ca^{2+}$-dependent mechanism. Astrocytes are endowed with secretory organelles: the small synaptic-like microvesicles (SLMV), the large dense-core granules (LDCGs) and lysosomes whith the function to "store and release". The gliotransmission activity is related to other functions that astrocytes support and that have been mentioned such as the brain potassium "housekeeper", neuron supporters, cerebral blood flow regulators. All of these processes occur at different timescale (micro and nano-scale) and different levels of involvement and organisation of single cluster or network of astrocytes, astrocytes-neurons, astrocytes-glia. Generally, the "old school" of studying neurotransmission considered the transfer of information in the brain as a process mediated between neurons alone. The most recent evidence of the last 15 years, demonstrated the presence of a bidirectional signalling between astrocytes and neurons, where the role of the gliotransmitters is fundamental to regulate neuronal excitability and synaptic transmission. These findings are precursors of a new concept of synaptic physiology, "the tripartite synapse," in which astrocytes exchange information with the neuronal synaptic elements[101]. As a consequence, astrocytes can be considered an integral part of the synapses (Fig. 1.8).

Glutamate is probably the best characterised gliotransmitter, able to modulate synaptic transmission. It is converted to glutamine by the enzyme glutamine synthetase (GS) before being passed back to synaptic terminals and back to glutamate. Cytoplasmic glutamate level is kept lower in astrocytes than in neurons, thus allowing its prompt uptake from astrocytes, when needed.

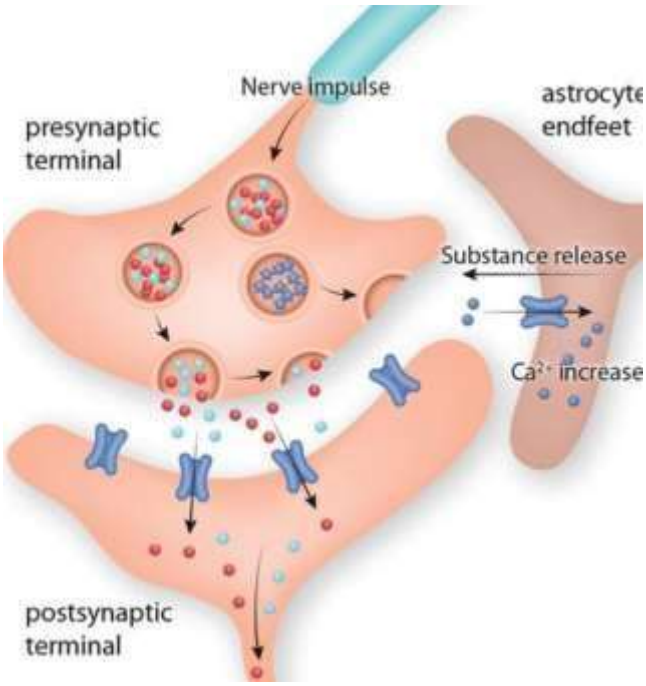


**Fig. 1.8: The tripartite synapse.** Astrocyte' endfeet is the third component of the synapsis made of pre and postsynaptic terminals of 2 neurons. The receptors can interact with the neurotransmitters released from the presynaptic terminal of the neuron. The process is responsible for the activating rises of calcium ions in astrocytes. Astrocytes release as a consequence diverse neurotransmitters and neuromodulators, such as ATP, glutamate[17]. Permission from: Copyright © 2020 Wiley-VCH GmbH.

This complex activity is potentiated by the participation of other gliotransmitters, such as GABA, ATP, adenosine (a metabolic product of ATP), or d-serine, to evoke neurons' response, while ATP has been observed to be released from astrocytes, *in vitro*, *in situ* and *in vivo*, by exocytosis and diffusion through membrane channels, GABA by specific transporter or by diffusion via anion channels, the release of the neuromodulator D-serine seems to occur after the conversion of L-serine by the enzyme serine racemase substrate[35]. Recent studies have also demonstrated the role of astrocytes in maintaining GABAergic neurotransmission through astroglial syncytium for $Cl^-$ homeostasis[102]. In conclusion, glutamate stimulates the astrocyte-to-neuron signalling through the elevation of $Ca^{2+}$, as demonstrated in the hippocampus and cortex area of the brain[101]. Astroglial processes are a structural part of the tripartite synapse made of pre and postsynaptic neuronal terminals. The model demonstrates a bidirectional, glial-neuronal communication where neurotransmitters induce glial $Ca^{2+}$ signalling causing the release of neurotransmitters from the astrocyte to the synaptic space. Astrocytes can control the initiation and shape of synaptic networks

by controlling ion and neurotransmitter homeostasis in the synaptic volume and contributing to synaptic pruning.

Here, the more recent *in vivo* evidence, indicating the functions in which astrocytes are implicated at the systemic level, are reported; in particular, cognitive processes alteration such as memory and learning, information processing, food intake, chemo-sensing, energy balance[17].

*Neuronal Oscillation in Cortical Network*

The cerebral cortex is a highly distributed system in which numerous cells operate in dynamic, through connections explicated from one to another coordinating center. This assumption raises two important questions: first, how is organized the architecture of connections that is assumed coordinating brains' functions? and second, how dynamics can be regulated in the spatio-temporal area. Neurons in the cortex are functionally organised in a network to enable appropriate excitations and inhibitions in the brain. To balance the dynamic of the neuronal networks in the mammalian brain several oscillatory bands in different frequencies from approximately slow 0.05 Hz to fast 500 Hz have been distinguished[30]. Oscillations in neurons are classified based on power and frequency band, with different frequency bands being associated with specific behaviors and activity. Following Berger's tradition, frequency bands were labelled with Greek letters and drawn (delta, 0.5–4 hertz; theta, 4–8 hertz; alpha, 8–12 hertz; beta, 12–30 hertz; gamma, > 30 hertz)[30], (Fig. 1.9). The frequency of bands can belong to the same neuronal network, stimulating a specific function or it can be associated with different brain states[104-107]. Because of it, a constant alternation between different dynamic states of the brain has been identified; several functions, controlled by the cortex, have been associated with a "natural rhythm". Cognitive functions represent the larger rhythmic pattern in the cortex. The nature of this rhythm is due to the voltage fluctuations emerging from the synchronization of individual neurons that are part of a neuronal network. The ordered and marked fluctuations are properties depending on the complex physical architecture of neuronal networks and on the limit of spreading the neuronal communication high in speed from the axons in the time and spatial scale[34]. The latter could cause chaotic oscillations and disruption of the network itself. Moreover, slow

rhythms synchronize large spatial domains and can spread higher frequency localised oscillations, for example sleeping is the result of multiple oscillations, but still poorly defined in its mechanism of development and spreading. Its state is determined by unperturbed multiple oscillations in the thalamus[108]. On the contrary higher frequency oscillation occurs in small neuronal network[106]. There is a correlation among the type of oscillation and the function that the brain is supporting[103]. Different mechanisms in different brain structures can oscillate the same band, but at least one distinct mechanism stimulates the oscillation network.

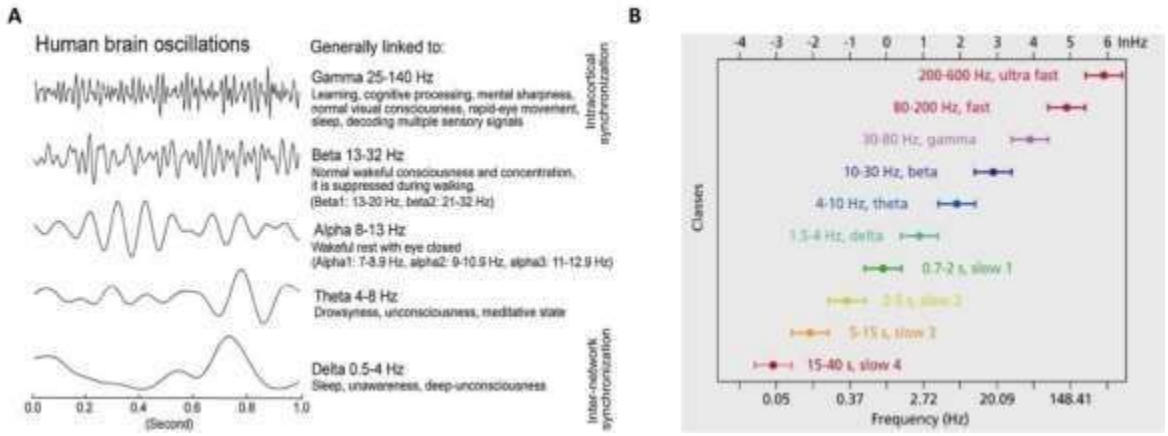


**Fig. 1.9: Cortical oscillations in human brain**. A) Cortical oscillations classified into frequency bands; each of them contributes in a healthy brain to different functions and activities for human life. B) Graph showing linear progression of the frequency classes on their natural logarithmic scale[3],[103]. Permission from: Copyright © Elsevier and Copyright Clearance Center and American Association for the Advancement of Science 2004.

The best performance in cognitive function is determined by tonic increase in alpha but a decrease in theta power, it depends also on the type of memory demands. The alpha frequency is related to age and memory performance decreasing from childhood to adulthood. Modulating the power of alpha is controversial but can be a solution to different neurological disorders. In addition, the phenomena of transition from waking to sleeping is correlated to an alpha power decrease, whereas theta power increase[109].

*Astrocytic Modulation of Cortical Oscillation in the Brain*

The mechanism behind the range of frequency in the cortical network needs to be regulated to a driven factor able to generate network oscillations, tuning different frequencies in time and space,coordinating neurons and activating intrinsic conductance by neuromodulators[110], receptors cellular

excitability and the hyperpolarization of inward current[110]. The intrinsic increase of Potassium concentration ($[K^+]o$) impacts the synaptic transmission and plasticity[111,112].

The increase in the accumulation leads to neuronal excitability and pathological conditions[113,114]. Sejnowski's group studied the impact of $K^+$ activity on the excitation of neurons and neuronal networks[115,116] by the formulation of a computational model. They found that possible modification of $K^+$, because of changing in the conductance of neurons, can lead to altering fast and slow oscillatory firing. Nedergaard's group showed the role of $K^+$ in the release of neuromodulators *in vivo*, he demonstrated that $K^+$ fluctuations could alter the synaptic activity[117].

$K^+$ homeostasis appears to be the main protagonist of a complex network, however, it is still not well identified and implicated in all the brain functions. Buskila and Bellot-Saez demonstrated that alteration of $[K^+]_o$ modulates network excitability, affecting both low and high-frequency oscillations, this could modify the membrane's properties[118]. The study of A. Araque's laboratory about astrocytes modulation of neuronal network activity introduces the idea of the quantification of sensory-evoked astrocyte responsiveness and the impact on sensory-evoked cortical neuronal network activity. The data of its studies determine the relationship between sensory stimuli and cortical astrocyte-neuronal network responses and confirm that astrocytes are active in the processing of cortical sensory information[119]. Supporting the theory of the active involvement of astrocytic signaling in cognitive function, V.M. Sardinhia and J.F. Oliveira analysed through electrophysiology experiments the hippocampus–prefrontal cortex network, giving emphasis to the role of astrocyte-derived signaling in corticolimbic circuits and cognitive processing[120]. In conclusion, the state-of-the art hypothesis on the role of astrocytes in the modulation of brain oscillations are related to their homeostatic capability. Since astrocytes are pivotal in maintaining the $K^+$ homeostasis, the modulation of their quality in the potassium re-uptake from the extracellular milieu, is a potential mechanism to tune the neural oscillations and to preserve the network disruption before the rising of impairments. Moreover, in a recent review about the understanding

of the regulation of rhythm behaviour, Drosophila and mice were compared to demonstrate the importance of astrocyte-neuron communication in the regulation of circadian behaviour and sleep by astrocytes. Both neurons and astrocytes contain circadian clocks that control rhythmic behaviour. In Drosophila,astrocytes are critical for normal behaviour, but it is unclear how astrocyte clocks participate in regulating circadian period. In contrast, mammalian astrocyte clocks determine behavioural rhythms including circadian period[119,122].

**Potential Role of Astroglial Ion channels in Cognitive Functions**

Several studies established astroglial cells' active contribution to emotions, learning, memory, and generation of thoughts in humans, as regulators of the synaptic transmission and of the intrinsic neuronal excitability. The second factor that allows us to consider astrocytes related to cognitive functions is that astrocytes occupied 20-fold larger volume in the human brain than that in rodents. The influence on process information in specific ways by integrating and computing data and by participating in the mechanisms of memory formation and learning cannot still recognize a real link with the concept of human intelligence and astrocytes, never demonstrated. The information travels through the brain and passes through the connections of neurons. Astroglial cells take part as the third fundamental member of the neuronal network; however, the mechanism that mediates this coupling is still not known[50]. Furthermore, pathophysiological data also support this hypothesis by demonstrating that the lack or the down or up-expression of astrocytic ion channels and water channels is observed in diseases characterised by cognitive impairment. In particular, KCNJ10, the gene encoding the potassium channel Kir4.1 or AQP4 dysfunctions, have been linked to autism and neuroinflammation. Additionally, the numerous techniques used to study astrocytes *in vitro* and *in vivo*, are not able to address the question of whether astrocytes directly contribute to cognitive functions or allow cognitive functions. Some observations *in vivo* demonstrate that calcium increase and signalling, which is responsible for the glial complex gliotransmission process, is suppressed during the anaesthesia in animals.

One of the studies analysed the impairment of working memory induced by cannabinoid.

Mice with conditional astrocytic deletion of CB1-cannabinoid receptors didnot display deficits in working memory in response to cannabinoid. In contrast, mice with conditional deletion of CB1 receptors in glutamatergic or inhibitory neurons exhibited the expected detrimental effects of cannabinoid. Thus, excessive stimulation of astrocytic CB1 receptors may mediate cannabinoid-related impairment of cognitive function. The emergence of new experimental techniques offers exciting possibilities in studying the importance of neuroglia signalling in the absence of pathology *in vivo* during the cognitive and learning functions[17,35,122]. Of interest is the implication that astrocytes have in the regulation of rhythmic behaviour *in vivo*, such as the circadian rhythms and in particular in sleeping. It is emerged that astrocytes are endowed with a "clock center"made of at least 396 genes localized in the suprachiasmatic nuclei in the anterior hypothalamus (CNS); [55] of them are responsible of wakefulness and sleep[35]. The endogenous clocks of astrocytes are suggested to be similar to those expressed in neurons and implicated in rhythmic behaviour. Thisobservation leads to considering astrocytes and neurons part of an oscillatory and rhythmic network[35]. In the plethora of hypotheses, our lab has pioneered the idea that astrocytes can actively contribute not only to the maintainance but also to the genesis of the brain rhythm. In particular, we believed that transmembrane ionic fluxes across the plasmamembrane occurring in such a minute space like the one of micrdomais can generate local current displacement that, on turn, might contribute to the genesisof oscillations or to tuning their balance by active ions uptake/secretion and bioelectrical signal. However, despite valuable data provided, the emerging problem on the difficulty to approach the question of the role of astrocytes in brain rhythm is the lack of specific ways and techniques or methods that can provide a unique and conclusive answer[17,100].

Thus, as demonstrated in **Chapter IV** we took advantage of nanostructured forest of electrodes to verify the occurrence of such spontaneous waves of voltages *in vitro*, and to set the scene to unveil amore deterministic role of astrocytes in cognitive function.

**Astrogliosis and Gliopathologies**

The brain, which is located in the skulls, can be exposed to different traumatic events; some insults affect

astrocytes' structural and functional properties and can alter neurons or the surrounding parenchyma. The term used to indicate damage to glial cells is *Gliosis.* It refers to structural and functional changes of astrocytes and microglia, in response to chronic or acute insults of the CNS. The kind of alteration, and the degree of the type of pathology are variable, but the features that characterise the acute and chronic damages are similar; it includes hypertrophic cellular proliferation,upregulated expression of several proteins, including GFAP and vimentin in astrocytes, the presenceof cytokines, chemokines, and growth factors and ultimately the formation of a persistent fibrous scar[123-125]. Biochemical signalling cascade, molecular paths, and structural changes of reactive astrocytes, as significant alteration in ions expression occurs in astrogliosis. In particular, dramatic changes in the membrane expression of inwardly rectifying potassium channel Kir 4.1, excitatory amino acid transporter as (EAAT2), gap junction protein connexin 43 (Cx43), calcium channel TRPV4 and of the water channel AQP4[126-129]. The uncontrolled proliferation of glial cells, as a consequence of the reactive gliosis, can cause a phenomenon of excessive neuro-inflammation that leads to neuronal death and tissue damage.

In this perspective, ion channels, water channels and other transporters present the target forengineering neural implants that aim to reduce the gliotic responses and to treat neuroinflammation.In this perspective designing and validating nanoglial interfaces materials and devices and aim to propose novel therapeutic opportunities for brain disorders where astrocytes structure and function are compromised[17].

It should be also noted that, the implant *in vivo* of a device in the brain is often accompanied by a gliotic response to electrodes. In these processes, microglia start secreting cytokines that, at the beginning, act as proinflammatory biomolecules. The final result of the gliotic cellular reaction is typically the formation of an encapsulation layer around the implant named *gliotic scar*[126-129](Fig.1.10). The biomedical engineering progress helps in the approach with new methods to minimise the effects of gliosis, tuning the mechanical mismatch between the brain and the device material, the bio-functionalization of the electrodes and the low-impedance nano-structure of the interface. However, the features of specific anti-gliotic devices are difficult to be established becauseof the extreme variability in

the human brain response; the thickness the ultra-flexibility, the stretchability and higher level of conformability can be a good strategy to minimise the impact of theimplant on the CNS. Besides, also a chemical approach based on the choice of materials, or biomodification of the implant interface by immobilisation of bioactive peptides, is a strategy that allows advantages (i.e., aminogroups to impact on neuronal adhesion and neurite outgrowth, integrinsbinding peptides to anchor astrocytes to the implants while inhibiting their gliotic hypertrophic proliferation or RGD mimicking motifs). Other interesting strategies to reduce the inflammatory reaction of glial cells in the brain are the use of anti-inflammatory agents on inorganic electrodes or the coverage of implants with biomimetic and bioactive coatings to mitigate the neuroimmune inflammatory reaction $\alpha$-Melanocyte-stimulating hormone ($\alpha$-MSH), a hormone usually secreted bypituitary cells, astrocytes, monocytes, and keratinocytes that have intrinsic functions inhibiting proinflammatory cytokines—or the local release of Dexamethasone, a synthetic glucocorticoid hormone)[17,130]. Glial fibrillary acidic protein (GFAP), the main constituent of astrocyte intermediatefilaments, is used as a marker of reactive astrocytes in human pathologies.

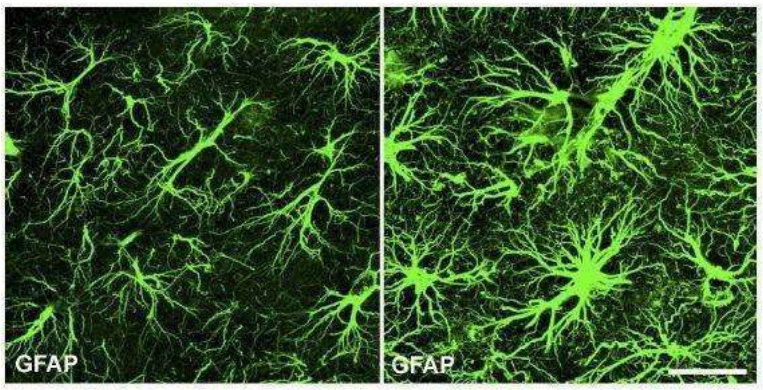


**Fig. 1.10:** Reactive astrocytes (right panel) show hypertrophy of their cellular processes marked with GFAP[132]. Permission from: Copyright © 2013 Wiley Periodicals, Inc.

Immunohistochemical experiments of the brain, spinal cord, or retinal tissue upregulate GFAP other signs of astrocyte reactivity and reactive astrogliosis in a whole range of neuropathologies, suchas neurotrauma, focal brain ischemia, brain haemorrhage, perinatal asphyxia, acute, subacute, or chronic CNS infections, epilepsy, primary or secondary CNS' tumours, retinal ischemia, diabetic retinopathy, Alzheimer's disease (AD), Parkinson's disease, multiple sclerosis, Batten disease (BD) or amyotrophic lateral sclerosis (ALS,

known also as Lou Gehrig's disease)[131]. GFAP markers can reveal gliosis *in vivo* and *in vitro* systems both in single astrocytes culture and in co-cultures with other CNS cells. The study of gliosis, also induced by astrocytes/materials interface in reliable cell culture system allows the essential understanding of the function of healthy astrocytes, including theirfunction in metabolism, neurotransmitter recycling, and calcium signalling and it allows to mimic various disease situations such as injury, hypoxia, or neurodegenerative diseases. However, 2D *in vitro* systems have several limitations, that include the highly reduced morphological complexity of astrocytes. This limitation can be overcome with the use of 3-D astrocyte cultures and the novel approach of technologies and methods to study astrocytes *in vitro*, mimicking the ECM (Fig. 1.11)[131].

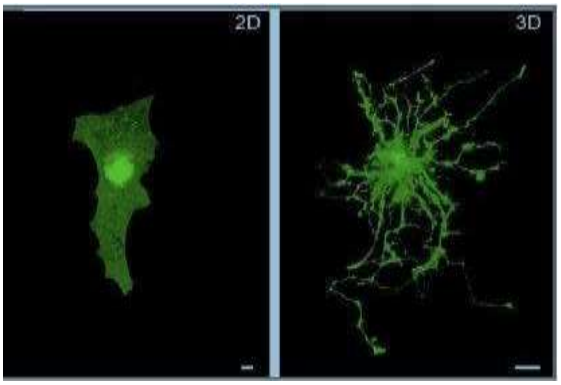


**Fig. 1.11:** Astrocytes labelled with GFAP, in 2D and 3D cultures. The right panel shows the preservation of some of the complex morphological and biochemical features of *in vivo* astrocytes that are normally lost in culture, compared to the left panel[133]. Permissionfrom: Copyright © 2013 Wiley Periodicals, Inc.

Several neuropathologies are characterized by loss of homeostatic properties of astrocytes: epilepsy (among the others), brain edema (ischemia, ictus), or neurodegenerative diseases (Alzheimer's Disease, Retinitis Pimentosa, Neuromielitis Optica).

Cerebral edema is excess accumulation of fluid (edema) in the intracellular or extracellular spaces ofthe brain. The influx of ions and water results in cellular swelling and in generation of cytotoxic edema, that is a critical event following ischemia/hypoxia. Astroglial ion channels and AQP4 are the dominant contributor to the formation and clearance of cerebral edema. Thus, studying nanomaterials interfaces capable of the modulation of their expression and function might be of use to define noveltherapeutic paths[134-136].

Epilepsy is one of the most common neurological conditions, while it was thought that epileptic activity was generated by neurons, recent evidence showed an astrocytic basis for epilepsy. Specifically, the alteration of astroglial potassium homeostasis, with a critical role for Kir4,1 and impaired potassium clearance is now in the spotlight as a major therapeutic target of intervention[136-138].

Actually, Valproic acid, a common antiepileptic drug, seems to reduce the loss of astrocyte domain organisation in an animal model of epilepsy[139-141]. However, the development of nanomedicine and nanoglial tools might be useful for selective drug delivery to astrocytic microdomains devoted to potassium homeostasis or to monitor the activity of astrocytes in Epileptic patients.

Brain Tumours are recognized as the most aggressive form of neoplasia, causing thousands of deaths. In particular, glioblastoma (GBM)[141] is an aggressive tumour of adults in particular that consists of neoplastic astrocytes highly invasive and characterised by an angiogenesis process[142-143]. During the GBM progression there is an alteration of the entire ECM and of the proliferation of several stromal cells, including microglia, pericytes, fibroblasts, and endothelial cells[144-146]. Typically, the morphological observation of glioma patients tissue presents an overexpression of GFAP correlated with astrocytes and with tumour size, but not with the degree of malignancy. The role of water transport, AQP4 polarization, potassium impairment and RVD process have been clearly demonstrated[147-150]. It has been shown that these processes lead/participate to uncontrolled proliferation, to infiltration and aggressiveness of glioma. Thus, these processes and involved channels should be considered as target for nanomedicine and for the study in neuroscience using protein nanoglial interfaces (see Chapter IV, paper 4).

Besides acute pathologies or brain tumor, alteration in astrocytes structure and function has been demonstrated in Alzheimer's disease, Psychiatric disorders, Neurodegenerative processes such as Amyotrophic Lateral Sclerosis or Neurological conditions related to Diabetic Disorders. All these evidence calls for a scenario allowing for a broader use and interest in the development of Nanoglial interfaces.

**State-of-the-art techniques to study astroglial cells**

The physiology and pathology of glial cells need different methodologies and approaches to elucidate their roles and behaviour. Since they were considered as an active unit of the CNS, typical applications used for neurons such as electrophysiology, calcium imaging, *in vivo* and *in vitro* imaging, conditional knockout animals have been employed trying to catch the complexity of their biological responses.

For what concerns the study of cells *in vitro* the culture systems in 2D were the first revolution in the understanding of the molecular and cellular pattern of brain cells, even though they represent a simplified model with respect to the *in vivo* brain network[101,120]. First models derived from primary rodent cultures of neuronal and glial immortalised cell lines in monocultures or co-cultures[151,152]. However, there is still a lack in studying glial cells, caused by the fact that most of the tools used *in vivo* and *in vitro* are dedicated to the exploration of neurons; recent new methodologies applied *in vivo*, especially in the optical imaging and in the development of genetically encoded sensors, transgenic mouse lines expressing fluorescent proteins, biosensors, opto/chemogenetic proteins, Cre recombinase, Cas9, represent an improvement in the knowledge about the glial role in the brain[153,154]. Among *in vivo* strategies, the genetic modification and manipulation of viral vectors are strategical to evaluate potential therapeutic approaches in brain disorders[197]. It is, usually, employed as a

technique to modulate the gene expression of neurons, but it can be applied to transduce glial cells in primary culture as well as gene silencing with small hairpin RNA (shRNA)[154-157]. The advent of mCRISPR technology could also be used to inactivate or modulate genes in glial cells. The most used technique to image brain cells, especially *in vivo,* through the two-photon method allows a more sophisticated dissection of the role of glial cells in the complex neuroglial networks, even with several limits emerging such as spatial and temporal precision. The two-photon microscopy combined with emission depletion (STED) microscopy is an optical tool used to detect calcium in astrocytes. There are many commercially available organic $Ca^{2+}$ indicators to properly observe $Ca^{2+}$ changes in astrocytes microdomains, but currently, the available methodologies are weak *in vivo* and *in vitro.* Although astrocytes are electrically silent cells as they cannot fire action potentials, calcium in astrocytes could be considered a kind of excitability[158,159]. Recently, optogenetics (a technique allowing genetically the control of membrane potential or intracellular signalling) defines cell populations by expressing opsins. Opsin acts on the membrane potential (light-sensitive proteins, ion pumps or ion channels) and stimulates the potential by light. The emission can be applied *ex vivo* via the microscope objective or *in vivo* through an optical fibre connected to a light source[160]. For example, optogenetic cation channels are perfect for neuronal activation, but not for astrocytic modulation. The aim is based on genetically encoded light-sensitive ion channels driven by rhodopsin isomerization to cause the opening of ion channels to allow the flow of certain cations or anions to alter the bioelectrical properties of the targeted cell; channelrhodopsin 2 (ChRs2) is a blue sensitive cation channel found in cyanobacteria, with light[161-166]. Experiments performed in astroglial cells *in vivo* showed that photoactivation of ChR2 induce gliotransmitter release while, *in vitro* experiments performed on mouse cortical astrocytes showed that activation of ChR2 triggered $Ca^{2+}$ elevations, very slowly in a timescale of minutes[167-170]. In conclusion, specific tools capable of modulating astrocyte activity are necessary in order to properly understand astrocytes' physiology and the interaction between neurons and astrocytes.

**Smart glial engineering and interfaces for measuring and probing astrocytes**

This thesis disserts about new smart glial engineering interfaces for the correct measure of astrocytes; it presents innovative interfaces in terms of research tools and therapeutic approaches. As mentioned keywords in determining the lifetime of neural interfaces are: bio-materials, the mechanical mismatch between the brain and the device material, specific bio-functionalization of the surface, nano-coating and low impedance[17]. The aim is to validate *gliointerface* where all the "key features" in terms of sensing and probing astrocytes can be elucidated. The multidisciplinary approach and coordination of different fields such as engineering, biology, physics and chemistry leads to the definition of neuroscience combined with nanoscience and result in nanoneuroscience. For example, the use of nanomaterials rather than microstructures allows to detect and reveal low frequency, slow, and long-lasting voltage membrane variations typical of astrocytes. The evolution in the study of glial cells and the new approach of sensing brain cells probing them targeting ions and water transport or gliotrasmitters with mechanical, electrical, and photonic stimuli is a challenge in the field of the technologies and it is relevant to define an interface as smart biomaterials, potentially implantable and not dangerous for tissue. In engineering and material science, these interactions are usually referred to as biotic and abiotic processes[171], meaning 1) control the cellular response to a foreign body and 2) control the impedance increase and the electrode corrosion. The biotic process leads to gliosis and includes hypertrophic cellular proliferation upregulated expression of several proteins, including GFAP and vimentin in astrocytes, presence of cytokines, chemokines, and growth factors, and ultimately the formation of a persistent fibrous scar, enabling the device[123]. All this evidence leads to a central question: which factors can be tuned to reduce the gliosis reaction in implants? Which are the major nanomaterials tunable for the glial cells probing and sensing?

To answer these questions, the choice of a biomaterial is the first crucial stumbling block to overcome in the interaction with a biological system. Biomaterials can be part of electronic devices, electrodes, diodes, transistors, main surface or components of the devices. Once a device is in contact with the

brain, it is recognised as a foreign body and a response to the implant is activated by the cell's body (Fig. 1.12).

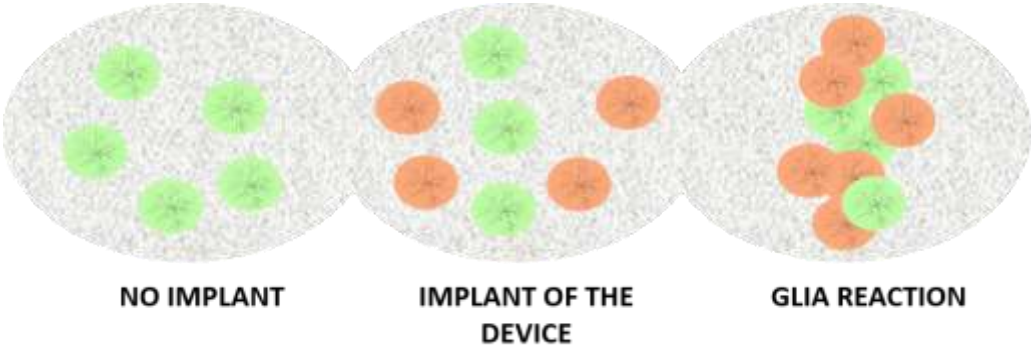


**Fig.1.12**: Scheme of the response of astrocytes to an implantable device recognized as a foreign body. Before implant (left), green viable and non reactive astrocytes, right after implant the acute inflammation phase starts and astrocyte (red) and microglia are active. In the chronic phase (right) takes place completely the glia reaction, the encapsulation of the implant, the inactivation of its function and the surrounding glial scar (created by Office PowerPoint ®).

To guarantee the performance of a potential implantable device the constituent material must have specific chemical, physical, mechanical properties and overall, it must be biocompatible to inhibit the possibility to be encapsulated and embedded by the inflammatory reaction mediated by glial cells[172]. Evidence shows that more than one approach has been tested to help the overcoming of this problem. Specifically, 1) functionalization of the surface with anti-inflammatory molecules[173-176], 2) softness and 3) reduced dimension of the topography area interacting with cells 4) micro - and nanostructuredmaterials can be helpful to promote an intimate contact of the device with the cells[177]. In particular, two dimensional (2D) nanomaterials have been widely used for interfacing with biological systems *in vitro* due to their diverse potential and unique physicochemical and morphological structures, but the 2D is still a limit, even if it represents a milestone in the brain understanding and glial interface science.

**Smart nanoglial interfaces**

Unlocking the secret circuits in the brain is a challenge of scientific technologies; equipments and tools aim to gain precision in time and scale revelation. The evolution of nanomaterials culminated in the employment of several agents and functionalized agents as novel diagnostic and therapeutic strategies,

including drug delivery or neuroprotection. To be considered a real functional therapy, itis important to discover the cause and the origin of pathologies, the latter represents a huge problemfor scientists[178]. The understanding of the constituents of the nervous system: neurons and their functional circuits, glial cells, neurons' plasticity, spatio temporal dynamic rearrangements, meets theneeds of the potential applications of the emerging attention to nano-size materials and molecules[179]. In this context, "Nanoneuroscience" employees' nanomaterials and nano-size to interact with the organ tissues and membranes or with BBB, try to prevent insults to the brain[180]. For example, the useof nanoliposomes, micelles or nanogels is cited as examples to overcome the problem of passing theBBB[181]. The principle of those molecules is based on nanoparticles[182](MNPs). Moreover, inflammatory or infectious processes represent another aspect that captured the attention of neuroscientists: it is fundamental to promote appropriate neural growth and electrical conductivity in a healthy brain. This issue requires materials, scaffolds and devices with exceptional properties[183]. Inthis context, ion channels are the basic elements in the transmission of signals, in neurons firing andglial cells communication[184]. Alterations of their activities are responsible for the mutation of genes expressing ligand- and voltage-gated ion channels, known as channelopathies[185] and detected by molecular-based technology and electrophysiology. The ion flow in the neuronal circuit pays attention to the recent development of nanoscale sensors or nanoprobes[186] to investigate the ion measurement of $Na^+$, involved in neural transmission. Another promising model is modelling an optical sensor to visualise ion flow in the nervous system by the application of an optical sensor thattransforms the captured light into an electrical signal that can be read by the instrument. Ion channels can be controlled also by the magnetic field, inducing heating NPs[187] to activate temperature-sensitiveion channels in cells such as temperature-sensitive transient receptor potential channels (TRPV1)[188]. HTlc are colloidal aqueous dispersions of ZnAl-HTlc having the formula $[Zn_{0.72}Al_{0.28}(OH)_2]$ $Br_{0.28}$ 0.69 $H_2O$ and prepared by the double-microemulsion technique. The chemical composition of the ZnAl-HTlc allows the following clays nanoparticles to be used in different configurations from nanoparticles to micro sheets[88,92]. Moreover, taking advantage of sucessful results obtained in terms

of morphological and functional differentiation of astrocytes that the same interfaces were prepared and investigated focusing on the functional interplays occurring between ion channels and AQP4 rely in the astrocytes microdomains and their role as regulator of cell volume and homeostasis in cells.

The last chapter of this thesis presents and discuss on going results and approach of specific category of nanotools we are studying in collaboration with ARL Laboratory of Aberdeen of the Prof. S. P. Karna. Nanoprobes, called nanoclusters (NCs): NCs-conjugated with Gold (Au), have never been explored with brain cells. They are small clusters of gold (Au) atoms ranging from 5 to 25 atoms[189-192]. P:NC exhibits several photo-physical properties such as tunable fluorescence and high photostability. The possibility to modify their chemistry makes the AuNC fluorescence available for the functionalization with proteins, stimulating the enzymatic activity, the cells metabolism, the cells morphology, or properties. A major hypothesis leads to the idea that NCs functionalized with bio-proteins increase their potential biocompatibility. However, the mechanism of biosynthesized AuNCs remains under investigation. Previous studies suggested that metal ions such as Au (III), Ag(II), Pt(IV), or Zn(II) diffuse through the cellular membrane and are reduced at specific sites in intracellular proteins and stabilised[193-196](Fig. 1.14). Wang et al. in 2013 demonstrated for the first time the *in situ* synthesis of green-fluorescent P:AuNCs in tumour cells, however still any studies have been presented on their application with brain disease[197]. In this context, atomic nanoclusters and biological sensing applications in the brain can represent a new frontier of investigation. For example, they could be part of thin-film polymers' devices and sensors, expoiting the unique opportunity to develop low-power, high-sensitivity, multifunctional future sensors technologies, where nanomaterials preserve their electronic and optical properties.

More generally, NCs exhibit unique properties at nanometer scale that are different from the atomic scale and can respond to external electrical, optical, magnetic, chemical, and biological stimuli.

Au possesses unique and tuneable plasmon resonance properties, unique magnetic properties, high signal-to-noise ratio; besides, it exhibits intense photoluminescence and high stability. The gold-

nanoclusters (AuNCs) offer considerable advantages in several applications of studying cell biology such as imaging applications thanks to fluorescence, versatility in nano-size, surface and hydrophilic or lipophilic characteristics. In addition, protein-synthesis fAuNCs *in vitro*, such as bovine serum albumin protein (BSA, fAuNCs/BSA) have been already shown to internalise into cervical, kidney, and fibroblast cell lines without negatively impacting cell viability[198].

Summarizing, the advantages of using AuNCs as nanoglial interfaces might be: 1) the intrinsic fluorescence that could allow to identifying cells' specific targets, 2) the intrinsic ultrasmall dimension, 3) the functionalization with proteins that allow AuNCs to be pharmacological vehicle; 4) the possible tunability of astrocytes properties by the modulation of time exposition and concentration of AuNCs with cells solution.

However, the identification of the mechanism that the NCs employ to interact with cells is still under investigation.

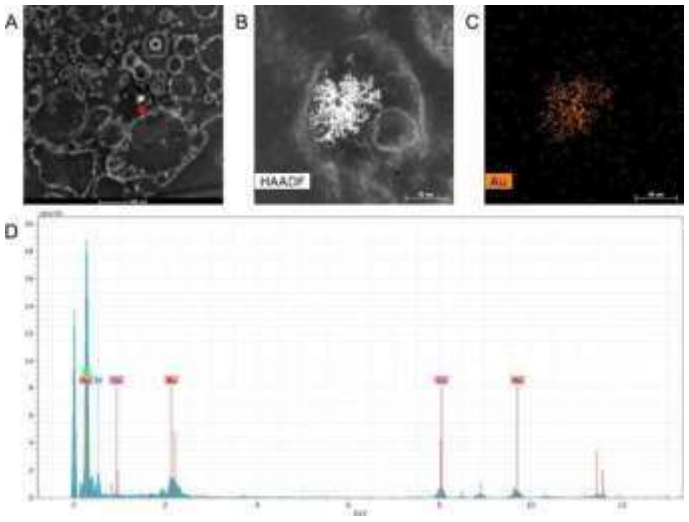


**Fig. 1.14:** Scanning transmission electron microscopy of human microglial cells exposed to AuNCs. (A) Gold was visible as bright white against the dark background (red arrow). (B–D) Gold verified through EDX analysis[198].

Thus, a dedicated section of this thesis discusses the possible application of f-AuNCs impact on astrocytes growth, functional and structural properties.

**Bioelectronic, optoelectronic and photonic glial interfaces**

It is becoming evident that driving and controlling the gliotic inflammatory reaction is central for the success of therapeutic approaches; new studies on glial cells are needed to understand and control the impact of neural interfaces considering the long cell viability, growth, proliferation, and functional properties. It is important to underline that silicon and metal neural interfaces may manifest technological and mechanical defects in terms of spatio-temporal resolution, selectivity, mechanical tissue mismatch, and long-term biocompatibility. Organic bioelectronic polymers, on the contrary, show a variant of intrinsic properties, such as electrical conductivity, biocompatibility, mechanical flexibility that offer advantages if compared to inorganic materials[17,199,200]. As a biocompatible organic interface, several materials have been investigated interacting with neurons and later with glial cells, *in vitro* and *in vivo* with the aim to collect ion current and to capture their specific signals. For example, (poly(3,4-ethylenedioxythiophene) polystyrene sulfonate (PEDOT:PSS), polypyrrole (PPy), and polyaniline (PANI)[201,202]. The study was focused on the increase of the conductive properties supported by increasing concentration of Ethylene glycol (EG), with a final conclusion that neurons' growth and survival were higher than astrocytes and the collected signals were opposite to that observed in primary astrocytes. Organic materials-based bioelectronics offer promising tools for the study of the physiology of astroglial cells. They are biocompatible, optically transparent in the visible range, iono-electronic transport promoters with light adsorbing and emitting properties. One of the most important questions about astrocytes and cell communication that remains is the astrocytic activity is independent from the neuronal activity. To address this issue, devices eliciting biochemical and electrical signals in astrocytes are needed, overcoming the limits of neural devices caused by biological instability, high electrical noise, tissue inflammation, primate studies and human clinical trials[203]. To solve this issue, Benfenati, Antognazza et al., exploits photoexcitation of a thin film polymer photovoltaic blend made of poly(3-hexylthiophene) with phenyl- C61-butyric-acid-methyl ester (P3HT:PCBM), previously used to excite hippocampal neurons, and later for neuronal firing *in vitro* of blinding retina[204-207]. The work demonstrated that P3HT:PCBM supports the growth of pure

primary cultured rat neocortical astrocytes; 543 laser light emission excite the whole-cell membrane conductance of astrocytes and depolarized the membrane potentials, suggesting that the ClC-2 protein channels are triggered. For the first time they demonstrated the effect of P3HT:PCBM blended photostimulation *in vitro* as a gliophotonic interface. On this basis in this thesis in **Chapter IV**, we described the results achieved in collaboration with Dr. Antognazza, IIT-CNST, Milan, on the use of nanopillars of P3HT:PCBM blend. Given the the importance to reveal intracellular calcium concentration ($[Ca^{2+}]i$) in primary rat astrocytes as fundamental in cells' signalling, Borrachero et al., used transparent organic cell-stimulating and sensing transistor (O-CST) made of perylene-diimide-derivative N, N'-ditridecyl perylene-3,4,9,10- tetracarboxylic diimide (P13), already validated to stimulate and record neurons, to explore the possibility to elicit calcium signalling in astrocytes. The work showed that an extracellular electrical stimulation given by a slow ramp of voltage spanned at the gauge electrode of the OCST induces a slow and persistent increase in $[Ca^{2+}]I$ by TRPV4 and TRPA1[208,209]. Thus, both organic bioelectronic and optoelectronic approaches are suitable as promising glia interfaces. Another important carbon-based material is graphene and its derivatives, with tunable electrical conductivity and mechanical flexibility. Graphene represents a potentially suitable material for neuronal interface. The properties of graphene include large surface area (2630 m2 g−1), strong mechanical strengths (Young's modulus∼1100 GPa, fracture strength ∼ 125 GPa) and high thermal conductivity (5000 W m−1 K−1)[210,211]. Furthermore, its all-carbon backbone structure can be easily functionalized via standard organic chemistry or electrochemistry[212,213]. The outstanding mechanical properties of graphene allow high tensile stiffness and strength and flexibility, which make graphene ideal electrodes to contact brain cells[214]. The family of graphene nanomaterials can be classified according to the number of layers, chemical modification of the surface, purity, lateral dimensions, the density of defects and composition[215]. A general nomenclature of graphene-related materials (GRMs) has been introduced by the EU project Graphene Flagship guidelines to discriminate single- and few-layered G (1–10 layers; GR), G oxide (single layer, 1[thin

space (1/6-em)]:[thin space (1/6-em)]1 C/O ratio; GO), reduced G oxide (rGO), graphite nano- and micro-platelets (more than 10 layers, but <100 nm thickness and average lateral size in the order of the nm and μm, respectively), G and G oxide quantum dots (GQDs and GOQDs, respectively) and a variety of hybridised G nanocomposites[216].

Chiacchiaretta et al., also observed that treatment with GO flakes induces a significant alteration of $K^+$ currents along with an increase in outward rectifying currents[217].

Additionally, they found that astrocytes treated with GO flakes had enhanced $Na^+$-dependent glutamate uptake capabilities as well as displayed alterations in calcium signalling[218].

In collaboration with the group of V. Palermo and Manuela Melucci at ISOF CNR in Bologna, we aim to improve the interaction with astrocytes exploiting the biomimetic approaches, and functionalization with (bio)molecules composed of a bilayer of phospholipids[219]. To this end, a phospholipid (PL) was linked on graphene oxide (GO) sheets and the resulting substrate was used as a bidimensional scaffold for growing primary rat cortical astrocytes. The adhesion of primary rat cortical astrocytes on GO-PL substrates was increased compared to standard systems (e.g., poly-D-lysine, PDL) and compared to that on non-functionalized GO. Primary rat cortical astrocytes grown on GO-PL showed no significant gliotic reactivity. GO films with a nanometric thickness can be easily fabricated via spin coating or filtering of aqueous solutions at different concentrations. Although GO is non-conductive, it can be transformed to highly conductive and reduced graphene oxide (rGO) via thermal, chemical, and electrochemical treatments[220].

Bioelectronic deals with all the electronic devices capable of interacting between biological signals and electronic systems. This means that in the study of brain cells, the ability to record extracellular signals is crucial. The development of MEAs based on more functional electrodes is promising both *in vivo* and *in vitro*; however, the present limit shows that the simultaneous recording of voltage changes in a big population of cells by several electrodes without causing damage to the plasma membrane and able to discern the neurons from the glial cells' signals, is still complicated[221,222].

Nonetheless astrocytes are considered electrically silent, although the basis for consistent transmembrane potential discharge is possible. Given the fact that most of these transmembrane ions dynamics occurs in the microdomains, nanostructured electrodes needed to be developed to allow efficient electrical coupling at the nanoscale.

Examples of successful results for neuronal cells recording have been achieved by an intracellular electrode platform of vertical metal-coated silicon nanowires for the intracellular recordings of neurons' activity. The same was obtained with a non-invasive gold-mushroom-shaped microelectrode and the reduction of the signal-to-noise[223,224]. In astrocytes Mestre et al., demonstrated that a similar approach can efficiently record voltage variations in primary non differentiated astrocytes[225-227]. On this basis during my PhD in collaboration with Annalisa Convertino and Luca Maiolo at CNR-IMM, we tested a gold coated silicon nanowire forest to grow astrocytes primary culture and to exploit the possibility to use the platform to record astrocytes. The results are reported in **Chapter IV**.

**Nanoglial Interfaces based on polymeric materials**

Polymers are materials made of long, repeating chains of molecules. The materials have unique properties, depending on the type of molecules being bonded and how they are bonded. Several medical applications have been recognized in polymers. Body proteins are natural polymers and consist of amino acids and the nucleic acids (DNA and RNA) are polymers of nucleotides[228]. In chemistry, the process of combining molecules, called monomers into a chain with different bonds is called polymerization. This term as the word macromolecules, guaranteed the Nobel Prize in Chemistry in 1953 to H. Staudinger, a professor of organic chemistry at the Eidgenössische Technische Hochschule (University of Applied Sciences) in Zurich for the first manipulation of natural and synthetic polymers. The American Chemical Society recognizes him as the "father of modern polymer development". Polymers have several advantages with respect to previous materials[229]. The synthetic ones are easy to use, ready to obtain by fabrication, tunable and low cost. The natural ones have the huge advantage of being biocompatible, biodegradable, reducing the gliotic

reaction and being long term available[230]. Among natural polymers, silk fibroin (SF) obtained by Bombyx mori cocoon, has been deeply investigated by our group, in interfacing with neural cells and glial cells. The versatility of the water SF solution called regenerated silk fibroin (RSF) can be processed in various forms (i.e., films, gels, fibres, porous scaffolds, and sponges) with the possibility to modulate the chemo physical properties (thickness, mechanical properties, time-controlled biodegradation, blending and functionalization) and to modulate its pharmacological and therapeutic properties[231-235]. Interestingly, primary astrocytes and primary neurons show different responses interfacing with SF, depending on the modulation of its quality such as the hydrophobic properties, that seem to contribute to the support of neurons attachment and astrocytes, respect to the neurite outgrowth that increase in hydrophilic conditions. Benfenati et al. was the first investigating on SF films and primary astrocytes' showing their ability to grow up to 3 weeks *in vitro*, without occurrence of any gliotic reaction[264,265]. In addition, the same study demonstrated the delivery of trophic compounds, such as the purine guanosine, which induced a large inward rectifying potassium conductance and parallel increase of Kir4.1 protein channel expression. *In vivo* investigations of SF were obtained by integration of the natural polymer into organic optoelectronic polymeric devices based on P3HT/PCBM[206,236], or as silk fibroin dielectric. Moreover, studies support the idea of the employment of natural polymers, used in bone surgery; more recently in the brain, thanks to the formulations based on Matrigel, hyaluronic acid derivatives, collagenous proteins, polysaccharides, self-assembling peptides proteins and alginates. For example, hyaluronic acid-based hydrogels with different molecular weights or with different peptides (i.e., RGD, YIGSR, IKVAV, and RDG adhesive peptides) respond to pluripotent stem cell-derived neural progenitor (hiPS–NPCs) in terms of spreading and cell attachment[237]. Several works have demonstrated that Collagen, the more diffused ECM protein in the adult nervous system, is a promising element in 3D remodelling brain tissue during regeneration[238,239]. The recent increase in the use of synthetic polymers for thegeneration of scaffolds is due to the complexity of the brain environment from which astrocytes and

other glial cells originate[241]. In particular, in glial science, the astrocytic adhesion, morphology, proliferation, migration, and gene and protein expression lead to the study of new polymers for the fabrication of 3D scaffolds that may fit well with the ECM and that allow being a guide in case of disease, where these features need to be modified and correct by engineering implantable long-term interface. The following new "smart" polymeric interface is first validated as a 2D system *in vitro* before being processed in 3D scaffolds and our lab is focusing on the validation of several materials where synthetic polymers properties such as stiffness, surface topography, porosity, and molecular transport, play important roles in determining the *in vitro* responses of astrocytes to the materials[241]. Current technological approaches for the fabrication of brain biodegradable or non-biodegradable, micro and nano-interfaces are generally based on innovative processes such as electrospinning, nano-emulsion[239]. Among them, FDA approved polymers are: polyesters of lactic and glycolic acid (PLA or PGA) or their co-polymers (PLGA), PLA:PGA, the chemistry of PLGA copolymers seem to improve the transport of therapeutic agents (i.e., antitumor drugs, glial derived neurotrophic factor) across the BBB in the treatment of neurodegenerative diseases[2423,243]. Polymeric synthetic materials can increase the level of expression of the cytoskeletal marker, GFAP, interfacing with astrocytes, we demonstrated that polycaprolactone (PCL) nanofibres, fabricated via electrospinning to mimic the ECM, are able to generate an architecture to regulate proliferation, cell shape, and motility of astrocytes[244,245], without inducing GFAP over-expression. Lau et al. demonstrated as first, that there was a role of random or aligned organisation of PCL fibres on the *in vitro* response of mouse astrocytes, via gene and protein expression studies, confirming the ability of PCL oriented nanofibres to down-regulate GFAP protein expression, while the actin, vinculin and chemokines, neurotrophic factors, antioxidants (glutathione S-transferase $\alpha$1) and the glutamate transporter were upregulated in astrocytes on PCL random nanofibres. Also, the results obtained with PCL electrospun nanofibers are described in the **Chapter IV** of the thesis. Moreover, PCL, as well as other polymers, can be chemically modified during synthesis to include different copolymers with properties suitable for the

CNS, for example with polymethyl methacrylate[246]. Besides, polymers endowed with electrical and conductive properties, (i.e., polythiophenes, polyanilines-PANI, etc.) are designed as smart bio-interfaces supporting neurite regeneration[247-249]. Our previous study about the role of PCL combined or not with natural protein such as gelatin, has been implemented with evidence regarding the copolymerization with PANI nanoneedles embedded in the random and aligned electrospun fibre[247-249]. Results are reported in **Chapter IV**.

Surprising results about no difference in the electrophysiological properties of astrocytes have been obtained, the increasing adhesion and growth properties were confirmed. This conclusion allows us to consider such polymers as a useful platform for neuroregenerative scaffold as well as for the understanding of how astrocytes behave in case of disease where the "signals network" and the cell communication between astrocytes and neurons or other glial cells is compromised.

Soft hydrogels are recently studied as non-biodegradable 3D implant for the brain; Among these polymers, PEG–dimethacrylate (DMA), poly(N, N-dimethylacrylamide) (PDMAA), poly(2-ethyloxazoline) (PEtOx), and poly([2-methacryloyloxy)ethyl] trimethyl ammoniumchlorid) (PMTA) are recognized as biocompatible for brain cells[250-251]. Our lab is now validating, in collaboration with ISTEC of CNR of Faenza a new approach based on the combination of different aspects presented here such as the copolymerization of conductive polymers based on PEDOT:PSS with proteins able to generate soft hydrogels to be useful in tissue regeneration. Our approach is based on interfacing with primary astrocytes *in vitro* and the understanding of morphological rearrangement induced by the 3D scaffold with the cells. Future perspectives will guide to suggest that conductivity of substrate can be an essential factor for differentiation and determination of cell fate in astrocytes in 3D hydrogels, on the base of neuronal differentiation and electrochemical currents mediated by conductive electrically cross-linked polymers substrate[253,254].

**Nanoglial Optical Stimulations**

Light has the potential to be considered a tool for neuromodulation in the brain, the sources to emit light can be differently modulated and can differently target the cells composing the brain. First approaches were obtained using Argon ion laser at a wavelength of 488 nm. Effects induced on tissueand on neurostimulation depend not only on the wavelengths but obviously on other parameters such as distance, time, space and biological targets. All these parameters are very tunable and approach the "Photostimulation" as depending on the request of investigation. Evidence of application of lasers to the study of the glia-neuron network seems to be more suitable for the research application rather than in the therapeutic approach where light techniques are validated in human tissue and therapy, such as the light emission in cancer therapy, the photodynamic therapy[254,255]. One of the major problems is the excessive stimulation of reactive oxygen, which causes tissue damages.Optogenetics, for example, even though used in rodents since 2005, is still lacking relevant results in primates and in humans because it is far from being safe. Generally light therapy (710 nm) in the brain showed neuroprotection in rat experimental stroke models[256]. While the use of low-level light therapy mostly involves red and near-infrared light. Alternatively, low-power light- emitting diodes (LED) using visible light are attractive because LEDs are safe on tissue. Nevertheless, in the application of light therapy, longer red/near infrared wavelengths are better to penetrate tissue than blue/green LED-wavelengths; pulsed infrared (IR) stimulation has been shown to be a clinical alternative to stimulate neural activity, as a label-free technique that does not require genetic manipulation[257]. Low-level laser light (800 nm) improves cognitive deficits and modulates neuroinflammation after traumatic brain injury[258,259]. Additionally, it presents several advantages over electrical stimulation demonstrated in rat sciatic nerve using a free electron laser. The mechanism of IR localised heating by the absorption of light by water molecules guarantee a high spatial precision. Zao et al., shows that an 800-nm near infrared (NIR) femtosecond laser induces $Ca^{2+}$ waves in astrocytes[260].

Our recent study showed for the first time, by means of calcium imaging experiments, the INS application in astrocytes *in vitro*. Using live-cell fluorescence imaging, pharmacology, electrophysiology, and genetic manipulation, we showed that INS can modulate astrocyte function through changes in intracellular $Ca^{2+}$ and water dynamics (Fig. 1.15). Interestingly, we were able to modulate the INS impact on standard *in vitro* systems, as well on nanostructured materials such as the mentioned HTlc, where glial cells resemble an *in vivo*-like phenotype. The hypothesis is to consider the water transport activated through the involvement of $IP_3R$, TRPA1, TRPV4, and AQP4[261]. Moreover, nanostructured organic biomaterials endowed with photoactive propertires based on poly(3-hexylthiophene-2,5-diyl) with phenyl-C61-butyric-acid-methyl ester (rr- P3HT:PCBM) coated with PLL was used to plate primary neurons and astrocytes. Visible light andany applied electric field was used[204,207]. The advent of photostimulation as tool of investigation for the stimulation of astrocytes functional properties has been exploited also in our lab with polythiopene-based interfaces. In collaboration with Dr. Antognazza, we are exploting the structural and functional impact of semiconducting polymer interface based on polythiophene (rr- P3HT-pillars), responsive to visible light and endowed with a particular 3D micro and nano-topography made of pillars on the top surface of the substrate. These studies, whose results are reported in Chapter IV, are based on previous evidence reported by Dr. Antognazza group. They observed that seeded neurons were not negatively affected in their adhesion and growth on the top ofrr-P3HT substrates; however, it was shown a decrease in dendritic arborisation and cell membrane thinning. The rr-P3HT pillars interface has the potential to doubly exploit the nanostructure of the pillars with the conductive and photoactive elements of the materials and become a promettent tool of investigation and application on photomechanical, photochemical, and photoelectrical modulationof cell activity, thus, our though was to investigate them as nano glia photonic interface[262].

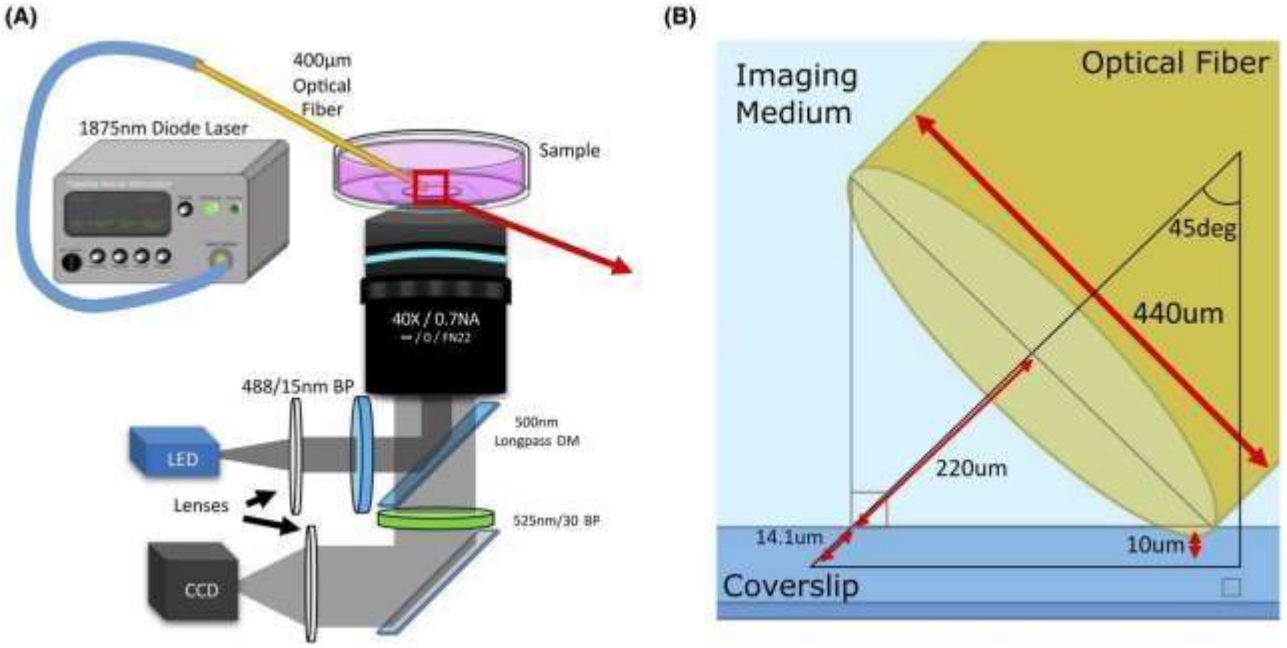


**Fig. 1.15:** Scheme representing two different approaches based on astrocytes photostimulation. A) Panel shows the experimental set-up for stimulation of astrocytes with INS (excitation wavelength source λ=1875 nm), B) Scheme of the fibre placement is in proximity of cells during the performed experiments of electrophysiology or calcium imaging[267].

# Aim of the Thesis

On the Basis of all the studies described above, about the role of astrocytes in the brain, they are definitely players in the physiological activity and the pathology of the brain.

The idea of astrocytes as "glue" in the brain tissue is completely overpassed, and their activity in the complex network of neurons is totally confirmed. Even though the excitability of neurons and the property of firing is still central in the study of several brain dysfunctions, the excitability system based on calcium signalling is still rising as a pioneer of the gliotransmission and diffusion of information. Information passes through temporal and spatial scales according to neurons' action potentials, synapse plasticity process and neurotransmitters[2,6,17]. At the same time, ion channels and water channels might play an unexplored key role in connectivity and cognitive functions. Nonetheless, the design of long term biocompatible implants demands permissive, non gliotic, nanoglial materials interfaces. Taking advantage of the ability of astrocytes to sense and react to extracellular chemophysical stimuli, *in vitro* studies demonstrated the selective ability of these cells to respond to different stimulation protocols (chemical, physical, mechanical, electrical or photonic stimuli).

However, probing glial cells, like astrocytes, needs the integration and the manufacture of specific innovative technologies into electronic devices to discriminate between the different nature of neuronal and astrocytic signalling. In this respect, Dr Benfenati's lab proposes glial engineering, glialinterfaces, and gliophotonics as emerging fields of investigation of the brain[17].

The vision relies on results achieved by a long-lasting work of multidisciplinary and fruitful collaborations. In such exciting and fertilizing environment, we put together the basis for the scope, the experimental design and the implementation of this thesis.

Accordingly, the rationale of the research work beyond my PhD thesis, was to define new insight intothe role of astrocytes in brain function, through the exploration and exploitation of new multifunctional nanoscale materials, interfaces and devices.

In order to characterize the impact of different materials and devices on astrocytes functionality we used *in vitro* primary astrocytes, a validate model where to study astrocytes in a controlled althoughsimplified manner. On these cells we performed experiments combining materials, interfaces and devices with validated protocols, technologies and systems of electrophysiological investigation, suchas the patch-clamp or extracellular recording by micro-electrode-array. The molecular analyses included western blot and immunofluorescence with confocal microscopy, while dynamics of actin or calcium were analyzed with fluorescent microscopy. Specifically, we tested nanostructuredmaterial interfaces made of 1) organic polymers based, electrospun nanofibers made of biopolymers and composites developed in collaboration with Vincenzo Guarino and the group of Prof. Luigi Ambrosio of CNR-IPCB and 2) gold silicon coated nanowires interfaces and devices developed in collaboration with the group of Dr. Annalisa Convertino and Luca Maiolo of CNR-IMM, 3) colloidalhydrotalcites films in collaboration with Dr. Tamara Posati and Roberto Zamboni at CNR-ISOF, 4) gold nano cluster tools tested in collaboration with Dr. P. Shashi Karna of Army Research Laboratory, 5) semiconducting polymer interfaces based on polythiophene in form of nanopillars in collaboration with Dr. Maria Rosa Antognazza at Italian Institute of Technology (Figure 2.1).

Finally,in collaboration with the group of Marco Capini at UNIBO FABIT, Grazia Paola Nicchia of the University of Bary and with the group of Prof Wolfgang Losert, at University of Maryland, we also exploit the use of nanostructured surfaces made of hydrotalcite, to evaluate the dynamics of water, cell volume in differentiated astrocytes and to describe for the first time the dynamics of cytoskeletal actin proteins and their difference in polygonal and differentiated astrocytes. As a mission, the long term goals to which these studies are devoted, is demonstrating the role of astrocytic dynamics in brain function and dysfunction by a novel cross-disciplinary and contaminated approach among Nanoscience and brain Science.

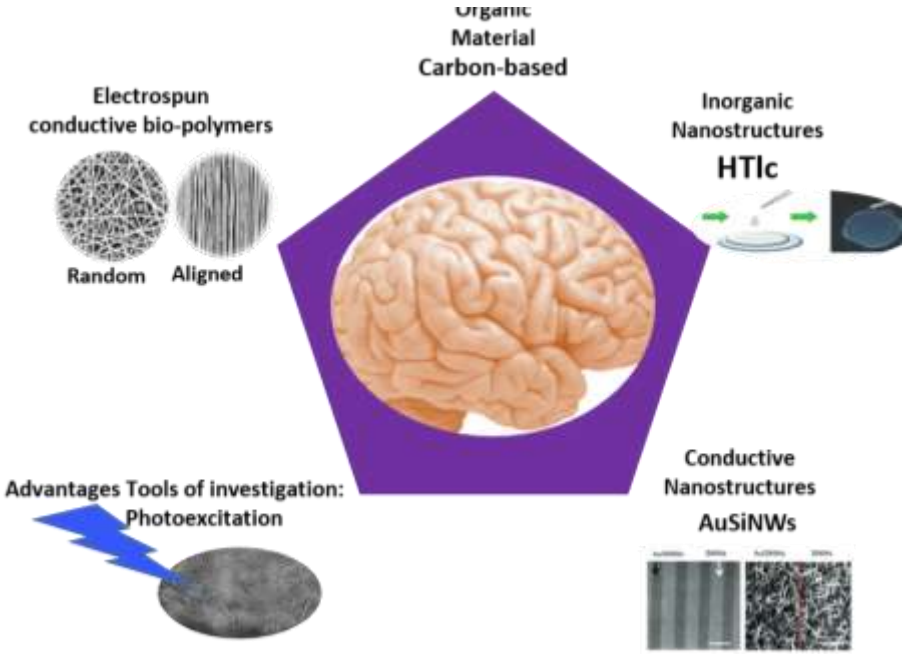


**Fig. 2.1:** A schematic representation of a key new class of interfaces here reported and enabling the investigation on astrocyte properties (created by Office PowerPoint®).

# Experimental Section

## Astroglial cells preparation, maintenance and plating

Primary astroglial cultures were prepared at the Department of Pharmacy and Biotechnology of the University of Bologna, in agreement with the Italian and European law of protection of laboratory animalsand the approval of the local ethical committee for animal experimentation (ethical Italian protocol numberID 1338/2020 PR, valid for 5 years). Every effort was taken to reduce the number of animals and their suffering. The procedure for astrocytes preparation is, briefly, reported in this paragraph and in the experimental section of each paper presented in **Chapter IV**. Neonatal rats p0-p2 (Sprague Dawley) were sacrificed to avoid the astrocytes cell culture preparations. Astrocytes culture were prepared from the most superficial layer of both cortical hemispheres and transferred into 1/2 ml of tissue culture medium containing 15% FBS (Table 1, media composition). The final step consisted of transferring the tissue cortex into a 25 $cm^2$ tissue culture flask and incubating at 37°C, 5% $CO_2$. Two days after preparation, the medium was carefully changed to remove the debris from preparation. Into two days from the cells preparation, the debris from cells preparation was eliminated by rinsing astrocytes flasks with pure Dulbecco's Modified Eagle Medium (DMEM). The "washing", accompanied by shaking the flasks, were repeated every two days to remove debris and undesired cell types. Reaching the confluence, astrocytes were maintained in culture medium containing 10% FBS; 2 weeks later astrocytes can be re-plated a (at specific concentration) onto the respective substrates, the re-plating of astrocytes is mediated by enzymatical dispersion with 0.25% trypsine-EDTA to detach cells from the flask[17,61,62,88,91,92,93].

| | **15 % FBS** | **10 % FBS** |
|---|---|---|
| **DMEM** | 84 ml | 89, 5 ml |
| **FBS** | 15 ml | 10 ml |
| **PenStrep* 1%** *penicillin-streptomycin (100U/mL and 100 mg/ml respectively) | 1 ml | 0, 5 ml |

**Table 4.1:** Composition of the 15% FBS media preparation and 10% FBS media maintenance of primary astrocytes. Values are reported for 100 ml total of media solutions.

**Biocompatibility Assays**

*Fluorescein diacetate assay*

The Fluorescein diacetate (FDA) Assay was used as the first approach to test the cell viability. FDA is a non-fluorescent fluorescein analogue, that could be hydrolysed to a fluorescent fluorescein analogue in living cells, by the enzyme activity of a cellular esterase. The enzyme works by cleaving off the acetate groups when the molecule is incubated with living cells. The preparation of the stock solution (5 mg/ml) consists of a stock solution diluted in acetone, secondary 3.3 µl of the stock solution was diluted in 1 ml ofphosphate buffered saline (PBS, Invitrogen). After 5 min at room temperature (RT), the cells seeded on thesubstrates and devices were washed with PBS and they could be observed by fluorescence or confocal microscopy (Nikon eclipse 80i fluorescence inverted microscope equipped with a 20X or 40X air magnification, Nikon TE 2000 inverted confocal microscope equipped with a 40X magnification and a 400nm diode, 488 nm Ar+ and 543 nm He–Ne lasers as exciting sources, Crisel Instruments- Olympus BX-63confocal time-lapse microscope equipped with a 40X, 60 X immersion and 100X oil magnification and 6 LED (390, 440, 475, 510, 555, 575 nm) e 2 NIR lasers (637, 748 nm) exciting sources). Living cells were counted by Imagej software and the number of cells/area was calculated at desired time points. ProLong Diamond Antifade Mounting (DAPI) blue staining was usually used in order to stain the cells' nuclei[201,88,225,234,248,249].

*Alamar blue Assay*

Astrocytes viability on different substrates and interfaces was analysed via Alamar Blue Assay (AB, Life Technologies), according to the Interchim technical sheet (66941P) and protocols in a microplate reader, (Thermo Scientifict Varioskan Flash Multimode Reader). AB Assay provides a time course of astrocytic viability by quantitatively measuring the cell number and the proliferation rate of living cells on the substrates per time. The proliferation rate was calculated as the increase in fluorescence, which is proportional to the number of cells and it was expressed as a percentage. Besides, AB Assay relies on the enzymatic activity related to aerobic cells respiration and REDOX reaction in the cytoplasm of living cells, given also information on the cell metabolism activity. Data were collected at least from three separate

experiments performed in triplicate and are expressed as means ±SE of the percentage of reduced[225,234,248,249,252].

**Morphological characterization of astroglial cells**

*Image processing and analysis*

The evaluation of the morphology of astrocytes, grown on different substrates, was performed by FDA analysis usually after 1 day *in vitro* (1 div), (3/4 div), (7 div) from the re-plating of cells seeded on different substrates. Data were collected at least from three separate experiments. A sequence of images (10 to 15 different fields for each sample) was taken using fluorescent or confocal microscopy. Images were analysedby ImageJ software. The morphological criterion, used to measure the cell differentiation, induced by growth of astrocytes on different substrates and interface, consists in: distinguishing between elongated andstar-like astrocytes or polygonal undifferentiated astrocytes. The differentiation of cells can be defined as "elongation" when the vertical Y axis for each cell was at least two times longer than the horizontal X axis,and "star-like" when a cell displays more than 2 branches[88]. Data are reported as means ±SE.

**Characterization of molecular properties of astrocytes**

*Immunostaining for fluorescence and confocal microscopy*

To perform immunofluorescence and confocal microscopy, cultured astrocytes plated on coverslips, substrates and films were fixed in 4% paraformaldehyde (PFA), washed in phosphate buffered saline (PBS); the nonspecificsites were blocked with 3% Bovine Serum Albumine (BSA) in PBS and permeabilized with 0.3% Triton X-100in PBS. After the blocking of nonspecific sites with BSA, cells were incubated with primary antibodies for 2h at RT, washed in PBS and incubated for 1h at RT with Alexa conjugated secondary antibodies. Finally, sampleswere mounted on slides, using ProLong Diamond Antifade Mounting with DAPI or the mounting medium (50%Glycerol, 0.01% N-Propil-Gallate in PBS) and images were taken. Primary antibodies used were: mouse anti- GFAP (Sigma Aldrich, Milan, Italy, dilution 1:300 in 3%BSA and 0.1% Triton X-100 in PBS) rabbit anti-Kir 4.1 (Alomone, Jerusalem, Israel, dilution 1:300), goat anti-AQP4

polyclonal (Santa Cruz Biotechnology, Santa Cruz, CA, dilution 1:200) and rabbit anti-Vinculin (Life Technologies, Monza, Italy, dilution 1:200). To stain F-actin fi-actinng ATTO 647N-Phalloidin (Fluka Analytical, St Louis, MO, dilution 1:200) and Phalloidin-FITC (Sigma Aldrich, Milan, Italy, dilution 1:200) were used. The common used secondary antibodies were: donkey anti-mouse CY3 (Jackson Labs), Alexa488-conjugated donkey anti-rabbit or goat anti-mouse and Alexa594-conjugated donkey anti-goat (Molecular Probes, Eugene, OR) at a dilution of $1{:}1000^{88,92,225,234,248,249}$.

**Monitoring of Actin dynamics**

*Transduction of cells with actin- Cell Light*

To visualise actin dynamics, astrocytes were transduced with CellLight Actin-GFP, BacMam 2.0 (ThermoFisher Scientific, MA, USA) at a concentration of 100 particles per cell. At 48h prior to live imaging, 5-10 µL (depending on the plating cells density) of the reagent was added to the cell culture media. A full media change was performed 16-20h after transduction, and imaging was performed 24h after the full media change. Transduced astrocytes were identified by a positive signal in the 488 laser channel of confocal imaging. A consistent z-plane was assured with Perfect Focus (Nikon PFS). Live imaging timelapses were acquired at the University of Maryland CMNS Imaging Core using a PerkinElmer spinningdisk confocal microscope with an oil immersion 40X objective (1.30 NA; 0.36 µm/pixel) and temperature and humidity control. The microscope was equipped with a Hamamatsu ImagEM X2 EM-CCD camera (C9100-23B), which recorded 16-bit images. Data acquisition was performed with Perkin Elmer's Volocitysoftware (version 6.4.0).

**Synthesis fabrication and functional characterization of smart glial engineering and interfaces**

This thesis reports a review on engineered technologies and innovative tools based on biomaterial interfacesand devices able to induce a response in astrocytes. It is highlighted that, while I have been performing every single experiment related to the characterization, all the process of synthesis preparation and characterization of the materials and substres were performed by respective partners as indicated below.

Stable polymers such as polycaprolactone (PCL) have been used successful in form of PCL nanofibers, obtained through electrospinning at CNR-IPCB in the group of Prof Ambrosio, by Dr Vincenzo Guarino and Anna Boriello. The idea to use electrospinning as a method of fibres' preparation was to mimic the specific extracellular matrix (ECM) of the brain to obtain a fibrous architecture of the substrates that can promote astrocytes' cytoskeleton rearrangement. All the experiments were performed at natural

environmental conditions (T = 18/21 °C, RH = 40–50%). In collaboration with Prof. Luigi Ambrosio and Dr. Vincenzo Guarino of IPCB-CNR electrospun fibres were processed by Poly-Ɛ-caprolactone (PCL, Mn45 kDa), bovine gelatin type B (Gel, ~225 bloom) in powder form, chloroform (CHCl3, 0.33 g/ml) and 1,1,1, 3, 3, 3, hexafluoro-2-propanol (HFP), (Sigma Aldrich, Italy), moreover PCL/Gelatin solution was obtained by dissolving PCL and Gelatin separately in HFP for 24 h to obtain the final polymer concentration of 0.1 g/ml (polymers ratio 1:1). Electrospun fibres were processed using commercialised electrospinning equipment (Nanon01 Mecc, Japan) optimised for the fibres deposition by vertical configuration. All the parameters (i.e., flow rate, voltage, electrodes distances, rotation speed) have been optimised; morphological analysis, fibres' mean diameter was calculated, fibres anisotropy and the spatial organisation of fibres, wettability are reported in the section of **Chapter IV** dedicated to PCL[248]. Moreover, the last decade focused on the use of biocompatible polymers with electrically conductive properties, which can promote cell adhesion. In this context, the use of electroactive polymers (EAPs) is emerging as a class of organic materials with intrinsic conductive properties and with different applicative uses (i.e., molecular targeting, biosensors, biocompatible scaffolds). The electrically conductive nanocomposite platforms havebeen investigated in this thesis as a promising platform potentially applied to stimulate and record astrocytesfor the recovery of neuronal structure and function. For this purpose, by embedding electro conductive PANi into electrospun fibres, PCL-based substrates with Gelatin and Polyaniline (in form of nano-needles) have been fabricated as it follows[248] in IPCB-CNR labs. For the synthesis of PnNs, aniline, ammonium peroxydisulfate (APS), camphor sulphonic acid (CSA), and emeraldine base polyaniline (EB, Mw 10 kDa),(Sigma Aldrich, Italy) were used. The morphology of the PnNs, the mean diameter of the fibres and fibrescharacterization have been analysed and reported in a dedicated section of **Chapter IV**[248]. As control, electrospun fibres without PnNs were fabricated under the same processing conditions.

*Electrospinning technique*

Polymeric materials are dissolved in a suitable solvent to become a solution that is placed in a syringe pump. An electrostatic repulsion forced by the application of charges of the same sign on the surface where

thedrops of polymers will be delivered. When these forces are such as to overcome the tension surface of the drop, a polymer jet is formed, due to the electric field. The jet is stretched and it allows the formation of thenanostructures. (Fig. 4.1).

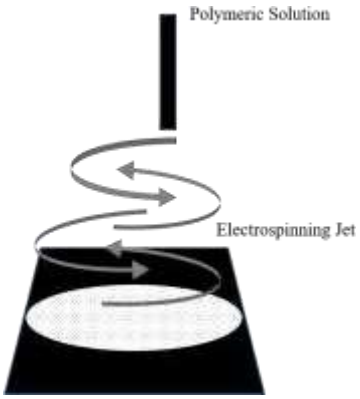


**Fig.4.1:** Scheme of the electrospinning technique (created by Office PowerPoint ®).

Silicon Nanowires (AuSiNWs) covered by gold represent a class of interface were produced by plasma enhanced chemical vapour deposition in collaboration with Dr. Annalisa Convertino and Dr. Luca Maiolo,from CNR-IMM in Rome. Technical details and the characterization of the substrates are reported in a dedicated section of **Chapter IV**.

*Vapor-liquid-solid (VLS) mechanism of nanowires growth.*

The following mechanism of nanowires growth occurs when an alloy droplet, formed from a solid substrate and metal catalyst, becomes supersaturated with a material coming from a gaseous reactant. As a second step, the material precipitates (from the solid-liquid interface) to form a nanowire. The liquid droplet must be stable and form an alloy or a eutectic mix at the right pressure and temperature. One of the downsides to this technique is that the metal catalyst dopes and creates impurities throughout the nanowire. In the caseof Au, the eutectic temperature (the lowest temperature before solidifying) is at 363˚C degrees.

*The Plasma-Enhanced Chemical Vapour Deposition (PECVD)*

PECVD is a variant of conventional CVD, in which the deposition process is not governed by the thermodynamic characteristics but by the kinetic ones. In fact, the dissociation reactions of the gaseous precursors are induced by electrical excitation within a plasma. Plasma is a rarefied gas of ionised

moleculesand atoms, electrons and neutral species that emits a characteristic discharge, plasma is made up of both positive and negative ions and overall it is neutral. It can be generated in different ways depending on the type of apparatus, in our case by means of an electrical signal alternating in radio frequency (RF) between two electrodes. In fact, this signal is able, under low-pressure conditions, to make the electrons acquire sufficient energy to trigger ionisation and dissociation processes of the gases present, with the formation ofhighly reactive radicals. The substrate is positioned on the positive electrode (anode) and when the radicalsreach it by diffusion they react with the catalyst. The growth continues as long as the radiofrequency signalon the negative electrode (cathode) is finished[225].

The implementation of inorganic nanostructures, such as*Hydrotalcite-like compounds (HTlc) synthesis and films preparation* HTlc substrates were formulated, synthesised by Dr. Tamara Posati, CNR-ISOF as described previously. The drop casting technique consists in depositing a drop of solution on a substrate. Then, the evaporation of the solvent used and the film densification are expected. This process is easy to carry out and does not require specific instrumentation. However, drop casting cannot be applied to large surfaces. It is hardly possible to obtain homogeneous and reproducible films[88,92] (Fig. 4.2).

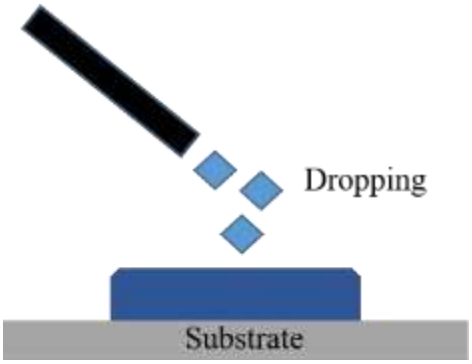


**Fig. 4.2:** Scheme of the drop casting solution on substrate (created by Office PowerPoint ®).

*Gold Nanocluster Preparation and Characterization*

fAuNCs solutions were prepared according to the ARL Laboratory of Aberdeen of Prof. S. P. Karna: 0,004 g of gold salt clusters were dispersed in PBS and dissolve after 30-60 sec. of sonication in 10% cell media, in order to obtain [1mM] solution. The same procedure was used to prepare [1mM] fAuNCs solution with any amount of BSA-blended. Cells were treated with the following solutions after 1 div from the re-plating; they were left for 24h of treatment in incubator 37°C and 5% of $CO_2$, later rinsed with PBS before performing single experiments.

*rr-P3HT pillars Preparation and Characterization*

rr-P3HT nanopillars have been processed by IIT according to the following protocol. Rr-P3HT (purity 99.995%, molecular weight 15000−45000), were purchased from Sigma Aldrich. PDMS elastomer (Sylgard184) was purchased from DowCorning. Glass/ITO substrates (15 Ω/sq) were purchased from Xin Yan Technology. PDMS precursor was mixed with the curing agent (10:1volume ratio) and left in vacuum for 30 min in order to remove air bubbles formed during the mixing process. P3HT was dissolved in o- dichlorobenzene (20 g L−1) and stirred for one night at 50 °C. A 1 μL drop of the rr-P3HT solution was pushed onto the cleaned glass/ITO surface using the micropatterned PDMS mold. After a thermal treatmentat 90 °C for 2 min, the mold was gently removed ending up with a 4 × 5 mm2 rr-P3HT pillar array surrounded by a flat rr-P3HT region deposited on top of glass/ITO substrates. Flat Glass/ITO/P3HT were prepared by spincoating and used as control for studying the structural and functional impact of astrocytes with the nanosized polymer pillars[262] (Fig. 4.3).

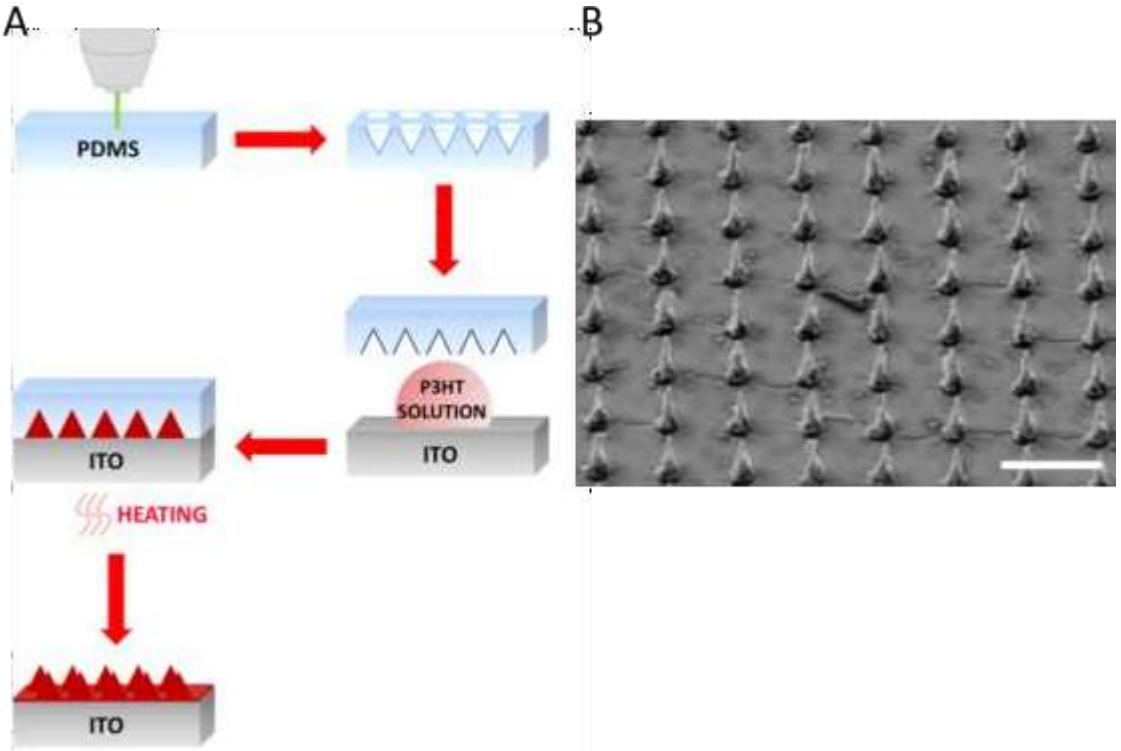

**Fig. 4.3:** Device fabrication and morphology. A) rr-P3HT micropillar fabrication process. B) SEM- Photograph of the rr-P3HT-pillar-based device, taken at the end of the fabrication process. Scale bar: 10 μm. Permission from: Copyright © 2019 American Chemical Society. Readapted from[262].

**Analysis of the Functional properties of brain cells:**

*Electrophysiology: The Patch Clamp Technique*

The origin of the patch clamp can be found in the 1660s, when Dutch and Swammerdam prepared a neuromuscular dissection from a frog leg. The aim was to stimulate the frog's nerve and observe what a trigger could cause in the muscle contraction. After the first successful results, they perfected the preliminary preparation, by attaching needles to each of the muscles to analyse, in order to monitor the muscle contraction. Slowly, Swammerdam started to understand the nature of signal propagation between nerves, but it was Isaac Newton, who first mentioned the electrical nature of nerve signals.The story of ionchannels, which are the main protagonist of the bioelectrical activity and properties studied in this thesis began in 1791, when Luigi Galvani published his fundamental work: "*De Viribus Electricitatis in Motu Musculari Commentarius on animal electricity*" as accurate work of 10 years of observations on contractionof isolated frog nerve–muscle preparations, which Galvani performed with his wife, Lucia Galeazzi, and his nephew, Giovanni Aldini. Galvani's prophecy allows the identification of the electrical excitation of thenerve–muscle preparation and the relationship between stimulus intensity and muscle contraction. He also described the refractory phenomenon due to the contractions, which can be restored after a period of rest. Itwas only in 1797 that Galvani settled the crucial experiment to demonstrate the action potential propagationand developed *the theory of electrical excitation*. Aldini, after the death of Galvani in 1798, continued to investigate animal electricity. He was the first to apply electrical currents to a mammalian brain. However,in the XIX century, the spread of "Galvanism theory" was so intensive in the word that it inspired, in 1817,writers such as Mary Shelly with "Frankenstein, or the Modern Prometheus"; the novel, addressed for the first time, the problem of the ethical responsibility of a scientist.In the development of the *theory of electrical excitation*, Matteucci succeeded Aldini, he measured the resting current between the intact and cut surface of a muscle, and only later Emile du Bois-Reymond was able to measure the electrical events accompanying the excitation of nerve and muscle. In 1850–1852, Hermann von Helmholtz was able to determine the delay between electrical stimulation of the nerve and muscle contraction. Finally, Bernstein made the first true recordings of resting and action

potentials, estimating that at rest, the nerve interior is about 60 Mv. In 1896, he applied the electrolytic theory of Walther Nernst to a biological system and he raised the theory of $K^+$ selectivity through the "*lipoidal membrane*" model of the plasmalemma. The bilayerstructure of the cellular membrane was confirmed in 1925 by Gorter and Grendel. This theory was further developed by Danielli and Dawson who introduced the concept of the "bilayer lipid membrane" including numerous proteins (i.e. ion channels). In 1939, Kenneth Cole and Howard Curtis performed the first impedance measurements, Cole and Curtis and Alan Hodgkin and Andrew Huxley developed the idea of anintracellular electrode, which could be inserted into the axon of a neuron. They were pioneers of the first direct recordings of action potentials. In 1949, the *voltage-clamp technique* was designed by Cole and Marmont, and almost immediately, employed by Hodgkin and Huxley to produce the ionic theory of *membrane excitation*. However, several problems arose such as the fact that excitation required recordingsnot only from axons; the need to control both the extra- and intracellular environments to precisely separatesingle ion currents and the understanding of the mechanisms of ion regulation. All these technical challengeswere analysed and solved by several groups of dedicated electrophysiologists that contributed to the development of the patch-clamp technique, here will be mentioned the most important novelties: the introduction of microelectrodes pulled from glass pipettes, suitable for low-traumatising penetrations of individual cells, developed in 1949 by Gilbert Ling and Ralf Gerard. In 1969, Erwin Neher and Hans DieterLux developed a conceptually similar technique to monitor membrane currents by pulling micropipettes toobtain an opening of about 100–150 μm in diameter; they applied a gentle suction (2–10 mmHg) which helped the approach to the neuronal membrane in the ganglia (normally covered by glial cells) and improvedthe interaction with the intracellular part of the membrane. In 1961 Peter Baker, Alan Hodgkin and Trevor Shaw introduced the double perfusion of intracellular and extracellular space. Even, the important progressand magnificent evolution in the patch-clamp history, all these techniques suffered from a *leakage*

*resistance* between the membrane surface and the recording pipette, which caused low-noise recordings. Ina single cell, the difficulty was to detect single-channel currents in the presence of background electrical noise. Neher and Sakmann pressing a smooth electrode tip on the surface of an isolated skeletal muscle fibre, were able to isolate a patch of the cell membrane and to record a signal with an intrinsic noise decrease. The lower noise levels allow recording picoampere (pA) currents flowing through single ion channels. The discovery of the1980 was called high resistance (giga-ohm) seal: *the giga-seal,* (cell-attached configuration). Actually, the patch-clamp technique exploits the same principle: all ions pass through this membrane patch flow into the pipette and can be recorded by a chlorinated silver electrode connected to anelectronic amplifier, while a grounded bath electrode is used to set the zero level. Thanks to this basilar mechanism, the complex biophysical properties of different ion channels can be studied deeper thanks to patch clamp setup (Fig. 4.4). However, a major limitation is due to the recording of single cells, neither suitable for high-throughput screening nor in more complex brain networks of neurons and glial cells. Thehistorical events of patch clamp discovery have been reported in this thesis because I found really fascinating the story of the evolution of this technique. Although, the invention of the patch clamp techniquehas been motivated by the desire to understand the function of the electrically excitable nerve and muscle cells. In 1982 the technique born for muscles and nerves was applied also to record single-ion-channel currents from non-excitable cells (not firing pancreatic acinar cells). In conclusion, this big invention in 1991 revealed its importance to the world with the Nobel Prize won by Neher and Sakmann.

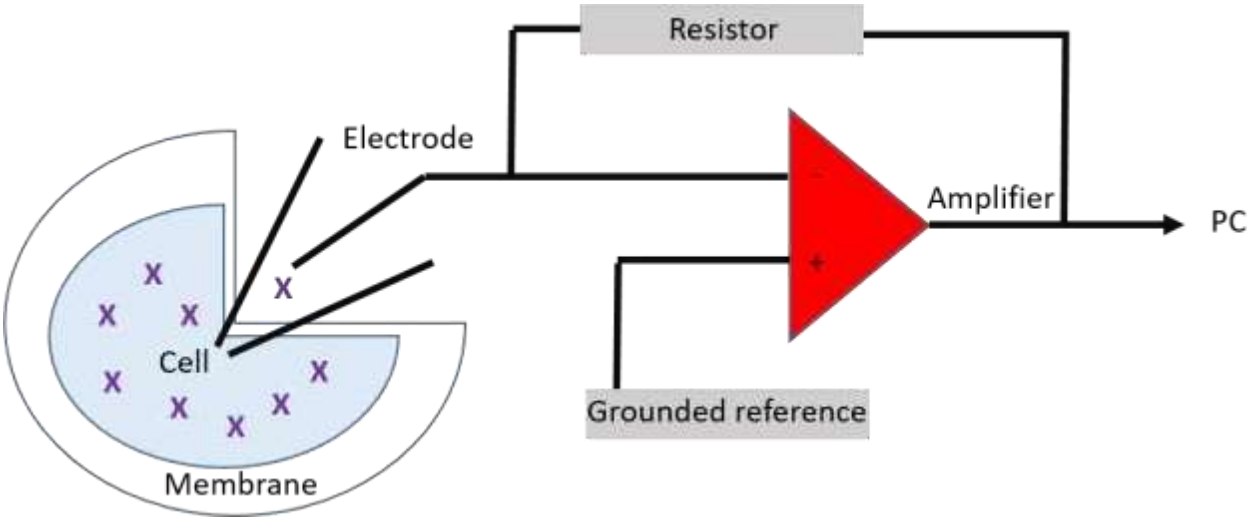


**Fig. 4.4:** Patch Clamp setup: electrical circuit exemplification (created by Office PowerPoint ®).

The electrophysiological experiments of single cell patch clamp, presented in this thesis, were performed following the voltage clamp mode, whole-cell configuration, after 24-72 h after cells re-plating; time depended on the relative experiment and by the substrates to be tested with the seeded primary cortical astrocytes. All the experiments were performed in the same setup at ISOF, CNR Bologna, equipped with aNikon Eclipse Ti-S microscope at RT using patch pipettes (2-4 M tip-resistance) pulled from thin-walled borosilicate glass capillaries. Responses were amplified (Multiclamp 700B, Axon Instruments), digitized (Digidata 1440A, Axon Instruments), (Fig. 4.5).

Capacitive transients were compensated by the nulling circuit of the recording amplifier. Because of the large current amplitude, the access resistance (below 10 MΩ) was corrected 70-90%.

**Fig. 4.5:** Patch Clamp setup located in the Faraday cage and settled at the CNR of Bologna where all the functional experiments have been performed. All the components needed for the electrophysiological recording are equipped.

Analysis was performed off-line using pClamp 10 (Axon Instruments) and Origin 10 (OriginLab Corporation). Passive properties of astrocytes were calculated as shown below[263](see paragraph 9. StatisticalAnalysis). Moreover, according to the concept of "Gliophotonic" defined by Dr Benfenati and implemented in the ASTROTECH Project Team, Maiolo et al., explores the role of light photo-stimulation as a tool of neuromodulation coupled with electrophysiology recording. Generally, optical tools can provide precise, fast, label-free control of ions, and water dynamicsto study the cellular and molecular mechanisms of astrocytes function and to potentially treat dysfunction. In particular, we define a protocol, never explored before, of pulsed infrared light on astrocytes to understand the mechanisms by which astrocytes may be modulated. Laser light emitted from a fiber can be coupled to an inverted epifluorescence microscope and attached to a micromanipulator (Sutter Inc), close to the plated cells[62]. Similar approaches are actually under investigations and aim to define new optical label-free tools able to stimulate glial cells (Fig. 4.6).

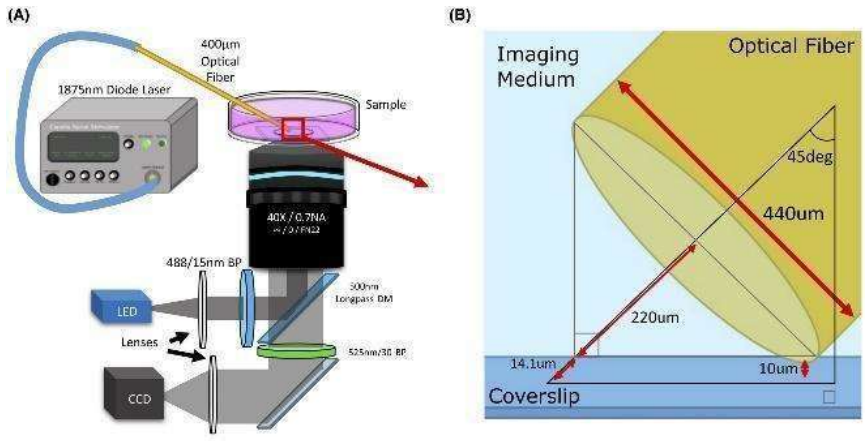


**Fig.4.6:** Scheme representing astrocytes photostimulation by means of pulsed infrared light (INS) to stimulate calcium imaging in cultured astrocytes. The experimental setup is setted to be performed togheter with an electrophysiological record. A) Panel shows the experimental set-up for stimulation of astrocytes with INS light by means of an optical fiber. B) Panel shows the fibre placement in proximity of cells during theexperiments. Light photostimulation can be delivered according to a specific protocol to astrocytes by application of fixed or pulsed LED illumination mediated by a source to the inverted microscope[62]. Permission from: © 2020 Federation of American Societies for Experimental Biology.

**Calcium Imaging**

*Calcium microfluorimetry*

The variation in free intracellular and extracellular calcium concentration ([$Ca^{2+}$ ]i/e) was monitored by calcium microfluorimetry using the indicator Fluo4-AM or X-RHOD 1 AM (Life Technologies, Milan, Italy), respectively in green or red single-wavelength fluorescent for $Ca^{2+}$dynamics. The protocol allowingthe $Ca^{2+}$ dynamics measurements was provided by the plating of a high number of astrocytes seeded on PDL or different substrates or pre-treated with specific treatment. Cells were loaded with 10 μM Fluo-4 AM/X-RHOD, dissolved in standard bath solution for 30 min to 45 min at room temperature (RT). Sampleswere next rinsed with standard bath solution. Measurements of [$Ca^{2+}$] were performed by using a fluorescence microscope (Crisel Instruments- Olympus BX-63 confocal time lapse) equipped with long- distance dry objective (40X) and appropriate filters. The excitation/emission of $Ca^{2+}$ bound form wavelengthwas 494/506 nm and 580/602 nm with a light pulse duration of 200 ms and a sampling rate of 1.5 Hz. Dataacquisition was controlled by MetaMorph software[62,92].

Solutions and chemicals

All saline solutions for patch-clamp experiments were prepared with salts of the highest purity grade (Sigma-Aldrich) and deionized and sterilised water. pH-adjustments were obtained with the respective acid or base, the osmolarity as well was adjusted by adding mannitol (Sigma-Aldrich). Solution composition are here reported:

1) Standard solution for astrocytes

NaCl 140 mM

MgCl2 2 mM

KCl 4 mM

CaCl2 2 mM

HEPES 10 mM

Glucose 5 mM

Mannitol 20mM

pH 7.4 with 1N NaOH, osmolarity~315 mOsm

2) Internal Standard solution for astrocytes

KCl 144 mM

MgCl2 2 mM

EGTA 5 mM

HEPES 10 mM

pH 7.2 with 1N KOH, osmolarity~295 mOsm

3) External Cesium standard solution for astrocytes

CsCl 140 mM

MgCl2 2 mM

CaCl2 2 mM

TES 10 mM

Glucose 5 mM

pH 7.4 with 1N CsOH, osmolarity~315 mOsm

4) Internal CsCl-solution for astrocytes

CsCl 126 mM

MgCl2 2 mM

EGTA 1 mM

TES 10 mM

pH 7.2 with 1N CsOH, osmolarity~295 mOsm

5) Internal CsGluconate solution for astrocytes

CsCl 22 mM

CaCl2 2 mM

MgCl2 2 mM

TES 10 mM

Glucose 5 mM

Gluconic acid 100 mM

pH 7.2 with 1N CsOH, osmolarity~295 mOsm

6) High $K^+$ [40-100 mm] solution for astrocytes

106 NaCl mM

40 KCl mM

2 $MgCl_2$ mM

2 $CaCl_2$ mM

10 HEPES

5 glucose

pH 7.4 with 1N NaOH, osmolarity 315 mOsm

The $Ca^{2+}$ free extracellular saline was prepared by omitting $CaCl_2$ salt and adding a calcium-chelating agent (EGTA 0.5 mM). The hypotonic saline (260 mOsm) was prepared without adding mannitol.

The different salines containing pharmacological agents were applied with a gravity-driven, local perfusion system at a flow rate of ≈200 μL min−1 positioned within ≈100 μm of the recorded cell [62,88,92,93,221,225,234,248,249].

Statistical Analysis

1) Analyses and statistics were performed with Imagej, Clampfit 10, Origin 8.5.1 programs to perform morphological and molecular imaging characterization, electrophysiology and calcium imaging analysis.

2) Calculation of astrocytic electrophysiological passive properties was obtained as follow a) the cell capacitance, b) resting membrane potential, c) reversal potential, d) maximal current density e) specific conductance (SG), f) input resistance (IR):

a) The *capacitance* of the cell membrane is proportional to the surface area of about 1µF/cm[264].The value of cell capacitance was taken directly before recording, using the cell capacitance compensation of the Multiclamp program of amplifiers.

b) The *resting membrane potential* (at 0 current potential) is calculated by setting the current in the amplifier value to zero.

c) *The reversal potential* was obtained by plotting the current vs the set voltage in the recorded ramp current trace.

d) *The maximal current density* (I *max*) was calculated by normalising the obtained current value (I) at a specific voltage (for the inward current density -120 mV, for the outward current density +60 mV) for the cell capacitance, (Cp): Imax = I/ Cp

e) *The specific conductance* (SG) was obtained from the reciprocal of the input resistance (IR), normalised by the cell capacitance (Cp):

$$SG = (1/IR) * Cp$$

f) *The input resistance* (IR) was obtained from recorded current traces, where the given stimulation was a voltage step (ΔV, from $V_H$= -60 mV to -120 mV for astrocytes). The change in current (ΔI) was then used to calculate the input resistance:

$$IR = \Delta V/\Delta I$$

3) In the calcium imaging experiments, the ratio of the fluorescence intensity at each time point (Ft) and the initial fluorescence (Ft0), that directly correlates with variation in $[Ca^{2+}]I$[265] was continuously recorded during the experiment. The percentage (%) of inhibition of fluorescence was calculated as follows [(Ftcontrol/Ft0control-Ftblocker/Ft0blocker)/Ftcontrol/Ft0control]x100, where Ftcontrol/Ft0control was the fluorescence ratio Ft/Ft0 recorded at the end of stimulation and 50 s after the end of the stimulation

when we used standard bath solution containing $Ca^{2+}$. Data were compared by one-way ANOVA with Bonferroni post-test. A statistically significant difference was reported if $p \leq 0.05$. The data was derived from at least 3 independent experiments performed at least in triplicate. Dataare reported as the mean _ Standard Error (SE).

*Note: Every modification to materials and methods with respect to the standard protocols, applied in the performed experiments, are discussed in **Chapter IV** and **Chapter V** dedicated to the presentation and discussion of the Results of each topic of this PhD thesis.

# Results

This chapter is dedicated to a collection (*papers' review*) of the paper related to the main focus of this PhDthesis, selected among those published, on the basis of major contributions I gave and alliance with the scope of the PhD program.

The papers' review reports the journal publications in PDF format, following both the chronological order of publication and the flow of the evolution of our studies.

Each paragraph is dedicated to a single paper and it will be introduced by a brief description of the aim of every single work.

The editor's policy has been verified for each journal where papers have been published and that are here reported; the guideline for publication follows the rules indicated in the database: SHERPA/ROMEO (http://www.sherpa.ac.uk/romeo/), as suggested by the ALMAMATER-University of Bologna for the final submission of "PhD thesis".

In this thesis results are reported on nanomaterials that i) provide advance in knowledge on mechanisms beyond the whole brain function and especially by providing new discoveries on astrocytes ii) provided a nanoscale interaction with astrocytes able to be used as topographical nanostructure for the design of braindevice iii) contribute to unraveling the astrocytes-neurons communication. To this end, nanoscale materialsare tested with astrocytes to understand first their impact on astrocytes viability and growth and mainly to address their impact on astrocytes' structure and function. The vision is to demonstrate the potential of astrocytes as a "dynamic system", overthrowing the idea of astrocytes as silent cells. Moreover, the conceptof astrocytes as a "dynamic system" has been exploited by demonstrating specific active regions, where astrocytes show active oscillations and generate a "natural rhythm". In this context, our lab is a pioneer of studying the interaction of astrocytes with inorganic nanostructures made of clay and named Hydrotalcite-like compounds. Specific chemical aspects of the material, build of positively charged layers and exchangeable interlayer anions allow the adhesion of astrocytes and their morphological differentiation byinducing cytoskeleton rearrangement, as large inward conductance with biophysical features of Kir4.1 and AQP4[88]. Based on the previous observations, we explored the functional relationship at microdomain levelof differentiated HTlc-astrocytes between AQP4 and calcium and chloride channels. The biophysical properties have been chronically investigated impacting on the extracellular environment with hypotonic alteration. Data confirmed the up- regulation of AQP4 expression in the membrane of differentiated astrocytes and showed an intracellular calcium response, typically mediated by TRPV4, as well as an activation of VRAC current as a consequence of hypotonic application. Our data allow us to observe that differentiated astrocytes might respond to osmotic changes, and guide the RVD and RVI process. However,the overexpression of AQP4 channels in astrocytes responds to cell volume changes and restorative effectsand it is tangible in the cell membrane of astrocytes on the contrary of TRPV4 and VRAC expression[92]. These findings are also confirmed by the implementation of other inorganic nanostructures based on silicon

nanowire. Recently, our lab demonstrated the efficacy of gold-coated silicon nanowire devices (Au/SiNWs)in recording extracellular currents from primary astrocytes *in vitro*. The signal detected has an amplitude from 17 to 132 μV and duration from 60 to 730 ms with an interval between two distinct events occurring in a range from 0.2 to 26s. Details will be explained better in a dedicated section of this thesis[225]. AuSiNWswere first fabricated as an interface, once they were tested, AuSiNWs device -MEA, were fabricated in collaboration with Dr. A. Convertino and Dr. L. Maiolo of Institute for Microelectronic and MicrosystemsIMM, CNR of Rome. The goal was to record the extracellular activity of such "silent" cells with respect toneurons. Results demonstrate that the random distribution of nanowires influence the astrocytes morphologyand adhesion; nanowires induce an *in vivo*-like differentiation of the cell body without the need of any biochemical functionalization of the surface. Accordingly, the obtained astrocytes phenotype on thenanowires was more hyperpolarized and displayed a higher resting permeability and capacitance, as well asincreased expression and function of the potassium channels Kir4.1. We suppose that such functional properties of the cells are due to the disordered topology of inorganic nanostructured materials that resemblethe neural and glial networks of the brain. Until our discovery, inorganic metal-based devices were used tointeract with other kinds of cells, such as cancer cells *in vitro*[226]. Our findings add new milestones to the results suggested by Mestre et al.; he was the first to perform extracellular recording in primary astrocytes using micro-structured mushroom interface, and observing spontaneous burst in astrocytes, comprised of quasiperiodic signals, with a frequency of ≈0.1 Hz and with a broad distribution in amplitudes from 10 to 60 μV, preceded by an increase on the average noise fluctuations[227]. In conclusion, both inorganic materialsHTlc and AuSiNWs are here reported as valid glial nano interfaces to provide an alternative path to study astrocytes in a more *in vivo* like state, useful to learn more about brain physiology, neuron-glia interaction, neuron-astrocyte crosstalk, and networks. As a natural consequence of this plan, we are working on the *in vitro* validation of protocols to study astrocyte-neuron co-cultures in order to discriminate between different signals. Future results will be helpful in the knowledge of numerous neuropathological states in which astroglial cells are crucial such as epilepsy, AD, depression, cognitive deficit[17].

## 1.1 Introduction to Paper 1

"*Structural and Functional Properties of Astrocytes on PCL based electrospun fibres*" by **Emanuela Saracino, Valentina Cirillo, Marica Marrese, Vincenzo Guarino, Valentina Benfenati, Roberto Zamboni, Luigi Ambrosio** has been published as Open Access publishing on Materials Science & Engineering C 118 (2021) 111363, contents lists available at ScienceDirect Materials Science (www.elsevier.com), DOI: https://doi.org/10.1016/j.msec.2020.111363.

Supplementary information accompanies this paper at:

https://www.sciencedirect.com/science/article/pii/S0928493120332811?via%3Dihub.



The design and engineering of biomaterials, that can drive the structural and functional properties of astrocytes, are of growing interest for neuro-regenerative medicine and for the treatment of brain dysfunctions. In particular, non neuronal cells, such as astrocytes, show their change in cytoskeleton and ion channels' function coincide with neuronal damage in acute neurological conditions or chronic disease. Poly-ε-caprolactone (PCL), is an FDA-approved, biodegradable and non-toxic semi-crystalline linear resorbable aliphatic polyester having excellent mechanical and chemical properties, that can be tailored, as its topography too, to obtain neural implants for regenerative purposes. Specifically, aligned electrospun fibres of PCL (−GEL) and blending of PCL and Gelatin protein (+GEL). are investigated as a tuneable interface to selectively alter astrocytes structural components (cytoskeleton and focal adhesion points), while preserving astrocytes function. In conclusion, the aligned nanostructure of PCL interface can be proposed as a validated easy to use and low-cost glial interface, where the astrocytes network can reinforce, guide and promote the outgrowth of neurons during a stroke.

**Tesi Gennaio\PDF -FORMATO PAPERS\Saracino E., et al., Mat Science and Engineering C 4.1.pdf**

Materials Science & Engineering C 118 (2021) 111363

Contents lists available at ScienceDirect

Materials Science & Engineering C

journal homepage: www.elsevier.com/locate/msec

# Structural and functional properties of astrocytes on PCL based electrospun fibres

Emanuela Saracino[a], Valentina Cirillo[b], Marica Marrese[b], Vincenzo Guarino[c,*], Valentina Benfenati[a,*], Roberto Zamboni[a], Luigi Ambrosio[c]

[a] Consiglio Nazionale delle Ricerche, Istituto per la Sintesi Organica e la Fotoreattività (CNR-ISOF), via Piero Gobetti 101, 40129 Bologna, Italy
[b] Former Temporary Researcher at Institute for Composite and Biomedical Materials, National Research Council of Italy, Mostra d'Oltremare, Pad. 20, V.le J.F. Kennedy 54, 80125 Naples, Italy
[c] Consiglio Nazionale delle Ricerche, Istituto dei Polimeri, Compositi e Biomateriali (CNR-IPCB), Mostra d'Oltremare, Pad. 20, V.le J. F. Kennedy 54, 80125 Naples, Italy

ARTICLE INFO

*Keywords:*
Poly-ε-caprolactone
Astrocytes
Electrospun nanofiber
Cell function
Instructive material

ABSTRACT

Increasing evidences are demonstrating that structural and functional properties of non-neuronal brain cells, called astrocytes, such as those of cytoskeleton and of ion channels, are critical for brain physiology. Also, changes in astrocytes structure and function concur to and might determine the outcome of neuronal damage in acute neurological conditions or of chronic disease. Thus, the design and engineering of biomaterials that can drive the structural and functional properties of astrocytes is of growing interest for neuroregenerative medicine. Poly-ε-caprolactone (PCL), is FDA-approved polyester having excellent mechanical and chemical properties that can be tailored to obtain neural implants for regenerative purposes. However, the study on the use of PCL substrates for neuroregenerative purposes are mainly aimed at investigating the interaction of the material with neurons. Here, we report on the long-term viability, morphology, structural and functional properties of primary astrocytes grown on electrospun fibres of PCL (−GEL) and on blending of PCL and Gelatin protein (+GEL). We found that topography and morphological features of the substrate are the properties that mainly drives astrocytes adhesion and survival, over the long term, while they do not alter the cell function. Specifically, aligned PCL fibres induced in astrocytes a dramatic actin-cytoskeletal rearrangement as well as focal adhesion point number and distribution. Interestingly, structural changes observed in elongated astrocytes are not correlated with alterations in their electrophysiological properties. Our results indicated that PCL electrospun fibres are a permissive substrate that can be tuned to selectively alters astrocytes structural components while preserving astrocytes function. The results open the view for the use of PCL based electrospun fibres to target astrocytes for the treatment of brain dysfunction such as injuries or chronical disease.

## 1. Introduction

Studies over the past four decades revealed that glial cells, called astrocytes, are structurally and functionally connected to neurons and blood vessels [1]. Astrocytes are crucial players in homeostatic control of the concentration of ions, bioactive molecules and water in the extracellular space, by means of trans-membrane proteins forming ion channels, water channels, transporters. More recently, *in vivo* studies demonstrate that astrocytes structural components and dynamics are important for synaptic plasticity, formation of memory, learning, regulation of sleep or metabolisms [2]. The role of astrocytes is even more relevant in brain and Nervous System pathologies. During acute and chronic neurological conditions, astrocytes undergo to inflammatory reaction, called astrogliosis that is characterized by increased proliferation, migration toward the lesion [3] site and augmented expression of the intermediate filament protein called Glial Fibrillary Acidic Protein (GFAP). The reorganization of actin cytoskeleton structure is also induced by injuries and accompanies gliotic reactivity [4]. Nevertheless, the modification of the function of potassium channels, that occur during astrogliosis, alters the homeostatic properties of astrocytes leading to detrimental impact on neuronal network communication. Finally, hypertrophic astrocytes reactivity ultimately leads to the formation of a gliotic scar *in vivo*, that hamper spontaneous axon sprouting of injured neurons limiting regenerative process [5]. All these evidences justify the increasing attention that is being paid to bio materials interfaces and devices enabling the control and the modulation

* Corresponding authors.
*E-mail addresses:* Vincenzo.guarino@cnr.it (V. Guarino), valentina.benfenati@isof.cnr.it (V. Benfenati).

https://doi.org/10.1016/j.msec.2020.111363
Received 25 February 2020; Received in revised form 3 July 2020; Accepted 3 August 2020
Available online 11 August 2020
0928-4931/ 

of structural and functional properties of astrocytes [1,6–9].

Synthetic biodegradable polymers represent a class of materials with a considerable potential to drive nerve or axonal regeneration processes [10,11]. Among them, poly-ε-caprolactone (PCL), is an FDA-approved polyester, combining favourable mechanical properties [12] with biocompatibility, controllable biodegradation and versatility that makes it elective materials for neural interfaces such as gel, sponge, and fibrous structure. In addition to exceptional features of the constituent materials, PCL electrospun fibres allow high surface/volume ratio, porosity, anisotropy suitable to develop three-dimensional models to explore the *in vitro* response of neuronal cells in the CNS. To date, PCL nano fibres have been extensively used to produce suitable platforms for adhesion and differentiation of neurons [13]. Nonetheless, the permissive behaviour of PCL with astrocytes primary culture in terms of viability has been demonstrated [14–16]. However, a study on the impact of PCL based materials chemistry and topography on ion channels functionality of astrocytes is completely lacking and the knowledge on the effect of chemical Vs topographic clues on structural properties of astrocytes demand further investigation.

Here, we aim to fill this gap by reporting on the preparation and the characterization of PCL (GEL) and PCL + Gelatin (+GEL) electrospun fibres and on the effect of topographical of electrospun fibres on the viability of primary rat cortical astrocytes over the long-term (1 month), on F-actin, Vinculin and GFAP expression levels and distribution pattern. Notably, we also define the functional properties of astrocytes grown on aligned PCL electrospun fibres by single cell patch-clamp. We show that aligned PCL electrospun fibres promote strong cell orientation, guide astrocytes cytoskeletal structure and preserve functional properties, essential for astrocytes homeostatic role *in vivo*.

Our results indicated that aligned PCL electrospun fibres are promising substrates to engineer scaffolds that drive astrocytes behaviour *in vitro*, setting the scene for biomaterials based therapeutic approaches targeting glial cells structure and function *in vivo*.

## 2. Materials and methods

### 2.1. Preparation of PCL and PCL/GEL electrospun fibres

Poly-Ɛ-caprolactone (PCL, Mn 45 kDa), bovine gelatin type B (Gel, ~225 bloom) in powder form, chloroform (CHCl3) and 1,1, 1, 3, 3, 3, hexafluoro-2-propanol (HFP) were all purchased by Sigma Aldrich (Italy). All chemicals were used as received without additional purification.

PCL/Gelatin solution was obtained by dissolving PCL and Gelatin separately in HFP for 24 h under magnetic stirring and then mixing them to get the final polymer concentration of 0.1 g/ml (polymers ratio 1:1). Meanwhile, PCL solution was prepared by dissolution in chloroform (0.33 g/ml). In both cases, the solution was left under stirring for further 24 h.

Electrospun fibres were processed by using a commercialized electrospinning equipment (Nanon01 Mecc, Japan) optimized for the fiber's deposition by vertical configuration. Solutions were loaded into a 5 ml plastic syringe with a 18G needle, connected to the positive output of the high voltage power supply. To impart a uniaxial alignment of fibres, they were collected onto small glass discs- 12 mm as diameter fixed on a rotating drum-190 mm as diameter for 1 h. All the parameters (i.e., flow rate, voltage, electrodes distances, rotation speed) have been optimized depending on the properties of the solution in order to obtain the best morphology. As a control, randomly dispersed fibres have been collected on glass discs placed over a grounded aluminium foil target. All the experiments were performed at natural environmental conditions (T = 18/21 °C, RH = 40–50%).

Process parameters optimized for the preparation of samples for *in vitro* tests have been reported in Table 1.

All the experiments were performed at natural environmental conditions (T = 18/21 °C, RH = 40–50%), (Supplementary S1A).

**Table 1**
Summary of process parameter conditions used for each sample.

| Solution | Type | Flow rate (ml/h) | Voltage (kV) | Electrode distance (mm) | Rotation rate (rpm) |
|---|---|---|---|---|---|
| −GEL | Random | 0.1 | 15 | 80 | 50 |
| +GEL | Random | 0.5 | 15 | 120 | 50 |
| −GEL | Aligned | 0.1 | 15 | 80 | 500 |
| +GEL | Aligned | 0.5 | 13 | 120 | 3000 |

### 2.2. Morphological analysis of electrospun nanofibres

Electrospun samples were analysed by scanning electron microscopy (SEM; QuantaFEG 200, FEI, The Netherlands) in order to assess fibres morphology and alignment. Specimens were sputter coated with a Pd-Au nanolayer (Emitech K550, Italy) and then observed under high vacuum conditions (10–5 mbar). Fibres mean diameter was calculated from selected SEM images (ca. 20 units) by using images analysis software (Image J freeware 1.52a) and reported as mean value ± standard deviation (SD). In order to collect further information about fibres anisotropy, the spatial organization of fibres was also investigated by using two different measurement algorithms available as plugins for the image elaboration software:

(a) "orientation staining" to carry out a qualitative map of structural anisotropy by variously staining fibres with different orientation;
(b) "Frequency Fourier Transform (FFT)" to extrapolate fibres orientation angles and quantifying the occurrence probability to characterize fibres alignment. The FFT function converts information present in an original data image from "real" space into mathematically defined "frequency" space [17]. The resulting FFT output image contains grayscale pixels that are distributed in a pattern that reflects the degree of fibres alignment present in the original data image.

### 2.3. Water contact angle analysis

The wettability of electrospun membranes was measured by a water contact angle system (WCA) supported by videocam equipment (OCA20 Dataphysics, Italy). A single droplet (volume, 0.5 μl) was used for each sample. Ten measurements were performed at time zero to remove any influence of perfusion flow through the membrane. Contact angle size was reported as the mean value ± standard deviation in triplicate.

### 2.4. Atomic force microscopy

The morphology of electrospun fibres was imaged by an Innova System Atomic Force Microscopy (Bruker Corporation, Santa Barbara, USA) with a 90 μm lateral range scanner. To minimize the damage of the sample during scanning, a dynamic force (tapping) mode and a commercially available RTESPA silicon cantilever with a spring constant of 57 N/m and a rotated tip of radius 8 nm were used. The scanning velocity was 8 μm s-1, while the scan size was 20 × 20 $\mu m^2$. Electrospun fibres, for AFM imaging, have been collected directly on a glass substrate for 2 min. The measurements were performed in air, at room temperature (25 °C) and after an accurate calibration procedure on a hard substrate, through the Thermal Tune Calibration method. The images of interest were first captured by AFM raster scanning, processed using the Nano Scope Analysis data processing software 1.40 (Bruker Corporation, USA) and then graphically reported in 2D and 3D form. The raw AFM data of the electrospun fiber have been filtered using procedures for plan-fit and flatten. Root mean square roughness (Rrms) of each electrospun membrane was calculated by manually applying a rectangular region of interest (ROI) box to different areas of the fiber surface. To obtain an average value of the surface roughness, this operation was repeated several times on different single fibres. The

adhesion properties were estimated by quantitative force spectroscopy AFM. The adhesion interaction between tip and sample was determined as force versus Z-piezo displacement and a mean value of each point was considered.

### 2.5. Rat cortical astrocyte culture preparation, maintenance and plating

Primary astroglial cultures were prepared at the University of Bologna, in concordance with the Italian and European law of protection of laboratory animals and the approval of the local bioethical committee, under the supervision of the veterinary commission for animal care and comfort of the University of Bologna and approved protocol from Italian Ministry of Health (ethical protocol number ID 360/2017 PR, released on May 2017, valid for 3 years). Astrocyte primary cultures were prepared as described previously [1,18] from new borns, at post-natal day 1–2, of Sprague-Dawley Rattus, Norvegicus, Wistar. Briefly, neonatal cerebral occipital cortices devoid of meninges were gently triturated, filtered with a 70 μm cell strainer (Falcon, BD Bioscience, Bedford, MA) and placed in cell culture flasks containing Dulbecco's Modified Eagle-glutamax medium with 15% fetal bovine serum (FBS) and penicillin/streptomycin (100 U/ml and 100 lg/ml, respectively). Cells were maintained in incubation at 37 °C and 5% of CO2 and proper humidity levels for three weeks. During this period, we replaced cell medium every three days and flasks were gently shaken when necessary to remove undesired microglial cells. After three weeks in culture, confluent astrocytes were dispersed using trypsin-EDTA 0.25% and the cell suspension was dropped on random and aligned samples of –GEL and +GEL at concentrations of $8 \times 10^3$ cells per sample and maintained in culture medium containing 10% FBS. We used cells grown on Poly-ɒ-Lysine as reference control for all the structural analyses (Fig. S2). We realized that during patch-clamp experiment, cells grown on random substrates cannot be reached by the patch-clamp pipette, as cells are highly interlaminated and infiltrated in the sample and thus cannot be properly visualized by optical microscopy. As cells plated on random fiber resemble structural features of those plated on PDL substrates (Fig. S2), and considering that the use of random substrate for patch-clamp was not technically possible, we used cells grown on Poly-ɒ-Lysine as reference control also for the analyses of electrophysiological properties of primary astrocytes.

### 2.6. Alamar Blue viability assay

Astrocytes viability and biocompatibility on fibrous PCL-based samples were analysed via Alamar Blue (AB) assay according to the Interchim technical sheet (66941P) and to protocols described previously [8]. Viable cells maintain a reducing environment within their cytoplasm. Time course of astrocytic viability on random and aligned PCL (−GEL) and PCL +GEL nanofibres was evaluated from 1 day *in vitro* (DIV) to 28DIV after re-plating cells on the substrates. On the day of the assay, AB reagent was added directly to culture medium at 10% volume of medium contained in each sample. After 3 h of incubation, 100 μl of AB containing medium were transferred in a 96 multiwell plate for fluorescence measurement at 545nmEx/590nmEm, using a Thermo Scientific Varioskan Flash Multimode Plate Reader. We included a negative control (CTRL-) (only medium with 10% AB and without cells) and positive control (CTRL+) of 100% reduced AB reagent without cells. Given that AB reagent does not alter cellular viability8, viability time course was evaluated on the same culture of astrocytes for each experimental trial. Analyses of the AB fluorescence and correlation with viability was performed as described previously [8]. Data were collected from three separate experiments performed in quadruplicate and are expressed as means ± SE of the percentage of reduced AB.

### 2.7. Fluorescein diacetate viability assay

Fluorescein diacetate assay (FDA) was performed on astrocytes plated on random and aligned -GEL, and +GEL as described previously [8,19–21]. Briefly, astrocytes plated on the different coverslips were incubated for 5 min with FDA (Sigma Aldrich). Samples were rinsed with PBS three times. A sequence of images (10 to 15 different fields for each sample) was taken using a Nikon TE 2000 inverted confocal microscope (40× objective). The staining was carried out after 4DIV.

### 2.8. Morphological analyses and alignment angle measurement

To evaluate the morphology of astrocytes grown on aligned -GEL +GEL electrospun fibres, FDA positive cells were imaged by using a Nikon TSi S inverted confocal microscope (20× objective). A sequence of 15 images for each replica was taken after 24 h (1DIV) and 96 h (4DIV) from the re-plating of astrocytes on the substrates. The orientation angle of an individual cell was defined as the angle between the longest cell axis and the nearest fibres to the cell body. The cell orientation angle values were expressed as the average of the orientation angle value of alive cells for each aligned condition, as described previously [22]. Results were analysed using the ORIGIN-PRO program.

### 2.9. Immunofluorescence and confocal microscopy

Astrocytes cultures plated on the different samples were fixed for 15 min with 4% para-formaldehyde (PFA) in 0.1 M phosphate buffer saline (PBS) at room temperature (RT, 20–24 °C) and then rinsed with PBS. The samples were incubated for 20 min in 3% bovine serum albumin (BSA) and 0.3% Triton X-100 solution in PBS, in order to permeabilize astrocytes membrane and to block reactive sites. Vinculin immunostainings was performed by using primary rabbit anti-vinculin (Life Technologies, Monza, Italy) 1:200 incubated 3 h at RT as primary antibody and donkey anti-rabbit Alexa Fluor 488-conjugated (1:1000, Molecular Probes-Invitrogen) as a secondary antibody, incubated for 1 h at room temperature (RT = 22–24 °C). F-actin fibres were stained for Phalloidin-TRITC (Sigma-Aldrich, Milan, Italy). Coverslips were mounted with Prolong Anti-Fade (Molecular Probes-Invitrogen). The optical images were taken with a Nikon TE 2000 inverted confocal microscope equipped with a 40× objective and 400 nm diode, 488 nm Ar+ and 543 nm He-Ne lasers as exciting sources. Data were collected from two experiments.

To perform focal adhesion (FA) vinculin quantification, at least 15 images for each replica of condition were analysed by ImageJ software. FA density was expressed as means ± SE of number of vinculin contacts counted for each image (300 μm x 300 μm) and divided for nuclei (blue staining) amount of the same image.

### 2.10. Electrophysiology

Current recordings were obtained in the whole-cell configuration of the patch-clamp technique, by customized patch-clamp set-up (Crisel Instruments, Rome, Italy). Experiments were performed after 24 h *in vitro* treatment. Patch pipettes were prepared from thin walled borosilicate capillaries (Harvard Apparatus) to have a tip resistance of 2–4 MΩ when filled with the standard internal solution. To ensure the comparability between the conditions, only elongated astrocytes were selected to evoke whole cell currents, cells in control intra- and extracellular saline were held at −60 mV and after stepping to −120 mV for 500 ms, a ramp from −120 mV to +60 mV (500 ms) (inset Fig. 9A).To investigate the voltage and time dependence of conductance of cells seeded on –GEL and +GEL substrates astrocytes were stimulated with 500 ms voltage steps (Vh = −60 mV) from −120 mV to +60 mV in increments of 20 mV (inset Fig. 8B). Membrane currents were amplified, filtered at 2 kHz and acquired at a sample rate of 5 kHz by Axopatch 200B amplifier in voltage-clamp mode. Responses were

amplified, low-pass filtered at 1 kHz, digitised at 20 kHz, stored and analysed with pCLAMP 10. Experiments were carried out at room temperature (22–24 °C). Cells were voltage-clamped at a holding potential (Vh) of −60 mV and, after stepping to −120 mV for 400 ms, a slow ramp (180 mV/600 ms) from −120 mV to 60 mV (inset in Fig. 9B) was applied to elicit whole-cell currents. Current amplitude was recorded, and values of the resting membrane potential (Vmem), input resistance (IR), specific conductance (SG) and capacitance (Cp) were calculated as described previously [19].

### 2.11. Solutions and chemicals

All salts and chemicals employed for the investigations were of the highest purity grade (Sigma). For electrophysiological experiments, the standard bath saline was (mM): 140 NaCl, 4 KCl, 2 $MgCl_2$, 2 $CaCl_2$, 10 HEPES, 5 glucose, pH 7.4 with NaOH and osmolarity adjusted to 315 mOsm with mannitol. The intracellular (pipette) solution was composed of (mM): 144 KCl, 2 $MgCl_2$, 5 EGTA, 10 HEPES, pH 7.2 with KOH and osmolarity 300 mOsm. When using external solutions with different ionic compositions, salts were replaced equimolarly.

### 2.12. Statistical methods

Data were elaborated using a one-way analysis of variance (ANOVA, with Bonferroni's test). A statistically significant difference was reported $P < 0.05$ or less. Data of biological experiments are reported as the mean ± standard error (SE). The number of experiments (n) is indicated in the text or in the figure legends. Results reported are the mean of at least 3 different experimental trials performed in triplicate or more.

## 3. Results and discussion

### 3.1. Fabrication and characterisation of PCL, PCL/Gel substrates

Electrospun fibres were produced by electrospinning technique by a vertical deposition of the fibres. In comparison with the standard configuration [23], the experimental setup was customized by using a rotating drum, working as collector [24], at different rotating rates in order to control the spatial organization and alignment of the fibres (Fig. 1). To obtain a random deposition of the fibres, the rotation rate was fixed at the minimum rate equal to 50 rpm in order to cover a large portion of the collector surface, minimizing the effect to the rotation rate on fibres dispersion and their spatial distribution. A preferential fibres alignment was reached by increasing the rotating rate from 500 to 3000 rpm, as a function of the peculiar features of the polymer solution. Process parameters including flow rate, voltage and needle to collector gap, were next further optimized in order to accurately improve the fibres morphology.

SEM images showed the morphology of random electrospun fibres (Fig. 2A) obtained by using optimized process parameters (Table 1). It can be observed that the typical diameters of bare PCL random fibres (−GEL) fall in the micrometer range. Data are in agreement with previous works on the use of apolar solvents (i.e., chloroform) and solutions with high polymer concentrations (over 20% w/v) for the preparation of PCL electrospun fibres [25]. SEM images of PCL/Gelatin (+GEL), processed by using polar solvents such as HFP, indicated an evident reduction of the fibres diameter. It is plausible that high polarity of HFIP promotes stronger molecular interactions with respect to chloroform in the presence of the applied electric fields, inducing a more remarkable stretching of the polymer jet from the needle to the counter electrode, during the electrospinning process. This effect, due to solvent polarity, is further corroborated by the integration of Gelatin molecules. Indeed, high polar groups along the protein chains further support the stretching of the polymer jet, thus promoting the formation of thin fibres with an average diameter falling in the sub micrometric size scale. As the rotation rate of the collector increases, the drawing forces applied to the polymer jet rise up, thus imparting a remarkable orientation to fibres until to be uniaxially oriented (see SEM images, Fig. 3A). Image elaboration via orientation staining and FTT gives a powerful tool to collect visual information useful to reveal differences in the fiber morphology (Fig. 2B–C). First of all, the presence of Gelatin does not alter the random organization of the fibres: a colorful fibres network due to the wide range of fibres orientation angles is recognized, independently upon the presence of Gelatin (Fig. 2B). Accordingly, FTT spectra – due to a radial summation of the pixel intensities plotted between 0° and180° shows a symmetric and circular pattern (Fig. 2C).

Contrariwise, in the case of aligned fibres, a uniform color of fibres, ascribable to the same orientation angle, can be detected (Fig. 3B) and a not homogeneous FFT image with a group of pixel intensities oriented in a preferential direction is generated (Fig. 3C), thus confirming that alignment degree is independent on the Gelatin contribution. Noteworthy, in the case of -GEL fibres, the use of highly concentrated solutions contributes to generate a more stable polymer jet, thus enabling to collect highly aligned fibres patterns by using moderate rotation rates (500 rpm). In the case of +GEL fibres, the higher permittivity of the polymer solution tends to generate whipping instabilities of the polymer jet, that nullify the contribution of rotation rate on the fibres stretching. Therefore, higher rotation rates, nearly 3000 rpm, need to be used to guarantee an uniaxial alignment of the fibres.

The qualitative trend of fibres diameters observed by SEM imaging

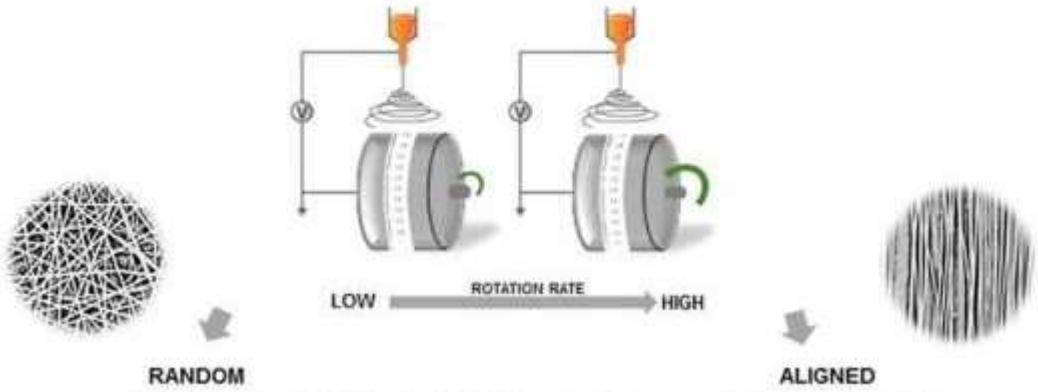


**Fig. 1.** Experimental setup tailored for the fabrication of electrospun fibres with random or aligned distribution.

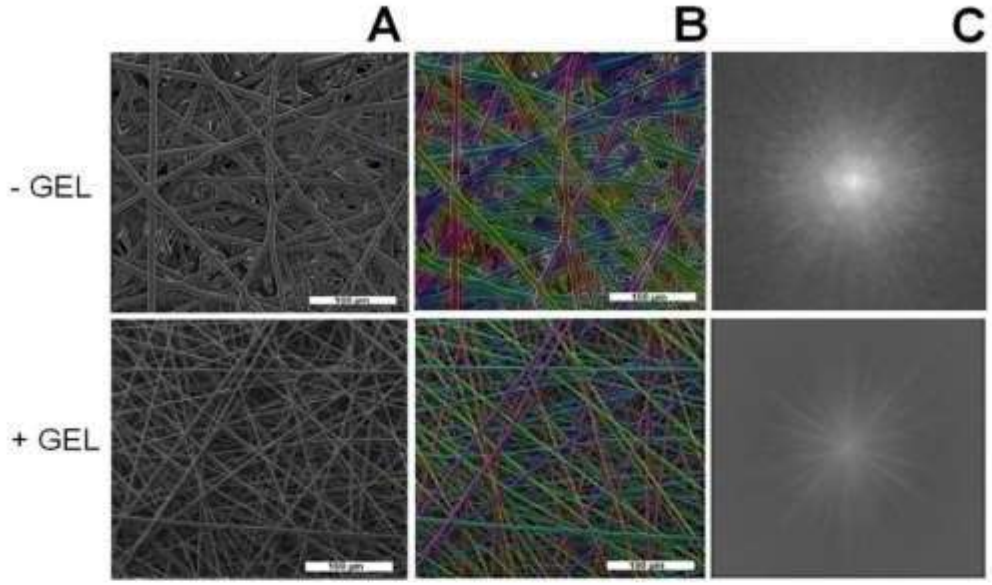


**Fig. 2.** Morphological analysis of random fibres: A) SEM images and qualitative evaluation of fibres orientation via B) fibres staining and C) FTT analysis.

was confirmed by the quantitative measurements obtained image analysis reported in Fig. 4.

To collect further morphological information in terms of surface roughness, the topography of -GEL and + GEL fibres was estimated by using AFM in tapping mode. The test was performed by considering cantilever oscillations close to the resonance frequency and short tip approaching times onto the surface for every oscillation cycle in agreement with previous works [25]. AFM data indicated a strong reduction of the surface roughness in the presence of Gelatin (Fig. 5A, + GEL), due to a reduction of the uniaxial normal stresses onto the surface, at the exit of viscoelastic fluid jet from the needle tip. AFM analyses was also used to measure the adhesion force between the tip and fibres surface. Adhesion force measured in -GEL was $0.15 \pm 0.06\mu N$ while GEL fibres displayed almost half of the value ($0.08 \pm 0.03\mu N$). This finding can be ascribed to the balance between the contribution of hydrophilic properties of Gelatin macromolecules and to the reduction of the fibres roughness, also related to the surface to volume ratio [26]. Wettability was also assessed by multiple

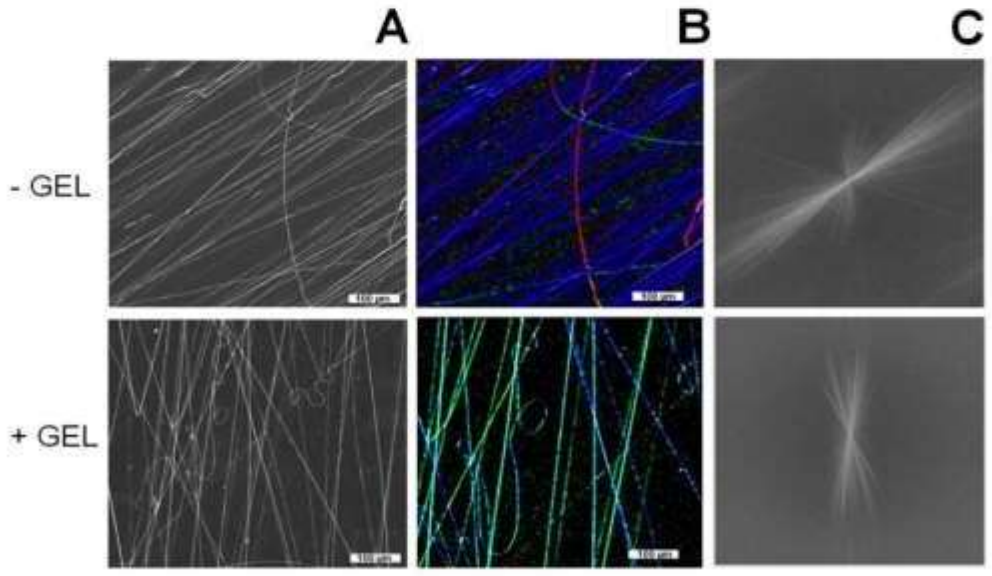


**Fig. 3.** Morphological analysis of aligned PCL fibres: A) SEM images, and qualitative evaluation of fibres orientation via B) fibres orientation staining and C) FTT method.

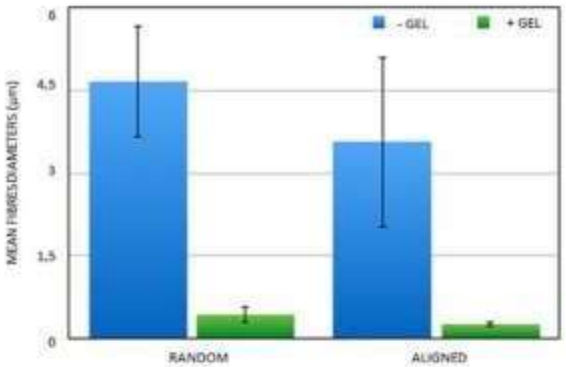


**Fig. 4.** Evaluation of average PCL fibres diameters. Random (blue) and Aligned (green) fibres of PCL -GEL and PCL +GEL. (For interpretation of the references to color in this figure legend, the reader is referred to the web version of this article.)

measurements of the contact angle at time zero to minimize any effect of flow perfusion through the fibres network (Fig. 5B). As expected, a remarkable difference in contact angle was detected between -GEL and +GEL fibres (Table 2). In line with adhesion force measurements, lower values of the contact angle were detected in the case of fibres +GEL, thus confirming the role of Gelatin on the improved hydrophilicity of the electrospun fibres.

### 3.2. Effects of PCL electrospun fibres on astrocytes growth, polarization and morphological elongation

In order to determine the impact of PCL based substrates on astrocytes adhesion and morphology, confluent primary rat cortical astrocytes were re-plated on random and aligned substrates of PCL (+GEL and –GEL). Bright field and fluorescent imaging analyses were performed on label free and fluorescein diacetate (FDA) labelled astrocytes after 2 and 4 days *in vitro* (2 DIV and 4 DIV) after re-plating on the substrates.

In Fig. 6, we report typical bright field images (Fig. 6A) and fluorescent images (Fig. 6B), captured at 2DIV and at 4DIV, of viable (green) astrocytes plated on random –GEL and +GEL (Fig. 6A–B, upper panels) and aligned –GEL, +GEL fibres (Fig. 6A–B, lower panels). Notably, astrocytes on random fibres are polygonal with a shape, typically observed when the same type of cultures were plated on Poly-D-Lysine (PDL, Supplementary S2A) or on other biopolymers and bioorganic interfaces [7,8,27].

On the other hand, astrocytes grown on aligned +GEL and -GEL fibres appear elongated and aligned with the orientation of the fibres (Fig. 6A–B, lower panel, white arrow). In agreement with previous studies [32], the elongation and stretching of astrocytes body seemed more pronounced when cells were grown on –GEL samples than on +GEL ones, in response to the different size scale of surrounding fiber pathway.

To evaluate the impact of electrospun PCL fibres on adhesion and growth of astrocytes, Alamar Blue (AB) viability assay was performed from 24 h up to 28 days *in vitro* on astrocytes plated on random and aligned -GEL, +GEL. Bar plot reported in Fig. 6, shows the percentage of AB reduced, with respect to the oxidazide one, a value that is proportional to the metabolic activity and, on turn, to the viability of the cells. After 1 day from the seeding of the cells on the substrates (1 day *in vitro*, 1 DIV), adherent astrocytes grown on PDL showed comparable values than those recorded in random and aligned PCL substrates. The presence of Gelatin was not affecting the adhesion of astrocytes, as indicated by the data that -GEL and +GEL samples values that were not significantly different. After 3DIV, the viability was significantly higher in aligned substrates compared with the random ones, thus, indicating that Gelatin disappeared and the topography of the nanostructure mainly impacts on the cell survival. Accordingly, a constant increase in cell viability was observed in aligned samples at all the time points analysed between 3DIV and 28DIV. On the other hand, the cell viability was always comparable between random samples +GEL and -GEL (Fig. 6C). This may be explained by the fast release of Gelatin as described in recent works [28], leaving adhered astrocytes only to respond to the isotropic topographic signals from the randomly organized network of fibres. Cell viability significantly increased in the case of aligned samples at 8DIV (+GEL), even when compared to PDL plated cells, also suggesting a synergic effect of fiber diameter and alignment on astrocytes response. Accordingly, the proliferation rate analysis (Supplementary S3) confirmed that the topographical organization, in terms of nanofibres distribution, majorly drive astrocytes growth on the samples, rather than the chemical signals. Of note, cells are still viable up to 28DIV in all the samples analysed. However, while the cell growth reaches a plateau on PDL, cells on aligned PCL substrates continue to grow up to 28DIV.

Next, we determine the orientation angle as quantitative measure of the cell alignment. The orientation angle was defined as the angle between the line crossing the major diameter of the cell body and the nearest fibres (scheme in Fig. 7A). The averaged cells orientation angle values measured in cells plated on aligned -GEL and +GEL substrates is reported in Fig. 7B. The presence of GEL is decreasing the orientation angle at 1 DIV while the average value is higher at 4 DIV. The higher number of cells with a small angle of orientation, observed at 1 DIV, in +GEL aligned samples indicated that, the presence of GEL is favouring the increase in cell alignment at 1 DIV (Figure Supplementary S4). After 4DIV it is evident that the alignment was lower in GEL samples.

### 3.3. Impact of PCL electrospun fibres on astrocytes structural properties

We next analysed the expression of GFAP, a well-known marker of astrogliosis. Confocal imaging of immuno-stained cells, performed after 3 DIV, give evidence of a comparable level of GFAP expression between the astrocytes grown on random -GEL and +GEL samples (Fig. 8A–B) and those grown on the aligned -GEL +GEL substrates (Fig. 8C–D). The data also indicated that the observed effect on increased proliferation in aligned samples was not related to a gliotic reaction as the expression of GFAP was comparable among substrates. However, the GFAP distribution pattern was altered on Aligned -GEL and +GEL and follow the shape of the substrates. To get further insight on the impact of PCL electrospun fibres topography and chemistry on astrocytes structural features, we performed the study of the actin cytoskeleton and vinculin focal adhesion points. Typical images of Phalloidin staining reported in Fig. 8C showed that astrocytes cultured on aligned -GEL and +GEL substrates express stressed F-actin fibres (Fig. 8C, arrows) that parallel the pattern of the PCL fibres. Cells on the random PCL display a disorganised structure of the F-actin fibres (Supplementary S3C), resembling those on PDL. The vinculin fluorescent signal analyses on cells grown on aligned -GEL substrates indicated an oriented distribution and expression of the protein in the elongations of the astrocytes (Fig. 8D, left panel). The vinculin expression of astrocytes plated on aligned +GEL substrates was patchy (Fig. 8D, right panel), whereas its distribution was mislocalized in cells plated on random PCL (Supplementary S2D). Quantitative analysis of focal adhesion points (FA) per cell (Fig. 8E), revealed a significatively higher number of FA points on aligned +GEL respect to aligned -GEL substrates.

### 3.4. Effects of PCL electrospun fibres on functional properties of astrocytes

Several works demonstrated that primary rodent astrocytes, grown on different substrates such as flat coverslips coated with poly-D-Lysine (PDL), poly-stirene Petri Dishes, silk fibroin, organic semiconductors,

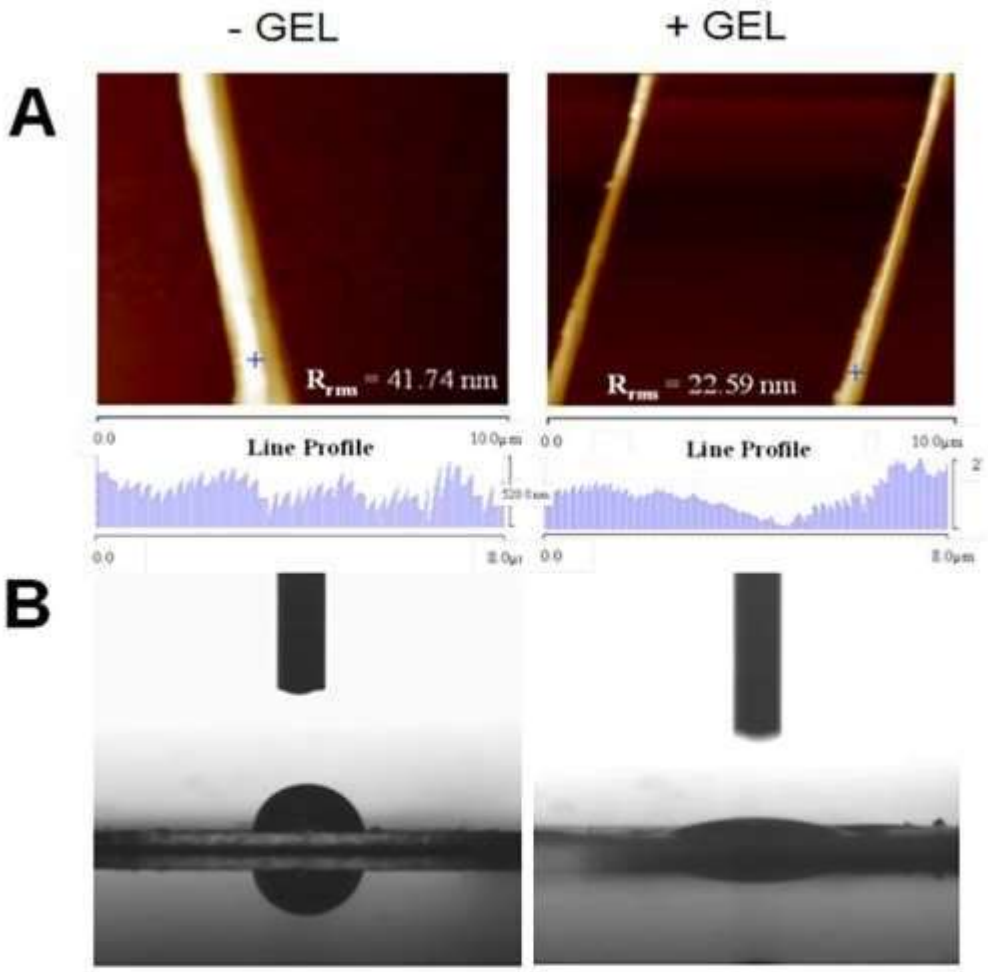


**Fig. 5.** Characterization of surface properties of -GEL and +GEL fibres: A) AFM images and surface roughness evaluation; B) fibres wettability via contact angle measurement.

**Table 2**
Roughness and wettability: summary of the experimental data in the case of -GEL and +GEL fibres.

| | Roughness (nm) | Contact angle (degrees) |
|---|---|---|
| -GEL | 41.74 ± 5.68 | 78.29 ± 5.69 |
| +GEL | 22.59 ± 7.50 | 22.02 ± 2.09 |

flat gold MEA display a polygonal morphology, which is parallel by comparable electrophysiological properties [8,14,18,29,30,36]. On the other hand, differentiated or elongated astrocytes have been shown to display peculiar alteration in their functional properties, with respect to those observed in polygonal cells [8,21,31,32,36].

To verify if elongation and structural modification observed in cells grown on aligned PCL substrates was accompanied by functional modifications, we performed electrophysiological analyses of the astrocytes plated on aligned -GEL and +GEL, we investigate the behaviour of $K^+$ channels that play a fundamental role in astrocytes physiology [1,8]. For this purpose, we performed whole-cell patch-clamp measurements on single cells after 24–48 h from re-plating on aligned -GEL and +GEL samples (Fig. 9). As cells plated on random fibres resemble structural features of those plated on PDL substrate, and considering that the use of random substrate for patch-clamp was hampered and technically not possible (see methods session), we used cells grown on Poly-D-Lysine as reference control for the analyses of also electrophysiological properties of primary astrocytes (Supplementary S5). The passive membrane properties were calculated (Table 3:) and revealed that the values of Voltage membrane (Vmem), Input Resistance (IR) and Specific Conductance (SpG) of the astrocytes on aligned -GEL and +GEL are very similar to those reported for primary astrocytes grown *in vitro* on PDL [1,21].

The typical current profiles obtained in response to the applied voltage ramp are shown in Fig. 9A for the astrocytes on both aligned -GEL, +GEL. The ramp-current traces displayed a strong outward rectification as witnessed by the negligible currents recorded at membrane potentials more hyperpolarized than −40 mV on astrocytes plated on aligned -GEL (Fig. 9A, left panel) as well as aligned +GEL plated (Fig. 9A, right panel) astrocytes.

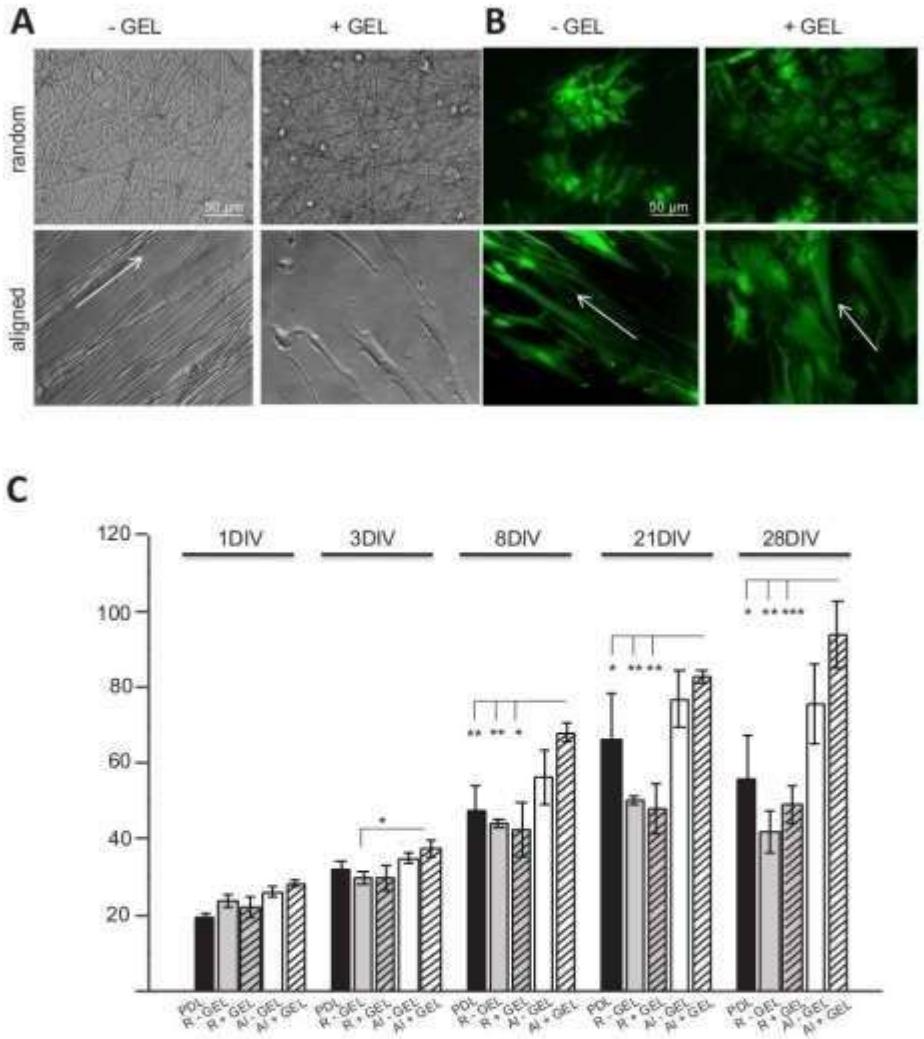


**Fig. 6.** Analyses of the effect of electrospun fibres on astrocytes morphology and viability. A) bright field 20 × micrographs representing astrocytes plated on random -GEL, +GEL (upper panel), and aligned -GEL, +GEL (below panel) substrates, captured after 4 DIV from cells re-plating. B) Single plane confocal images of FDA stained astrocytes, representing viable cells plated on random -GEL, +GEL (upper panel), and aligned -GEL, +GEL (below panel) substrates, captured after 4 DIV from cells re-plating. C) Time course of astrocytes viability on random and aligned -GEL, +GEL investigated by AB assay at different time points (1 to 28 DIV) from cells re-plating. Data are plotted as the averaged percentages of reduced AB ± Standard Error (SE) versus DIV, Student's *t*-test, * = pval < 0.05, ** = pval < 0.01, *** = pval < 0.001. (For interpretation of the references to color in this figure legend, the reader is referred to the web version of this article.)

Rapidly activating, non-inactivating, voltage-dependent whole-cell currents were elicited with the family of voltage-step protocols at potentials positive to −40 mV (Fig. 9B) either on astrocytes plated on aligned -GEL and +GEL. A comparative analysis, obtained by an I/V plot of averaged values of maximal current, recorded for each voltage step (Fig. 9C), revealed a similar voltage-dependent profile of whole-cell peak and steady state currents of astrocytes plated on aligned –GEL and +GEL samples. The latter ramp and step current profile was comparable to the one recorded on cells plated on PDL (Supplementary S5). All the data indicate that astrocytes plated on -GEL, +GEL have voltage-gated K+ channels activated at membrane potentials more positive than −40 mV and that the properties among the conditions are preserved and not altered by the topography nor by the blended gelatin.

The present work aimed to analyse the impact of topographical and chemical cues of electrospun fibres on the viability as well as on the structural and functional properties of astrocytes.

For this purpose, we provided a comparative study of the response of astrocytes on −GEL and +GEL fibres. Recent literature demonstrated that PCL electrospun fibres accurately replicate the physical dimensions and fibrillary organization of the collagen network into the native extracellular matrix [33]. However, PCL electrospun fibres present some lacks in terms of cell affinity and biorecognition, mainly due to their intrinsic hydrophobic properties [34]. Hence, the integration by different ways (i.e., blending, grafting, adsorption) of bioactive proteins

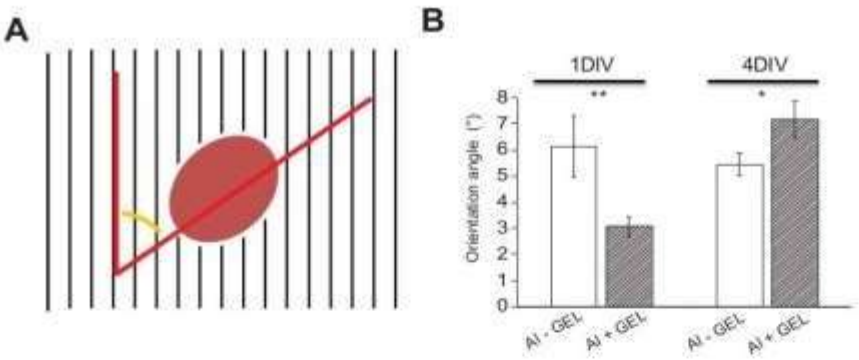


**Fig. 7.** Alignment of astrocytes on PCL fibres. A) Scheme representing the criteria used to measure cell alignment angle. B) Bar plot reporting the averages of orientation angles measured between astrocytes and fibres (1 DIV, 4 DIV) plated on aligned -GEL samples (Al-GEL, white bar, n = 38 at 1 DIV, n = 40 at 4 DIV) and aligned PCL +GEL (Al + Gel, n = 60 at 1 DIV, n = 35 at 4 DIV) substrates. Student's *t*-test, * = pval < 0.05, ** = pval < 0,01.

from collagenous source can improve the interface interactions between cells and the surrounding fibres, by promoting basic recognition (i.e., adhesion, spreading, migration) and physiological mechanisms (i.e., proliferation, differentiation) [34].

Our results showed that the fibres alignment and, thus, the topography are the key feature that promote astrocytes adhesion, viability and growth, while chemical clue such as GEL and hydrophobicity play a major role in promoting cell alignment. Previous studies reported that chemical blending of PCL with Gelatin enhances the hydrophilicity of the polymer, and promoting the adhesion of neuronal-like cell lines as well as their neurite outgrowth [35].

Here we found that GEL blending to the PCL fibres allows significantly improving the hydrophilic properties of the fibres as confirmed by contact angle measurements (Fig. 2). However, the increase in hydrophilicity of +GEL samples compared to -GEL substrates is not further improving adhesion of astrocytes to the PCL fibres. Accordingly, we found that, in the case of protein films (i.e., silk fibroin), the adhesion and growth of astrocytes was higher on more hydrophobic surface [9,36], whereas the surface hydrophilicity improved neurite outgrowth of primary dorsal root ganglion neurons. Moreover, +GEL samples display peculiar sub micrometric sizes lower than those of -GEL ones (Fig. 4) which is not favouring astrocytes adhesion. This data is in line with recent studies reporting that astrocytes showed significantly increase in elongation and adhere preferentially, when seeded on the large diameter fibres, with respect to values of cells plated on small diameter fibres [37]. In addition, more efficient extension of astrocytes on larger diameter fibres allow better outgrowth of neurites of dorsal root ganglia neurons plated on them [37].

It is not surprising that neurons and astrocytes respond differently to the surface topography and chemistry. While neurons adhesion to substrates depends upon the presence of extracellular matrix factors and components [37], astrocytes cell cultures are capable to release adhesive and repulsive ligands, including collagen, laminin, fibronectin and to chemically shape the surrounding environment [37,38]. Interestingly, aligned astrocytes on polydioxanone improve neurite outgrowth of DRG neurons compared with substrates with unaligned fibres or with those without astrocytes.

The ability of astrocytes to sense surface topography is well documented. Notably, adhesion of astrocytes on flat inorganic substrates or highly hydrophobic surfaces like organic semiconductors needs to be improved by coating with ECM components or poly-ionic substances such as Poly-o-Lysine or anchoring molecules such as Phospholipids [7,21,39,40]. On the other hand, nanotopographic clues such as nanoislands, nanorods or electrospun nanofibres are sufficient to improve astrocytes adhesion and viability [8,9] with respect to unstructured ones. In this view, our data are in agreement with the literature

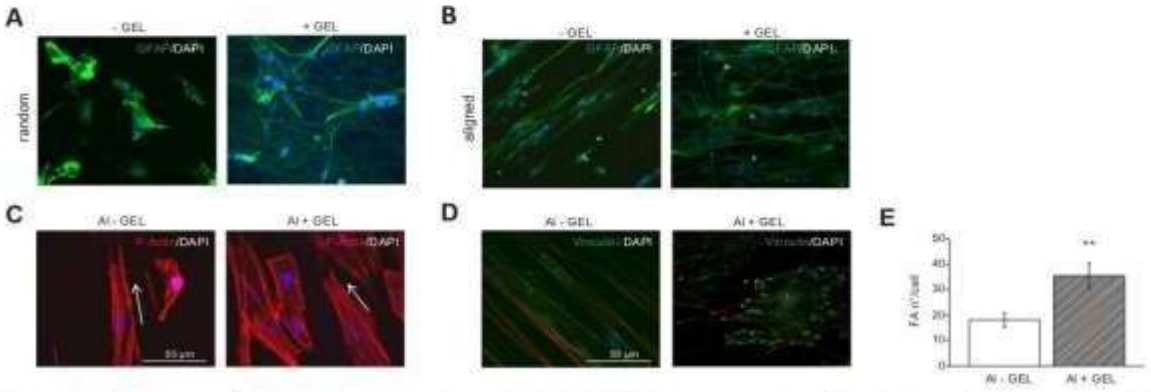


**Fig. 8.** Impact of PCL electrospun fibres on astrocytes structural properties. (A–B) Confocal images representative of GFAP/DAPI expression in astrocytes seeded on random -GEL, +GEL (A), and aligned −GEL, +GEL (B), captured after 3 DIV from cell re-plating. C) Confocal images of Phalloidin-TRITC staining of the cytoskeleton (red) and of DAPI in the nuclei (blue) of astrocytes plated on aligned -GEL and +GEL substrates, collected after 3 DIV from the re-plating. White arrows show the oriented F-actin fibres directions. D) Confocal images of astrocytes plated on aligned −GEL and +GEL substrates immune-stained for Vinculin (green) and with DAPI (blue staining), collected after 3 DIV from the re-plating. E) Bar plot shows the number of vinculin contacts per cell, counted after 3 DIV from the cells re-plating in cells plated on aligned −GEL and +GEL substrates. Data are expressed as means ± S.E. (n: −GEL = 124; +GEL = 138), Student's *t*-test, ** = pval < 0.01. (For interpretation of the references to color in this figure legend, the reader is referred to the web version of this article.)

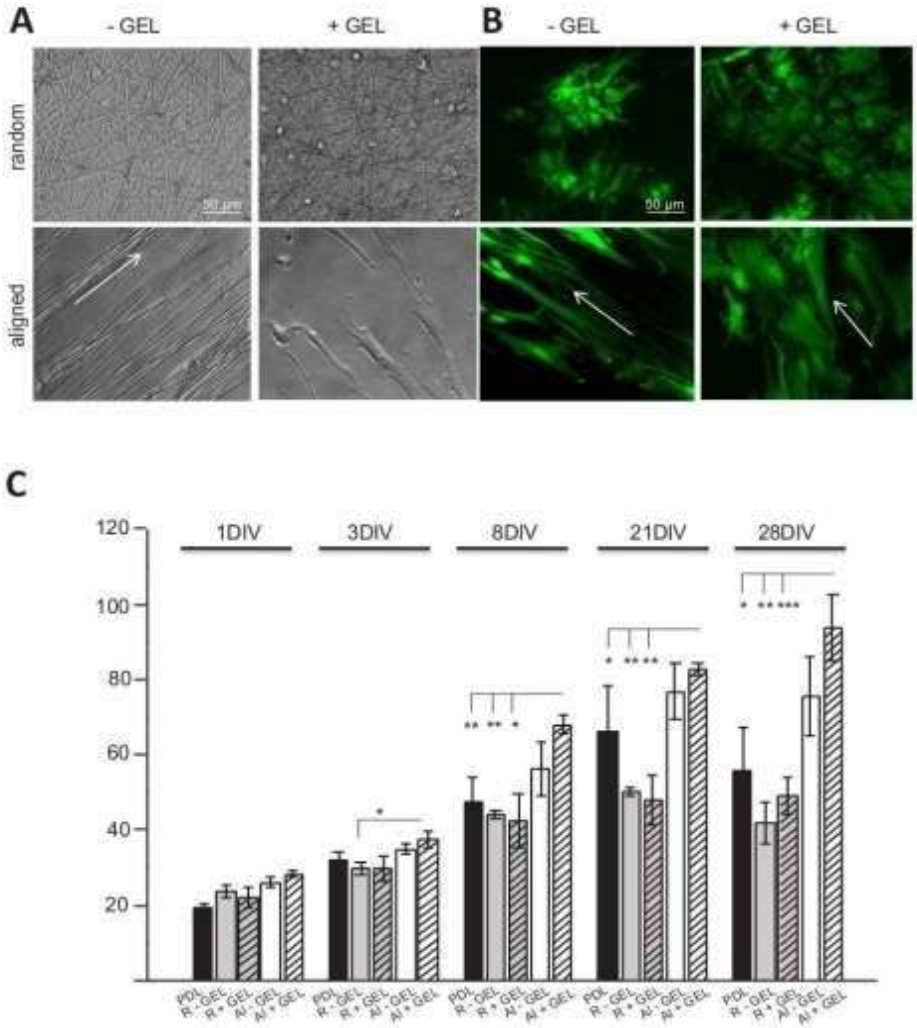


**Fig. 6.** Analyses of the effect of electrospun fibres on astrocytes morphology and viability. A) bright field 20 × micrographs representing astrocytes plated on random -GEL, +GEL (upper panel), and aligned -GEL, +GEL (below panel) substrates, captured after 4 DIV from cells re-plating. B) Single plane confocal images of FDA stained astrocytes, representing viable cells plated on random -GEL, +GEL (upper panel), and aligned -GEL, +GEL (below panel) substrates, captured after 4 DIV from cells re-plating. C) Time course of astrocytes viability on random and aligned -GEL, +GEL investigated by Alb assay at different time points (1 to 28 DIV) from cells re-plating. Data are plotted as the averaged percentages of reduced AB ± Standard Error (SE) versus DIV, Student's *t*-test, * = pval < 0.05, ** = pval < 0.01, *** = pval < 0.001. (For interpretation of the references to color in this figure legend, the reader is referred to the web version of this article.)

Rapidly activating, non-inactivating, voltage-dependent whole-cell currents were elicited with the family of voltage-step protocols at potentials positive to −40 mV (Fig. 9B) either on astrocytes plated on aligned -GEL and +GEL. A comparative analysis, obtained by an I/V plot of averaged values of maximal current, recorded for each voltage step (Fig. 9C), revealed a similar voltage-dependent profile of whole-cell peak and steady state currents of astrocytes plated on aligned –GEL and +GEL samples. The latter ramp and step current profile was comparable to the one recorded on cells plated on PDL (Supplementary S5). All the data indicate that astrocytes plated on -GEL, +GEL have voltage-gated K+ channels activated at membrane potentials more positive than −40 mV and that the properties among the conditions are preserved and not altered by the topography nor by the blended gelatin.

The present work aimed to analyse the impact of topographical and chemical cues of electrospun fibres on the viability as well as on the structural and functional properties of astrocytes.

For this purpose, we provided a comparative study of the response of astrocytes on −GEL and +GEL fibres. Recent literature demonstrated that PCL electrospun fibres accurately replicate the physical dimensions and fibrillary organization of the collagen network into the native extracellular matrix [33]. However, PCL electrospun fibres present some lacks in terms of cell affinity and biorecognition, mainly due to their intrinsic hydrophobic properties [34]. Hence, the integration by different ways (i.e., blending, grafting, adsorption) of bioactive proteins

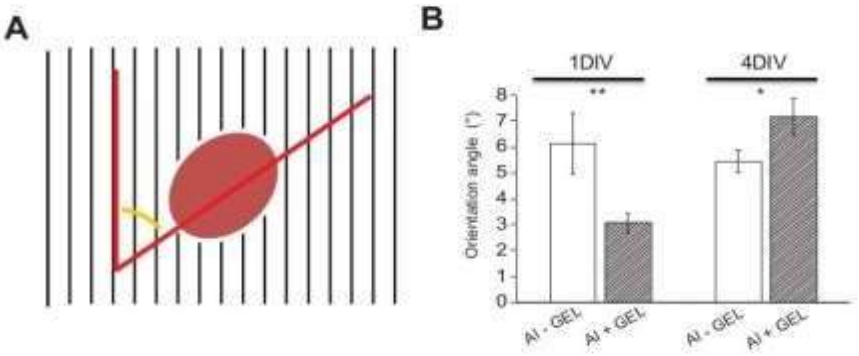


**Fig. 7.** Alignment of astrocytes on PCL fibres. A) Scheme representing the criteria used to measure cell alignment angle. B) Bar plot reporting the averages of orientation angles measured between astrocytes and fibres (1 DIV, 4 DIV) plated on aligned -GEL samples (Al-GEL, white bar, n = 38 at 1 DIV, n = 40 at 4 DIV) and aligned PCL +GEL (Al + Gel, n = 60 at 1 DIV, n = 35 at 4 DIV) substrates. Student's *t*-test, * = pval < 0.05, ** = pval < 0,01.

from collagenous source can improve the interface interactions between cells and the surrounding fibres, by promoting basic recognition (i.e., adhesion, spreading, migration) and physiological mechanisms (i.e., proliferation, differentiation) [34].

Our results showed that the fibres alignment and, thus, the topography are the key feature that promote astrocytes adhesion, viability and growth, while chemical clue such as GEL and hydrophobicity play a major role in promoting cell alignment. Previous studies reported that chemical blending of PCL with Gelatin enhances the hydrophilicity of the polymer, and promoting the adhesion of neuronal-like cell lines as well as their neurite outgrowth [35].

Here we found that GEL blending to the PCL fibres allows significantly improving the hydrophilic properties of the fibres as confirmed by contact angle measurements (Fig. 2). However, the increase in hydrophilicity of +GEL samples compared to -GEL substrates is not further improving adhesion of astrocytes to the PCL fibres. Accordingly, we found that, in the case of protein films (i.e., silk fibroin), the adhesion and growth of astrocytes was higher on more hydrophobic surface [9,36], whereas the surface hydrophilicity improved neurite outgrowth of primary dorsal root ganglion neurons. Moreover, +GEL samples display peculiar sub micrometric sizes lower than those of -GEL ones (Fig. 4) which is not favouring astrocytes adhesion. This data is in line with recent studies reporting that astrocytes showed significantly increase in elongation and adhere preferentially, when seeded on the large diameter fibres, with respect to values of cells plated on small diameter fibres [37]. In addition, more efficient extension of astrocytes on larger diameter fibres allow better outgrowth of neurites of dorsal root ganglia neurons plated on them [37].

It is not surprising that neurons and astrocytes respond differently to the surface topography and chemistry. While neurons adhesion to substrates depends upon the presence of extracellular matrix factors and components [37], astrocytes cell cultures are capable to release adhesive and repulsive ligands, including collagen, laminin, fibronectin and to chemically shape the surrounding environment [37,38]. Interestingly, aligned astrocytes on polydioxanone improve neurite outgrowth of DRG neurons compared with substrates with unaligned fibres or with those without astrocytes.

The ability of astrocytes to sense surface topography is well documented. Notably, adhesion of astrocytes on flat inorganic substrates or highly hydrophobic surfaces like organic semiconductors needs to be improved by coating with ECM components or poly-ionic substances such as Poly-o-Lysine or anchoring molecules such as Phospholipids [7,21,39,40]. On the other hand, nanotopographic clues such as nanoislands, nanorods or electrospun nanofibres are sufficient to improve astrocytes adhesion and viability [8,9] with respect to unstructured ones. In this view, our data are in agreement with the literature

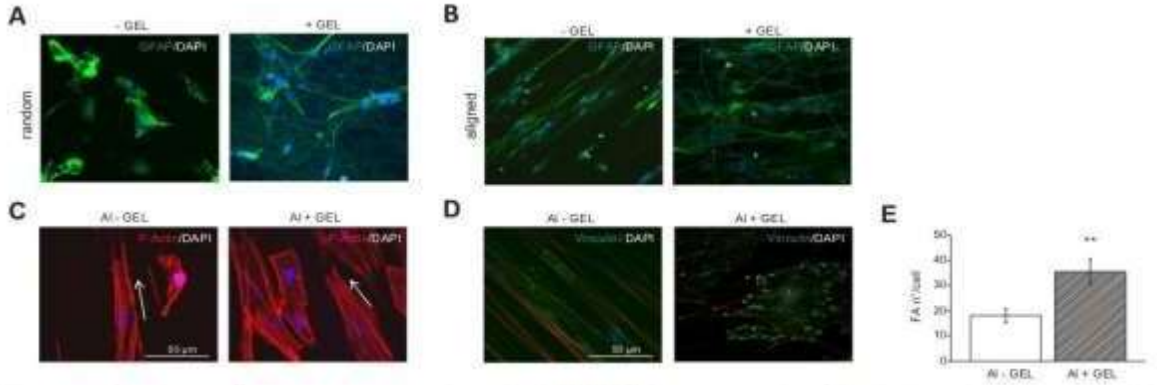


**Fig. 8.** Impact of PCL electrospun fibres on astrocytes structural properties. (A–B) Confocal images representative of GFAP/DAPI expression in astrocytes seeded on random -GEL, +GEL (A), and aligned −GEL, +GEL (B), captured after 3 DIV from cell re-plating. C) Confocal images of Phalloidin-TRITC staining of the cytoskeleton (red) and of DAPI in the nuclei (blue) of astrocytes plated on aligned -GEL and +GEL substrates, collected after 3 DIV from the re-plating. White arrows show the oriented F-actin fibres directions. D) Confocal images of astrocytes plated on aligned −GEL and +GEL substrates immune-stained for Vinculin (green) and with DAPI (blue staining), collected after 3 DIV from the re-plating. E) Bar plot shows the number of vinculin contacts per cell, counted after 3 DIV from the cells re-plating in cells plated on aligned −GEL and +GEL substrates. Data are expressed as means ± S.E. (n: −GEL = 124; +GEL = 138), Student's *t*-test, ** = pval < 0.01. (For interpretation of the references to color in this figure legend, the reader is referred to the web version of this article.)

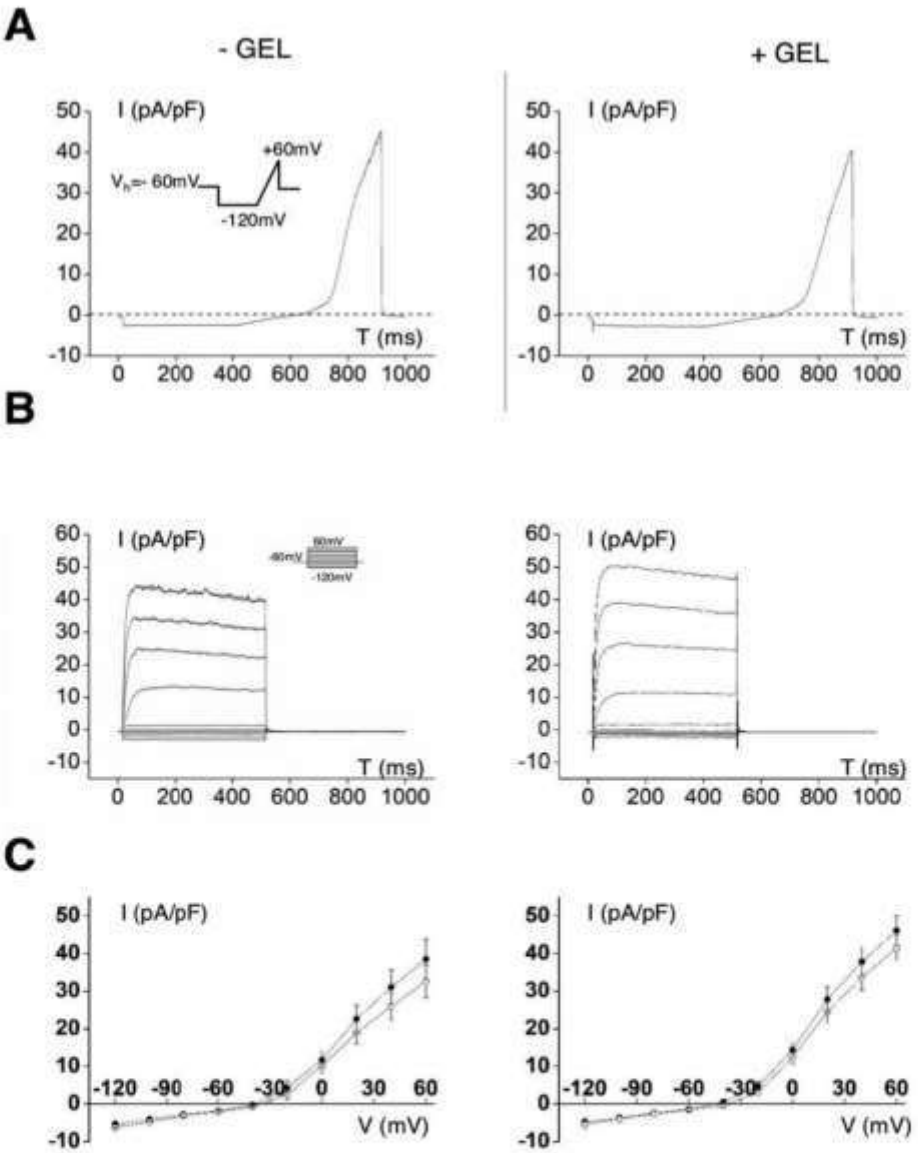


**Fig. 9.** Functional properties of astrocytes plated on aligned -GEL and +Gel substrates. A) Current traces recorded stimulating astrocytes with a voltage ramp protocol (inset A) from Vh of −60 mV from −120 to +60 mV (500 ms), in cells plated on aligned–GEL and +GEL substrates. B) Representative current traces elicited by the response to a voltage step protocol from Vh of −60 mV, from −120 mV to +60 mV with potential steps of 20 mV, recorded in aligned -GEL and +GEL. C) I-V plots: Mean values of maximal current values of astrocytes plated on PCL -GEL and +GEL. I-V plots have been generated by calculating the average of the maximal current values recorded at potential steps of 20 mV at peak (black circles) and steady state (white circles) and normalized for the relative cell capacitance values. No statistical were observed on averaged currents in I/V plot (n = 10 for -GEL and n = 11 for +GEL); ANOVA test, pval > 0.05.

demonstrating that the proliferation and survival of astrocytes on aligned -GEL substrates are the highest with respect to other samples tested over the long term.

Of note, the higher proliferation rate is not due to the gliotic reaction as GFAP expression, a typical marker of gliosis is not enhanced by the growth of astrocytes on electrospun nanofiber with respect to PDL.

We found that aligned fibres induce a strong orientation of astrocytes along the fibres showing the ability of the PCL substrates to impact astrocytes morphology (Fig. 6). These data are in agreement with previous studies showing the potential of nanotopography to regulate astrocytes cell shape, polarity and differentiation [8,40]. Accordingly, our studies using nanostructured films made of hydrotalcite or gold-coated silicon nanowire [36] induce dramatic differentiation of astrocytes with a long process extending randomly over the substrates.

Here, we found that PCL electrospun nanofibres strongly impact on astrocytes morphology inducing a more elongated phenotype with

**Table 3**
Electrophysiological properties of astrocytes plated on -GEL and +GEL substrates. Cp, membrane capacitance; Vmem, resting membrane potential; SG, mean specific conductance; IR, input resistance; I, current density. n = 9 for -GEL and n = 12 for +GEL. None of the electrophysiological properties recorded in astrocytes grown on different substrates were significantly different (pval > 0.05).

| | Cp (pF) | $V_{mem}$ (mV) | SG (ns/pF) | IR (MΩ) | I(pA/pF) −120 mV | I(pA/pF) +60 mV |
|---|---|---|---|---|---|---|
| PDL | 51.8 ± 6.8 | −34.5 ± 2.7 | 0.04 ± 0.01 | 877 ± 327 | −4.8 ± 0.8 | 47.7 ± 5.7 |
| −GEL | 66.1 ± 16.2 | −36.5 ± 3.6 | 0.05 ± 0.01 | 566 ± 72 | −4.5 ± 0.8 | 40.0 ± 6.7 |
| +GEL | 64.9 ± 10.1 | −49.7 ± 7.1 | 0.04 ± 0.01 | 812.3 ± 293.3 | −4.4 ± 0.7 | 45.6 ± 4.5 |

respect to polygonal form observed on random and PDL coated substrates. We hypothesise that nanofibres can interact with astrocytes cytoskeletal proteins such as F-Actin and vinculin to induce their rearrangement that, in turn, affect cell shape balance between blast-like, polarized, elongated proliferating/migrating cells. Accordingly, we found that aligned PCL electrospun nanofibres promoted vinculin rearrangement and patchy distribution over the fibres. We also observed F-actin fibres stress and alignment with the fibres. Noteworthy, cell alignment is also supported by the presence of Gelatin at 1DIV. Indeed, the distribution of vinculin was more polarized on cells plated on Aligned +GEL samples and the number of FA was much higher in +GEL samples than in aligned -GEL ones (Fig. 8). Thus, it is plausible that GEL has a favourable effect on movement and alignment of the cell along the fibres, and that the chemical cue has a dominant effect with respect to the one of the dimension the fiber [37]. The effect of lower alignment, observed at 4 DIV in aligned GEL samples, can be ascribed to the gradual release of blended GEL from the PCL samples. The latter phenomena might then favour the dimensional cue of the nanofibers. As a result, according to previous studies [37], at 4 DIV, the alignment of astrocytes is higher on fiber with larger diameter fibres (−GEL). On the other side, GEL had no impact on stressed fibres presence, that were sufficiently induced by nanotopographic cues.

The main finding of the present work is that PCL aligned electrospun nanofibres do not impact on $K^+$ channels functionality, required for astrocytes homeostatic properties. Importantly, data reported on passive membrane properties of astrocytes plated on aligned +GEL and -GEL, resemble those of previous studies with primary astroglia plated on PDL (Supplementary S5), polystyrene Petri dishes, silk fibroin or organic semiconductor coated with PDL [36,41]. Similarly, analyses of time and voltage dependency revealed similar biophysical features of cell current on +GEL and -GEL that overlaps those of delayed rectifier potassium current previously characterized in immature glial cells [8]. Collectively the results indicated that +GEL and -GEL preserve astroglia electrophysiological properties while alignment is not paralleled by alteration of $K^+$ conductance.

We have previously shown that the stellation and differentiation, that characterize astrocytes grown on inorganic nanostructured bidimensional films, was accompanied by an alteration in the expression and function of potassium channels [8,36]. In the present work, we found that changes in cell morphology, are not impacting on astrocytes functionality and that astrocytes on aligned substrates essentially behave as on a flat surface. As confirmed by Alamar Blue analyses, astrocytes remain on a proliferating functional phase, which is typically characterized by the presence of potassium delayed rectifier potassium conductance. The data is in line with evidence indicating that potassium conductance is critical for cell proliferation and differentiation. Accordingly, recent evidence showed that potassium conductance changes and drive stem cell differentiation to counteract neurodegeneration [42,43].

Potassium channels have a fundamental role in astrocytes as they set the membrane potential and allow its changes occurring after neuronal activity. Following acute brain insults, they are altered in astrocytes surrounding the lesion site, where reactive gliosis occurs [31,35]. In addition, protein expression and function of potassium channels are considered critical for cell invasion and the formation of metastatic brain glioma [44,45].

Since there is no effect on the $K^+$ current in astrocytes, we conclude that PCL represents a suitable substrate for studying and manipulating brain astroglial ion channels by means of tailored functional/molecular chemical modification of PCL skeleton.

Of note, the long-term survival (almost 1 month) is a unique data reported in the present work, thus validating the use of PCL as a platform for future *in vivo* testing in neurological conditions.

On this regard, the recent critical role highlighted for astrocytes protein channels in neuropathic pain derived from peripheral nerve injury opens the perspective for the use of PCL electrospun scaffold as glial interface for the therapy of gliopathies.

## 4. 5. Conclusion

The validation of the use of PCL electrospun fibres for CNS injuries regeneration requires, as a first step, an understanding of appropriate neural cells-substrate interactions (growth, morphology, differentiation, functional properties). Considering the well documented role of astrocytes for the nervous system function, we aim at investigating the structural and functional impact of topographical and chemical cue sof PCL electrospun fibres on the response of astrocytes *in vitro* [8,20,46].

Here, we demonstrate that the aligned electrospun -GEL and +GEL fibres, enable long term viability, growth and alignment of astrocytes even after weeks of culture, and that the mechanisms underpinning the differentiation, involves the actin cytoskeleton rearrangement and focal adhesion complex. Also, we showed that astrocytes elongation along the fibres occurs without altering the properties of potassium channels, indicating that PCL electrospun fibres are permissive substrate to drive specific astrocytes properties depending on the targeted applications [47,48]. It was suggested the stability of implant devices, targeting neuroregenerative medicine, requires tight and permissive interactions between the cell membrane of astrocytes and the biomaterials interface [49]. Our results suggested that the favourable interaction of astrocytes with PCL nanosubstrates, as well as the active ability of the substrate to drive astrocytes behaviour, further strengthen the application of PCL electrospun fibres in neuroregenerative strategies aiming to support the axonal outgrowth. It is worth noting how recent studies evidence the possibility to rescue brain functionality in degenerative disease models, by changing structural and functional features of astrocyte [43,50,51]. The versatility of the presented PCL based approach, that allows to add functionalities to the scaffold such as drug delivery or conductivity, broadens the spectrum of approaches that can be used to drive the behaviour of astrocytes for an astrocytes-targeted regenerative therapeutic approach.

## CRediT authorship contribution statement

E.S. prepared and maintained rat primary culture, performed and analysed patch-clamp experiments, contributed to the manuscript preparation and editing, performed immunofluorescence staining and alignment image analyses. V. C., M. M. and V.G. synthetized and fabricated the fibres samples, performed the SEM and AFM imaging and analyses. L. A. and R. Z. contributed to the discussion of the results and to the editing of the manuscript. V.G. and V.B. coordinated the research

effort, designed the experiments, wrote the manuscript.

## Declaration of competing interest

The authors declare that they have no known competing financial interests or personal relationships that could have appeared to influence the work reported in this paper.

## Acknowledgements

This work has been financially supported by Air Force Office of Scientific Research- AFOSR with the following grants: AFOSR, grant name: 3D NEUROGLIA, grant number, FA9550-18-1-0255; AFOSR, grant name ASTROMAT, grant number, FA9550 16-1-0502; AFOSR, grant name ASTRONIR, grant number, FA9550-17-1-0502 and by Emilia-Romagna Region, Por-Fers 2014–2020, grant name MAT-2-REP.

We are grateful to Dr. Marco Caprini, Francesco Formaggio and Dr. Alessia Minardi from the Dept. of Pharmacy and Biotechnology (FABIT) at the University of Bologna for their assistance with astrocyte cell culture preparation. Scanning Electron Microscopy was supported by the Transmission and Scanning Electron Microscopy Labs (LAMEST) of the National Research Council.

## Appendix A. Supplementary data

Supplementary data to this article can be found online at https://doi.org/10.1016/j.msec.2020.111363.

## References

[1] V. Benfenati, S. Ferroni, D. Rozzo, S.A. Masino (Eds.), Homeostatic Control of Brain Function, first edition, vol. 1, Oxford University Press, 2015, pp. 3–40.
[2] A. Verkhratsky, M. Nedergaard, Physiol. Rev. 98 (2018) 239–389.
[3] C.L. Luo, M. Kinnavane, et al., J. Neurochem. 130 (2014) 215–226.
[4] V. Pérez, C. Fernandez, et al., J. Neurosci. 21 (2005) 26–32.
[5] J.W. Salatino, K.A. Ludwig, D.Y. Kozai, E.K. Purcell, Nat. Biomed. Eng. 1 (2017) 862–877.
[6] A. Chvátal, M. Anderová, et al., J. Neurosci. Res. 85 (2007) 260–271.
[7] M. Dumas, A.I. Barrachina-Cuesta, et al., J. Mater. Chem. B 6 (2018) 5335–5342.
[8] T. Pouti, A. Pistone, et al., Sci. Rep. 6 (2016) 1–16.
[9] M. Bramini, S. Sacchetti, et al., ACS Nano 10 (2016) 7154–7171.
[10] V. Cirillo, V. Guarino, et al., J. Mater. Sci. Mater. Med. 25 (2014) 2323–2332.
[11] J. Xie, M.R. MacEwan, A.G. Schwartz, Y. Xia, Nanoscale 2 (2010) 35–44.
[12] V. Cirillo, B.A. Clements, et al., Biomaterials 35 (2014) 8970–8982.
[13] P.S. Donoghue, R. Lammel, et al., Tissue Eng. Part A 19 (2013) 497–507.
[14] S.K. Min, C.R. Kim, S.H. Kim, H.S. Shin, J. Nanomater. 2014 (2014) 1–8.
[15] S.K. Min, S.H. Kim, C.R. Kim, S.M. Paik, et al., Neurosci. Lett. 8 (2013) 80–84.
[16] R.J. Gilbert, M.K. Gorsuch, J.M. Zuidema, Cells Tissues Organs 205 (2018) 372–393.
[17] J.K. Alexander, R. Fuss, R.J. Colello, Neuron Glia Biol. 2 (2006) 93–103.
[18] S. Ferroni, C. Marchini, P. Schubert, C. Rapisarda, FEBS Lett. 367 (1995) 319–325.
[19] V. Benfenati, S. Toffanin, et al., Biomaterials 31 (2010) 7883–7891.
[20] A. Signelli, A. Pistone, et al., RSC Adv. 6 (2016) 9304–9314.
[21] V. Benfenati, N. Martino, et al., Adv. Healthcare Mat. 3 (2014) 392–399.
[22] E.S. Gil, S.H. Park, J. Marchant, et al., Macromol. Biosci. 10 (6) (2010) 664–673.
[23] V. Guarino, V. Cirillo, R. Altobelli, L. Ambrosio, Expert Rev. Med. Devices 12 (2015) 1113–1120.
[24] M. Marrese, V. Guarino, L. Ambrosio, J. Funct. Biomater. 8 (2017) 1–26.
[25] A. Guarino, V. Guarino, et al., Biotechnol. Bioeng. 108 (2011) 8.
[26] M. Marrese, V. Guarino, Int. J. Polym. Mater. 67 (2018) 961–966.
[27] A. Barrachina-Cuesta, E. Saracino, et al., Adv. Healthc. Mater. 8 (2019) 1–12.
[28] M. Marrese, V. Cirillo, V. Guarino, L. Ambrosio, J. Funct. Biomater. 9 (2) (2018) 27.
[29] V. Benfenati, M. Caprini, M. Nobile, J. Neurochem. 98 (2) (2006) 430–445.
[30] M. Bramini, A. Riccio, P. Benfenati, P. Cesca, Adv Neurobiol. 22 (2019) 53–79.
[31] S. Ferroni, C. Marchini, M. Nobile, C. Rapisarda, Glia (1998) 1099–1136.
[32] V. Benfenati, M. Amtmy-Meghaddam, M. Caprini, Neurosci. 146 (4) (2007) 876–892.
[33] J. Fernández-Pérez-ah, K.E. Kadreabc, A.P. Lynchaih, M. Ahearneah, Mater. Sci. Eng. 108 (2020) 110415.
[34] M. A. Alvarez-Perez, V. Guarino, V. Cirillo, L. Ambrosio, Biomacromolecules, 11, 9, 2238–2246.
[35] V. Guarino, V. Cirillo, L. Ambrosio, Expert Rev. Med. Devices, 13,83–102.
[36] E. Saracino, L. Mainiu, et al., Adv. Biosystems (2020) 1901264.
[37] D.L. Christopher, J.M. Johnson, et al., ACS Appl. Bio Mater. 2 (2019) 104–117.
[38] W.N. Chow, D.G. Simpson, J.W. Bigbee, R.J. Colello, Neuron Glia Biol. 3 (2007) 119–126.
[39] E. Guadagno, H. Moukhles, Glia 47 (2004) 138–149.
[40] S. Marchetto, L. Ballerini, et al., Science 9 (2017) 1010–1011.
[41] E. Rut, D. Blum de Oliveira, et al., Tissue Eng. Part A 16 (2010) 3173–3184.
[42] S. Sandelacznr, M. Levin, D.L. Kaplan, Stem Cell Rev. 5 (2009) 231–246.
[43] K.L. Turner, H. Sontheimer, Philos. Trans. R. Soc. Lond. Ser. B Biol. Sci. 369 (2014) 1–9.
[44] R.R. Ji, C.R. Donnelly, M. Nedergaard, Nat. Rev. Neurosci. 11 (2019) 667–685.
[45] H. Pivonkova, M. Anderova, Curr. Pharm. Des. 23 (2017) 5056–5074.
[46] J. Gerardo-Nava, T. Führmann, et al., Neuromolecular 9 (2008) 1.
[47] N. Saadatkish, S.N. Kheraani, J. Biomed. Mater. Res. Part A 106 (2018) 2394–2401.
[48] R. Bai, G. Gao, Y. Xing, H. Xun, Neural Regen. Res. 8 (2013) 2656–2665.
[49] W. Salatino, K.A. Ludwig, D.Y. Kozai, et al., Nat. Biomed. Eng. 1 (2017) 862.
[50] H. Qian, X. Kang, J. Hu, et al., Nat. 582 (2020) 550–556.
[51] H. Zhou, J. Su, X. Hu, et al., Cell 181 (3) (2020) 580–603.

### 1.2 Introduction to Paper 2

"*Polyaniline nano-needles into electrospun bio active fibres support in vitro astrocyte response*" by **Emanuela Saracino,* Simona Zuppolini, Vincenzo Guarino,* Valentina Benfenati, Anna Borriello,* Roberto Zambonia Luigi Ambrosio,** has been published as Open Access publishing on RSC Advances Journal, 2021, 11, 11347, DOI: 10.1039/d1ra00596k.

https://pubs.rsc.org/en/content/articlelanding/2021/RA/D1RA00596K.

Supplementary information accompanies this paper at:

https://www.rsc.org/suppdata/d1/ra/d1ra00596k/d1ra00596k1.pdf?_ga=2.65611501.2583609.1639495321-97415880.1639495320



The bioelectrical response of glial cells represents a key of interest in the neuroregenerative study. Taking advantage of the previous results published in the work presented in the paragraph 1.1, **Chapter IV**, here electrospun nanofibres based on PCL: PCL (−GEL) and blending of PCL and Gelatin protein (+GEL). are embedded with the nanostructure of a conductive polymer, polyaniline (PANi), synthesised in the form of nano-needles (PnNs), where peculiar is the fibre nanoscale size and alignement. The final scaffold is an electrically conductive interface able to support the growth and elongation of astrocytes' body without affecting an inflammatory reaction, accordingly the functional properties of astrocytes are measured by patch clamp. experiments reveal that PnNs do not alter the bioelectrical properties of resting astrocytes. Both the electrospun PnNs substrates result as biocompatible and not toxic for glial cells even at long time

points of investigation. The following substrate opens the way to a new perspective of investigation on the biophysical properties of astrocytes, by the use of a specific and tuneable glia interface that can be potentially used to stimulate and possibly record astrocytes, aiming at the recovery of neuronal structure and function.

**PDF -FORMATO PAPERS\Saracino E., et al., RSC Advance 4.2.pdf**

RSC Advances



PAPER

View Article Online
View Journal | View Issue



Cite this: RSC Adv., 2021, 11, 11347

# Polyaniline nano-needles into electrospun bio active fibres support *in vitro* astrocyte response†

Emanuela Saracino,[*a] Simona Zuppolini,[b] Vincenzo Guarino,[*b] Valentina Benfenati,[a] Anna Borriello,[*b] Roberto Zamboni[a] and Luigi Ambrosio[b]

Recent studies have proposed that the bioelectrical response of glial cells, called astrocytes, currently represents a key target for neuroregenerative purposes. Here, we propose the fabrication of electrospun nanofibres containing gelatin and polyaniline (PANi) synthesized in the form of nano-needles (PnNs) as electrically conductive scaffolds to support the growth and functionalities of primary astrocytes. We report a fine control of the morphological features in terms of fibre size and spatial distribution and fibre patterning, *i.e.* random or aligned fibre organization, as revealed by SEM- and TEM-supported image analysis. We demonstrate that the peculiar morphological properties of fibres – *i.e.*, the fibre size scale and alignment – drive the adhesion, proliferation, and functional properties of primary cortical astrocytes. In addition, the gradual transmission of biochemical and biophysical signals due to the presence of PnNs combined with the presence of gelatin results in a permissive and guiding environment for astrocytes. Accordingly, the functional properties of astrocytes measured *via* cell patch-clamp experiments reveal that PnNs do not alter the bioelectrical properties of resting astrocytes, thus setting the scene for the use of PnN-loaded nanofibres as bioconductive platforms for interfacing astrocytes and controlling their bioelectrical properties.

Received 22nd January 2021
Accepted 5th February 2021

DOI: 10.1039/d1ra00596k

rsc.li/rsc-advances



## 1. Introduction

Recent studies have demonstrated that external electric field stimulation can accelerate nerve regeneration by supporting the exchange of information by neurons both *in vitro* and *in vivo*.[1] This effect can be corroborated by the use of biocompatible polymers with electrically conductive properties, which can promote cell adhesion by a controlled transfer of electrical signals and by the administration of moderate currents that avoid killing nerve tissue and cells.[1–4] In the last decade, several studies have investigated the use of electro-conductive materials as building blocks to design active interfaces between electronic and biological fields for various applicative uses (*i.e.*, molecular targeting, biosensors, biocompatible scaffolds).[5] Among them, electroactive polymers (EAPs) are emerging as a class of organic materials with intrinsic conductive properties, similar to those of metals and semiconductors, which can be accurately controlled by modifying chemical and physical surface properties in order to directly influence the charge mobility along the backbone of the polymer chain.[6–8] In this context, polyaniline (PANi) is a widely recognized EAP that shows good biocompatibility, high environmental stability and switchable properties between conductive and resistive states *in vitro*.[9] The peculiar chemistry of PANi, based on repeating units of aniline monomers with alternate single and double bonds, including phenyl rings with nitrogen atoms, promotes the formation of different oxidation states (*e.g.*, emeraldine, nigraniline, and leucoemeraldine) with chemical/physical properties that are suitable to fight inflammatory response and support cell growth.[10,11] According to recent studies, the biological response can be properly addressed as a function of the electronic properties of conjugated polymers, which are finely tuneable by manipulating topological (*i.e.*, the structure of the polymer backbone) and/or chemical factors (*i.e.*, nature/concentration of the dopant ions).[7,10–13]

With respect to nerve regeneration, while several studies have demonstrated the favourable interaction of neuronal cells with PANi and PANi-loaded fibres, allowing for the regeneration of neurites and functional excitability *in vitro* and *in vivo*,[12,14,15] studies are lacking on the effect of PANi on brain glial cells, called astrocytes. Astrocytes are cells in the central nervous system that are primarily involved in the regulation of the homeostatic balance of ions, water, and molecules in the extracellular space.[16] Although they are incapable of action potential, astrocytes express ion channels and bioelectric properties[17] with critical roles in brain cognitive functions such

[a]Institute of Organic Synthesis and Photoreactivity (ISOF), National Research Council of Italy, via Gobetti, 101, 40129, Bologna, Italy. E-mail: emanuela.saracino@isof.cnr.it

[b]Institute for Polymers, Composites and Biomaterials (IPCB), National Research Council of Italy, Mostra d'Oltremare, Pad. 20, V. le J. F. Kennedy 54, Naples, Italy. E-mail: vguarino@unina.it; vincenzo.guarino@cnr.it; borriell@unina.it

† Electronic supplementary information (ESI) available. See DOI: 10.1039/d1ra00596k

as learning and memory. Alteration in the morphology, cytoskeletal structure and ion channel function of astrocytes is implicated in acute and chronic pathologies.[17] It is worth noting that the inflammatory response to brain and nerve implants is mainly driven by alteration in glial cells and in particular to astrogliosis reactions, which cause dramatic changes in astrocyte morphology, increased expression of glial fibrillar acid protein (GFAP) and loss of or alteration in the expression and function of ion channels.[16-18]

Despite their inability to generate action potential, astrocytes can respond to electrical, mechanical and topographical stimuli provided by nanostructured material interfaces and devices.[18-20] However, nanostructured devices based on conductive substrates enable the recording of bioelectrical signals from primary differentiated astrocytes at a precise slow frequency. This evidence highlights the possibility and the need to generate glial interfaces that target structural and bioelectrical properties of astrocytes to induce signal promoting/supporting of neuroregenerative processes[19] or functional recovery of neurons.[21] Despite the rising interest in astrocytes in biomaterials design, a comprehensive study of the impact of conductive PANi biomaterials on the morphology, the cytoskeletal properties and above all on the ion channel function of astrocytes has never been reported. In this work, to address this lack of knowledge, we report the fabrication of a novel composite platform made of poly-ε-caprolactone (PCL) and embedded with gelatin and PnNs; it was fabricated *via* an electrospinning technique.

Electrospinning is the leading technology to fabricate fibrous scaffolds with random or aligned fibres that mimic the architecture of the extracellular matrix of natural tissues.[20] In order to improve the biological response, the blending of synthetic polymers with natural proteins, *i.e.*, collagen, gelatin, and zein, currently represents a consolidated strategy to impart selected biochemical cues that can more actively support *in vitro* cell interaction.[22]

Herein, electrically conductive nanocomposite platforms were obtained by embedding electro-conductive PANi into electrospun fibres, and the response of primary astrocytes grown on PANi nano-needles (PnNs) was evaluated in terms of adhesion, proliferation, morphology and bioelectrical activity.

## 2. Materials and methods

### 2.1 Materials

Poly-ε-caprolactone (PCL, $M_n$ 45 kDa), bovine gelatin type B (gel ~ 225 bloom) in powder form, chloroform ($CHCl_3$), and 1,1,1,3,3,3-hexafluoro-2-propanol (HFiP) were all purchased from Sigma Aldrich (Italy). For the synthesis of PnNs, aniline, ammonium peroxy disulphate (APS), camphor sulphonic acid (CSA), and emeraldine base polyaniline (EB, $M_w$ 10 kDa) were purchased from Sigma Aldrich (Italy). All chemicals were used as received without additional purification.

**2.1.1 PnNs synthesis and characterization.** Ultrafine short fibres of polyaniline doped with CSA were prepared as follows (Fig. 1A): 0.8 mmol of APS (*i.e.*, initiator) and 3.2 mmol of aniline (*i.e.*, monomer) were separately dissolved in a 1.0 MCSA-doped acid solution and rapidly mixed all at once. The appearance of bluish-green droplets of polyaniline were noticed within 30 minutes of the start of the reaction, and the synthesis was left to proceed for 2 hours at room temperature.

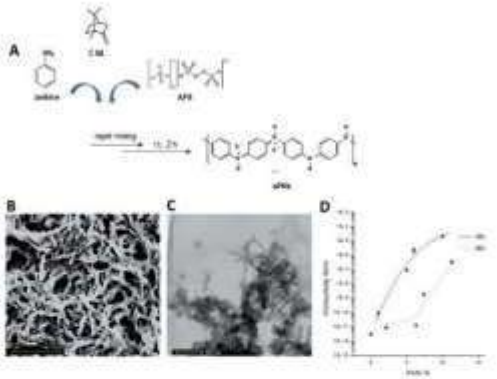


Fig. 1 Optimization of PnNs: (A) scheme of synthesis. Morphological analysis *via* (B) SEM and (C) TEM. Image analysis showed diameters ranging from 50 to 100 nm and lengths from hundreds of nanometers to several micrometers for a nanoneedle shape factor varying from 1 : 9 to 1 : 15. (D) Comparison of conductive curves of PnNs and EBPs obtained by fitting two-probe DC electrical resistance measurements.

The (as-prepared) nanofibres can be purified by centrifugation, a common solid–liquid separation technique. PNs were obtained in powder form after drying at 80 °C under vacuum. The dry powders of polyaniline were re-dispersed in HFIP by mild sonication. In order to validate the conductive properties of the PnNs, two-probe DC electrical resistance measurements were performed using a Signatone 1160 probe station connected to a picometer/voltage source meter (National Instrument) in ambient conditions. A custom cell was designed and realized in polytetrafluoroethylene (PTFE) to efficiently perform conductivity tests on these films.

In order to prevent surface current errors, the cell has an internal platinum circular electrode with a diameter of 10 mm and a guard ring placed at a distance of 0.5 cm. For these experiments, samples with different PCL/PnNs ratios (100/0, 99/1, 95/5, 90/10, and 80/20 wt/wt) were optimized to prepare thin casted films by solvent evaporation. As a control, EB-doped PANi samples (EBP) were prepared by doping of EB *via* CSA (50/50 wt/wt) and dissolution of the subsequent polymer in HFIP ($6 \times 10^{-3}$ M) at room temperature under magnetic stirring (2 h).

**2.1.2 Preparation of PnNs-loaded electrospun fibres.** The polymer solution was obtained by dissolving PCL in HFIP for 24 h under magnetic stirring. Then, gelatin was separately mixed to obtain a final polymer concentration of 0.1 g $ml^{-1}$ (1 : 1 w/w ratio).

Lastly, PnNs (5% wt with respect to the total polymer concentration) were added by gently stirring for a further 24 h. PnNs-loaded electrospun fibres were produced using electrospinning equipment (Nanon01, Mecc, Fukuoka, Japan) with an 18G needle and vertical configuration. Random and aligned

fibres were collected on small glass discs (diameter 12 mm) fixed on a rotating drum (diameter 19 cm) for 1 h. All the parameters (*i.e.*, flow rate, voltage, electrode distance, rotation speed) were optimized in order to obtain the best fibre morphology. As a control, electrospun fibres without PnNs were fabricated under the same processing conditions. The process parameters for all the electrospun fibres are summarized in Table 1. All the experiments were performed at room temperature within a range of relative humidity (RH) = 45–55%.

**2.1.3 Morphological analysis.** The morphology of the PnNs was preliminarily analyzed *via* bright field transmission electron microscopy (TEM, Jeol, JEM 1220, Japan) by re-dispersing PnNs in chloroform and subsequently depositing one drop of the dispersed solution on a copper grid covered with carbon. For these analyses, an acceleration voltage of 80 kV was set.

PnNs and PnNs-loaded fibres were analyzed by scanning electron microscopy (SEM; Quanta FEG 200, FEI, The Netherlands) in order to assess the morphology of the fibres. The specimens were sputter-coated with a Pd–Au nano layer (Emitech K550, Italy) and then observed under high vacuum conditions ($10^{-5}$ mbar) at a low voltage electron emission (lower than 10 kV) to minimize beam invasiveness on the polymer matrices. The mean diameter of the fibres was calculated from selected SEM images (*ca.* 20 units) by using image analysis software (ImageJ freeware 1.52a) and reported as diameter distribution and mean value ± standard deviation.

### 2.2 *In vitro* studies

**2.2.1 Rat cortical astrocyte culture preparation, maintenance, and plating.** Primary astroglial cultures were prepared at the University of Bologna, in concordance with the Italian and European law of protection of laboratory animals and the approval of the local bioethical committee (ethical Italian protocol number ID 1338/2020 PR, released in February, valid for 5 years). Astrocyte cultures were prepared as described previously.[16,35] After 3 weeks in culture, confluent astrocytes in 15% fetal bovine serum (FBS) were dispersed using trypsin–EDTA 0.25%, and the cell suspension was dropped on random and aligned samples of PCL–gelatin (−PANi) and PCL–gelatin blended with PnNs (+PANi) at concentrations of $8 \times 10^3$ cells per sample and maintained in culture medium containing 10% FBS. Flat portions of the substrates and cells plated on poly-D-lysine (PDL) were used as internal and comparative controls.

**2.2.2 Alamar Blue, fluorescein diacetate viability assay and confocal microscopy.** The viability and biocompatibility of astrocytes on fibrous PCL–gelatin-based samples were analysed *via* Alamar Blue (AB) assay according to the Interchim technical sheet (66941P) and to protocols previously described.[35,47] The time course of astrocytic viability on random and aligned −PANi and +PANi nanofibres was evaluated from 1 day *in vitro* (DIV) to 8 DIV after re-plating cells on the substrates. Analyses of the AB fluorescence and correlation with the viability were performed as described previously.[23] Data were collected from three separate experiments performed in quadruplicate and are expressed as means ± SE of the percentage of reduced AB.

The fluorescein diacetate assay (FDA) and evaluation of the morphology of astrocytes grown on aligned −PANi and +PANi electrospun fibres was performed 24 h (1 DIV) and 96 h (4 DIV) from the re-plating of astrocytes on the substrates.[23,24] A sequence of images (10 to 15 different fields for each sample) was taken using a Nikon TE 2000 inverted confocal microscope (40× objective). The orientation angle measurement of an individual cell was defined as previously described.[23] Results were analysed using the ORIGIN-PRO (Microcal) program. All the immune fluorescence and confocal microscopy experiments on astrocytes plated on different samples were performed as previously described.[26] The primary antibodies used were rabbit anti-vinculin (Life Technologies, Monza, Italy); anti GFAP (Sigma Aldrich); and donkey anti-rabbit Alexa Fluor 488-conjugated as a secondary antibody (1 : 1000, Molecular Probes-Invitrogen). F-actin fibres were stained for phalloidin-TRITC (Sigma-Aldrich, Milan, Italy). Coverslips were mounted with Prolong Anti-Fade with DAPI (Molecular Probes-Invitrogen). The optical images were taken with a Nikon TSE 2000 inverted confocal microscope and a Photometrics camera (Crisel Instruments). Data were collected at least from three different experiments performed in triplicate. At least 15 images for each replica of a condition were analysed by ImageJ software. The focal adhesion (FA) point density was expressed as means ± SE of the number of vinculin contacts counted for each image (300 μm × 300 μm) and divided by the number of nuclei (blue staining) in the same image.

**2.2.3 Electrophysiology and functional properties.** Current recordings were obtained in the whole cell configuration with the patch-clamp technique. Experiments were performed after 24 h of *in vitro* treatment. To ensure comparability between the conditions, only elongated astrocytes were selected to evoke whole cell currents; cells in control intra- and extracellular saline were held at −60 mV, and after stepping to −120 mV for 500 ms, a ramp was performed from −120 mV to +60 mV (500 ms) (inset Fig. 6A). To investigate the voltage and time-dependence of the conductance of cells seeded on −PANi and +PANi substrates, the astrocytes were stimulated with 500 ms voltage steps ($V_h$ = −60 mV) from −120 mV to +60 mV in increments of 20 mV (inset Fig. 6B).

**2.2.4 Statistical methods.** Data were elaborated using one-way analysis of variance (ANOVA, with Bonferroni's test). A statistically significant difference was reported as $P < 0.05$ or less. Data of biological experiments are reported as the mean ± standard error (SE). The number of experiments ($n$) is indicated in the text or in the figure legends. The results reported are the mean of at least 3 different experimental trials performed in triplicate or more.

## 3. Results and discussion

### 3.1 PANi electrospun nanofibre fabrication and characterization

Herein, we propose the fabrication of nanocomposite fibres containing PnNs – namely polyaniline synthesized in the form of nano-needles that can transfer electrical signals to support the growth and functionalities of primary astrocytes,

minimizing the cytotoxic effects. Indeed, the peculiar needle-like shape of the PnNs enables the formation of a percolative pathway of electrically conductive phases, drastically reducing the irrelative fraction into the fibre body. PnNs were endowed into bicomponent fibres obtained by blending PCL and gelatin, largely validated in terms of *in vitro* biodegradation and biomechanical and biocompatible response.[27–29] The morphology of the PnNs was investigated by SEM and TEM with the support of image analysis. Fig. 1B and C show PnNs with diameters in a range from 50 to 100 nm and average lengths from hundreds of nanometres up to a few micrometres. Conductivity tests confirmed that the electrical conductivity of the PnNs equaled 0.05 S $cm^{-1}$ in air and was not affected by the synthesis procedure, in comparison with previous data in literature.[28] Moreover, it was demonstrated that the properties of the PnNs were significantly higher than those of the EBPs, as confirmed by the comparison of the conductivity curves of the PnNs and EBP-loaded films (Fig. 1D). As a function of the conductive phase content, the results demonstrated a higher attitude of charge transport of the dispersed PnNs with respect to EBPs at the same volume fraction. Indeed, in the case of low fractions of EBPs, the peculiar globular shape tends to promote more limited contacts due to a large average distance among adjacent conducting phases. Indeed, the EBPs fraction must reach a critical value to generate an adequate number of punctual bridges that are suitable to form a conductive path that can percolatively transfer the electrical signal. In the case of PnNs, the peculiar shape factor of the nano-needles allows more efficient support of the formation mechanism of the contact points, thus originating percolative conductive pathways in the presence of lower amounts of the conductive phases. Therefore, it was identified that the critical value for PnNs corresponded to 5 wt% (Fig. 1D), and this concentration was used to fabricate electrospun fibres to investigate the biological response with astrocytes. In Fig. 2A and B, SEM images of random and aligned PnNs-loaded electrospun fibres are reported. As for the fibre processing, HFIP was selected to greatly dissolve gelatin and PCL and promote a fine dispersion of PnNs into the solution. Moreover, the high polarity of HFIP allows strong interactions with the electric field, thus promoting remarkable jet stretching with low-concentrated solutions (*i.e.*, 10% w/v).[30,31] As a consequence, the fibres showed a narrowed distribution of sizes, with mean diameters in the submicrometric range, equal to 0.44 ± 0.07 μm (Fig. 2C). No relevant differences in fibre size and distribution can be recognized due to the presence of PnNs (+PANi) in comparison with the controls (−PANi), as

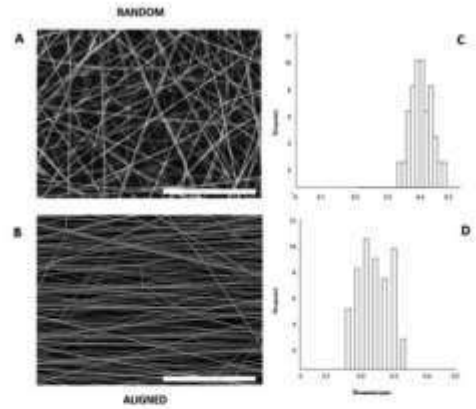


Fig. 2 Morphological analyses of PnNs-loaded electrospun scaffolds: SEM images of (A) random and (B) uni-axial aligned fibres (scale bar 10 μm); and (C and D) fibre diameter distributions *via* image analysis.

investigated in previous work.[27,32] Indeed, the presence of conductive phases mainly tends to promote the formation of free charges in solution; this helps stabilize the dispersion without altering the mechanism of fibre formation during the electrospinning process.[8,33] Hence, the resulting PnNs-added fibres were beadless and homogeneously dispersed. A different effect was recognized in the case of aligned fibres fabricated by collecting fibres onto the surface of a rotating collector. In this case, the mechanical drawing due to the high rotating rates significantly influences the solvent evaporation, consequently reducing the final diameters of the fibres to 0.25 ± 0.04 μm (Fig. 2D). No relevant differences in the fibre diameters can be recognized with respect to the aligned fibres without the presence of PnNs.[34] Instead, the PnNs mainly help promote a more efficient alignment of fibres due to the polarization of inherent charged groups of PANi in the solution, which tends to promote remarkable jet instabilities, *i.e.*, the whipping effect.

### 3.2 Effects of PANi electrospun nanofibre on the viability and morphology of primary astrocytes

In order to determine the impact of PnNs on astrocyte adhesion and morphology *in vitro*, confluent primary rat cortical astrocytes were re-plated on random and aligned substrates of +PANi and −PANi used as controls. We report typical bright field images (Fig. 3A) and fluorescent images (Fig. 3B) of viable (green) astrocytes captured at 2 DIV and at 4 DIV, plated on

Table 1 Summary of the electrospinning process parameters used

| | | Flow rate (ml $h^{-1}$) | Voltage (kV) | Electrode distance (mm) | Rotation speed (rpm) |
|---|---|---|---|---|---|
| Random | CTR<br>PANI | 0.5 | 13 | 120 | 50 |
| Aligned | CTR<br>PANI | 0.5 | 13 | 120 | 3000 |

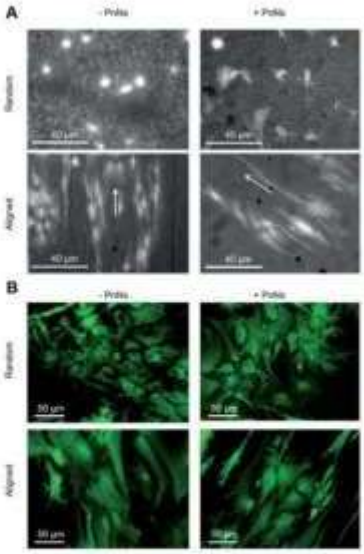

Fig. 3 Analyses of the effect of electrospun fibres on the morphology, viability and structural properties of astrocytes. (A) Bright field 20× micrographs representing astrocytes plated on random −PnNs, +PnNs (upper panel), and aligned −PnNs, +PnNs (below panel) substrates, captured after 4 DIV from cell re-plating. (B) Single plane confocal images of FDA-stained astrocytes, representing viable cells plated on random −PnNs, +PnNs (upper panel), and aligned −PnNs, +PnNs (below panel) substrates, captured after 4 DIV from cell re-plating.

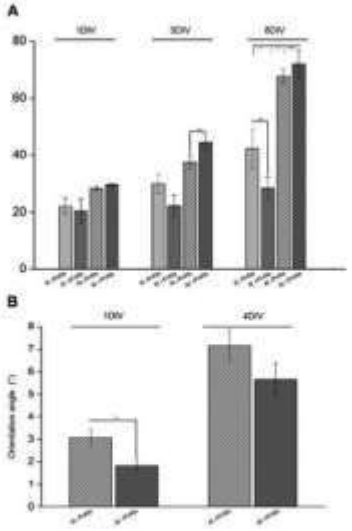

Fig. 4 (A) Time course of viability of astrocytes on random (R) and aligned (Al), −PnNs, +PnNs, investigated by AB assay at different time points (1 to 8 DIV) from cell re-plating. Data are plotted as the averaged percentages of reduced AB ± standard error (SE) *versus* DIV. (B) Bar plot reporting the averages of orientation angles measured between the astrocytes and fibres (1 DIV, 4 DIV) plated on aligned −PnNs, +PnNs samples (Al −PnNs, $n = 60$, Al +PnNs, $n = 36$ at 1 DIV) and (Al +PnNs $n = 35$, Al +PnNs $n = 42$ at 4 DIV) substrates.

random −PANi and +PANi (Fig. 3A and B, upper panels) and aligned −PANi and +PANi fibres (Fig. 3A and B, lower panels). Notably, the astrocytes on random substrates are polygonal, with a shape typically observed when the same type of culture is plated on PDL or on other biopolymers and bioorganic interfaces.[25,26] On the other hand, astrocytes grown on aligned −PANi and +PANi fibres appear elongated and aligned with the orientation of the fibres (Fig. 3A and B, lower panel, white arrows).

The bar plot reported in Fig. 4A shows the percentage of reduced AB with respect to the oxidized one; the value is proportional to the metabolic activity and, in turn, to the presence of viable cells. After 3 DIV, the viability value of +PANi samples was significantly higher compared to the value of aligned −PANi samples. A constant increase in cell viability was observed in −PANi and +PANi samples in both random and aligned conditions at 8 DIV. However, the cell proliferation rate was higher in both aligned −PnNs and +PnNs samples (ESI, S1†). The cells in the aligned samples with respect to random samples indicates that the topography of the nanostructure could positively impact cell survival. At 8 DIV, the presence of PnNs is associated with a higher cell viability only on the aligned samples.

The presence of PANi decreased the orientation angle at 1 DIV as well as at 4 DIV, indicating that the degree of alignment of cells is higher in the presence of the conductive polymer (Fig. 4B).

Astrocyte adhesion, growth and morphology can be altered or even driven by interactions with nanomaterials.[18,20,26,27,35,36] With respect to electrospun nanofibres, previous data indicated that the topography is the major superficial clue driving adhesion and growth of astrocytes.[25] Accordingly, in the present work, the aligned nanofibres display the best performance in terms of viability and growth of primary astrocytes over time. In addition, the presence of PnNs is associated with a higher viability of astrocytes, but only in the aligned samples. Different distributions or orientation patterns of PnNs in the aligned samples may account for the observed effect.

We next analyzed confocal imaging of immunostained cells, performed after 3 DIV, to give evidence of the comparable levels of the expression of glial fibrillar acid protein (GFAP), a well-known marker of the inflammatory reaction called astrogliosis, among cells grown on different samples (Fig. 5A, upper panel, random samples and Fig. 5A, lower panel, aligned samples). The typical images of phalloidin-stained cells reported in Fig. 5B show that astrocytes cultured on aligned −PANi and +PANi substrates express both stressed F actin fibres parallel to the pattern of −PANi fibres (Fig. 5B, white arrows).

Cells plated on random substrates (ESI S2†) displayed a disorganized structure of the F-actin fibres resembling those on PDL, as previously demonstrated.[37] The vinculin fluorescent signal analyses on cells grown on aligned −PANi substrates (Fig. 5C, left panel) indicated patchy but marked expression of the protein at the boundaries of the astrocytes, while the vinculin expression of astrocytes plated on aligned +PANi was more

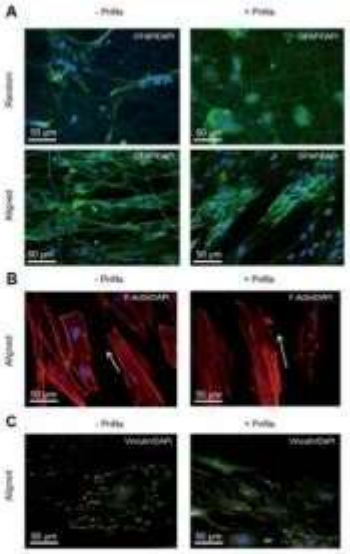

Fig. 5 (A) Confocal images representative of GFAP/DAPI expression in astrocytes seeded on random (upper panel) and aligned (below panel) −PnNs, +PnNs, captured after 3 DIV from cell re-plating. (B) Confocal images of phalloidin-TRITC staining of the cytoskeleton (red) and of DAPI in the nuclei (blue) of astrocytes plated on aligned −PnNs, +PnNs substrates, collected after 3 DIV from re-plating. White arrows are indicative of the oriented F-actin fibre directions. (C) Confocal images of astrocytes plated on aligned −PnNs, +PnNs, substrates immune-stained for vinculin (green) and with DAPI (blue), collected after 3 DIV from re-plating.

mislocalized in the cell body (Fig. 3G, right panel). Quantitative analysis revealed a higher number of focal adhesion (FA) points/cell on aligned −PANi with respect to the aligned +PANi substrates (ESI, S3†).

In our previous work, we demonstrated the effects of topography in a nanocomposite formed by electrospun PCL fibres and gelatin on the orientation and cytoskeletal properties of astrocytes. We have demonstrated that topography is the major factor affecting the morphology, alignment and structure of the cytoskeleton properties of astroglial cells, while the inclusion of adhesion-promoting protein gelatin shows a nonsignificant variation of the observed effect. In the present work, the presence of PANi nanoneedles induced a better degree of alignment. The ability of nanoneedle-shaped substrates to induce a mechanosensitive response, leading to cell alignment or morphological rearrangement, has been demonstrated.[37] The direct interaction of nanoneedles with cells prevents the formation and maturation of focal adhesions (FAs) at the cell–material interface and remodels the actin cytoskeleton proteins.

In line with this evidence, we found that PANi Nn reduced the FA number; however, it reshaped the actin cytoskeleton, promoting the expression of stressed fibres. These molecular events are associated with the presence of PANi and may account for (i) the morphological rearrangement of astrocytes and for (ii) the higher degree of alignment of the astroglial cell body with PCL fibres +PANi nanoneedles when compared to cells grown on PCL −PANi samples.

We observed a morphological rearrangement of astrocytes and redistribution of the cytoskeletal proteins vinculin and actin in the aligned nanofibres. In addition, in the presence of PnNs, we observed a higher degree of alignment of the cells to the fibres. We hypothesize that these effects are due to (1) the response of astrocytes to the nano-topographical cues conferred by the alignment of fibres. The data are in line with previous evidence indicating that the nano-topography of PCL nanofibres is sufficient to promote primary adhesion and alignment of astrocytes to the substrates.[35] (2) The data that cells grown on the substrates with embedded PnNs–PCL showed a higher degree of alignment, suggesting that the presence of PnNs in the PCL scaffold is implicated in the modification of the cell morphology and of the observed cell alignment. The latter phenomena can be ascribed to the nanostructure or the nanoneedles but also to the presence of conductivity properties in the needles. It has been widely demonstrated that changes in the functional properties of primary astrocytes can occur when these cells are grown on a nanostructured surface or on biocomposites with different compositions.[18,20,26,35,37] Recent and growing literature also describes that every cell type, including stem cells and glial cells, can sense the extracellular environment and change their electrical properties accordingly.[38]

However, changes in the electrical properties of astrocytes can be observed during gliotic reactions occurring in response to biomaterial implants.[18–20,23,28,80]

Thus, to analyze the impact of PANi on the bioelectrical properties of astrocytes, we next performed whole-cell patch-clamp measurements on single cells 24–48 h after re-plating on aligned −PANi and +PANi samples (Fig. 6).[20,26]

The passive membrane properties were calculated (ESI Table S1†) and revealed that the values of the voltage membrane ($V_{mem}$), input resistance (IR) and specific conductance (SpG) of the astrocytes on aligned −PANi and +PANi are very similar to those reported for primary astrocytes grown *in vitro* on PDL and simple PCL-based samples, while the membrane capacitance ($C_p$) of astrocytes seeded on +PANi substrates is significantly lower than that of those seeded on −PANi.[20,40] The capacitance of cells is a measure of the cell surface area.[39–41] Thus, the lower value of the cell capacitance of the cells grown on +PANi substrates confirms the morphological changes observed with the microscopical analyses.

The ramp-current traces for the astrocytes on both aligned −PANi and +PANi (Fig. 6A) as well as the voltage step family-evoked current analyses (Fig. 6B) indicated that astrocytes plated on −PANi and +PANi displayed voltage-gated delayed rectifier $K^+$ channels, previously observed in non-differentiated astrocytes *in vitro* and essential for astrocyte physiology *in vivo* (Fig. 6). The graph in panel 6C shows the *I*–*V* plots built with the mean values of the maximal current values of astrocytes plated on aligned −PANi and +PANi. *I*–*V* plots were generated by calculating the averages of the maximal current values recorded at the peak (black circles) and steady state (white circles) and normalized for the relative cell capacitance values in cells grown on −PANi and +PANi substrates. The plot quantitatively

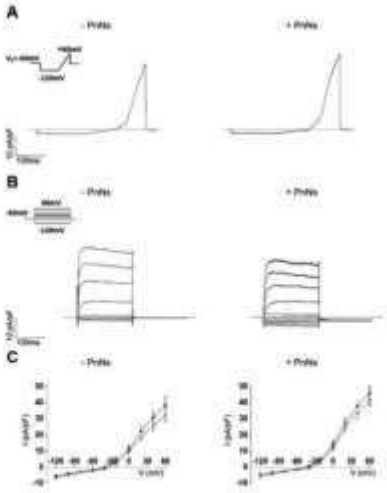


Fig. 6 Functional properties of astrocytes plated on aligned −PANi and +PANi substrates. (A) Current traces recorded by stimulating astrocytes with a voltage ramp protocol (inset A) from $V_h$ of −60 mV from −120 to +60 mV (500 ms) in cells plated on −PANi and +PANi substrates. (B) Representative current traces elicited by the response to a voltage step protocol from $V_h$ of −60 mV from −120 mV to +60 mV with potential steps of 20 mV, recorded in aligned −PANi and +PANi. (C) *I*–*V* plots: mean values of maximal current values of astrocytes plated on aligned −PANi and +PANi. *I*–*V* plots have been generated by calculating the average of the maximal current values recorded at potential steps of 20 mV at the peak (black circles) and steady state (white circles) and normalized for the relative cell capacitance values. No statistical differences were observed on averaged currents in *I*/*V* plot ($n$ = 12 for −PANi and $n$ = 16 for +PANi); ANOVA test, $p$ value >0.05.

represents the voltage and time dependency of the recorded currents. The data suggested that voltage and time-dependency of the whole-cell currents of astrocytes are not altered by the presence of PANi nanoneedles embedded in the PCL scaffold. Thus, the presence of PANi nanoneedles does not alter the biophysical properties of the whole cell currents of the astrocytes. Moreover, the analyses revealed that the magnitude and the biophysical profile of those currents was comparable to those previously described for astrocytes grown on PCL electrospun nanofibres, supporting the tenet that inclusion of PnNs in the fibres preserves the function of astrocytes *in vitro*.

It is known that the presence of a conductive substrate may rearrange the electric fields that can be locally generated by living cells, which in turn may affect cell morphology and behavior, even without the need for the application of an extracellular field.[42] The local electric fields generated by the cells correlate with the bioelectrical activity of the cells and, in turn, with the function or the expression of ion channels on the cell plasma-membrane. The resting bioelectrical properties as well as the voltage- and time-dependency of the currents recorded in the astrocytes are unchanged in the presence of PnNs. Given that the functional properties of the astrocytes observed in the presence or absence of PnNs are comparable, we cannot rule out that in line with other work on different substrates, the expression pattern of the protein channels can be altered by the presence of PANi and that this effect may be accompanied by or account for changes observed in the cell morphology.[20,26] Further investigations are needed with respect to this issue.

Previous studies reported different cell behaviours elicited in response to electrical stimulation, influencing directional cell movement, cell migration rate, cell alignment, cell division rate and orientation, and cell morphology.[2,4,38–41] With regard to astrocytes, recent studies indicated that is possible to modulate the structural and functional properties of astrocytes by acute and chronic application of extracellular electric fields.[38–41] Alexander *et al.* showed that orientation of astrocytes can be achieved by continuous extracellular electrical stimulation.[44] Nonetheless, astrocyte orientation promotes neurite outgrowth of neurons of the same co-culture.[13,44] The possibility to induce astrocyte migration by application of an extracellular electric field has also been demonstrated.[43] In addition, our group has recently demonstrated that an extracellular electric field applied by means of an organic cell stimulating and sensing transistor[44–47] evoked specific calcium signalling in astrocytes *in vitro*,[36] which is important for their cross-talk with neurons *in vivo*. All these data indicate that electrical stimulation of astrocytes is a potential therapeutic target (i) to drive astroglial cell migration at the lesion sites during inflammatory gliotic reaction, (ii) to promote the alignment of astrocytic processes that may support and direct neurite outgrowth of the injured area, or (iii) to acutely modulate their functional properties, which is essential for proper neuronal cell synaptic activity.

## 4. Conclusions

In the present work, we have investigated the effects of PnNs embedded into bioactive electrospun fibres on the viability as well as on the structural and functional properties of primary astrocytes. The integration of PnNs in the scaffold (i) allows adhesion and growth of astrocytes over time; (ii) supports actin cytoskeleton rearrangement and a focal adhesion complex by promoting a higher degree of cell alignment (iii) without relevant effects on the active/passive bioelectrical properties of the astrocytes.

It is well known that conductivity is a key material property for successfully recovering nerve injury and nerve outgrowth.[45,46] Our data confirm that the presence of PnNs in addition to peculiar topographic and chemical cues of the electrospun substrates may provide a functional interface that is permissive of the adhesion, growth and function of astrocytes. Given the clear evidence from other authors that driving the properties of astrocytes may further reinforce the outgrowth of neurons promoted by the nanostructured scaffold,[18,21,47] the electrospun fibre embedded with PnNs herein reported could represent a novel glial interface[18,49] that can be potentially used to stimulate and possibly record astrocytes, aiming at the recovery of neuronal structure and function.

## Conflicts of interest

There are no conflicts to declare.

## Acknowledgements

This work has been financially supported by AFOSR (ASTRO-MAT FA9550 16-1-0502, ASTRONIR FA9550-17-1-0502 3D NEUROGLIA FA9550-18-1-0255, ASTRODYN FA9550-19-1-0370) and Por Fesr Emilia Romagna 2014-2020 (MAT2REP PG/2018/626605).

## Notes and references

1 N. Yamamoto and G. Lopez-Bendito, *Eur. J. Neurosci.*, 2012, **35**, 1595–1604.
2 Q. Wang and W. Teng, *Int. J. Nanomed.*, 2016, **11**, 131–145.
3 C. E. Schmidt, V. R. Shastri, J. P. Vacanti and R. Langer, *Proc. Natl. Acad. Sci. U. S. A.*, 1997, **19**, 8948–8953.
4 Q. Zhang, D. Esrafilzadeh, J. M. Crook, R. Kapsa, E. M. Stewart, E. Tomaskovic-Crook, G. G. Wallace and X. F. Huang, *Sci. Rep.*, 2017, **7**, 42525, DOI: 10.1038/srep42525.
5 R. Balint, N. J. Cassidy and S. H. Cartmell, *Acta Biomater.*, 2014, **10**, 2341–2353.
6 K. Feron, R. Lim and P. C. Dastoor, *Int. J. Mol. Sci.*, 2018, **8**, 2382.
7 B. Li, V. Agarwal, D. Ho, J. P. Vede and K. L. Swaminathan, *New J. Chem.*, 2018, **42**, 7237–7240.
8 V. Guarino, S. Zuppolini, A. Borriello and L. Ambrosio, *Polymers*, 2016, **8**, 185.
9 L. Yu-Sang, C. Bei-Fan, L. Xiao-Jun, K. Z. Wei and T. He-Bin, *PLoS One*, 2014, **9**, e107361, DOI: 10.1371/journal.pone.0107361.
10 S. Kamalesh, P. Tan, J. Wang, T. Lee, E. T. Kang and C. H. Wang, *J. Biomed. Mater. Res.*, 2000, **52**, 467–478.
11 R. Sarvari, B. Massoumi, M. Jayman, Y. Beygi-Khosrowshahic and M. Abdollahid, *RSC Adv.*, 2016, **6**, 19437–19451.
12 L. Huang, X. Zhuang, J. Hu, L. Lang, P. Zhang, Y. Wang, X. Chen, Y. Wei and X. Jing, *Biomacromolecules*, 2008, **9**, 850–858.
13 P. R. Bidez, S. Li, A. G. Mac Diarmid, E. C. Venancio, Y. Wei and P. I. Lelkes, *J. Biomater. Sci., Polym. Ed.*, 2006, **17**, 199–212.
14 A. Borriello, V. Guarino, L. Schiavo, M. A. Alvarez-Perez and L. Ambrosio, *J. Mater. Sci.: Mater. Med.*, 2011, **22**, 1053–1062.
15 Q. Zhang, S. Beirne, K. Shu, D. Esrafilzadeh, X. F. Huang and G. G. Wallace, *Sci. Rep.*, 2018, **8**(1), 9855, DOI: 10.1038/s41598-018-27784-5.
16 V. Benfenati and S. Ferroni, *Neuroscience*, 2010, **168**(4), 926–940.
17 A. Verkhratsky and M. Nedergaard, *Physiol. Rev.*, 2018, **98**, 239–389.
18 L. Maiolo, V. Guarino, E. Saracino, M. Melucci, A. Convertino, L. Ambrosio, M. Muccini, R. Zamboni and V. Benfenati, *Adv. Healthcare Mater.*, 2021, **10**, 2001268.
19 J. W. Salatino, K. A. Ludwig, D. Y. Kozai and E. K. Purcell, *Nat. Biomed. Eng.*, 2017, **1**, 862–867.
20 S. Ferraris, S. Spriano, A. C. Scalia, A. Cochis, L. Rimondini, I. Cruz-Maya, V. Guarino, A. Varesano and C. Vineis, Topographical and Biomechanical Guidance of Electrospun Fibers for Biomedical Applications, *Polymers*, 2020, **12**(12), 2896.
21 J. M. Zuidema, R. J. Gilbert and M. K. Gottipati, *Cells Tissues Organs*, 2018, **205**, 372–395.
22 I. Cruz-Maya, A. Varesano, C. Vineis and V. Guarino, Comparative Study on Protein-Rich Electrospun Fibers for in Vitro Applications, *Polymers*, 2020, **12**, 1671, DOI: 10.3390/polym12081671.
23 E. Saracino, L. Maiolo, D. Polese, M. Semprini, A. I. Borrachero-Conejo, J. Gasparetto, M. Sola, L. Tomasi, F. Valle, L. Pazzini, F. Formaggio, M. Chiappalone, S. Hussain, M. Caprini, M. Muccini, L. Ambrosio, G. Fortunato, R. Zamboni, A. Convertino and V. Benfenati, *Adv. Biosyst.*, 2020, 1900264, DOI: 10.1002/adbi.201900264.
24 V. Benfenati and S. Ferroni, in *Homeostatic control of brain function*, ed. D. Boison and S. A. Masino, Oxford University Press, 1st edn, 2015, 1, pp. 3–40.
25 V. Benfenati, S. Toffanin, R. Capelli, L. M. Camassa, S. Ferroni, D. L. Kaplan, F. G. Omenetto, M. Muccini and R. Zamboni, *Biomaterials*, 2010, **31**, 7883–7891.
26 V. Benfenati, N. Martino, M. R. Antognazza, A. Pistone, S. Toffanin, S. Ferroni, G. Lanzani and M. Muccini, *Adv. Healthcare Mater.*, 2014, **3**, 392–439.
27 E. Saracino, V. Cirillo, M. Marrese, V. Guarino, V. Benfenati and R. Zamboni, *Mater. Sci. Eng., C*, 2021, **118**, 111363.
28 T. Posati, A. Pistone, E. Saracino, F. Formaggio, M. G. Mola, E. Troni, A. Sagnella, M. Nocchetti, M. Barbalinardo, F. Valle, S. Bonetti, M. Caprini, G. P. Nicchia, R. Zamboni, M. Muccini and V. Benfenati, *Sci. Rep.*, 2016, **6**, 1–16.
29 Y. Li, B. Chen, X. Li, W. K. Zhang and H. Tang, *PLoS One*, 2014, **9**, 107361, DOI: 10.1371/journal.pone.0107361.
30 M. Marrese, V. Guarino, I. Fasolino, V. Cirillo and L. Ambrosio, *Int. J. Polym. Mater.*, 2017, **67**, 961–966.
31 V. Cirillo, B. A. Clements, V. Guarino, J. Kohn and L. Ambrosio, *Biomaterials*, 2014, **35**, 8970–8982.
32 M. A. Alvarez Perez, V. Guarino, V. Cirillo and L. Ambrosio, *J. Biomed. Mater. Res., Part A*, 2012, **100**(11), 3008–3019.
33 V. Guarino, V. Cirillo, R. Altobelli and L. Ambrosio, *Expert Rev. Med. Devices*, 2015, **12**, 113–129.
34 V. Cirillo, V. Guarino, M. A. Alvarez-Perez, M. Marrese and L. Ambrosio, *J. Mater. Sci.: Mater. Med.*, 2014, **25**, 2323–2332.
35 V. Benfenati, M. Caprini, M. Nobile, C. Rapisarda and S. Ferroni, *J. Neurochem.*, 2006, **98**, 430–445.
36 A. Borrachero-Conejo, E. Saracino, M. Natali, F. Prescimone, S. Karges and S. Bonetti, *Adv. Healthcare Mater.*, 2019, **8**, 1801139, DOI: 10.1002/adhm.201801139.
37 M. Bramini, S. Sacchetti, A. Armirotti, A. Rocchi, E. Vázquez, V. L. Castellanos, T. Bandiera, F. Cesca and F. Benfenati, *ACS Nano*, 2016, **10**, 7154–7171.
38 M. Bramini, M. Chiacchiaretta, A. Armirotti, A. Rocchi, A. Kale, D. Deepali, M. C. E. Vázquez, T. Bandiera,

S. Ferroni, F. Cesca and F. Benfenati, *Small*, 2019, **15**, 1900147.

39 C. S. Hansel, S. W. Crowder, S. Cooper, S. Gopal, M. João Pardelha da Cruz, L. de Oliveira, D. M. Keller, S. Rothery, M. Becce, A. E. G. Cass, C. Bakal, C. Chiappini and M. M. Stevens, *ACS Nano*, 2019, **13**, 2913–2926.

40 S. Sundelacruz, M. Levin and D. L. Kaplan, *Stem Cell Rev. Rep.*, 2009, **5**, 231–246.

41 T. A. Banks, P. S. B. Luckman, J. E. Frith and J. J. Cooper-White, *Integr. Biol.*, 2015, **7**, 693–712.

42 C. Chen, X. Bai, Y. Ding and Y. I. S. Lee, *Biomater. Res.*, 2019, **23**, 25.

43 H. W. Funk Richard, *Front. Physiol.*, 2015, **6**, 143.

44 J. K. Alexander, B. Fuss and R. J. Colello, *Neuron Glia Biol.*, 2006, **2**, 93–103.

45 B. R. Borgens, R. Shi, T. J. Mohr and B. J. Christine, *Exp. Neurol.*, 1994, **128**, 41–49.

46 C. Yang, W. Lei, W. Weiji, S. Wang, M. Yuxiao, Q. Mao, G. Gao, R. Chen and J. Feng, *Exp. Cell Res.*, 2019, **374**, 282–289.

47 V. Benfenati, S. Toffanin, S. Bonetti, G. Turatti, A. Pistone, M. Chiappalone, A. Sagnella, A. Stefani, G. Generali, G. Ruani, D. Saguatti, R. Zamboni and M. Muccini, *Nat. Mater.*, 2013, **7**, 672–680.

48 T. W. Hsiao, P. A. Tresco and V. Hlady, *Biomaterials*, 2015, **39**, 124–130.

49 R. Fabbri, E. Saracino, E. Treossi, R. Zamboni, Palermo and V. Benfenati, *Nanoscale*, 2021, DOI: 10.1039/D0NR07824G.

### 1.3 Introduction to Paper 3

*"A glial-silicon nanowire electrode junction enabling differentiation and non-invasive recording of slow oscillations from astrocytes"* by

**Emanuela Saracino, Luca Maiolo, Davide Polese, M. Semprini, Ana Isabel Borrachero-Conejo, Jacopo Gasparetto, Stefano Murtagh, Margherita Sola, Lorenzo Tomasi, Francesco Valle, Luca Pazzini, Francesco Formaggio, Michela Chiappalone, Saber Hussain, Marco Caprini, Michele Muccini, Luigi Ambrosio, Guglielmo Fortunato, Roberto Zamboni, Annalisa Convertino,* and Valentina Benfenati*** has been published on Advance Biosystems (www.adv-biosys.com), DOI: https://doi.org/10.1002/adbi.202070044.

https://onlinelibrary.wiley.com/doi/10.1002/adbi.202070044.

Supplementary information accompanies this paper at: https://onlinelibrary.wiley.com/action/downloadSupplement?doi=10.1002%2Fadbi.201900264&file=adbi201900264-sup-0001-SuppMat.pdf.



Astrocytes guide the human brain function. Studying non neuronal cells such as glial cells and their connection with neurons network is fundamental to unravel specific pathways of the complexity of the brain. In particular, biomedical engineering aims to develop reliable approach to study the role of astrocytes function in brain physiology and pathologies. However, bioelectrical properties of glial cells, and specifically of astrocytes *in vitro* are not close to those displayed *in vivo*; this feature was already mentioned and largely explored in paragraph 1.3, **Chapter IV**, dedicated to the conductive polymers interface.

In this regard, the *in vitro* non-invasive electrophysiological recording of astrocytes remains challenging for biomedical engineering. Here, primary astrocytes are grown on a device formed by a forest of randomly oriented gold coated-silicon nanowires (AuNWs), resembling the complex structural and functional phenotype expressed by astrocytes *in vivo*. The device enables non-invasive extracellular recording of the slow-frequency oscillations generated by differentiated astrocytes as a new approach to study the role of astrocytes function in brain physiology and pathologies.

**PDF -FORMATO PAPERS\Saracino E., et al., Advanced Biosystems 4.3.pdf**

ADVANCED BIOSYSTEMS
www.adv-biosys.com

# A Glial-Silicon Nanowire Electrode Junction Enabling Differentiation and Noninvasive Recording of Slow Oscillations from Primary Astrocytes

*Emanuela Saracino, Luca Maiolo, Davide Polese, M. Semprini, Ana Isabel Borrachero-Conejo, Jacopo Gasparetto, Stefano Murtagh, Margherita Sola, Lorenzo Tomasi, Francesco Valle, Luca Pazzini, Francesco Formaggio, Michela Chiappalone, Saber Hussain, Marco Caprini, Michele Muccini, Luigi Ambrosio, Guglielmo Fortunato, Roberto Zamboni, Annalisa Convertino,* and Valentina Benfenati**

**The correct human brain function is dependent on the activity of non-neuronal cells called astrocytes. The bioelectrical properties of astrocytes in vitro do not closely resemble those displayed in vivo and the former are incapable of generating action potential; thus, reliable approaches in vitro for noninvasive electrophysiological recording of astrocytes remain challenging for biomedical engineering. Here it is found that primary astrocytes grown on a device formed by a forest of randomly oriented gold coated-silicon nanowires, resembling the complex structural and functional phenotype expressed by astrocytes in vivo. The device enables noninvasive extracellular recording of the slow-frequency oscillations generated by differentiated astrocytes, while flat electrodes failed on recording signals from undifferentiated cells. Pathophysiological concentrations of extracellular potassium, occurring during epilepsy and spreading depression, modulate the power of slow oscillations generated by astrocytes. A reliable approach to study the role of astrocytes function in brain physiology and pathologies is presented.**

## 1. Introduction

Recent studies have moved the neurocentric attention of the neuroscientists toward nonexcitable glial cells, called astrocytes. Although astrocytes are incapable of generating and propagating action potentials, these cells display bioelectrical activity mediated by ion channel proteins, that allow transmembrane movement of ions and organic molecules.[1] In particular, local transmembrane $K^+$ and $Ca^{2+}$ dynamics at astrocytic process are critical for brain function, from synapse to memory and learning. Gap junctional communication channels also allow astrocytes to work as a syncytial network.[5] Notably, alteration in structure and function of astrocyte ion channels, occurring during astrogliosis, has a causal role in

E. Saracino, J. Gasparetto, S. Murtagh, M. Sola, L. Tomasi, Dr. R. Zamboni, Dr. V. Benfenati
Consiglio Nazionale delle Ricerche
Istituto per la Sintesi Organica e la Fotoreattività
via Gobetti 101, 40129 Bologna, Italy
E-mail: valentina.benfenati@isof.cnr.it

Dr. L. Maiolo, Dr. D. Polese, L. Pazzini, Dr. G. Fortunato, Dr. A. Convertino
Consiglio Nazionale delle Ricerche
Istituto per la Microelettronica e i Microsistemi
Via del Fosso del Cavaliere n.100, 00133 Roma, Italy
E-mail: annalisa.convertino@cnr.it

M. Semprini, Dr. M. Chiappalone
Fondazione Istituto Italiano di Tecnologia (IIT)
Rehab Technologies IIT-INAIL Lab
Via Morego 30, 16163 Genova, Italy

Dr. A. I. Borrachero-Conejo, Dr. M. Muccini, Dr. F. Valle
Consiglio Nazionale delle Ricerche
Istituto per lo Studio dei Materiali Nanostrutturati
via Gobetti 101, 40129 Bologna, Italy

F. Formaggio, Prof. M. Caprini
Università di Bologna
Dipartimento di Farmacia e Biotecnologie FaBit
University of Bologna
via San Donato 19/2, 40127 Bologna, Italy

Dr. S. Hussain
US Air Force Research Laboratory
Wright-Patterson AFB
Dayton, OH 45433, USA

Prof. L. Ambrosio
Istituto per i Polimeri Compositi e i Biomateriali
Viale J.F. Kennedy 54, Mostra d'Oltremare, Pad 20, 80125 Napoli, Italy

The ORCID identification number(s) for the author(s) of this article can be found under https://doi.org/10.1002/adbi.201900264.

**DOI: 10.1002/adbi.201900264**

 

such pathologies as ischemia, epilepsy, and glioma.[2–5] Dysfunction of bioelectrical properties of astrogliotic cells surrounding brain implants facilitates the spread of inflammation and the formation of gliotic scarring, reducing the performance of implants over the long term.[6] Thus, the complex ion dynamics of astrocytes require the adoption of bioelectronic tools to enable high-resolution analyses of events occurring at different spatio-temporal scales.[8] In the traditional patch-clamp method the spatial resolution is limited to the electrical signal recorded from the cell body of a single astrocyte, and the invasiveness of the probe reduces the monitoring timeframes to minutes. Perturbation of physiological functions, caused to the employed dyes or light source, affect also the optical fluorimetric methods.[9]

To date, extracellular recording systems based on planar microelectrode arrays (MEAs) are the optimal electrophysiological equipment for noninvasive long-term analysis studying of neuronal circuit-connectivity in vitro and in vivo.[7] While stimulation of astrocytes signaling has been achieved successfully with organic field effect transistor devices, the use of MEA for the recording of astroglial cells signaling in vitro still displayed critical issues.[9–14] First, astrocyte primary cultures, grown on flat substrates lose structural and functional features,[11a,b,12] essential for their homeostatic and physiological function in vivo.[13] This issue strongly reduces the validity and the potential of the findings with traditional MEA in vitro. Second, low-impedance recording is crucial for extracellular signals, as it determines high signal to noise ratio (SNR) and, therefore, the capability to record slow and low variations of transmembrane potentials, expected from local displacement current typically occurring in astrocytes. Strategies achieved low electrode impedance focusing on increasing the effective surface area by using nanostructured electrodes.[9,14–20] In this regard, silicon nanowires (SiNWs) are promising neural interface, allowing real-time, spatial-resolved recording and manipulation of bioelectrical activity in neurons.[19–24] Silicon nanowires' 3D nanostructured morphology promotes interactions with micro/nanoscale features of the cell surface.[25–27] Moreover, the nanosize, large surface-to-volume ratio, and surface chemistry engineering make SiNWs suitable for bielectronic probing and sensing of mammalian cells. However, the work attempting to interface SiNWs with astrocytes is limited to biocompatibility.[6,27–29] Here, we show that gold coated SiNWs (Au/SiNWs), randomly organized into a forest of heterogeneous sizes, are capable to promote the growth/proliferation of astrocytes that recapitulate the structural and functional properties similar to those they display in vivo. Furthermore, the use of Au/SiNWs device allows for the recording of variations in actrocytes transmembrane potentials in a noninvasive manner. The advantages of this engineered bioelectronic platform are: decreased electrode impedance due to a large effective surface area;[10,31] high-yield, low-cost and low temperature fabrication techniques compatible with transparent supports.[32–35] The latter feature meets the demand of a large number of samples with a high reproducibility and transparent substrates for reliable electrophysiological recordings.

We studied the cumulative bioelectrical activity of primary cortical astrocytes coupled to a device based on Au/SiNWs and discovered that differentiated astrocytes generate transmembrane potentials in the slow frequency band that cannot be recorded with planar MEA. Pathophysiological concentrations of extracellular potassium occurring in dysfunction as epilepsy and spreading depression can modulate astrocytes excitability at a specific frequency range, thus validating our approach for the study of astrocytes in neurological conditions.

## 2. Results

### 2.1. Fabrication and Characterization of the Au/SiNWs Device

We developed an Au/SiNWs device as illustrated in **Figure 1**. The device consists of 4 stripe shaped recording sites based on "a forest" of randomized Au/SiNWs, embedded in a mat of insulating SiNWs (Figure 1A). The stripes are 1 cm long and 25 µm wide with an electrode spacing of 25 µm (Figure S1, Supporting Information). Initially, to induce the NWs growth, a 2 nm thick Au film was selectively evaporated onto the specific area (1 cm × 1 cm large) of a microscope glass slide (Figure 1B, 1). The SiNWs were grown by plasma enhanced chemical vapor deposition (PECVD) via vapor liquid solid (VLS) mechanism (Figure 1B, 2). The SiNWs were covered by an insulating film of $SiO_2$.[35]

Finally, the electrodes and connecting tracks, based on Au, were patterned and fabricated (Figure 1B, 3). Figure 1C shows an example of the fabricated device; the electrodes are inside the dashed red oval. The scanning electron microscopy (SEM) images of the nanostructured MEA (Figure 1D) reveal a dense ensemble of disordered and randomly oriented NWs, where the dark areas are the metal electrodes. The conducting and insulating NWs are ≈2–3 µm long, with an averaged diameter of about 100–150 and 50–80 nm, respectively. Electrical performances were investigated by using impedance spectroscopy. Specifically, we evaluated the differences between our Au/SiNWs device and a conventional planar MEA device. For this purpose, we fabricated a reference MEA (planar Au MEA) consisting of planar Au stripes, fabricated directly onto the glass substrate, with the same size and features of the nanostructured device. Figure 1E compares the typical Bode plots of the impedance modulus, |Z|, obtained from the two electrode systems in the range 0.1 Hz–100 KHz and in aqueous KCl solution. As expected, a significant reduction in the low frequency range (0.1–100 Hz) impedance is observed in the nanostructured electrode with respect to the planar one due to the enlargement of the effective surface area induced by the presence of the underlying nanostructures.

### 2.2. Structural, Molecular, and Functional Differentiation of Astrocytes on Au/SiNWs

The study of the cellular adhesion, growth and differentiation of primary rat cortical astrocytes was performed by staining cells with Fluorescein diacetate (FDA) and Hoechst 33342, that marks respectively cytoplasm and nucleus of living cells. **Figure 2**A shows the fluorescent images, representing the cell morphology observed in astrocytes plated on Au/SiNWs 5 days after re-plating. As a control experiment, we also used

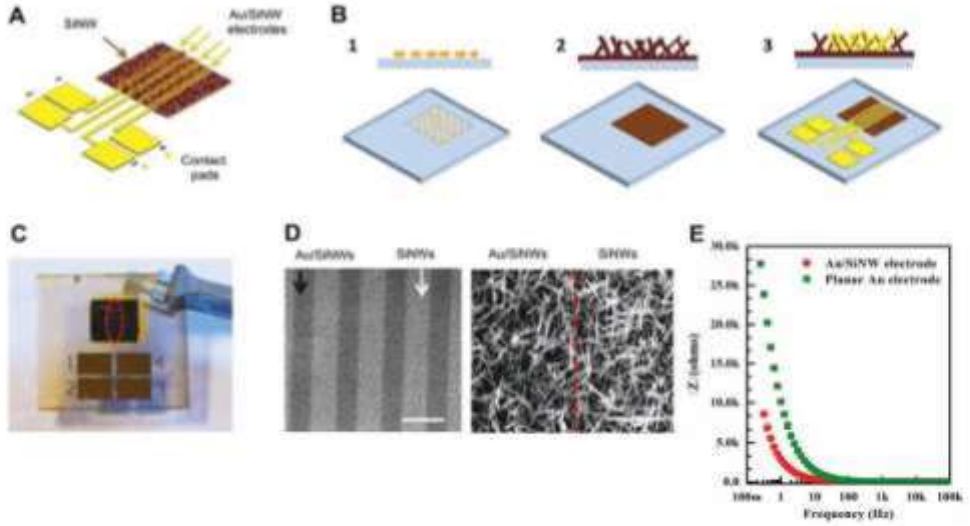


**Figure 1.** Au/SiNWs MEA fabrication and characterization. A) Schematic configuration of the 4-channel Au/SiNWs MEA. B) Schematic representation of the device fabrication steps: 1) evaporation of the Au catalyst (layer thick 2 nm) onto a selected area of a glass substrate; 2) VLS growth of SiNWs and passivation with a $SiO_2$ layer (50 nm thick); 3) fabrication of the electrodes by evaporating Au onto the selected rectangular area of passivated SiNW mat. C) Photograph of the device. D) SEM images of the 4 Au/SiNWs electrodes (dark stripes in the left panel, scale bar is 50 µm) in the insulating SiNW mat (light areas). In the right panel a detail of the border conductive/insulating NWs (scale bar is 5 µm). E) The Bode plot of the impedance modulus, |Z|, of an Au/SiNWs electrode (red dotted symbols) compared with that recorded from a planar Au one (green squared symbols).

a planar Au/Si substrate, obtained by evaporating a thin film (150 nm thick) of Au on Si wafer. The astrocytes on the control substrate (Figure 2A, left panel) display a polygonal flat shape, typically observed in in vitro experiments when they are plated on Poly-D-lysine coated coverslips, polystyrene petri dishes or flat biopolymers.[12,36–38] Conversely, astrocytes grown on bare Au/SiNWs (Figure 2A, right panel) show a differentiated morphology with elongations extending from the cell body for several micrometers. Alamar Blue (AB) viability assay was performed on astrocytes plated on Au/SiNWs and planar Au/Si, after 1, 5, and 15 days in vitro (DIV). The plot in Figure 2B compares the AB percentage, a measure of cell viability and proliferation rate of astrocytes on Au/SiNWs, to that of the cells plated on control Au/Si samples at all selected time points. While AB percentage is comparable, plots indicate the long-term survival of astrocytes on the substrate.

To overcome any concern that morphological features expressed by the astrocytes on Au/SiNWs, might be due to an inflammatory reaction of the cells to the nanostructured substrate, we next analyzed glial fibrillar acid protein (GFAP) expression, a well-known marker of astrogliosis in vitro and in vivo. Confocal imaging of immuno-stained cells performed after 5 DIV, shows a comparable level of GFAP expression between the astrocytes on Au/SiNWs (Figure 2C, right panel) and those grown on the control Au/Si substrate (Figure 2C, left panel), with a significantly lower amount of GFAP fluorescence in astrocytes on Au/SiNWs (Figure 2D).

We next performed the actin cytoskeleton study with phalloidin F-actin staining analyses. The results demonstrate that the astrocytes grown on Au/SiNWs have a well-organized pattern of stressed F-actin fibers (Figure 2E, right panel) compared to the cells on the control substrate, which have disorganized and randomly structured F-actin fibers (Figure 2E, left panel). In addition, the vinculin fluorescent signal analyses indicate a patchy distribution and expression of protein in the elongations of the astrocytes on Au/SiNWs versus a mislocalized distribution in cells on planar Au/Si (Figure S2A,B, Supporting Information). To get further insight into the interaction between astroglial cells and Au/SiNWs, we performed SEM imaging after 5 DIV (Figure 2F–H). Morphological analyses confirmed that most of the astroglial cells grown on Au/SiNWs (98.2% ± 3) were differentiated, displaying branches departing from the cell body (Figure 2F,G and Figure S2C, Supporting Information). Moreover, higher magnification images reveal that astrocyte elongations have lateral projections allowing junctions between cells and enwrapping nanowires (Figure 2H). Atomic force microscopy (AFM) analysis confirmed the tight interaction of the astrocytes processes with the NWs surface (Figure 2I). To study the functionality of the astrocytes plated on Au/SiNWs, we investigated the behavior of $K^+$ channels that play a fundamental role in the physiology of astrocytes in vivo.[1,13] For this purpose, we performed whole-cell patch-clamp measurements on single cells after three days from re-plating on Au/SiNWs and, as comparison, on planar Au/Si substrate. In particular, to correlate the morphology with functionality, we analyzed the cells on Au/SiNWs with "starlike" shape that resemble the morphology of astrocytes in vivo. The passive membrane properties were calculated (Table S1, Supporting Information)[13] and revealed that the values of voltage membrane ($V_{rest}$), input resistance (IR), and specific conductance

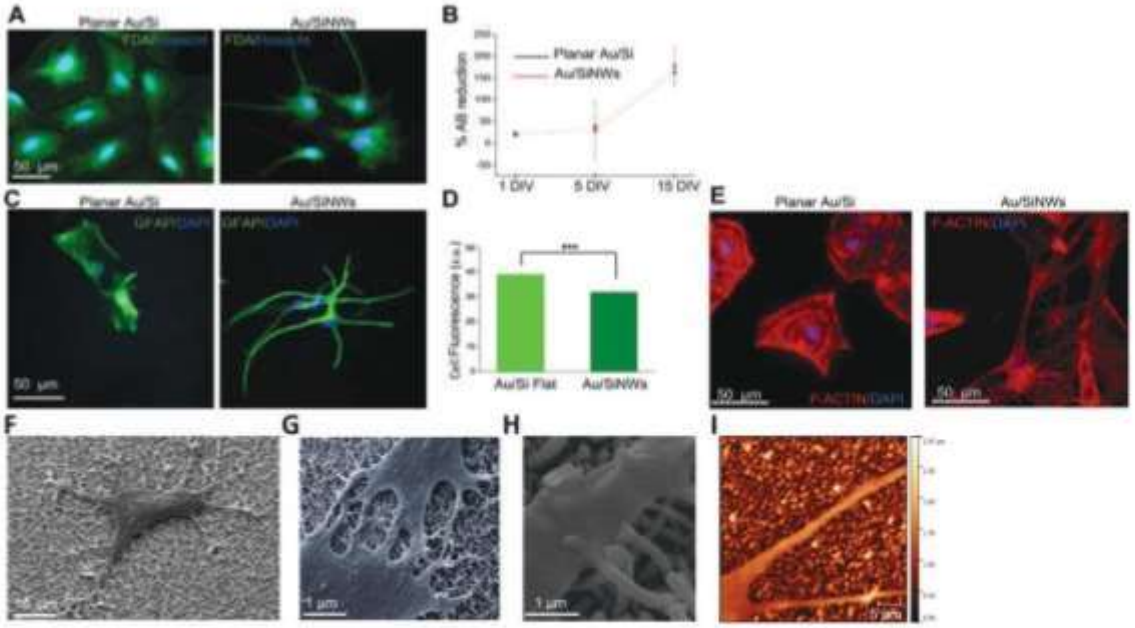


**Figure 2.** Viability and morphology of astrocytes on Au/SiNWs. A) Single plane confocal images of FDA and Hoechst 33342 stained astrocytes, representing viable cells plated on control planar Au/Si (left panel) and Au/SiNWs (right panel) at 5 DIV. B) Time course of astrocyte viability on planar Au/Si (black trace) and Au/SiNWs (red trace), investigated by AB assay at different time points (DIV) from cell re-plating. Data are plotted as the averaged percentages of reduced AB ± Standard Error (SE) versus div, $n = 3$ (number of experiments performed in triplicate), pval > 0.05 in all the condition tested: pval = 0.42 at 1 DIV; pval = 0.85 at 5 DIV, pval = 0.95 at 15 DIV, Student's *t*-test. C) Confocal imaging of astrocytes stained with GFAP plated on planar Au/Si (left panel) and Au/SiNWs (right panel) captured after 5 DIV from cell re-plating. D) Quantification of the GFAP protein expression level in astrocytes plated on planar Au/Si and Au/SiNWs. $n$ = number of analyzed images per condition = 7 for planar Au/Si and $n = 14$ Au/SiNWs pval = $5.6 \times 10^{-4}$; Student's *t*-test, ***: $p < 0.001$. E) Micrographs representing astrocytes immunostained for actin plated on planar Au/Si (left panel) and Au/SiNWs (right panel). F–H) SEM imaging of cells plated on Au/SiNWs. Elongated branches departing from the cell body are clearly visible (F). G) Higher magnification images showing astrocytes coupling and H) astrocytes endfoot enwrapping a nanowire. I) AFM image of astrocyte elongation on Au/SiNWs.

(SpG) values of the astrocytes on the planar Au/Si substrates, are very similar to those reported for primary astrocytes grown in vitro on different planar substrates,[11,12,36] whereas the astrocytes on the NW are more hyperpolarized with a lower IR and a higher capacitance. The typical current profiles obtained in response to the applied voltage ramp are shown in **Figure 3** for the astrocytes on both the planar Au/Si (Figure 3A) and the Au/SiNWs (Figure 3B). In the inset of Figure 3A the applied voltage ramp is plotted. A strong outward rectification, as confirmed by negligible currents recorded at membrane potentials below −40 mV (Figure 3A), was shown by the astrocytes on the planar Au/Si. Conversely, we observed a double rectification profile with large inward currents activated at membrane potentials more negative than −40 mV for the astrocytes on the Au/SiNWs (Figure 3B, arrow). The averaged calculation of current density ($I$ pA/pF) at −120 mV confirmed that astrocytes plated on Au/SiNWs display a significant increase in inward current density (Table S1, Supporting Information).

It is interesting to note that the inward current of the astrocytes on the Au/SiNWs increased when the extracellular saline contained higher potassium concentration ($40 \times 10^{-3}$ M, High $[K^+]_o$) (Figure S3, Supporting Information, red line) with a positive shift in the reversal potential ($E_{rev}$). The inward current is inhibited by sub-millimolar concentrations ($200 \times 10^{-6}$ M) of Barium ($Ba^{2+}$) to the High $[K^+]_o$ saline solution (Figure S3, Supporting Information, green line). The biophysical features observed in astrocytes on Au/SiNWs resemble those of inward rectifier $K^+$ (Kir) channels in astrocytes in situ and differentiated in vitro.[11,36] Among the Kir channels, Kir 4.1 is recognized as the protein channel mainly involved in homeostatic regulation of $K^+$ operated by astrocytes in vivo.[3,39] Thus, we hypothesized that the growth of astrocytes on Au/SiNWs might induce Kir4.1 expression. Accordingly, confocal images of cells immunostained for Kir4.1 (Figure 3D,E) showed that expression of the channel is increased in the membrane of astrocytes soma and processes when cells are grown on Au/SiNWs (Figure 3E).

### 2.3. Extracellular Recordings from Astrocytes Plated on Au/SiNWs MEA

Extracellular recordings were performed by measuring the electrochemical voltage of cortical rat astroglial cell popula-

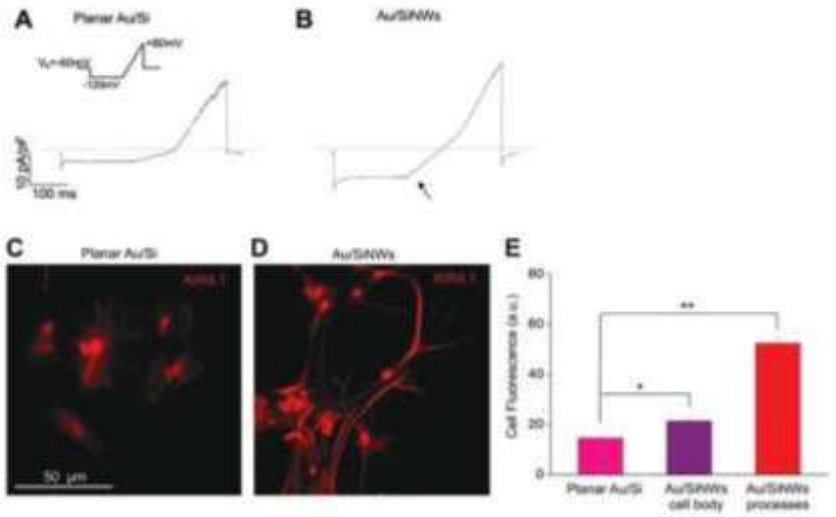


**Figure 3.** Functional properties of astrocytes plated on Au/SiNWs. A,B) Typical current traces evoked from a holding potential (Vh) of −60 mV stimulating astrocytes with a voltage ramp (inset). Astrocytes plated on planar Au/Si A) display only voltage-dependent outward rectification. Astrocytes plated on Au/SiNWs B) display an inward conductance in response to hyperpolarizing stimulus (arrow). C,D) Confocal imaging of stained Kir4.1 astrocytes on C) planar Au/Si and D) Au/SiNWs. E) Bar plot of the fluorescence levels detected in the soma and endfeet of astrocytes stained for Kir 4.1 grown on planar Au/Si and Au/SiNWs, $n$ = number of analyzed images per condition = 19 for planar Au/Si and $n$ = 22 Au/SiNWs; pval = 0.0473 for Au/SiNWs cell body, pval = $1 \times 10^{-3}$, Student's t-test, *: $p < 0.05$, **: $p < 0.01$.

tions grown on Au/SiNWs MEA over a frequency range of 0.1–1 kHz. In addition, to evaluate the differences between nanostructured and a traditional planar MEA, we fabricated a planar Au MEA consisting of Au stripes evaporated directly onto glass slides having the same size and features of the nanostructured ones. A PMMA well was glued on top of the area of the MEAs. This well served for the astrocyte culture and successively as a container for the electrolyte solution, as sketched in **Figure 4**A. The device was then accommodated in a specifically developed sample stage (Figure S3A, Supporting Information), specifically developed, which allowed four probes and the reference electrode to access as well as to contact the pads and the solution. The system was connected to a portable acquisition board. Astrocyte coverage of the electrodes was verified on live cells by optical microscopy for live cells and by SEM analysis for fixed cells both before and after the experiment, respectively, revealed astrocytes abundantly covering the electrode surface (Figure 4B and Figure S4B, Supporting Information). Recording was performed 5 days after re-plating astrocytes on the devices. Figure 4C shows the typical voltage versus time traces recorded from Au/SiNWs electrodes without (Figure 4C, upper trace) and with cells (Figure 4C, lower trace). Recording was performed in the same experimental conditions in planar Au MEA without (Figure 4D, upper trace) and with cells for comparison (Figure 4D, lower trace).

The power spectral density (PSD) of the voltage as a function of frequency in Figure 4E, revealed that activity was clearly detected at below 100 Hz, when astrocytes are plated on Au/SiNWs device. Analysis of supra-threshold events (i.e., astrocytes "oscillations") confirmed that signals were detected only when cells are plated on Au/SiNWs, whereas the same device, without any cells, shows negligible activity in both counts and in amplitude (Figure S5C,D, Supporting Information).

The features of the events of interest were variable in duration and frequency. Amplitude varies from 17 to 132 µV (Figure S5D, Supporting Information), duration from 60 to 730 ms in duration (Figure S5E, Supporting Information) and interval between two distinct events occurs in a range from 0.2 to 26 s (Figure S5F, Supporting Information). The PSD analysis shows that signals recorded with the Au/SiNWs have 10 times higher power magnitude with respect to the planar device in the frequency ranges $\delta$ (0.1–5 Hz), $\theta$ (5–9 Hz), and $\beta$ (9–30 Hz), as reported in Figure 4E (Mann-Whitney test, $p < 0.05$). The power of signals recorded in planar Au MEA with and without cells is not significantly different (Figure 4E). Interestingly, the power of signal recorded when astrocytes are plated on Au/SiNWs MEA can be modulated when cells are exposed to saline with elevated and pathophysiological concentrations of potassium (Figure 4G, High $[K^+]_0$) or when barium ($BaCl_2$, $200 \times 10^{-6}$ M), is added to the High $[K^+]_0$ saline solution (Figure 4H, High $[K^+]_0 + Ba^{2+}$).

## 3. Discussion

First, we found that Au/SiNWs promote adhesion, growth and differentiation of astrocytes with star-like morphology (Figure 2F–I), typically shown in vivo, without the need of additional coating. We noted that in vivo astrocytes are physiologically devoted in responding to the environmental changes. In particular, they are equipped with an array of polymodal receptors[1,3] possibly responsible for their ability to sense and

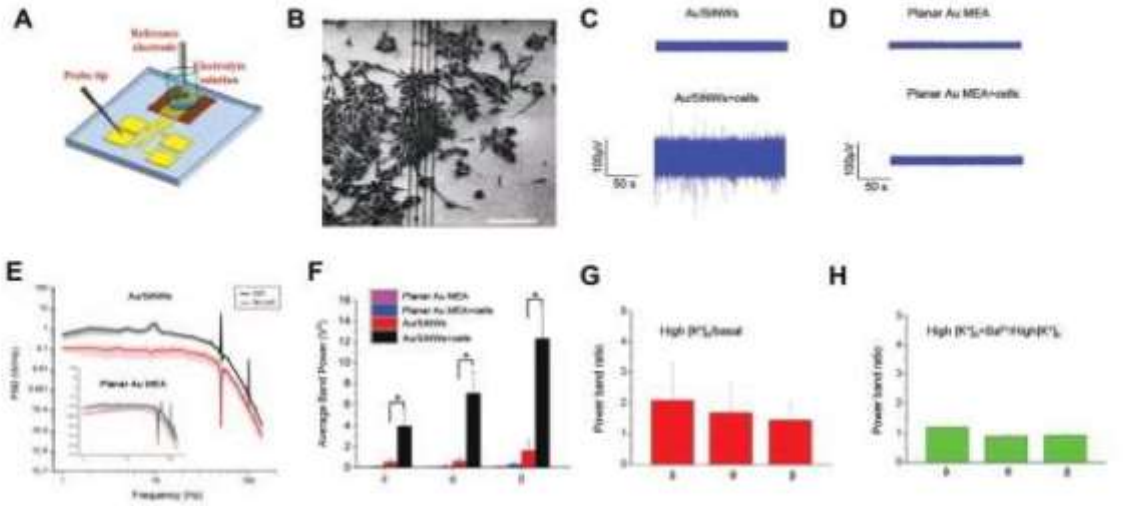


**Figure 4.** Extracellular recording and analysis of astrocyte transmembrane potentials. A) Schematic illustration of the setup used for the detection of the activity in cortical rat astrocytes grown on 4-channel Au/SiNW MEA device. B) SEM images of astrocytes cultured on the 4-channel Au/SiNW MEA. C) Voltage versus time traces obtained by the Au/SiNW electrodes without (upper trace) and with cells (lower trace). D) Voltage versus time traces recorded from planar Au planar electrodes without (upper trace) and with cells (lower trace). E) Power spectral density (PSD) of the voltage as a function of frequency in a population of astrocytes on Au/SiNWs electrode (black line). For comparison the PSD obtained by measuring the voltage without cells is also plotted (red line). The inset shows the power spectral density calculated for the flat MEA with (black line) ad without (red line) cells. F) Bar graphs of the average power band calculated in the different frequency range: $\delta$ (0.1–5 Hz), $\theta$ ( 5–9 Hz), and $\beta$ (9–30 Hz) for the planar Au and Au/SiNWs electrodes with and without cells. G,H) Bar graphs of the averaged ratio of the power band in the $\delta$, $\theta$, and $\beta$ obtained from the astrocyte population on Au/SiNWs electrode after G) increasing potassium concentration and H) successively adding barium with respect to recordings in baseline conditions. Pharmacological manipulation on a subset of 9 recordings with an extracellular solution containing a high concentration of potassium (High $[K^+]_e$) and by addition with barium chloride (200 μm) to the latter solution (High $[K^+]_e$ + $Ba^{2+}$). $n$ = number of recordings = 3 for planar Au, $n$ = 11 for planar Au +Cells, $n$ = 5 for Au/SiNWs and $n$ = 17 recordings for Au/SiNWs+Cells, $p$ = 0.04, Mann-Witney test.

adapting to topographical features. Guided by these findings, we suppose the star-like shape observed in the astrocytes plated on Au/SiNWs could be promoted by the disordered arrangement and heterogeneous size distribution of the NWs "forest," which resembles the neural and glial thread-like structures in the brain. In addition, in vitro experiments have demonstrated that the astrocyte cellular functions, including adhesion, proliferation, migration, differentiation and expressed physiological functionality, can be influenced by nanoscale features of nanomaterials.[11a,b,17,38,40,41] Accordingly, we note that the stellar shape of astrocytes on Au/SiNWs is also accompanied by an alteration in the cell cytoskeletal architecture (Figure 2E and Figure S2B, Supporting Information), ascribable to nanoscale cell/material interaction likely initiated by molecular events involving focal adhesion point (FAP) protein complex.[11b,40]

Of note, the unaltered GFAP expression (Figure 2C,D) suggests that the forest of Au/SiNWs does not induce any gliotic reaction. Thus, the forest of Au/SiNWs may be a promising contribution to implantable devices with reduced inflammatory response.[8]

In addition, astrocytes on Au/SiNWs express the $K^+$ channel called Kir 4.1 (Figure S3, Supporting Information), which is fundamental in the clearance of extracellular $K^+$ accumulation ($[K^+]_e$), occurring after the efflux of $K^+$ ions from neurons during repolarization phase of action potential.[3,4,42] Abnormalities in Kir4.1 gene protein expression and functions have been reported in different forms of epilepsy, ischemia, spreading depression and autism spectrum disorders (ASD).[43]

Collectively these results indicate that the forest of Au/SiNWs induces morphological, molecular and functional differentiation of astrocytes by prompting the cells to display a phenotype with properties observed also in astrocytes in vivo. In this respect, our approach will be useful to identify factors involved in the structural and functional regulation of astrocytes and helpful in guiding the development of novel treatments options for neuropathologies characterized by astrocyte dysfunction.

The remarkable signal detection from Au/SiNWs device is ascribed to: i) the large effective surface area of the nanostructured electrodes; ii) the tight junction NW/astrocyte-endfeet; iii) the absence of functionalization coatings, which are typically used to favor the growth and the cell-electrode contact stability but cause the increase of leak currents at the cells/device interface and iv) a possible NW engulfment into the cell membrane as reported for nanowires with the same length utilized here.[44]

Because of the performed signal detection capability of the Au/SiNW device, it has been possible to identify for the first time the spectral range of differentiated astrocytes transmembrane voltage oscillations and their power in the $\delta$, $\theta$, and $\beta$ frequency range (Figure 4F). Remarkably, this result has been obtained from differentiated astrocytes with structural, morphological and functional features closer to astrocytes

in vivo. The presented approach provides an advantage with respect to previously reported studies[9,10] where the recording was performed on cultures astrocytes displaying polygonal morphology, far from resembling the properties of astrocytes in vivo, thus having a lower potential of reproducibility of their findings in vivo. In addition, the Au/SiNWs device allowed us to obtain a signal detection from the beginning of the recording and 5 days after the plating of the cells on the device, indicating the potential to analyze astrocytes functionality over different time scales. Au/SiNWs device was able to detect the signal modulation, (Figure 4G,H) that occurs when the ionic content of the extracellular milieu is tuned by increasing $K^+$ concentration to pathological concentrations occurring during epilepsy, ischemia or spreading depression.[48]

Our results impact current scientific debate about the role played by astrocytes in higher cognitive functions and in cortical slow frequency oscillations. Indeed, electrophysiological recording and analyses performed in vivo and in situ are based on the statement that astrocytes are electrically silent and equipotential. Thus, as they cannot generate all-in one events, it is commonly thought that they cannot directly contribute to slow the voltage oscillations, recorded extracellularly from the brain bulk. However, a variety of ion channels are localized at astrocytes endfeet and can generate local "displacement ionic currents" that in situ and in vivo might concur to slow transmembrane voltage variations observed in extracellular recordings. In addition, recent hypotheses[1,42] advance the idea that, at astrocytes thin processes, surface ionic conduction dominates over volume conduction. Our findings support these recent assumptions. In particular, the tight junction observed between Au/SiNWs and the astrocyte process (Figure 2H,I) suggests that ionic signals, localized in the microdomains, majorly contributed to the observed slow oscillations. Concerning the ions responsible for the observed transmembrane potential oscillation, we can hypothesize a role of extracellular $Ca^+$ influx[1,13] without excluding $Na^+$ dynamics as recently described in astrocytes microdomain.[43]

Eventually, increasing evidences indicate that astrocytes modulate brain network oscillations, tuning their synchronization and contributing to cognitive functions as sleep and memory performance.[46] Studies in situ showed that astrocytes capability to clear $K^+$ from the extracellular milieu[47] and their $Ca^+$ activity are potential mechanism through which astrocytes tune network excitability in the slow-frequency range. The unprecedented observation of astrocyte activity at a precise slow frequency range raises the question as to whether the observed bioelectrical graded and slow frequency signals, recorded in the bulk brain in vivo and physiological and pathological conditions, might also be derived from astrocytes. Our data are even more relevant if considering that an increase in $[K^+]_o$ to the ceiling and pathophysiological levels observed in spreading depression and epilepsy[48] perturbs astrocyte oscillations, especially in the $\beta$ frequency range. The signal power is also sensitive to addition of $Ba^{2+}$, an inhibitor of ion channels (Figure S3, Supporting Information) involved in potassium spatial buffering, indicating that the phenomena are correlated with the homeostatic function of astrocytes. Differential PSD, events detection and waveform tools for analyses are needed to discern between astrocyte and neuronal signals in coculture as well in vivo or in pathophysiological models.[49] However, our work, providing resolved slow-frequency oscillations in differentiated astrocytes sets the scene for future transformative findings on brain communication processes and for bioengineering of reliable bioelectronic device that can actively dialogue with astrocytes to record and modulate their function during pathologies.

## 4. Experimental Section

*Fabrication of Au/SiNW Device*: Au catalyzed SiNWs were produced by plasma enhanced chemical vapor deposition on both microscope glass and Si wafer. To induce the NW growth, a 2 nm thick Au film was selectively evaporated onto the specific area, defined using photolithography and wet etching processes. The growth was performed with $SiH_4$ and $H_2$ as precursor at a total pressure of 1 Torr and substrate temperature of 350 °C. The flow ratio $SiH_4/(H_2+SiH_4)$ was fixed to 1:10. A 13.6 MHz radio frequency with power fixed at 5 W was used to ignite the plasma. The growth time was fixed at 7 min. A passivating $SiO_2$ layer (50 nm thick) was then deposited by Electron Cyclotron Resonance (ECR)-PECVD at room temperature, starting from a gas mixture of $O_2$, $SiH_4$ and He.[31] The insulating film was deposited at a working pressure of $4 \times 10^{-3}$ mbar and at microwave power of 700 W. Successively, a Ti (20 nm)/Au (150 nm) bilayer was thermally evaporated to produce the Au/SiNW electrodes and connecting tracks, obtained after a lift-off process. The role of the thin layer of Ti was solely devoted to improve the adhesion between the gold layer and the substrate. The morphology of the NWs was verified by scanning electron microscopy. A ZEISS EVO MA10 SEM was used at an accelerating voltage of 5 kV. The size of the NWs was determined by combined measurements from plan and cross views.

*Impedance Characterization of the Au/SiNWs Device*: Impedance spectroscopy was performed by using a potentiostat versa STAT 4 by PAR, in $100 \times 10^{-3}$ M aqueous KCl solution with a three-electrode configuration (Au wire as a counter electrode and Ag/AgCl as a reference electrode). The spectra were measured over 0.1 Hz–100 kHz frequency range with 10 mV rms input signal amplitude. Each measurement was performed with a minimum of four repetitions on the same electrode over a period time of 1 h.

*Rat Cortical Astrocyte Culture Preparation, Maintenance and Plating*: Primary astroglial cultures were prepared at the University of Bologna. They were performed in concordance with the Italian and European law of protection of laboratory animals and the approval of the local bioethical committee, under the supervision of the veterinary commission for animal care and comfort of the University of Bologna and approved protocol from Italian Ministry of Health (ethical protocol number no. 360/2017 PR, released on May 2017, valid for 3 years). Astrocyte primary culture were prepared as described previously,[11] from newborns at post-natal day 1–2 of Rattus, Norvegicus, Wistar. Briefly, neonatal cerebral occipital cortices devoid of meninges were gently triturated, filtered with a 70-lm cell strainer (Falcon, BD Bioscience, Bedford, MA) and placed in cell culture flasks containing Dulbecco's Modified Eagle-glutamax medium with 15% fetal bovine serum (FBS) and penicillin/streptomycin (100 U $mL^{-1}$ and 100 lg $mL^{-1}$, respectively). Cells were maintained in incubation at 37 °C and 5% of $CO_2$ and proper humidity levels for three weeks. During this period, cell medium was replaced in every three days and flasks were gently shaken when necessary to remove undesired microglial cells. After three weeks in culture, confluent astrocytes were dispersed using trypsin–EDTA 0.25%, and the cell suspension was dropped on planar Au/Si substrates as well as on Au/SiNWs samples plated into Petri Dishes at a density of $4 \times 10^5$ cells per sample.

*Cell Differentiation Measurement*: Differentiation induced by growth of astrocytes on Au/SiNWs was evaluated following morphological analyses described previously.[11] Cells differentiation was considered

when the vertical *Y* axis for each cell was at least two times longer than the horizontal *X* axis and star-like when cells were displaying more than 2 branches. Quantitative analysis was carried out by counting differentiated and undifferentiated cells from astrocytes FDA-positive plated on Au/SiNWs films and imaged after 5 DIV. The number of differentiated cells was expressed in percentage of total number of cells (Planar Au/Si $n = 114$ cells/10 images, Au/SiNWs $n = 65$ cells/18 images).

*Immunofluorescence and Confocal Microscopy*: Primary antibody used were: Mouse anti-GFAP (Sigma Aldrich, Milan, Italy) rabbit anti-Kir 4.1 (Alomone, Jerusalem, Israel) both diluted to 1:300 and Rabbit anti-Vinculin (Life Technonogies, Monza, Italy) 1:200. The secondary antibodies used for immunofluorescence included donkey anti-mouse CY3 (Jackson Labs), Alexa488-conjugated donkey anti-rabbit at a dilution of 1:1000. Cultured astrocytes plated on coverslips were fixed in 4% paraformaldehyde, washed in phosphate buffered saline (PBS), and permeabilized with 0.3% Triton X-100 in PBS. After blocking with 1% BSA in PBS, cells were incubated with primary antibodies for 2 h at RT, washed in PBS and incubated for 1 h at RT with Alexa conjugated secondary antibodies and with ATTO 647N-Phalloidin (Fluka Analytical, St Louis, MO) and Phalloidin-FITC (Sigma-Aldrich, Milan, Italy) to stain F-actin filaments. Coverslips were mounted on slides, using a mounting medium (50% Glycerol, 0.01% N-Propil-Gallate in PBS) and examined with a confocal microscope (TCS SP5, Leica) or with Nikon TE 2000 inverted confocal microscope equipped with 20x and 60x oil-objectives and 400 nm diode, 488 nm $Ar^+$ and 543 nm He–Ne lasers as exciting sources. Micrometric images of Vinculin-stained cells were captured with Nikon Eclipse 80i fluorescent microscope equipped by 20x and 40x objectives.

*Scanning Electron Microscopy*: Astrocytes plated on Au/SiNWs were fixed with 2.5% glutaraldehyde in phosphate buffer saline (PBS) at 4 °C, for 1 h. Each sample was then rinsed three times in PBS for 5 min before being stained 1 h in 1% Osmium tetra-Oxide ($O_sO_4$) at room temperature; three further rinsing with distilled water were then performed. Then samples were sequentially dehydrated in 50%, 75%, 95%, and 99% ethanol. Dried specimens were sputter-coated (QR150RS, Quorum Technologies Ltd, East Sussex, UK) with gold (10 nm thickness) before analysis with a ZEISS EVO MA10 SEM.

*Atomic Force Microscopy*: AFM imaging was performed on a Multimode 8 microscope equipped with a Nanoscope V controller and type E and J piezoelectric scanners (Bruker, USA). Samples were scanned in PeakForce mode with ScanAsyst-Air probes (Bruker, USA).

*Electrophysiology*: Current recordings were obtained with the whole-cell configuration of the patch-clamp technique. Patch pipettes were prepared from thin-walled borosilicate glass capillaries to obtain a tip resistance of 2–4 MΩ when filled with the standard internal solution. Membrane currents were amplified, filtered at 2 kHz and acquired at a sample rate of 5 kHz by Axopatch 200B amplifier in voltage-clamp mode. Responses were amplified, low-pass filtered at 1 kHz, digitized at 20 kHz, stored and analyzed with pCLAMP 10. Experiments were carried out at room temperature (22–24 °C). When necessary, current values were plotted as current densities calculated by dividing the current values measured at each membrane potential by the cell capacitance obtained by the correction of the capacitive transients of the recorded cells by means of the digital circuit of the patch-clamp amplifier. The passive properties of astrocytes were calculated as described previously,[11] by controlling the chemical composition of intracellular and extracellular saline, cells were voltage-clamped at a holding potential ($V_h$) of −60 mV and, after stepping to −120 mV for 400 ms, a slow ramp (180 mV/600 ms) from −120 to 60 mV (inset in Figure 3A) was applied to elicit whole-cell currents. Current amplitude was recorded, and values of the resting membrane potential ($V_{mem}$), input resistance (IR), specific conductance (SG), and capacitance (Cp) were calculated as described previously[11] (Table S1, Supporting Information) for the astrocytes on both control and nanostructured substrates.

*Solutions and Chemicals*: All salts and chemicals employed for the investigations were of the highest purity grade (Sigma). For electrophysiological experiments, the standard bath saline was (millimolar): 140 NaCl, 4 KCl, 2 $MgCl_2$, 2 $CaCl_2$, 10 HEPES, 5 glucose, pH 7.4 with NaOH and osmolarity adjusted to ≈315 mOsm with mannitol. The intracellular (pipette) solution was composed of (millimolar): 144 KCl, 2 $MgCl_2$, 5 EGTA, 10 HEPES, pH 7.2 with KOH and osmolarity ≈300 mOsm. The solution containing high potassium concentration was composed of (millimolar): 106 NaCl, 40 KCl, 2 $MgCl_2$, 2 $CaCl_2$, 10 HEPES, 5 glucose, pH 7.4 with NaOH and osmolarity adjusted to ≈315 mOsm with mannitol. The different salines containing pharmacological agents were applied with a gravity-driven, local perfusion system at a flow rate of ≈200 µL $min^{-1}$ positioned within ≈100 µm of the recorded cell.

*Electrophysiological Tests of the Au/SiNWs MEA*: The nanostructured MEA with the PMMA container were housed in a custom measuring chamber equipped with spring contacts to connect the MEA fingers. An external common Ag/AgCl reference electrode was used during the measurements. The testing apparatus was been placed in a Faraday cage to minimize external noise. All the tests have been carried out at room temperature. The spontaneous activity of astrocytes was collected by a custom recording system called NeuroDaq based on INTAN chip. Neurodaq consists of an ultra-compact 32-channel board, that can amplify, filter and digitized the signal and that can be placed very close to the signal source, thus further lowering the noise level.[70] The signal was collected over a frequency range between 0.1 Hz and 10 kHz by using standard saline solution for electrophysiological recording and Ag/AgCl as a reference electrode. The time acquisition was fixed at 5 min with a sampling frequency of 25 kHz. Each measurement was performed with a minimum of four repetitions on the same electrode over a time period of 30 min. A custom pc program made in Matlab (the Mathworks) was used to acquire, visualize and analyze the recorded traces.

*Statistical Analysis*: *Statistical Analysis—Patch-Clamp Experiments*: Data are reported as the mean average ± standard error (S.E) of the number of patched cells ($n$). Experiments were performed 5 times on five different primary culture, each experimental session was performed at least in triplicate, where each replica was a different Au/SiNWs substrate. The analyses and statistics of electrophysiological membrane properties of astrocytes plated on Au/Si planar and Au/SiNWs have been performed with Origin MicroCal Ver 6.0. with $n$ = number of recorded cells, Au/Si Planar ($n = 13$) and Si/NWs ($n = 19$); Cp = membrane capacitance, pval = 0042; $V_{mem}$, resting membrane potential, pval = 00058; SG, mean specific conductance, pval = $965 \times 10^{-6}$; IR, input resistance, pval = $133 \times 10^{-3}$; I (pA/pF) pval = 0.042; * $p < 0.05$, ** $p < 0.01$, *** $p < 0.001$ independent t-test.

*Statistical Analysis—Extracellular Recordings*: The dataset comprises acquisitions in four different conditions:

- Recordings from planar electrodes in a solution of astrocytes (planar Au+Cells–4 experimental sessions);
- Recordings from planar electrodes with in saline solution (planar Au+No Cells–2 experimental sessions);
- Recordings from NW electrodes in a solution of astrocytes (Au/SiNWs+Cells–6 experimental sessions);
- Recordings from NW electrodes in saline solution (Au/SiNWs+No Cells–3 experimental sessions).

Recording channels were spaced 25 µm; thus, given this distance, data was treated from the three single channels belonging to the same recording session as independent. Contaminated traces were removed by external noise sources or those that showed abrupt noise change. The final dataset thus consisted in 3 recordings for planar Au, 10 recordings for planar Au+Cells, 5 recordings for Au/SiNWs and 14 recordings for Au/SiNWs+Cells. As described in the Result section, during experimental sessions with Au/SiNWs MEA+Cells, on a subset of 9 recordings, pharmacological manipulation was also performed by using extracellular solution containing high concentration of potassium and by addition with barium chloride (200 µm) to the latter solution.

Each recording was low pass filtered in the 0.1–30 Hz frequency band with a 2nd order elliptic filter in Matlab, first 20 s of data was removed in

order to get rid of data distortion induced by filter application. The power spectral density was calculated of each recorded trace in the following frequency bands: delta (0.1–5 Hz), theta (5–9 Hz), beta (9–30 Hz).[51] Finally, the average PSD was computed of each band for the different experimental groups (Planar Au and Au/SiNWs electrodes with and without cells). To statistically assess the difference of band power across different conditions (cells plated over Au/SiNWs versus planar Au MEA), were performed, per each frequency band, the Mann-Whitney test using OriginPro (OriginLab).

*Event Detection Analysis*: Each recording was low pass filtered below the powerline frequency, with a Chebyshev type II IIR filter with order 20, stop band frequency of 50 Hz, using Matlab filter design tool. Then, the filter was applied using the "filtfilt" function in order to prevent phase distortion, and each recording was down sampled by a factor of 50 (i.e., keeping 1 data point every 50) in order to make the subsequent computation faster, thus obtaining a sampling frequency of 500 Hz.

In order to have a smoother and cleaner signal, the Maximal Overlap Discrete Wavelet Transform (MODWT) was performed,[51] which convolves the input with a discrete set of wavelet functions, splitting the whole frequency spectrum in sub-bands. The discrete set was obtained from a mother wavelet that was set equal to "sym4" (symlets wavelet with four vanishing moments). Four levels of decomposition, obtaining 5 components per recording (four "detailed" and one "approximated") were used.

Since MODWT does not preserve the temporal alignment of the input, a MODWT Multiresolution Analysis (MODWTMRA) was subsequentially performed to restore the original phase. This allows reconstructing the original signal, summing up all the previously obtained components. Then, only the last two components were kept, eventually obtaining the reconstructed trace, as shown in the Figure S5 (Supporting Information) (black line), with a frequency bandwidth of 0–31 Hz.

To detect electrophysiological events, symmetric amplitude thresholds applied on the reconstructed traces were used. For each trace, thresholds were computed automatically from the data distribution, as proposed by Quiroga et al.[52] The threshold values were estimated using the Median Absolute Deviation (MAD) of the distribution, as follows

$$\vartheta_{thr} = \pm n \cdot \frac{\text{MAD}}{0.6745} \tag{1}$$

where $n$ is a positive dimensionless parameter. For this work, $n = 5$ was chosen because it was empirically observed that it the minimum value for $n$ that guaranteed a negligible number of detected signals in the no-cell configurations.

Once events were detected as points of the trace above/below the thresholds, the time range of an event as the second left and second right zero-crossings (Figure S5A, Supporting Information, red line) were defined. Figure S5B (Supporting Information) shows the events detected on three different channels on a single recording, using the automatic thresholding method.

## Supporting Information

Supporting Information is available from the Wiley Online Library or from the author.

## Acknowledgements

This work was supported by the AFOSR Research Projects ASTROMAT, FA9550-17-1-0502 (V.B., A.C.) and 3D NEUROGLIA, FA9550-18-1-0255 (V.B., R.Z., L.A.), ASTRONIR, FA9550-17-1-0052 (E.S.) and by EU Marie Curie Project OLIMPIA (GA 316832) (M.M., V.B., A.B.), POR-FERS 2014–2020 of Emilia Romagna Region, MAT-2-REP (E.S., V.B.). Dr. Alessia Minardi from FABIT Dept. of the University of Bologna, Bologna, Italy, for her help in the preparation and maintenance of astrocytes primary culture. The authors are grateful to Marianna Barbalinardo, from CNR ISMN, for her help in acquisition of SEM images and to Vincenzo Ragona and Paolo Mei CNR-ISMN for their technical support.

## Conflict of Interest

The authors declare no conflict of interest.

## Author Contributions

E.S and L.M equally contributed to this work and share the first authorships. D.P, M.S. equally contributed to this work and share the second authorship. J.G and S.M. equally contributed to this work. E.S. prepared and maintained rat primary culture, performed and analyzed patch-clamp experiments, performed extracellular recordings, contributed to the manuscript preparation and editing. L.M. fabricated the device, performed impedance measurements, performed extracellular recordings, designed the experiments and wrote the manuscript. A.B. prepared and maintained rat primary culture, performed immunofluorescence staining and image analyses. D.P. and L.P. performed extracellular recordings, designed and fabricated the chamber and the set-up for extracellular recordings measurements. F.V. performed the AFM imaging. F.F. and M.C. Performed confocal imaging acquisition. M.S. and M.CH. performed PSD data analyses of extracellular recording. J.G. designed the spike detection method, wrote the algorithm. S.M. reviewed and filtered the data, conceived the spike detection method. M.SO. reviewed and filtered the data, revised the software. L.T. supervised the data analysis. L.A, S.H., G.F., M.M. and R.Z. contributed to the discussion of the results and to the editing of the manuscript. A.C. and V.B. coordinated the research effort, designed the experiments, wrote the manuscript.

## Keywords

astrocytes, extracellular recording, gold coated silicon nanowires, nanostructured electrode array, slow oscillations

Received: November 7, 2019
Revised: January 22, 2020
Published online: February 18, 2020

[1] A. Verkhratsky, V. Untiet, C. R. Rose, *J. Physiol.* **2019**, https://doi.org/10.1113/JP277478.
[2] A. Chvátal, M. Anderova, H. Neprasova, I. Prajerova, J. Benesova, O. Butenko, A. Verkhratsky, *Physiol. Res.* **2008**, *57*, S101.
[3] P. Kofuji, E. Newman, *Neuroscience* **2004**, *129*, 1043.
[4] V. Benfenati, S. Ferroni, *Neuroscience* **2010**, *168*, 926.
[5] E. Scemes, D. C. Spray, *Neurochem. Res.* **2012**, *37*, 2310.
[6] J. W. Salatino, K. A. Ludwig, D. Y. Kozai, E. K. Purcell, *Nat. Biomed. Eng.* **2017**, *1*, 862.
[7] M. E. Spira, A. Hai, *Nat. Nanotechnol.* **2013**, *8*, 83.
[8] A. Borrachero-Conejo, E. Saracino, M. Natali, F. Prescimone, S. Karges, S. Bonetti, G. P. Nicchia, F. Formaggio, M. Caprini, R. Zamboni, F. Mercuri, S. Toffanin, M. Muccini, V. Benfenati, *Adv. Healthcare Mater.* **2019**, *8*, 1801139.
[9] A. L. G. Mestre, M. Cerquido, P. M. C. Inácio, S. Asganfar, A. S. Lourenço, M. L. S. Cristiano, P. Aguiar, M. C. R. Medeiros, I. M. Araújo, J. Ventura, H. L. Gomes, *Sci. Rep.* **2017**, *7*, 14284.

 

[10] A. L. G. Mestre, P. M. C. Inácio, Y. Elamine, S. Asgarifar, A. S. Lourenço, M. L. S. Cristiano, P. Aguiar P., M. C. R. Medeiros, M. Araújo, J. Ventura, H. L. Gomes, *Front. Neural Circuits* **2017**, *11*, 1.
[11] a) T. Posati, A. Pistone, E. Saracino F. Formaggio, M. G. Mola, E. Troni, A. Sagnella, M. Nocchetti, M. Barbalinardo, F. Valle, S. Bonetti, M. Caprini, G. P. Nicchia, R. Zamboni, M. Muccini, V. Benfenati, *Sci. Rep.* **2016**, *6*, 1; b) C. Vallejo-Giraldo, K. Krukiewicz, I. Calaresu, J. Zhu, M. Palma, M. Fernández-Yague, B. McDowell, N. Peixoto, N. Farid, G. O'Connor, L. Ballerini, A. Pandit, M. J. P. Biggs, *Small* **2018**, *14*, e1800863.
[12] V. Benfenati, S. Toffanin, R. Capelli, L. M. Camassa, S. Ferroni, D. L. Kaplan, F. G. Omenetto, M. Muccini, R. Zamboni, *Biomaterials* **2010**, *31*, 7883.
[13] A. Verkhratsky, M. Nedergaard, *Physiol. Rev.* **2018**, *98*, 239.
[14] M. David-Pur, L. Bareket-Keren, G. Beit-Yaakov, D. Raz-Prag, Y. Hanein, *Biomed. Microdevices* **2014**, *16*, 43.
[15] E. Castagnola, A. Ansaldo E. Maggiolini, N. Angotzi, M. Skrap, D. Ricci, L. Fadiga, *ACS Nano* **2013**, *7*, 3887.
[16] X. Cui, D. C. Martin, *Sens. Actuators, A* **2003**, *103*, 384.
[17] M. Dankerl, S. Eick, B. Hofmann, M. Hauf, S. Ingebrandt, A. Offenhäusser, M. Stutzmann, J. A. Garrido, *Adv. Funct. Mater.* **2009**, *19*, 2915.
[18] B. M. Blaschke, M. Lottner, S. Drieschner, A. Bonaccini Calia, K. Stoiber, L. Rousseau, G. Lissourges, J. A. Garrido, *2D Mater.* **2016**, *3*, 25007.
[19] F. Patolsky, B. P. Timko, G. Yu, Y. Fang, A. B. Greytak, G. Zheng, C. M. Lieber, *Science* **2006**, *313*, 1100.
[20] T. Cohen-Karni, D. Casanova, J. F. Cahoon, Q. Qing, D. C. Bell, C. M. Lieber, *Nano Lett.* **2012**, *12*, 2639.
[21] B. Tian, J. Liu, T. Dvir, L. Jin, J. H. Tsui, Q. Qing, Z. Suo, R. Langer, D. S. Kohane, C. M. Lieber, *Nat. Mater.* **2012**, *11*, 986.
[22] C. Xie, Z. Lin, L. Hanson, Y. Cui, B. Cui, *Nat. Nanotechnol.* **2012**, *7*, 185.
[23] Q. Qing, Z J. Lin, X. R. Gao, L. Mai, C. M. Lieber, *Nat. Nanotechnol.* **2014**, *9*, 142.
[24] J. T. Robinson, M. Jorgolli, A. K. Shalek, M. H. Yoon, R. S. Gertner, H. Park, *Nat. Nanotechnol.* **2012**, *7*, 180.
[25] M. Kwak, L. Han, J. J. Chen, R. Fan, *Small* **2015**, *11*, 5600.
[26] A. Convertino, V. Mussi, L. Maiolo, M. Ledda, M. G. Lolli, F. A. Bovino, G. Fortunato, M. Rocchia, A. Lisi. *Nanotechnology* **2018**, *29*, 415102.
[27] G. Hong, C. Lieber, *Nat. Rev. Neurosci.* **2019**, *20*, 330.
[28] A. Ledesma, X.H. Li, J. L. Carvalho-de-Souza, W. Wei, F. Bezanilla, B. Tian, *Nat. Nanotechnol.* **2019**, *14*, 645.
[29] L. Gällentoft, L. M. E. Pettersson, N. Danielsen, J. Schouenborg, C. N. Prinz, C. Eriksson Linsmeier, *J. Nanobiotechnol.* **2016**, *14*, 64.
[30] H. Monai, O. Masamichi, M. Tanaka, Y. Oe, A. Konno, H. Hirai, K. Mikoshiba, S. Itohara, J. Nakai, Y. Iwai, H. Hirase, *Nat. Commun.* **2016**, *7*, 11100.
[31] A. Convertino, V. Mussi, L. Maiolo, *Sci. Rep.* **2016**, *6*, 25099.
[32] L. Maiolo, D. Polese, A. Pecora, G. Fortunato, Y. S. Diamond, A. Convertino, *Adv. Healthcare Mater.* **2016**, *5*, 575.
[33] M. Cuscunà, A. Convertino, L. Mariucci, G. Fortunato, L. Felisari, G. Nicotra, C. Spinella, A. Pecora, F. Martelli, *Nanotechnology* **2010**, *21*, 255601.
[34] A. Convertino, M. Cuscuna, G. Nicotra, C. Spinella, L. Felisari, G. Fortunato, F. Martelli, *J. Cryst. Growth* **2011**, *335*, 10.
[35] L. Maiolo, A. Pecora, G. Fortunato, N. D. Young, *J. Vac. Sci. Technol., A* **2006**, *24*, 280.
[36] S. Ferroni, C. Marchini, P. Schubert, C. Rapisarda, *FEBS Lett.* **1995**, *367*, 319.
[37] M. K. Gottipati, J. J. Samuelson, I. Kalinina, E. Bekyarova, R.C. Haddon, V. Parpura, *Nano Lett.* **2013**, *13*, 4387.
[38] M. Bramini, S. Sacchetti, A. Armirotti, A. Rocchi, E. Vázquez, V. L. Castellanos, T. Bandiera, F. Cesca, F. Benfenati, *ACS Nano* **2016**, *10*, 7154.
[39] H. Pivonkova, M. Anderova, *Curr. Pharm. Des.* **2017**, *23*, 5056.
[40] A. S. G. Curtis, M. Varde, *J. Natl. Cancer Res. Inst.* **1964**, *33*, 15.
[41] C. Cimmino, L. Rossano, P. A. Netti, M. Ventre, *Front. Bioeng. Biotechnol.* **2018**, *6*, 190.
[42] K. Breslin, J. J. Wade, K. F. Wong-Lin, J. Harkin, B. Flanagan, H. Van Zalinge, S. Hall, M. Walker, A. Verkhratsky, L. McDaid, *PLoS Comput. Biol.* **2018**, *14*, 1006151.
[43] G. Seifert, K. Schilling, C. Steinhäuser, *Nat. Rev. Neurosci.* **2006**, *7*, 194.
[44] H. Persson, C. Kebler, K. Malhave, L. Samuelson, J. O. Tegenfeldt, S. Oredsson, C. N. Prinz, *Small* **2013**, *9*, 4006.
[45] C. R. Rose, J. Y. Chatton, *Neuroscience* **2016**, *323*, 121.
[46] M. Santello, N. Toni, A. Volterra, *Nat. Neurosci.* **2019**, *22*, 154.
[47] A. Bellot-Saez, G. Cohen, A. van Schaik, L. Ooi, J. W. Morley, Y. Buskila, *Sci. Rep.* **2018**, *8*, 11565.
[48] E. Dossi, F. Vasile, N. Rouach, *Brain Res. Bull.* **2018**, *136*, 139.
[49] K.V. Kastanenka, R. Moreno-Bote, M. De Pittà, G. Perea, A. Eraso-Pichot, R. Masgrau, K.E. Poskanzer, E. Galea, *Glia* **2019**, *68*, 5.
[50] L. Pazzini, D. Polese, J. F. Weinert, L. Maiolo, F. Maita, M. Marrani, A. Pecora, M. V. Sanchez-Vives, G. Fortunato, *Sci. Rep.* **2018**, *8*, 16717.
[51] D. Percival, A. Walden, *Wavelet Methods for Time Series Analysis*, Cambridge University Press, Cambridge **2000**.
[52] R. Q. Quiroga, Z. Nadasdy, Y. Ben-Shaul, *Neural Comput.* **2004**, *16*, 1661.

 

### 1.4 Introduction to Paper 4

"*Cell Volume Regulation Mechanisms in Differentiated Astrocytes*" by

**Maria Grazia Mola, Emanuela Saracino, Francesco Formaggio, Arcangela Gabriella Amerotti, Barbara Barile, Tamara Posati, Antonio Cibelli, Antonio Frigeri, Claudia Palazzo, Roberto Zamboni, Marco Caprini, Grazia Paola Nicchia, Valentina Benfenati** has been published as Open Access publishing on Cell Physiol Biochem. 2021 Nov 5;55(S1):196-212. DOI: 10.33594/000000469 (https://www.cellphysiolbiochem.com/Articles/000469/).

Supplementary information accompanies this paper at:

https://www.cellphysiolbiochem.com/Articles/000469/SM/SM_1033594000000469.pdf.



In a previous study conducted in Benfenati lab, (Posati T., et al., *A Nanoscale Interface Promoting Molecular and Functional Differentiation of Neural Cells*, Scientific Reports J., 2016 (www.nature.com/scientificreports, https://www.nature.com/articles/srep31226)), it was demonstrated that nanostructured interfaces are potential tools to generate reliable models to study astrocytes *in vitro*. In the specific hydrotalcite-like compounds (HTlc) were interfaced with cortical rat primary astrocytes, showing that HTlc were layered nanostructured materials that promote astrocytes differentiation, molecular and functional up-regulation of inward rectifying potassium channel Kir 4.1 and AQP4. At the astrocytic microdomain Here, taking advantage of the same substrates (HTlc), it is reported the mechanism underpinning astrocytic cell volume regulation, critical for brain function and pathology. The ability of astrocytes to control extracellular volume homeostasis (RVD) and its correlation with the expression and function of AQP4 as well as with Transient Receptor Potential Vanilloid 4 (TRPV4) and Volume Regulated

Anion Channel (VRAC), together with Kir 4.1 are here investigated. The main hypothesis is that there is a functional interaction between AQP4 and each of these anion and cation channels, mainly expressed in the microdomains of astrocytes *in vivo*. In conclusion, HTlc represent a valid guide to structural and molecular investigation of astrocytes role in the brain and they can be useful in identifying novel therapeutic targets for neurological conditions, such as those characterized by imbalances to hydro saline challenges (i.e. edema) or by altered cell volume regulation (i.e in glioma).

**PDF -FORMATO PAPERS\Mola MG., Saracino E.,et al., Cellular Phisiology and Biochemistry PDF 4.4.pdf**

Cellular Physiology and Biochemistry

Cell Physiol Biochem 2021;55(S1):196-212
DOI: 10.33594/000000460
Published online: 5 November 2021
Accepted: 8 September 2021



**Original Paper**

# Cell Volume Regulation Mechanisms in Differentiated Astrocytes

Maria Grazia Mola[a] Emanuela Saracino[b] Francesco Formaggio[c]
Arcangela Gabriella Amerotti[a,b] Barbara Barile[a] Tamara Posati[b]
Antonio Cibelli[a] Antonio Frigeri[d] Claudia Palazzo[d] Roberto Zamboni[b]
Marco Caprini[c] Grazia Paola Nicchia[a] Valentina Benfenati[b]

[a]Department of Biosciences, Biotechnologies and Biopharmaceutics, University of Bari Aldo Moro, Bari, Italy, [b]Consiglio Nazionale delle Ricerche (CNR), Istituto per lo Sintesi Organica e la Fotoreattività (ISOF), Bologna, Italy, [c]Department of Pharmacy and Biotechnology, University of Bologna, Bologna, Italy, [d]Department of Basic Medical Sciences, Neurosciences and Sense Organs, School of Medicine, University of Bari Aldo Moro, Bari, Italy

**Key Words**
Astrocytes • Volume regulation • AQP4 and ion channels • Differentiation • Bio-nanomaterials

**Abstract**
***Background/Aims:*** The ability of astrocytes to control extracellular volume homeostasis is critical for brain function and pathology. Uncovering the mechanisms of cell volume regulation by astrocytes will be important for identifying novel therapeutic targets for neurological conditions, such as those characterized by imbalances to hydro saline challenges (as in edema) or by altered cell volume regulation (as in glioma). One major challenge in studying the astroglial membrane channels involved in volume homeostasis in cell culture model systems is that the expression patterns of these membrane channels do not resemble those observed *in vivo*. In our previous study, we demonstrated that rat primary astrocytes grown on nanostructured interfaces based on hydrotalcite-like compounds (HTlc) *in vitro* are differentiated and display molecular and functional properties of *in vivo* astrocytes, such as the functional expression of inwardly rectifying $K^+$ channel (Kir 4.1) and Aquaporin-4 (AQP4) at the astrocytic microdomain. Here, we take advantage of the properties of differentiated primary astrocytes *in vitro* to provide an insight into the mechanism underpinning astrocytic cell volume regulation and its correlation with the expression and function of AQP4, Transient Receptor Potential Vanilloid 4 (TRPV4), and Volume Regulated Anion Channel (VRAC). ***Methods:*** The calcein quenching method was used to study water transport and cell volume regulation. Calcium imaging and electrophysiology (patch-clamp) were used for functional analyses of calcium dynamics and chloride currents. Western blot and immunofluorescence were used to analyse the expression and localization of the channel proteins of interest. ***Results:*** We found that the increase in water permeability, previously observed in differentiated astrocytes, occurs simultaneously

M. G. Mola and E. Saracino contributed equally to this work.

Valentina Benfenati and Grazia Paola Nicchia
Consiglio Nazionale delle Ricerche (CNR), Istituto per lo Sintesi Organica e la Fotoreattività (ISOF), Via Gobetti 101, 40129 Bologna (Italy)
Tel. +390516399786, E-Mail valentina.benfenati@isof.cnr.it

Department of Biosciences, Biotechnologies and Biopharmaceutics, University of Bari Aldo Moro Via Orabona 4, 70125 Bari (Italy)
Tel. +390805443335, E-Mail graziapaola.nicchia@uniba.it

Cellular Physiology and Biochemistry
Cell Physiol Biochem 2021;55(S1):196-212
DOI: 10.33594/000000469
Published online: 5 November 2021



with more efficient regulatory volume increase and regulatory volume decrease. Accordingly, the magnitude of the hypotonic induced intracellular calcium response, typically mediated by TRPV4, as well as the hypotonic induced VRAC current, was almost twice as high in differentiated astrocytes. Interestingly, while we confirmed increased AQP4 expression in the membrane of differentiated astrocytes, the expression of the channels TRPV4 and Leucine-Rich Repeats-Containing 8-A (LRRC8-A) were comparable between differentiated and non-differentiated astrocytes. ***Conclusion:*** The reported results indicate that AQP4 up-regulation observed in differentiated astrocytes might promote higher sensitivity of the cell to osmotic changes, resulting in increased magnitude of calcium signaling and faster kinetics of the RVD and RVI processes. The implications for cell physiology and the mechanisms underlying astrocytic interaction with nanostructured interfaces are discussed.



## Introduction

Every cell is constantly challenged with osmolyte microgradient alterations as a result of metabolic cellular activity, nearby cell function and cell processes such as cell migration, proliferation, differentiation, signaling and apoptotic cell death. As a result, cell volume perturbation occurs both locally and globally [1–5]. Accordingly, the homeostasis of cell volume is efficiently preserved by processes referred to as Regulatory Volume Decrease (RVD) and Regulatory Volume Increase (RVI), driving the efflux or influx of ions and water for the cell to reach a new steady state.

A wealth of data indicates that astrocytes are essential for the maintenance of volume homeostasis in the brain since they are in charge of maintaining ions, water and osmolytes at their homeostatic concentrations [6–11]. In particular, astrocytes control ions and water dynamics at processes contacting synapses and siphon the excess of osmolytes and water to the blood vessels. Among protein channels involved in astrocytic regulation of the cell volume, the roles of water channel aquaporin-4 (AQP4), of calcium channels (belonging to the family of Transient Receptor potential Vanilloid 4 (TRPV4)), and of chloride channels (Volume Regulated Anion channels (VRAC)) are particularly important [12–15]. AQP4 is selectively expressed in astrocytic endfeet that face blood vessels, and it mainly accounts for faster, hydrostatically and osmotically driven water transport and distribution in the brain [16, 17]. TRPV4 is a polymodal sensor that can be gated by different stimuli, including thermal stress, cell volume and anisotonic challenge across the plasma membrane [18–23]. In the cortex, TRPV4 is expressed mainly on astrocytic membranes that face blood vessels. In astrocytes *in vitro* and in Müller cells *in situ*, TRPV4 mediates osmotically induced calcium signaling involved in the cell volume regulation mechanism [6]. The efflux of Chloride ($Cl^-$) and organic osmolytes (such as taurine, glutamate, and aspartate) through VRAC allows for the recovery of physiological cell volume during the RVD process [24–26]. Recent studies have identified the protein called LRRC8-A in the plasma membrane of primary cortical astrocytes and *in situ* at the perivascular interface with endothelial cells. Moreover, LRRC8-A protein expression is essential for proper VRAC mediated osmolyte release [27] and currents as well as for astrocytic RVD and is a key factor for astroglial volume homeostasis [9, 28].

Cooperation between different molecular players has also been reported *in vitro*. TRPV4 cooperates with AQP4 in RVD in astrocytes [19, 20], possibly by molecular partnerships that occur in specific domains *in situ* [19]. The VRAC and AQP4 functional interaction has been demonstrated in primary astrocytes [26]. Notably, the alteration in expression and function of AQP4, TRPV4 and VRAC is widely recognized as pathogenic in neurological conditions characterized by dysregulation of astrocytic homeostatic control of volume [25]. All this evidence highlights that uncovering the mechanisms of cell volume regulation in astrocytes is of great interest. However, major technical issues arise in the study of astroglial cell volume regulation that limit the knowledge acquired thus far on the mechanisms behind it. To reach the resolution required for studying dynamics of microdomains in two photon-imaging experiments *in vivo*, higher power exposure is required that can lead to phototoxicity [29]. On

the other hand, a major pitfall in the study of astroglial membrane channels involved in volume homeostasis *in vitro* is that, in standard cell culture conditions, their expression pattern does not resemble that observed *in vivo* [30–32]. In this context, we have demonstrated that plating astrocytes on a nano-structured interface, called hydrotalcite (HTlc), is an efficient method to obtain differentiated astrocytes *in vitro*, in terms of morphology differentiation and both molecular and functional features [33, 34]. In particular, HTlc astrocytes displayed highly branched morphology, accompanied with increased expression of Kir4.1 protein and conductance and overexpression of AQP4, that was paralleled with increased swelling-induced water permeability [32].

Given the peculiarity of this cell culture approach, which allows for the study of astrocytes *in vitro* in a way that recapitulates important features of astrocytes *in vivo*, we sought to study cell volume regulation mechanisms in these differentiated astrocytes. In particular, we aimed to investigate the functional and molecular roles of the increased AQP4 mediated-water permeability associated with astrocyte differentiation, on TRPV4 mediated $Ca^{2+}$ dynamics and on VRAC conductance in the so-called RVD and RVI mechanisms.

We found that RVD and RVI were more efficient in differentiated astrocytes. Moreover, while the expression of AQP4 is increased in the cell membrane, the expression of VRAC and TRPV4 is not. Surprisingly, swelling induced calcium increase as well as volume regulated chloride conductance are higher in magnitude in differentiated astrocytes compared to polygonal ones. The results presented here indicate that differentiated astrocytes respond to exposure to anisosmotic conditions with larger cell volume changes and larger restorative effects because overexpression of AQP4 channels leads to larger volume changes that in turn activate the volume regulatory effector mechanisms. Collectively, these data confirmed that AQP4 expression is critical for VRAC and TRPV4 function [18–20] and support the hypothesis that AQP4 upregulation in the cell membrane might serve as a driver for improved sensing and effector mechanisms responsible for astrocytic involvement in RVD and RVI.

## Materials and Methods

*Primary astrocyte culture preparation and plating*

Primary cultures of cortical astrocytes were isolated from brains of postnatal Wistar rats, as described in [35]. Cells were grown in cell culture flasks containing DMEM-GlutaMAX medium supplemented with 10% fetal bovine serum (FBS) and penicillin/streptomycin (100 U/mL and 100 µg/mL, respectively). Astrocytes were maintained for 3-4 weeks in culture, and the medium was changed twice per week. Microglia and oligodendrocyte contaminating cells were removed by gently shaking the flasks, when necessary. Glial fibrillary acidic protein (GFAP) immunolabeling demonstrated that cells were >95% type-1 cortical astrocytes [5, 31, 35]. Once confluent, astrocytes were detached using trypsin-EDTA 0.025% and replated as a single-cell suspension onto either Poly-D-lysine (PDL) or hydrotalcite (HTlc) -coated petri dishes or glass coverslips, depending on the need. HTlc films were prepared according to protocols described previously [32]. Experiments were performed 5 days after re-plating. Astrocytes were seeded at a high density for western blot and calcein quenching experiments ($10^4$ cells/cm$^2$). For immunofluorescence experiments, cells were plated at a low density ($2 \times 10^3$ cells/cm$^2$). All cell culture products were purchased from Euroclone (Milan, Italy).

*Antibodies and Dyes*

The following primary antibodies were used: rabbit anti-AQP4 (Cat: sc-20812; Santa Cruz, Biotechnology, Dallas, Texas, USA) dilution 1:500, mouse anti-GFAP (Cat: G3893; Sigma, Saint Louis, Missouri, USA) dilution 1:500, rabbit anti-TRPV4 (Cat: ACC-034; Jerusalem BioPark, Israel) dilution 1:200, rabbit anti-LRRC8A (generated by Twin Helix, [28]; Western blot 8 µg/ml; immunofluorescence 0.8 µg/ml). The following secondary antibodies were used at dilutions of 1:1000 for immunofluorescence: AlexaFluor 488-conjugated donkey anti-mouse IgG (Cat: A21202) and AlexaFluor 488-conjugated donkey anti-rabbit IgG (Cat: A21206), both purchased from Thermo Fisher Scientific, Waltham, Massachusetts, USA. The following secondary antibodies were used at dilutions of 1:5000 for Western blots: horseradish peroxidase

(HRP)-conjugated goat anti-rabbit IgG (sc-2004) and goat anti-mouse IgG (Cat: sc-2005), both purchased from Santa Cruz, Biotechnology, Dallas, Texas, USA. AlexaFluor 647-phalloidin (Cat: A22287) diluted 1:1000 was used to stain F-actin.

*Protein sample preparation for SDS-PAGE, Western blotting and densitometric analysis*

Astrocytes grown for 5 days on 60 mm petri dishes coated with either PDL or HTlc-films were washed once in ice-cold phosphate-buffered saline (PBS) and dissolved in five volumes of RIPA lysis buffer (10 mM Tris-HCl, pH 7.4, 140 mM NaCl, 1% Triton X-100, 1% Na deoxycholate, 0.1% SDS, 1mM $Na_3VO_4$, 1 mM NaF, 1 mM EDTA and 1× Protease Inhibitor Cocktail). Cell lysis was performed on ice for 1 h, and the samples were then centrifuged at 22,000g for 30 min at 4°C. Supernatants were collected and their protein content was measured using a bicinchoninic acid (BCA) Protein Assay Kit (Thermo Fisher Scientific, Waltham, Massachusetts, USA). 20 ug of membrane proteins/lane was dissolved in Laemmli Sample Buffer (Bio-Rad, Hercules, California, USA) and 50 mM dithiothreitol, heated to 37°C for 10 min, resolved on a 10% polyacrylamide gel, and transferred to polyvinylidene fluoride (PVDF) membranes (Merck Millipore, Burlington, Massachusetts, USA) for immunoblot analysis. Blocked membranes were incubated with primary antibodies, washed, then incubated with the appropriate peroxidase-conjugated IgG secondary antibodies. Reactive bands were revealed using enhanced chemiluminescence (Thermo Fisher Scientific, Waltham, Massachusetts, USA) and visualized on a Chemidoc imaging system (Bio-Rad, Hercules, California, USA). The density values of target bands were quantified with Image Lab software 5.2.1 and normalized to the Coomassie blue-stained membrane.

*Immunofluorescence and confocal microscopy analysis*

Cultured astrocytes grown on 12 mm diameter glass coverslips coated with PDL or HTlc were fixed in 4% paraformaldehyde solution, rinsed 3 times in PBS (Euroclone, Milan, Italy) and permeabilized for 15 min with 0.3% Triton X-100 (Sigma, Saint Louis, Missouri, USA) in PBS. After blocking with 0.1% gelatin (Sigma, Saint Louis, Missouri, USA) in PBS (blocking solution), cells were incubated for 1 h with primary antibodies, washed with blocking solution, and incubated for 45 min with the appropriate Alexa Fluor-conjugated secondary antibodies or AlexaFluor 647-phalloidin. Cover-slips were mounted on slides, using a medium containing 50% Glycerol and 0.01% N-Propylgallate in PBS, and immunostained cells were observed with a confocal laser-scanning microscope (Leica TSC-SP8, Leica-Microsystems, Wetzlar, Germany). Single or well-spread cells were preferentially imaged for the analysis under 100X magnification. Fluorescence emission was obtained by laser excitation of Alexa Fluor 488 at 488 nm and for Alexa Fluor 647 at 640 nm. Emission was collected between 510 and 540 nm and 670 to 720 nm, respectively. Two empty areas with no cells in the field were also acquired and collected as sample background images for each condition. The auto contrast function was applied to the captured images as a whole using Adobe Photoshop CS6 software to improve the visual quality of images in terms of colour and contrast.

*Confocal microscopy analysis*

Image analysis was performed using Fiji software (NIH). After background subtraction, a minimum of three square-shaped ROIs with an area of 100 $\mu m^2$ was drawn at the edge of single and isolated astrocytes or on their processes, when expressed. The two-channel ROIs were analysed using the JACoP plug-in. The software defines an automatic threshold for each single-channel image and allows calculation of Pearson's coefficient r, which is a measure of correlation between actin (red channel) and membrane proteins (green channel). Pearson's coefficient values range from +1 to -1, where +1 indicates a perfect positive relationship, -1 indicates a perfect negative relationship, and a 0 indicates no relationship. In this work, a high degree of correlation has been ascribed to the values lying between + 0.50 and + 1, while coefficients lying between +0.1 and +0.49 have been interpreted as a moderate or poor degree of correlation. The results are the average of three independent experiments where 3 ROIs were analysed for each cell.

*Fluorescence-quenching Assay*

Cell-volume changes in primary cultured astrocytes were assessed using calcein-quenching fluorescence assay as described previously [35]. Astrocytes were seeded on black, clear-bottom, 96-well plates (Corning, New York, USA) coated with either PDL or HTlc at a density of 3,500 cells per well, and water permeability measurements were taken 5 days after plating.

Nearly 90% confluent cells were loaded with 10 µM membrane permeable calcein-AM (Molecular Probes, Eugene, Oregon, USA), which is trapped intra-cellularly after cleavage by esterases and exhibits a fluorescence intensity directly proportional to changes in cell volume. Calcein fluorescence kinetics in response to altered extracellular osmolarity were recorded on a FlexStation3 plate reader, equipped with a liquid handling module (Molecular Devices, San Jose, California, USA) able to transfer reagents from a source plate to the read plate during data acquisition. Fluorescence was excited at 490 nm and detected at 520 nm using dual monochromators.

Cells were rinsed in isotonic PBS, and the osmotic shift was applied by automated addition of an appropriate volume of hypotonic (NaCl-free PBS) or hypertonic (D-mannitol 0.5 M) solution in order to obtain the required final extracellular osmolarity [20, 35–39]. Calcein fluorescence intensity increased upon addition of hypotonic media due to water influx and cell swelling and decreased in response to hypertonic stimulation due to water efflux and cell shrinkage. Data acquisition was performed by SoftMax Pro software, and the data were analysed with Prism software (GraphPad Software, La Jolla, CA, USA).

The time constants of cell volume changes upon either the osmotic stimuli or regulatory volume decrease (RVD) were obtained by fitting the data with an exponential function. The time constant of the regulatory volume increase (RVI) kinetics registered after the hypertonic-induced cell shrinkage was calculated by the linear fitting of the tangent line to the initial region of the recovery curve and expressed as 1/slope (s). The percentage of volume recovery was calculated from the maximum intensity of fluorescence reached after the osmotic shock (the amplitude of cell volume variation) and the level of fluorescence reached after the regulatory mechanism.

*Intracellular Calcium Measurements*

Intracellular calcium changes in response to hypotonic gradient were measured using the FlexStation3 plate reader, as previously described [20]. Astrocytes were seeded on black, clear-bottom, 96-well plates (Corning, New York, USA) coated with either PDL or HTlc at a density of 3,500 cells per well, and calcium measurements were done 5 days after plating. Cells were loaded with the ratiometric calcium indicator Fura-2-AM (8 µM; Molecular Probes, Eugene, Oregon, USA) in DMEM for 30 min at 37°C. Cells were then washed with DPBS and stabilized in the same buffer for 10 min at 37°C. The hypotonic stimulus was induced 20 s after the beginning of the data acquisition by adding an appropriate volume of hypotonic solution (NaCl-free DPBS) in order to obtain the required final extracellular osmolarity, and the fluorescence was recorded for 100 s. Intracellular calcium level was monitored by the ratio of the fluorescence intensity at 510 nm excited alternatively by 340 nm and 380 nm (F340/F380). The fluorescence ratio F340/F380 was used as an indicator of cytosolic [$Ca^{2+}$] changes, and the maximum intensity of F340/F380 ratio reached after the osmotic shock corresponds to the peak of calcium response. The relative time to reach this maximum was also measured. Data analysis was performed using SoftMaxPro and Prism 5 (Graph Pad).

*Electrophysiology*

Whole-cell recordings of swelling-activated $Cl^-$ currents were performed in cultured astrocytes as previously described [26]. Astrocytes plated both on PDL and HTlc were mounted on an inverted microscope (Nikon Diaphot; Nikon Italy, Firenze, Italy). Currents were recorded with the patch-clamp technique in a whole-cell configuration [40]. Patch pipettes were prepared from thin-walled borosilicate glass capillaries to obtain a tip resistance of 2–4 MΩ. Membrane currents were amplified with an EPC-7 amplifier (List Electronic, Darmstadt, Germany) and low-pass filtered at 2 kHz (3 dB). Data were acquired with a sample rate of 5 kHz. Traces were analysed offline with pClamp 6 software (Axon Instrument, Foster City, CA, USA) and Origin 6.0 (MicroCal, Northampton, MA, USA). Experiments were performed at room temperature (22–24°C).

Saline solutions for patch-clamp experiments were prepared with salts of the highest purity grade deionized and sterilized water (Millipore Sigma, Merck KGaA, Darmstadt, Germany). For electrophysiological recordings, the standard bath solution was the following (mM): 140 NaCl, 4 KCl, 2 $MgCl_2$, 2 $CaCl_2$, 10 HEPES, 10 glucose, pH 7.4 adjusted with NaOH, and the osmolarity was adjusted to 315 mOsm/L with mannitol. To isolate the $Cl^-$ current, the external bath perfusion, termed control saline, was the following (mM): 120 CsCl, 2 $MgCl_2$, 2 $CaCl_2$, 10 2-[Tris (hydroxymethyl)-methylamino]-ethanesulfonic acid (TES), 10 glucose, pH 7.4 adjusted with CsOH, and the osmolarity was adjusted to 320 mOsm/L with mannitol (60 mM). The intracellular (pipette) solution consisted of the following (mM): 126 CsCl, 2$MgCl_2$, 1 EGTA,

10 TES, pH 7.2 adjusted with CsOH, and the osmolarity was adjusted to 300 mOsm/L with mannitol. The hypotonic extracellular solution of 260 mOsm/L was obtained by omitting mannitol in the control solution. To block VRAC currents selectively, carbenoxolone (CBX) was freshly added to the hypotonic solution at a concentration of 100 μM [41].

*Statistical analysis*

Three independent experiments were performed on different astrocyte primary culture preparations for quantitative analysis. Statistically significant differences between PDL and HTlc astrocyte cultures exposed to a range of osmotic gradients were computed using one-way ANOVA analysis with a subsequent Newman-Keuls Multiple Comparison Test. Shapiro–Wilk normality test was performed on Pearson's correlation coefficients; then statistical significance between conditions per channel was evaluated using the unpaired t-test. Data are shown as mean ± SEM by using GraphPad Prism 5 software, and the level of significance was set at $p < 0.01$.

## Results

*HTlc astrocytes displayed faster cell volume changes and higher efficiency of cell volume regulation compared to PDL astrocytes*

The availability of a reliable *in vivo*-like model of astrocytes [32] allowed us to study the AQP4-mediated water transport considering the well-known molecular up-regulation of this channel promoted by the HTlc interface. Measurements were made on primary cultures of rat astrocytes 5 days after re-plating on poly-D-Lysine (PDL) or HTlc.

The impact of HTlc nanoparticles on osmotically induced changes in cell volume was characterized by calcein quenching-based assay [32, 35]. The osmotic behaviour of astrocytes grown on HTlc with respect to those grown on PDL was compared for their responsiveness in both hypotonic and hypertonic conditions. We also evaluated the dependence of water permeability parameters on the osmotic pressure gradient. Fig. 1A and B show representative data for the time courses of cell swelling in response to a series of hypotonic gradients between 20 and 100 mOsm/L recorded in PDL and HTlc plated astrocytes, respectively. Each shown kinetic includes a swelling phase related to the osmotic water influx and a regulatory volume phase that reached a steady-state cell volume (RVD phase). The time course of fluorescence signal was analysed in terms of swelling and RVD rate, swelling magnitude and percentage of volume recovery and measured parameters were compared between cells grown on PDL and HTlc substrates.

The analysis of the swelling phase revealed that HTlc astrocytes exhibited faster osmotic swelling compared to PDL astrocytes and that the measured swelling rate values were independent of the extracellular osmolarity in both growing substrates, as expected (Fig. 1C) [35, 42]. In agreement with previous studies [20, 37, 42, 43], we found a linear dependence of calcein signal ($\Delta F/F_0$) on the relative change in cell volume in the whole range of osmotic gradients tested on both PDL and HTlc substrates (Supplementary Fig. S1A – for all supplementary material see www.cellphysiolbiochem.com). Interestingly, astrocytes plated on HTlc films showed a significantly higher maximal amplitude of cell swelling for all osmotic gradient size compared to PDL astrocytes (Fig. 1D). Looking at the RVD phase, a higher efficiency of cell volume regulation in terms of rate of recovery (Fig. 1E) was detected in differentiated astrocytes in all hypotonic challenges. Similar to the trend observed in the swelling phase, the rate of the RVD phase was insensitive to the size of the osmotic gradient in both growing substrates. However, the percentage of volume recovery (Fig. 1F) was significantly enhanced at low osmotic gradients (20 and 25 mOsm/L) in differentiated cells. In parallel, the impact of HTlc nanoparticles on the glial functional response to hypertonic shock was explored. Fig. 2A and B show representative time courses of cell shrinking in response to a range of hypertonic gradients between 20 and 100 mOsm/L recorded in PDL and HTlc plated astrocytes, respectively. Each shown kinetic response includes a shrinking phase triggered by the osmotic water efflux and a regulatory volume phase that tends to

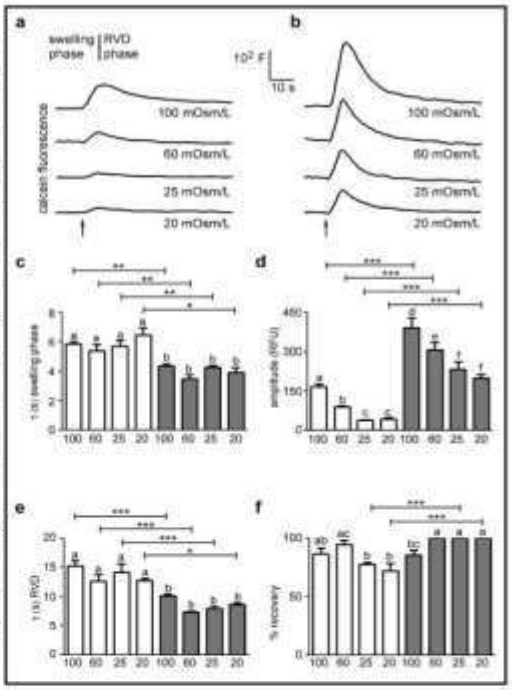


**Fig. 1.** Comparison between water transport properties of PDL and HTlc plated astrocytes under hypotonic conditions. a, b) Representative time courses of cell swelling (swelling phase) followed by RVD kinetic (RVD phase) recorded from calcein-AM loaded PDL (a) and HTlc (b) astrocytes. The time course shows changes in fluorescence (F, expressed in arbitrary units, RFU) over time (s) induced by the indicated hypotonic gradients applied. The arrows indicate the switch in the external osmolarity. c, d) Quantitative analysis of the cell swelling time constants (τ) and of the swelling amplitude (in RFU) in astrocytes plated on PDL (white bars) and HTlc (gray bars) for each gradient size (20, 25, 60,100 in mOsm/L). e, f) Quantitative analysis of values of the time constants (e) and of the extent of volume recovery (%) of the RVD phase (f) at the indicated hypotonic gradients. Note that AQP4 upregulation promotes faster swelling and RVD kinetics and higher efficiency of RVD. Data were obtained from 20 to 24 different measurements of three independent experiments performed using different astrocyte cultures. Significant differences of the means were calculated by One-way ANOVA and Newman-Keuls Multiple Comparison Test. ***P<0.0001; **P<0.001; *P<0.01. Different letters on top of each bar indicate significant difference between them and equal letters indicate no significant difference.

restore cell volume (RVI phase). The cell shrinking rates, computed from the time course data, were found to be remarkably enhanced in HTlc astrocytes compared to PDL astrocytes. Again, both PDL and HTlc astrocytes were insensitive to the entity of the osmotic shock (Fig. 2C). As observed in hypotonic conditions, the maximal amplitude of cell shrinkage was enhanced in differentiated astrocytes (Fig. 2D) and linearly related to the extracellular buffer osmolarity both in HTlc and PDL astrocytes (Supplementary Fig. S1B). Finally, HTlc films also promoted RVI efficiency in terms of rate (Fig. 2E) and extent of volume recovery at all hypertonic osmolarities in HTlc compared to PDL plated astrocytes (Fig. 2F). Similar to the RVD, the RVI response was also independent of the extracellular osmolarity in both differentiated and undifferentiated cells.

*Swelling-induced calcium and chloride current response was up-regulated in astrocytes grown on HTlc nanoparticles*

The osmotic swelling of cultured astrocytes in response to hypotonic stress has been associated with a transient rise in cytosolic calcium [19, 20]. Here, we used HTlc-differentiated astrocytes to evaluate whether faster cell swelling and higher volume increase observed in HTLc cells could have an effect on hypotonicity induced calcium influx (Fig. 3A and B). To this end we exposed astrocytes plated on PDL and HTlc plated astrocytes to hypotonic challenge (Osm=60mOsm/L) at room temperature, a condition essential to distinguish the response of TRPV4 to diverse modalities of activation [44]. Notably, the hypotonic challenge induces comparable calcium increase in PDL and HTlc (Fig. 3A, B). The role of TRPV4 in hypotonic induced calcium signaling in astrocytes was evaluated by adding the TRPV4 activator 4-alpha-phorbol-12,13-didecanoate (4αPDD) [18, 19] and then the TRPV4 antagonist RN1734 to the hypotonic solution [45, 46]. We demonstrate that both PDL and HTlc astrocytes respond to the addition of TRPV4 agonist 4αPDD to the hypotonic

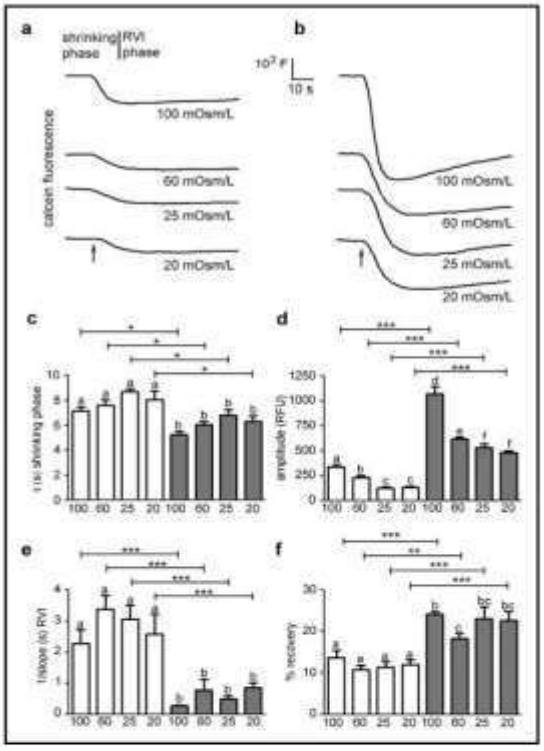


**Fig. 2.** Comparison of water transport properties of PDL and HTlc plated astrocytes under hypertonic conditions. a, b) Representative time courses of calcein-AM loaded cells during the shrinking phase followed by RVI kinetic (RVI phase) recorded on PDL (a) and HTlc (b) substrates and showing changes in fluorescence signal (F, expressed in arbitrary units, RFU) elicited by hypertonic stimulations, as indicated. The arrows indicate the switch in the external osmolarity. c, d) Quantitative analysis of the cell shrinking time constants (τ) and of the shrinking amplitude (in RFU) measured in astrocytes plated on PDL (white bars) and HTlc (gray bars) for each gradient size (20, 25, 60, 100 in mOsm/L). e, f) Quantitative analysis of the rate of the RVI phase (1/slope, s) (e) and of the extent of volume recovery (%) (f) at the applied hypertonic gradients. Note that AQP4 upregulation promotes faster shrinking and RVI kinetics and higher efficiency of RVI. Data were obtained from 21 to 24 different measurements of three independent experiments performed using different astrocyte cultures. A One-way Anova and Newman-Keuls Multiple Comparison Test were performed. ***P<0.0001; **P<0.001; *P<0.01. Different letters on top of each bar indicate significant difference between them and equal letters indicate no significant difference.

solution with an increase in intracellular calcium signaling. Notably, the magnitude of the increase in calcium response, observed after application of the agonist 4αPDD to hypotonic solution, was significantly higher in HTlc-differentiated cells compared to PDL cells (Fig. 3A, B). Accordingly, the increase induced by the TRPV4 agonist is significantly reduced after sequential addition of TRPV4 antagonist RN1734. Next, we studied intracellular calcium variations induced by hypotonic challenge at a physiological temperature of 37°C, at which TRPV4 is constitutively activated in heterologous system and in cortical astrocytes *in situ* [21, 45]. We found that hypotonicity induced calcium increase was higher in amplitude in HTlc differentiated astrocytes than in PDL astrocytes at all the hypotonic gradients tested between 20 and 100 mOsm/L. The magnitude of the response increases proportionally with osmotic challenge. On the other hand, the time-to-peak values remained unaffected (Supplementary Fig. S2).

To analyze hypotonicity-activated current, we applied protocols previously reported [26, 28]. Accordingly, astrocytes were clamped at the holding potential (Vh) of 0 mV, next to the astrocyte zero-current potential under our experimental conditions, and stimulated with voltage ramps of 1-s duration from -80 to 80 mV (Fig. 4A, B). Whole-cell membrane conductance recorded in extracellular isotonic saline (Fig. 4A, trace 1) was small in magnitude and increased upon exposure to hypotonic solution (ΔOsm = 60 mOsm) in PDL astrocytes [46], (Fig. 4A, trace 2). Of note, steady-state ramp currents were inhibited by a micromolar concentration of VRAC inhibitor carbenoxolone (Fig. 4A, trace 3) [39]. In HTlc plated astrocytes, hypotonic challenge proved to elicit a significant increase in the magnitude of whole-cell currents compared to PDL plated astrocytes (Fig. 4B, E).

Cellular Physiology and Biochemistry
Cell Physiol Biochem 2021;55(S1):196-212
DOI: 10.33594/000000469
Published online: 5 November 2021



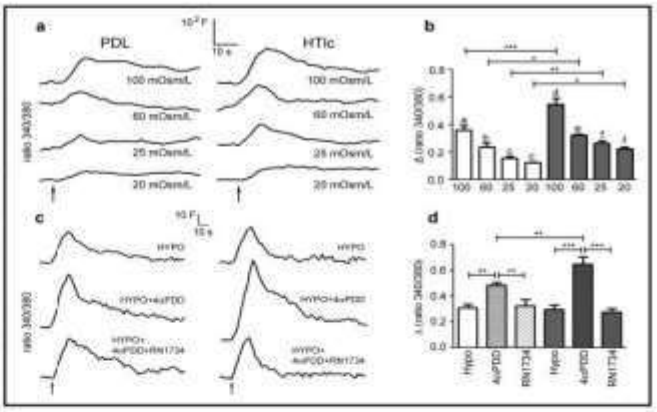


**Fig. 3.** Hypotonicity-induced calcium increase in PDL and HTIc differentiated astrocytes. a) Representative trace of hypotonicity-induced $Ca^{2+}$ response recorded from cells grown on PDL and HTIc films observed after exposing the cells to hypotonic solution (ΔOsm= 60 mOsm/L, lane 1) or to hypotonic solution with TRPV4 agonist 4αPDD or with 4αPDD +TRPV4 antagonist RN1734. The arrows indicate the time at which solutions were added to the control saline. Experiments were performed at RT. b) Barplot showing the mean±SE values of the increased $Ca^{2+}$ amplitudes measured in the conditions reported in A. Data were obtained from 12 to 15 different measurements of three independent experiments performed using 3 different astrocyte cultures. One-way ANOVA and Newman-Keuls Multiple Comparison Tests were performed. ***P<0.0001; **P<0.001; *P<0.01. c) Representative traces reflecting variations of cytosolic calcium $Ca^{2+}$ concentration recorded in cells grown on PDL and on HTIc films. Experiments were performed at 37°C. The osmotic challenges were obtained by addition of NaCl-free PBS in order to apply the indicated osmotic gradient size, at the timepoint indicated by the arrow. d) Bar plot showing the mean±SE values of calcium variations measured in the conditions reported in c. Data were obtained from 20 to 24 different measurements of three independent experiments performed using different astrocyte cultures. One-way ANOVA and Newman-Keuls Multiple Comparison Tests were performed. ***P<0.0001; **P<0.001; *P<0.01.

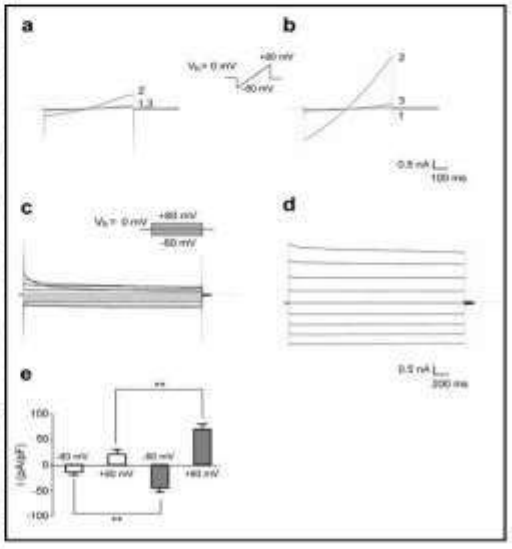


**Fig. 4.** VRAC-mediated current in astrocytes plated on PDL and HTIc. Representative current traces recorded in astrocytes plated on PDL (a) and HTIc (b) in response to ramp current protocol (inset). The reported current traces were recorded in isotonic solution (trace 1), at the maximal amplitude observed after exposure to the hypotonic solution (trace 2, Δ = 60 mOsm/L), and after addition of [100μM] CBX, a VRAC inhibitor [44] to the hypotonic solution (trace 3). Dashed lines represent the zero-current value. c,d) Representative current traces of hypotonic-challenge-activated current recorded in astrocytes plated on PDL (c) and HTIc (d) in response to family of voltage steps protocol (inset). Astrocytes were voltage clamped at the holding potential (Vh) of 0 mV, and families of voltage steps of 20 mV increments were delivered from -80 mV to +80 mV, every 10 sec. Hypotonic-challenge-activated current traces were obtained by digital subtraction of the steady-state current, recorded in isotonic condition, from the maximal value of current amplitude, recorded after exposure of the cell to hypotonic saline (Δ = 60 mOsm/L). e) Bar plot of maximal hypotonicity-activated current densities recorded at -80 and +80 mV in PDL (white bars) and HTIc plated astrocytes (gray bars). Data are expressed as mean±SE (n=6; **p<0.01, with Student's t test).

In order to analyze whether HTlc plating affects biophysical properties of VRAC, the voltage- and time-dependency of VRAC was analyzed in PDL (Fig. 4C) and in HTlc (Fig. 4D) plated astrocytes. To this end, $Cl^-$ currents were elicited with a voltage step protocol (Fig. 4C, inset), consisting of a family of voltage steps from Vh 0 mV from -80 to +80 mV in 20 mV increments delivered every 10 sec.

Hypotonicity-activated currents were obtained by digital subtraction of current traces recorded after 5–7 min of exposure to hypotonic saline from the currents recorded in control saline (Fig. 4C). Consistently with the VRAC biophysical profile, the currents in HTlc astrocytes activated instantaneously at all voltages and did not inactivate at potentials between -40 and +40 mV (Fig. 4D). At membrane potentials higher than +40 mV, the hypotonicity-evoked currents displayed a typical time-dependent inactivation, the rate and extent of which became larger at more depolarized potentials.

*The expression levels of TRPV4 and VRAC channels are not altered in HTlc differentiated astrocytes*

In line with our previous results, GFAP staining (Fig. 5A) revealed a polygonal shape in astrocytes grown on PDL and a remarkable morphological differentiation in HTlc plated astrocytes. Immunoblotting analysis confirmed comparable expression levels of GFAP, a well-known gliotic inflammatory marker (Fig. 5B and C) in cells grown on both substrates as well as the molecular up-regulation of AQP4 in HTlc-plated astrocytes. On the other hand, TRPV4 and VRAC protein expression levels remained unaltered in cells grown on HTlc compared to those grown on PDL.

To assess whether a gain in functionality was associated with a different expression pattern of the channels in the membrane, fixed astrocytes labelled for F-actin and the three aforementioned proteins were imaged using confocal microscopy (Fig. 6). The F-actin label was chosen in order to easily discriminate between differentiated and undifferentiated astrocytes as well as to identify the median focal planes within the cells with well-defined cell edges. Pearson's coefficients obtained from co-localization analysis between the membrane channels and F-actin showed that, while TRPV4 and VRAC were similarly distributed in both differentiated and undifferentiated cells without correlation to the F-actin distribution, AQP4 localization exhibited a profound rearrangement in differentiated star-shaped astrocytes grown on HTlc with a continuous plasma membrane staining strongly colocalized with cortical actin.

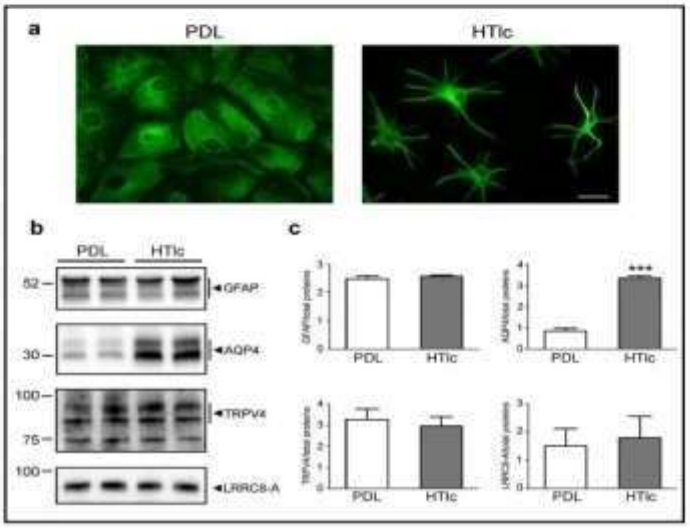


**Fig. 5.** Expression of GFAP, AQP4, TRPV4 and LRRC8-A proteins in astrocytes plated on PDL and HTlc. a) GFAP staining of PDL and HTlc astrocytes. (Scale bar: 50 μm). b) Representative Western blot analysis of GFAP, AQP4, TRPV4 and LRRC8-A expression in primary astrocytes grown on PDL and HTlc. c) Comparative densitometric analysis of GFAP, AQP4, TRPV4 and LRRC8-A corresponding signal in PDL and HTlc samples, normalized to the Coomassie blue-stained membrane. Data are means±SE, ***p<0.001.

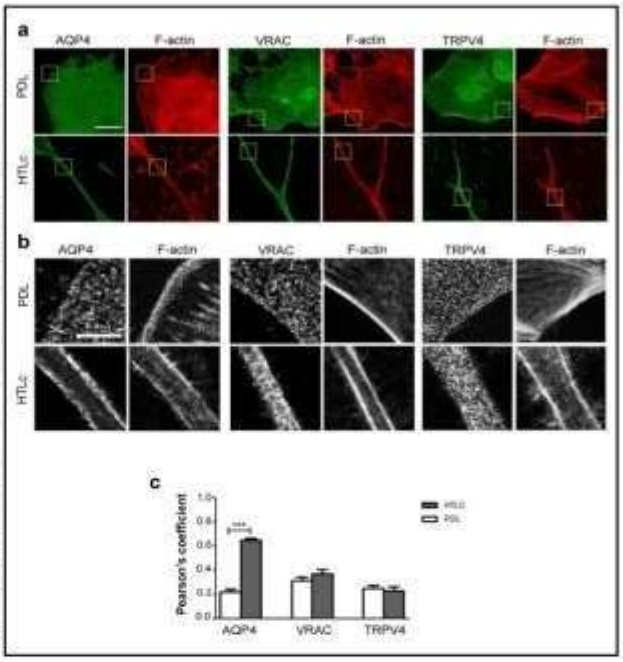


**Fig. 6.** AQP4, VRAC and TRPV4 protein expression and localization. a) Single-plane confocal images of astrocytes grown on PDL (upper panel) and HTlc (lower panel) immunostained for the channels (green) and F-actin (red) (Scale bar: 25 um). b) Magnification of the yellow-boxed regions from (a) (insets: 10 um x 10 um). c) Pearson's Correlation Coefficients resulting from colocalization analysis between membrane proteins and F-actin. In HTlc-grown astrocytes, AQP4 and F-actin colocalize with a greater extent compared to undifferentiated cells/ controls (Pearson's coefficient (r) = 0.65 ± 0.01, n = 27 for HTlc; r= 0.21 ± 0.02, n = 45 for PDL). No changes in the degree of overlap between VRAC or TRPV4 and F-actin were detected in differentiated astrocytes (r VRAC HTlc = 0.382 ± 0.03, n = 45; r VRAC PDL = 0.31 ± 0.02, n = 45; r TRPV4 HTlc = 0.229 ± 0.03, n = 48; r TRPV4 PDL = 0.24 ± 0.02, n = 45). Unpaired t-test; ***P ≤ 0.0001.

## Discussion

Several studies highlight that the astroglial syncytium strategically regulates homeostasis within the brain environment through a pool of ion and water channel proteins specifically distributed in microdomains facing diverse fluid-filled spaces [1, 47]. Astrocytic cell volume regulation in response to anisotonicity results from 1) sensing anisotonic environment and cell volume changes caused by osmotically driven water flux across the cell membrane; and 2) activation of effector mechanisms that restore the original cell volume. However, the mechanism behind cell volume regulation needs further insights.

In this work, we sought to investigate cell volume regulating mechanisms in differentiated astrocytes *in vitro* [32], that recapitulate morphological, molecular and functional features of astrocytes *in situ*. We confirm that AQP4-overexpression is accompanied with enhanced rate of water transport in astrocytes under hypotonic conditions and, as herein demonstrated, also under hypertonic conditions. Notably, the amplitude of the anisotonicity-induced cell volume responses of glial cells were considerably higher in differentiated astrocytes. One of the major novel findings of the present work is the improved response of differentiated astrocytes in terms of volume recovery.

To obtain insight into this phenomenon, we studied the hypotonicity induced calcium signalling and volume regulated anion conductance in PDL and HTlc astrocytes because they are mainly responsible for the cell sensing and effector mechanisms activated by anisotonicity.

We found that hypotonicity induced calcium signals is increased in its magnitude in differentiated astrocytes only when TRPV4 is activated by the selective agonist (Fig. 4A, B) or by temperature above 25°C. Thus, the upregulation might be either dependent or independent of the higher swelling observed in experiments performed at 22°C.

Notably, the amplitude of the swelling kinetics was half as large as the amplitude of shrinking kinetics [48]. Cell swelling processes are more complex than cell shrinkage as the plasma membrane exhibits a very limited stretch capacity and is constrained by extensive cytoskeletal networks [10].

Astrocytes grown on HTlc films display faster active RVD and RVI together with a more efficient volume recovery compared to undifferentiated cells.

It can be argued that the different surface-to-volume ratio between flat and stellate astrocytes should be taken into account with respect to the increased water transport kinetic properties measured in cells grown on HTlc. However, in line with previous manuscripts published by our group in which a morphological change of astrocytes was obtained, [31, 32, 49, 50] we have considered here the time constant of cell swelling or cell shrinkage a sufficient indicator of the water flux rate. In general, we have demonstrated that cell differentiation promotes the polarized expression of AQP4 on the cell plasma membrane associated with an increased water transport rate, suggesting that the selective AQP4 plasma membrane localization positively affects the permeability and the cell volume recovery mechanism in differentiated astrocytes.

It is plausible that AQP4 dependent increases in the plasma membrane stretching abilities are able to drive higher sensitivity of the cell to osmotic changes, thereby resulting in increased magnitude of osmotic induced calcium signaling (Fig. 3A and B) and faster kinetics of the RVD and RVI processes. Accordingly, we previously demonstrated [19, 20] that the hypotonicity-induced calcium transients recorded from WT and KO astrocytes were significantly different in terms of amplitudes and kinetics, indicating that the more rapid cell swelling provided by AQP4-mediated water influx plays a major modulatory role on TRPV4-mediated calcium signalling events.

Recent works have also indicated that TRPV4 is more of a volume-sensor than an osmo-sensor [51]. The results provided at room temperature are, however, more in favor of the ability of TRPV4 increased magnitude to sense osmolarity more than the cell volume. Indeed, increased magnitude of calcium signal in HTLc is observed only when TRPV4 is already activated by temperature or by an agonist, two conditions where discrimination among stimuli cannot be achieved [44, 52]. Our results support the tenet that AQP4 is a crucial player in the RVD and RVI mechanisms and that a molecular and functional interaction with TRPV4 exists in differentiated astrocytes [19, 20, 33, 53]. Our results have also demonstrated a dramatic increase in VRAC current in response to hypotonic challenge in differentiated astrocytes. The result observed might explain the more efficient kinetics of RVD observed in these cells following rapid osmotic influx or efflux of water in response to an anisotonic stimulus. The result is not surprising since, indeed, VRAC channels are known to be critical contributors to the cell volume regulation in astrocytes [27, 28, 34]. Moreover, in a previous work we found that AQP4-KD induced a down regulation of VRAC current [26]. Thus, a functional cooperation between AQP4 mediated swelling and VRAC is confirmed in differentiated astrocytes. We recently found that the expression of LRRC8A subunit of VRAC was essential for the amplitude of astrocytic VRAC conductance and RVD. However, in the present work, the increase in magnitude of VRAC current was not paralleled by an increase in LRRC8A total protein amount nor by higher expression in the astrocytic membrane. Thus, it is plausible that, in the case of VRAC, the higher cell volume achieved is linked to the higher expression of AQP4 in the cell membrane, resulting in a more effective stimulus for the activation of VRAC.

*Cell volume regulation nanostructure induced differentiation*

The herein reported nano-scale interface, HTlc, is known to promote differentiation of astrocytes with mechanisms involving the cytoskeleton rearrangement [32, 55, 56]. The tight interaction of the cell with the nano-scale environment might continuously challenge the cell, locally, to rearrange its surface and volume. Thus, RVD and RVI molecular and functional components could be improved. In this regard, a prominent role for RVD and AQP4 in glioma cells has been highlighted [57, 58]. The latter condition is typically characterized by

alterations in mechanical properties of the extracellular environment, and AQP4 mediated water flux seems to play a key role orienting glioma cell fate toward increased migration properties (AQP4 dependent increase in cell migration) or apoptosis (AQP4 dependent apoptotic volume decrease) [57]. In addition, it has been recently shown that TRPV4 might act as mechano-sensor in astrocytes. Thus, the increased response of TRPV4 in differentiated astrocytes might be a consequence of the nanomechanical challenge induced by HTlc. This, on turn, might set a lower threshold to activate TRPV4 in response to osmotic challenge or to cell volume. In this respect, the data herein provided and the growth of astrocytes on HTlc will be useful to understand the molecular mechanisms of differentiation and migration, as two typical traits of astrocytes in health and disease.

We can also speculate that the cell/material interface induces gene expression driving a molecular and functional phenotype that is more similar to the one observed *in vivo*, as previously described, which includes recapitulation of microdomains serving homeostatic function to which AQP4, Kir4.1 [32], TRPV4 and, more recently, VRAC have been demonstrated to belong [26, 28]. In this view, our work provides new insight into cell physiology and biophysics by controlled *in vivo*-mimicking - *in vitro* cell culture model.

## Conclusion

Here we demonstrate that the differentiation of astrocytes is associated with an increased AQP4 dependent water permeability. We hypothesized that the enhanced transmembrane osmotic water flux, conferred by the upregulated water channel protein and function, might drive higher sensitivity of the cell to osmotic changes. This enhanced flux results in increased magnitude of calcium signaling and faster kinetics of the RVD and RVI processes by functionally recruiting both TRPV4 and VRAC ion channels, even though the total protein levels of both TRPV4 and VRAC remain unaltered.

The present *in vitro* cell culture method to obtain differentiated astrocytes represents an important tool to study the dynamics underpinning the cellular localization and functionality of channel proteins belonging to astrocytic microdomains and has allowed us to test the hypothesis that volume transmission is a new communication path in non-excitable cells.

## Acknowledgements

The authors would like to thank Alessia Minardi (University of Bologna) for assistance in the astrocyte preparation, Gaetano Devito (University of Bari) for his excellent technical assistance, and Kate O'Neill (University of Maryland) for her assistance in revising the English of the article.

*Author Contributions*

M.G. Mola designed and performed water transport experiments, wrote the paper. E. Saracino set the protocol for differentiated astrocytes, performed calcium imaging experiments, wrote the paper. F. Formaggio performed patch-clamp experiments, analyzed electrophysiology data, wrote the paper. A. G. Amerotti and A. Cibelli performed western blot experiments and analyses. B. Barile and C. Palazzo performed immunofluorescence and confocal microscopy. T. Posati synthetized HTlc films. A. Frigeri discussed the data, wrote and corrected the manuscript. R. Zamboni discussed the data and corrected the manuscript. M. Caprini discussed the data, designed electrophysiology experiments and wrote the paper. G. P. Nicchia and V. Benfenati designed and supervised the research, discussed the data, wrote the manuscript.

*Funding Sources*

The work is supported by AFOSR Research Projects FA9550-19-1-0370: "Decoding astrocytes rhythm"; ASTROMAT: FA9550-16-1-0502; 3D NEUROGLIA: FA9550-18-1-0255; ASTRONIR: FA9550-17-1-0502; ASTROLIGHT: FA9550-20-1-0386; MSCA-ITN-2020-ASTROTECH (GA956325); E.S. is supported by POR-FESR 2014-2020 of Emilia Romagna Region, Fondo per lo Sviluppo e la Coesione (MAT-2-REP-FSC), and Grant sponsor Italian Ministry of the University and Research-FIRB Futuro in Ricerca (RBFR12SJA8).

*Statement of Ethics*

Experiments were performed in accordance with the European guidelines on the ethical use of animals for research and the Italian law on animal care. The animal use protocol for this study was approved by the Institutional Committee on Animal Research and Ethics of the University of Bari and Bologna and by the Italian Ministry of Health (protocol number no. 2020/1338-PR, renewed on February 2020 and valid for 5 years). Wistar rats provided by Charles River were bred in the Animal Facilities of the Universities of Bari and Bologna, and the pups were used for brain explant and cell culture preparation. Rats were kept under a 12-h dark to light cycle, at constant room temperature and humidity (22 ± 2°C, 75%), with food and water *ad libitum* in 1290D Eurostandard Type III cages (Tecniplast, Varese, Italy). Experiments were designed to minimize the number of animals used and their suffering.

## Disclosure Statement

The authors have no conflicts of interest to declare.

## References

1 Benfenati V, Ferroni S: Water transport between CNS compartments: Functional and molecular interactions between aquaporins and ion channels. Neuroscience 2010;168:926–940.
2 Lang F, Busch GL, Ritter M, Völkl H, Waldegger S, Gulbins E, Häussinger D: Functional Significance of Cell Volume Regulatory Mechanisms. Physiol Rev 1998;78:247–306.
3 Hoffmann EK, Lambert IH, Pedersen SF: Physiology of cell volume regulation in vertebrates. Physiol Rev 2009;89:193–277.
4 Wehner F, Olsen H, Tinel H, Kinne-Saffran E, Kinne RK: Cell volume regulation: osmolytes, osmolyte transport, and signal transduction. Rev Physiol Biochem Pharmacol 2003;148:1–80.
5 Sardella E, Mola MG, Gristina R, Piccione M, Veronico V, De Bellis M, Cibelli A, Buttiglione M, Armenise V, Favia P, Nicchia GP: A Synergistic Effect of Reactive Oxygen and Reactive Nitrogen Species in Plasma Activated Liquid Media Triggers Astrocyte Wound Healing. Int J Mol Sci 2020;21:3343.
6 Lafrenaye AD, Simard JM: Bursting at the Seams: Molecular Mechanisms Mediating Astrocyte Swelling. Int J Mol Sci 2019;20:330.
7 Verkhratsky A, Parpura V, Vardjan N, Zorec R: Physiology of Astroglia. Adv Exp Med Biol 2019;1175:45–91.
8 Nagelhus EA, Ottersen OP: Physiological Roles of Aquaporin-4 in Brain. Physiol Rev 2013;93:1543–1562.
9 Chen L, König B, Liu T, Pervaiz S, Razzaque YS, Stauber T: More than just a pressure relief valve: Physiological roles of volume-regulated LRRC8 anion channels. Biol Chem 2020;400:1481–1496.
10 Wilson CS, Mongin AA: Cell Volume Control in Healthy Brain and Neuropathologies. Curr Top Membr 2018;81:385–455.
11 Pivonkova H, Hermanova Z, Kirdajova D, Awadova T, Malinsky J, Valihrach L, Zucha D, Kubista M, Galisova A, Jirak D, Anderova M: The Contribution of TRPV4 Channels to Astrocyte Volume Regulation and Brain Edema Formation. Neuroscience 2018;394:127–143.
12 Jung JS, Bhat R V, Preston GM, Guggino WB, Baraban JM, Agre P: Molecular characterization of an aquaporin cDNA from brain: Candidate osmoreceptor and regulator of water balance. Proc Natl Acad Sci U S A 1994;91:13052–13056.

13 Frigeri A, Gropper MA, Turck CW, Verkman AS: Immunolocalization of the mercurial-insensitive water channel and glycerol intrinsic protein in epithelial cell plasma membranes. Proc Natl Acad Sci U S A 1995;92:4328–4331.
14 Nielsen S, Nagelhus EA, Amiry-Moghaddam M, Bourque C, Agre P, Ottersen OP: Specialized membrane Domains for Water Transport in Glial Cells: High- Resolution Immunogold Cytochemistry of Aquaporin-4 in Rat Brain. J Neurosci 1997;17:171–180.
15 Amiry-Moghaddam M, Ottersen OP: The molecular basis of water transport in the brain. Nat Rev Neurosci 2003;4:991–1001.
16 Neely JD, Amiry-Moghaddam M, Ottersen OP, Froehner SC, Agre P, Adams ME: Syntrophin-dependent expression and localization of Aquaporin-4 water channel protein. Proc Natl Acad Sci U S A 2001;98:14108–14113.
17 Hoddevik EH, Khan FH, Rahmani S, Ottersen OP, Boldt HB, Amiry-Moghaddam M: Factors determining the density of AQP4 water channel molecules at the brain–blood interface. Brain Struct Funct 2017;222:1753–1766.
18 Benfenati V, Amiry-Moghaddam M, Caprini M, Mylonakou MN, Rapisarda C, Ottersen OP, Ferroni S: Expression and functional characterization of transient receptor potential vanilloid-related channel 4 (TRPV4) in rat cortical astrocytes. Neuroscience 2007;148:876–892.
19 Benfenati V, Caprini M, Dovizio M, Mylonakou MN, Ferroni S, Ottersen OP, Amiry-Moghaddam M: An aquaporin-4/transient receptor potential vanilloid 4 (AQP4/TRPV4) complex is essential for cell-volume control in astrocytes. Proc Natl Acad Sci U S A 2011;108:2563–2568.
20 Mola MG, Sparaneo A, Gargano CD, Spray DC, Svelto M, Frigeri A, Scemes E, Nicchia GP: The Speed of Swelling Kinetics Modulates Cell Volume Regulation and Calcium Signaling in Astrocytes: A Different Point of View on the Role of Aquaporins. Glia 2016;64:139–154.
21 Dunn KM, Hill-Eubanks DC, Liedtke W, Nelson MT: TRPV4 channels stimulate Ca2+-induced Ca2+ release in astrocytic endfeet and amplify neurovascular coupling responses. Proc Natl Acad Sci U S A 2013;110:6157–6162.
22 Toft-Bertelsen TL, Larsen BR, MacAulay N: Sensing and regulation of cell volume – We know so much and yet understand so little: TRPV4 as a sensor of volume changes but possibly without a volume-regulatory role? Channels 2018;12:100–108.
23 Kanju P, Liedtke W: Pleiotropic function of TRPV4 ion channels in the central nervous system. Exp Physiol 2016;101:1472–1476.
24 Pasantes-Morales H, Franco R, Torres-Marquez ME, Hernández-Fonseca K, Ortega A: Amino Acid Osmolytes in Regulatory Volume Decrease and Isovolumetric Regulation in Brain Cells: Contribution and Mechanisms. Cell Physiol Biochem 2000;10:361–370.
25 Kimelberg HK: Astrocytic swelling in cerebral ischemia as a possible cause of injury and target for therapy. Glia 2005;50:389–397.
26 Benfenati V, Nicchia GP, Svelto M, Rapisarda C, Frigeri A, Ferroni S: Functional down-regulation of volume-regulated anion channels in AQP4 knockdown cultured rat cortical astrocytes. J Neurochem 2007;100:87–104.
27 Hyzinski-García MC, Rudkouskaya A, Mongin AA: LRRC8A protein is indispensable for swelling-activated and ATP-induced release of excitatory amino acids in rat astrocytes. J Physiol 2014;592:4855–4862.
28 Formaggio F, Saracino E, Mola MG, Rao SB, Amiry-Moghaddam M, Muccini M, Zamboni R, Nicchia GP, Caprini M, Benfenati V: LRRC8A is essential for swelling-activated chloride current and for regulatory volume decrease in astrocytes. FASEB J 2019;33:101–113.
29 Hopt A, Neher E: Highly Nonlinear Photodamage in Two-Photon Fluorescence Microscopy. Biophys J 2001;80:2029–2036.
30 Benfenati V, Caprini M, Nobile M, Rapisarda C, Ferroni S: Guanosine promotes the up-regulation of inward rectifier potassium current mediated by Kir4.1 in cultured rat cortical astrocytes. J Neurochem 2006;98:430–445.
31 Nicchia GP, Rossi A, Mola MG, Procino G, Frigeri A, Svelto M: Actin Cytoskeleton Remodeling Governs Aquaporin-4 Localization in Astrocytes. Glia 2008;56:1755–1766.
32 Posati T, Pistone A, Saracino E, Formaggio F, Mola MG, Troni E, Sagnella A, Nocchetti M, Barbalinardo M, Valle F, Bonetti S, Caprini M, Nicchia GP, Zamboni R, Muccini M; Benfenati V: A Nanoscale Interface Promoting Molecular and Functional Differentiation of Neural Cells. Sci Rep 2016;6:31226.

33 Jo AO, Ryskamp DA, Phuong TTT, Verkman AS, Yarishkin O, MacAulay N, Križaj D: TRPV4 and AQP4 Channels Synergistically Regulate Cell Volume and Calcium Homeostasis in Retinal Müller Glia. J Neurosci 2015;35:13525–13537.
34 Yang J, Vitery M del C, Chen J, Osei-Owusu J, Chu J, Qiu Z: Glutamate-Releasing SWELL1 Channel in Astrocytes Modulates Synaptic Transmission and Promotes Brain Damage in Stroke. Neuron 2019;102:813–827.
35 Mola MG, Nicchia GP, Svelto M, Spray DC, Frigeri A: Automated Cell-Based Assay for Screening of Aquaporin Inhibitors. Anal Chem 2009;81:8219–8229.
36 Farinas J, Simanek V, Verkman AS: Cell volume measured by total internal reflection microfluorimetry: application to water and solute transport in cells transfected with water channel homologs. Biophys J 1995;68:1613–1620.
37 Solenov E, Watanabe H, Manley GT, Verkman AS: Sevenfold-reduced osmotic water permeability in primary astrocyte cultures from AQP-4-deficient mice, measured by a fluorescence quenching method. Am J Physiol Cell Physiol 2004;286:426–432.
38 Chen Z, Zhang Z, Gu Y, Bai C: Impaired migration and cell volume regulation in aquaporin 5-deficient SPC-A1 cells. Respir Physiol Neurobiol 2011;176:110–117.
39 Peckys DB, Kleinhans FW, Mazur P: Rectification of the water permeability in COS-7 cells at 22, 10 and 0°C. PLoS One 2011;6:e23643.
40 Hamill OP, Marty A, Neher E, Sakmann B, Sigworth FJ: Improved patch-clamp techniques for high-resolution current recording from cells and cell-free membrane patches. Pflügers Arch 1981;391:85–100.
41 Benfenati V, Caprini M, Nicchia GP, Rossi A, Dovizio M, Cervetto C, Nobile M, Ferroni S: Carbenoxolone inhibits volume-regulated anion conductance in cultured rat cortical astroglia. Channels 2009;3:323–336.
42 Heo J, Meng F, Hua SZ: Contribution of Aquaporins to Cellular Water Transport Observed by a Microfluidic Cell Volume Sensor. Anal Chem 2008;80:6974–6980.
43 Fenton RA, Moeller HB, Nielsen S, De Groot BL, Rützler M: A plate reader-based method for cell water permeability measurement. Am J Physiol Renal Physiol 2010;298:224–230.
44 Gao X, Wu L, O'Neil RG: Temperature-modulated diversity of TRPV4 channel gating. J Biol Chem 2003;278:27129–27137.
45 Butenko O, Dzamba D, Benesova J, Honsa P, Benfenati V, Rusnakova V, Ferroni S, Anderova M: The Increased Activity of TRPV4 Channel in the Astrocytes of the Adult Rat Hippocampus after Cerebral Hypoxia/Ischemia. PLoS One 2012;7:e39959.
46 Vincent F, Acevedo A, Nguyen MT, Dourado M, DeFalco J, Gustafson A, Spiro P, Emerling DE, Kelly MG, Duncton MAJ: Identification and characterization of novel TRPV4 modulators. Biochem Biophys Res Commun 2009;389:490–494.
47 Kimelberg HK: Water homeostasis in the brain: Basic concepts. Neuroscience 2004;129:851–860.
48 Borrachero-Conejo AI, Adams WR, Saracino E, Mola MG, Wang M, Posati T, Formaggio F, De Bellis M, Frigeri A, Caprini M, Hutchinson MR, Muccini M, Zamboni R, Nicchia GP, Mahadevan-Jansen A, Benfenati V: Stimulation of water and calcium dynamics in astrocytes with pulsed infrared light. FASEB J 2020;34:6539–6553.
49 Nicchia GP, Frigeri A, Liuzzi GM, Svelto M: Inhibition of AQP4 expression in astrocytes by RNAi determines alterations in cell morphology, growth, and water transport and induces changes in ischemia related genes. FASEB J 2003;17:1508–1510.
50 Nicchia GP, Srinivas M, Li W, Brosnan CF, Frigeri A, Spray DC: New possible roles for aquaporin-4 in astrocytes: cell cytoskeleton and functional relationship with connexin43. FASEB J 2005;19:1674–1676.
51 Liedtke W, Choe Y, Marti-Renom MA, Bell AM, Denis CS, Sali A, Hudspeth AJ, Friedman JM, Heller S: Vanilloid Receptor-Related Osmotically Activated Channel (VR-OAC), a Candidate Vertebrate Osmoreceptor. Cell 2000;103:525–535.
52 Vriens J, Watanabe H, Janssens A, Droogmans G, Voets T, Nilius B: Cell swelling, heat, and chemical agonists use distinct pathways for the activation of the cation channel TRPV4. Proc Natl Acad Sci U S A 2004;101:396–401.
53 Thrane AS, Rappold PM, Fujita T, Torres A, Bekar LK, Takano T, Peng W, Wang F, Thrane VR, Enger R, Haj-Yasein NN, Skare Ø, Holen T, Klungland A, Ottersen OP, Nedergaard M, Nagelhus EA: Critical role of aquaporin-4 (AQP4) in astrocytic Ca2+ signaling events elicited by cerebral edema. Proc Natl Acad Sci U S A 2011;108:846–851.

54 Haj-Yasein NN, Jensen V, Østby I, Omholt SW, Voipio J, Kaila K, Ottersen OP, Hvalby Ø, Nagelhus EA: Aquaporin-4 regulates extracellular space volume dynamics during high-frequency synaptic stimulation: A gene deletion study in mouse hippocampus. Glia 2012;60:867–874.

55 Saracino E, Cirillo V, Marrese M, Guarino V, Benfenati V, Zamboni R, Ambrosio L: Structural and functional properties of astrocytes on PCL based electrospun fibres. Mater Sci Eng C Mater Biol Appl 2021:118:111363.

56 Saracino E, Maiolo L, Polese D, Semprini M, Borrachero-Conejo AI, Gasparetto J, Murtagh S, Sola M, Tomasi L, Valle F, Pazzini L, Formaggio F, Chiappalone M, Hussain S, Caprini M, Muccini M, Ambrosio L, Fortunato G, Zamboni R, Convertino A, et al.: A Glial-Silicon Nanowire Electrode Junction Enabling Differentiation and Noninvasive Recording of Slow Oscillations from Primary Astrocytes. Adv Biosyst 2020;4:e1900264.

57 Simone L, Pisani F, Mola MG, De Bellis M, Merla G, Micale L, Frigeri A, Vescovi AL, Svelto M, Nicchia GP: AQP4 aggregation state is a determinant for glioma cell fate. Cancer Res 2019;79:2182–2194.

58 Ernest NJ, Weaver AK, Van Duyn LB, Sontheimer HW: Relative contribution of chloride channels and transporters to regulatory volume decrease in human glioma cells. Am J Physiol Cell Physiol 2005;288:1451–1460.

**EMBARGO REQUEST- data not yet published**

# Overview on ongoing activities and unpublished results

1.1 Introduction to Paper 1

"*Decoding natural astrocyte rhythms: dynamic actin waves result from environmental sensing by primary rodent astrocytes*" by

**Kate M. O'Neill, Emanuela Saracino, Barbara Barile, Nicholas J. Mennona, Maria Grazia Mola, Spandan Pathak, Tamara Posati, Roberto Zamboni, Grazia P. Nicchia, Valentina Benfenati, Wolfgang Losert** has been published as pre print on bioRxiv 2021.09.13.460152; DOI: https://doi.org/10.1101/2021.09.13.460152.This article is a preprint and has not been certified by peer review. (https://www.biorxiv.org/content/10.1101/2021.09.13.460152v1 ).

 In a previous study conducted is widely recognized that astrocytes, once defined as passive glue cells, play an active role in determining excitability in the brain. Astrocytes are key regulators of brain homeostasis in the extracellular milieu of the brain and it is essential for the cognitive function. In particular, in the CNS, the homeostasis of $K^+$ is critical in the extracellular space and it is maintained by homeostatic process at 4 mM in physiological condition. Alterations in membrane properties including the decrease of IR, depolarization of the resting membrane potential could result in disorders such as epilepsy, or syndromes that affect behavioural tasks, such as sleep, learning, and attention[266,267.] Our study introduces actin dynamics in astrocytes as a potential carrier of information and actuator of the astrocytic response to changes in the local environment; actually, the role of cytoskeletal dynamics in this critical regulatory process is still unknown, although the importance that actin behave as an excitable system is increasing. The following work focuses on the dynamics of actin in specific

subcellular regions, near the cell boundary, called “hotspot” regions that selectively respond to certain chemo-physical stimuli. The induced stimuli, we applied, are targeted to simulate homeostatic challenges of ion or water concentration increases. This hypothesis has been validated through astrocytes actin-GFP transduction, optical flow algorithms and shape analysis[212,213]. Images were performed by means of live time-lapse confocal microscopy. The same approach was performed on HTlc-substrate topography. The role that HTlc nanostructured topography can have on astrocytes homeostasis properties have been reported in the dedicated paragraph 1.4 of **Chapter IV**. Here, taking advantage of the previous results, we define actin dynamics also on the following system where differentiated astrocytes grow. These rhythmic behaviours are associated with the transition between distinctive network oscillation frequencies of discrete neural networks, which are associated with different oscillation frequencies in neurons, as a reaction to the ever-changing environment.

Here it is reported a preprint version of our manuscript.

**\PDF -FORMATO PAPERS\K. O'Neill, Saracino E., et al., BioRxiv 5.1.pdf**

# Decoding natural astrocyte rhythms: dynamic actin waves result from environmental sensing by primary rodent astrocytes

Kate M. O'Neill[1]†, Emanuela Saracino[2]†, Barbara Barile[3], Nicholas J. Mennona[1,4], Maria Grazia Mola[3], Spandan Pathak[1], Tamara Posati[2], Roberto Zamboni[2], Grazia P. Nicchia[3], Valentina Benfenati[2*], Wolfgang Losert[1,4*]

[1] *Inst. for Physical Science and Technology, Univ. of Maryland, College Park, MD, USA*
[2] *Inst. of Organic Synthesis and Photoreactivity, National Research Council of Italy, Bologna, Italy*
[3] *Dept. of Bioscience, Biotechnology and Biopharmaceutics, Univ. of Bari Aldo Moro, Bari, Italy*
[4] *Physics Dept., Univ. of Maryland, College Park, MD, USA*

† *equal contributions as co-first authors*
* *valentina.benfenati@isof.cnr.it and wlosert@umd.edu (equal contributions as co-corresponding authors)*

**Abstract**

Astrocytes are key regulators of brain homeostasis, which is essential for proper cognitive function. The role of cytoskeletal dynamics in this critical regulatory process is unknown. Here we find that actin is dynamic in certain subcellular regions, especially near the cell boundary. Our results further indicate that actin dynamics concentrates into "hotspot" regions that selectively respond to certain chemophysical stimuli, specifically the homeostatic challenges of ion or water concentration increases. Substrate topography makes actin dynamics more frequent yet weaker, and it also alters actin network structure. Superresolution images analyzed with a filament extraction algorithm demonstrate that surface topography is associated with a predominant perpendicular alignment of actin filaments near the cell boundary whereas flat substrates result in an actin cortex mainly parallel to the cell boundary. Thus, actin structure and dynamics together integrate information from different aspects of the environment that might steer the operation of neural cell networks.

**Short Title**

Homeostatic actin dynamics in astrocytes

**Teaser**

Astrocytes display dynamic actin that is modulated by combinations of chemophysical stimuli and environmental topographies.

## Introduction

The ability of the brain to receive and compute information depends on the unique abilities of its component brain cells. In particular, astrocytes play crucial roles in cognitive function by maintaining electrochemical gradients of ions and both responding to and counteracting changes in the chemophysical environment of the extracellular milieu [1-3]. More recently, the importance of astrocytes' structural and functional properties has been highlighted for organ- and system-level functions, including synaptic plasticity, memory formation, learning, and regulation of sleep and metabolic activity [4, 5].

Astrocytes exhibit a branched morphology [1, 3] and express a variety of transmembrane proteins and receptors in a specific, patchy distribution throughout the cell, resulting in so-called functional microdomains. This molecular and structural patchwork allows astrocytes to uptake and pump ions, osmotically drive water and neurotransmitters across the cell, and redistribute and spatially "buffer" solute concentrations [6]. In this way, astrocytes precisely control the extracellular environment locally by continuously monitoring, sensing, and balancing changes in response to the neuronal network activity. At the same time, the gap junction coupling between astrocytes serves as a signaling path enabling synchronicity and lateral communication within the larger astroglia syncytia [7].

Though gap junctional communication coupling enables dynamic exchange at the ionic and molecular scales [8, 9], questions remain how these dynamics couple with, modulate, and impact responses of cell networks or of the whole brain. Here we investigate the actin cytoskeleton as an integrator from the molecular to the systems scale due to its ability to self-assemble into dynamic networks.

Indeed, experiments on fixed samples indicate that the astrocytic actin cytoskeleton plays a role in several homeostatic processes, such as volume regulation and potassium spatial buffering [10-12]. However, much less is known about the dynamics of the actin cytoskeleton in these cellular processes. For migrating cells – such as neutrophils, metastatic cancer cells, and even microglia – actin dynamics has been mostly considered as a facilitator of changes in cell morphology. For example, a recent study in T cells demonstrated the importance of global (whole cell) actin dynamics in facilitating immunological synapse formation [13].

Moreover, recent studies across multiple cell types have demonstrated not only that the actin cytoskeleton is dynamic when a cell changes shape and moves but also that the actin cytoskeleton is an excitable system with its own intrinsic dynamics, including sustained waves and oscillations that persist independently of changes to cell shape [14-21]. The source of actin dynamics is thought to be twofold: i) a cytoskeletal excitable network of proteins (CEN) that drives cycles of polymerization and depolymerization typically lasting a few seconds, and ii) a signal transduction excitable network (STEN) that can self-organize these local oscillations into larger scale waves that drive cell migration [17, 18, 22, 23].

Indeed, CEN waves can carry information. Actin waves have been shown to be sensitive to extracellular local topography upon which cells are cultured [24, 25] and are important for biological function [22, 26], such as surveillance of the brain parenchyma by microglia [27].

These waves are due to the second scale polymerization and depolymerization dynamics that occur locally due to CEN and are usually obscured by the longer timescale wave dynamics, but they can be revealed by suppression of STEN [17, 18, 22, 23].

We propose that, in astrocytes, CEN dynamics dominate, thus leading to local actin dynamics that are stationary in space and occur on a second timescale. Thus, cytoskeletal excitable networks carry information about homeostatic challenges that occur at the nanometer, ionic, and molecular scales. The actin cytoskeleton therefore serves as the bridge from these smaller scales to larger scales and facilitates the global homeostatic response of astrocytes.

To evaluate our hypothesis, we use optical flow algorithms and shape analysis on images of primary astrocytes transduced with actin-GFP. We demonstrate that actin dynamics occurs in astrocytes and that it can be triggered by extracellular environment modifications, such as an increase in ion concentrations or a change in nanomechanical features. The spatial distribution of the actin dynamics is localized near the boundary of the cell and is concentrated into patches we term "hotspots".

Notably, the strength of the actin dynamics is different depending on whether the exposure is to an increase in extracellular potassium or to hypotonic challenge (referred to as "triggering" conditions and abbreviated as "high K+" and "hypotonic", respectively). In addition, activity identified in the processes of differentiated astrocytes, induced by nanotopography, is weaker but more frequent when compared to undifferentiated cells. Superresolution imaging by STimulated Emission Depletion (STED) microscopy and analysis with a filament extraction algorithm demonstrates that the specific orientation of actin filament structures occurs only in differentiated cells, indicating that both structure and dynamics carry information about the environment.

Overall, our results indicate that actin is dynamic in astrocytes and behaves collectively by clustering into "hotspot" regions that respond in distinct ways to different stimuli and may drive the homeostatic response of the neural cell network.

## Results

### Primary astrocytes display actin dynamics in response to chemical cues

Our live imaging results demonstrate that astrocytes consistently display actin dynamics, particularly near the boundary of the cell. Representative overlays of fluorescent images are shown in **Figure 1A** (A1, inset A3 for representative control timelapse and A2, inset A4 for representative "triggering" timelapse). In this representation, a perfectly stationary cell would appear all white; the appearance of different colors indicates non-overlapping structures at either earlier (more blue) or later (more red) times. To quantify actin dynamics, we employ an optical flow method [28] similar to that used in our previous work [19]. We additionally use shape analysis [16, 29, 30] to separately consider actin dynamics within the whole cell, boundary region, and bulk region (see **Figure 1B** and **1C** for schematics and *Materials and Methods* for more detail).

To obtain an overall picture of how actin dynamics changes between control and triggering conditions, we first examined the strength of actin dynamics within specific regions (**Figure 1C2**). Both triggering conditions show increased strength of actin dynamics within the boundary region ($p=0.014$ and $p=0.028$ for high K+ and hypotonic, respectively) but not within the bulk region ($p=0.050$ and $p=0.057$ for high K+ and hypotonic, respectively) when compared to paired controls (p-values determined by paired t-tests).

We then wanted to understand whether actin dynamics becomes relatively more probable in the boundary region and/or in the bulk region after a triggering stimulus. To accomplish this, we calculate a relative fraction and find a significant shift in actin dynamics towards the boundary under high K+ conditions compared to paired controls; there is no significant difference for hypotonic conditions compared to paired controls (**Figure 1C3**; $p=0.026$ and $p=0.466$, respectively, as determined by paired t-test).

To delve into distance dependence of actin dynamics more closely, we quantify the distance from instances of actin dynamics to the cell boundary (true boundary shown in **Figure 1B**). Curves of the representative cells shown in **Figure 1A** are shown in **Figure 1D1** with the boundary region and bulk region labeled. Since we are most interested in the high actin activity near the boundary, we compare how the probability of actin dynamics changes over distance when comparing the two triggering conditions to their matched controls. High K+ cells are significantly less likely to show actin dynamics near the boundary edge compared to their matched controls, though the mean difference is extremely small ($p=0.019$ for 3.24 μm and $p=0.021$ for 3.6 μm, determined by repeated measures ANOVA). On the other hand, hypotonic cells are significantly more likely to show actin dynamics within the boundary region compared to matched controls, specifically between 0.36 and 2.52 μm from the boundary ($p<0.05$ for all distances as determined by repeated measures ANOVA; refer to **Figure 1D3** legend for exact p-values). Taken together with the data from **Figure 1C3**, we show that a higher probability of actin dynamics at specific distances is not necessarily accompanied by an overall shift to the boundary region.

These results indicate the following: i) actin dynamics has a higher probability of occurring under high K+ conditions (**Figure 1C2**), ii) a relative shift of actin dynamics to the boundary is observed when cells are exposed to high K+ (**Figure 1C3**), iii) increased probability of actin dynamics at specific distances is observed when cells are exposed to hypotonic challenge (**Figure 1D3**), and iv) for both triggering conditions, the strength of actin dynamics increases within the boundary region but not within the bulk region (**Figure 1C2**).

Actin dynamics within astrocytes is clustered into active "hotspot" regions

While characterizing actin dynamics within astrocytes, we noticed that many cells seemed to have active regions near the boundary (**Figure 2A1**) that we suspected were responsible for most of the actin dynamics. To identify these "hotspot" regions, we applied the image processing techniques of erosion and dilation to identify areas of persistent activity (**Figure 2A2**). After applying thresholds for activity magnitude and probability and hotspot size, we segment regions that meet these criteria (**Figure 2A3**, inset **Figure 2A4**).

We first compared the strength of actin dynamics within the hotspot regions, considering the boundary and bulk regions separately as in **Figure 1C2**. Following the trend of activity within the whole cell, we found that actin dynamics is stronger in cells exposed to both high K+ and hypotonic, specifically within the boundary region ($p=0.015$ and $p=0.032$, respectively, as determined by paired t-test) and not within the bulk region ($p=0.464$ and $p=0.527$, respectively, as determined by paired t-test) as shown in **Figure 2B1**. We also investigated the relative strength of hotspot dynamics where the average magnitude within hotspots is normalized by the average magnitude of dynamics within the whole cell (**Figure 2B2**). When comparing this relative strength between cells in triggering conditions and their matched controls, we found that only high K+ cells displayed significantly stronger actin dynamics within hotspot regions compared to the whole cell ($p=0.028$ for control vs. K+ and $p=0.087$ for control vs. hypotonic as determined by paired t-test). Finally, we investigated whether actin dynamics in these hotspot regions is more persistent and found that the duration is not significantly different for either high K+ cells or hypotonic cells compared to matched controls ($p=0.095$ and $p=0.831$, respectively, as determined by paired t-test), as shown in **Figure 2B3**.

To provide a static visualization of actin dynamics within these hotspots, we show traditional actin fluorescence kymographs (**Figure 2C1**) and novel actin dynamics kymographs (**Figure 2C2**) for the three largest hotspot regions (reg, orange, and yellow) in the representative cell. Both types of kymographs clearly show stronger dynamics in the triggering condition. Taken together, these results show that hotspot regions respond distinctly to different stimuli and that they are particularly active in general and specifically reactive to the high K+ chemical stimulus.

Astrocytes respond to nanotopographic surfaces with distinct actin dynamics

Finally, we took advantage of the topographic features in hydrotalcyte-like compound (HTlc) films to understand how actin dynamics is altered by mechanical stimuli at the nanometer scale. HTlc films direct polygonal astrocytes to develop a highly branched and differentiated morphology, thus recapitulating in *in vitro* astrocytes the functional microdomains regulating water and potassium homeostasis that would be seen *in vivo* [31, 32].

To this end, we cultured primary rat astrocytes on PDL-coated glass or on HTlc nanoparticle films and imaged them under control conditions using the same parameters as before. Morphological and functional differences between cells grown on these two surfaces have been thoroughly characterized previously [31], and similar differences are observed in our system as shown in **Figure 3A**.

We first compared how actin dynamics differs in the various regions of PDL cells versus HTlc cells. We found that PDL cells show significantly stronger dynamics both within the boundary region and within the bulk region (**Figure 3B1**, $p<0.001$ as determined by unpaired t-test). Surprisingly though, when comparing boundary to bulk within each nanotopographic surface (**Figure 3B2**), we found that both PDL and HTlc show significantly stronger boundary dynamics compared to bulk dynamics ($p<0.001$ for PDL and $p=0.021$ for HTlc as determined by paired t-test).

We next compared how likely cells on the different surfaces are to show actin dynamics. When comparing within each region, we found that HTlc cells are significantly more likely to have actin dynamics, both within the boundary region and within the bulk region compared to PDL cells (**Figure 2C1**; p=0.014 and p=0.020, respectively, as determined by unpaired t-test). In this case, there is no significant difference between boundary and bulk for either surface (**Figure 2C2**; p=0.072 for PDL and p=0.184 for HTlc as determined by paired t-test).

Finally, we evaluated distance dependence in **Figure 3D** similar to in **Figure 1D**. We show the full distance curves in **Figure 1D1** for the representative cells. When comparing the individual distances within boundary region, we see that HTlc cells are significantly more likely to have actin dynamics (**Figure 3D2**; $p<0.05$ for all distances between 0.36 and 3.6 μm as determined by two-way ANOVA). Finally, when normalizing for size of the boundary (**Figure 3D3**), we do not find any difference in the relative fractions of actin dynamics within the boundary region compared to the bulk region for either surface (p=0.287 for PDL and p=0.058 for HTlc as determined by paired t-test). Taken together, these results indicate that HTlc cells show more frequent and weaker actin dynamics than PDL cells.

Astrocytes sense nanotopographic cues through actin orientation near the boundary

Inspired by our analysis of actin dynamics in live astrocytes, we sought to understand i) why certain "hotspots" of actin activity are more prevalent in cells grown on PDL than in cells grown on HTlc and ii) whether the characteristics of actin dynamics are related to the underlying actin structure. To this end, we cultured primary rat astrocytes on PDL-coated glass or on HTlc films and performed STED microscopy on fixed cells stained for F-actin and the intermediate filament protein glial fibrillary acid protein (GFAP). Representative images are shown in **Figure 4**. HTlc preferentially induces stellate morphology characteristic of differentiated astrocytes, whereas astrocytes grown on PDL-coated glass display the polygonal shapes characteristic of undifferentiated astrocytes.

Confocal images of F-actin labeled astrocytes reveal that there is a marked tendency for cells grown on PDL (**Figure 4A**) to display a non-differentiated and dynamic phenotype with distinct leading and trailing edges and several motile structures (i.e. lamellipodia, filopodia, stress fibers; **Figure 4C**). Conversely, in the "star" shaped cells grown on HTlc (**Figure 4B**), the same motile elements that would indicate direction of propagation are not clearly visible (**Figure 4D**). Moreover, the astrocytic actin is seen to "burst" out of the actin cortex in HTlc cells (**Figure 4D**). This bursting or "flaring" behavior is indicative of a functional microdomain, known to be present in differentiated astrocytes grown on HTlc [31]. Although many regions in the representative HTlc cell display this microdomain morphology, the actin dynamics of astrocytes plated on HTlc is of lower magnitude than that of astrocytes grown on PDL (refer to **Figure 3B**). Therefore, we chose to investigate how astrocytic actin senses the different mechanical environments presented by PDL-coated glass and HTlc films and the subsequent cytoskeleton remodeling at a nanoscale level via superresolution imaging. We used a method for quantitative, semi-automated analysis of the actin bundles' preferential orientation [33] to assess the involvement of actin organization in sensing the local mechanical environment around astrocytes.

Image analysis was performed by combining segmentation via an anisotropic, rotating Laplacian of gaussian (LoG) kernel with a hierarchical cluster analysis (see **Figure 5A** for a schematic overview and *Materials and Methods* for a detailed description). These image processing methods allow for the analysis of actin angle organization and the determination of fractions of actin roughly parallel versus roughly perpendicular to the leading edge of the cell boundary (**Figure 5B**). From our clustered data, we determine that PDL astrocytic actin is oriented more parallel relative to the leading edge of the astrocyte, whereas HTlc astrocytic actin is oriented more perpendicular (**Figure 5C**). The difference seen between the actin of cells grown on PDL versus on HTlc is significant as the cluster algorithm identifies two clusters within the data. Moreover, we see the cluster groups largely correspond with the chosen nanotopography, with an error of seven out of 37 cells: one HTlc cell is misclustered, and six PDL cells are misclustered (i.e. six PDL cells can be found in the cluster of predicted HTlc actin fractions). While the differences observed between astrocytes grown on HTlc and those grown on PDL at a dynamic, micron scale do not necessarily correspond to the differences seen in structure at the nanometer scale, our analytical approach reveals that the underlying nanoscale organization of actin within astrocytes does indeed change when the cells are exposed to different nanotopographic surfaces.

## Discussion

We show for the first time, by means of live timelapse confocal microscopy, that astrocytes respond to changes in the chemophysical environment with changes in actin dynamics. Actin is spatiotemporally organized into micron scale territories that enhance the dynamics in response to chemophysical stresses. Topography enhances the frequency of these dynamics but lowers their strength.

Our study reveals that actin dynamics occurs persistently and on different spatial scales, with local actin dynamics detectable near the boundary even when the boundary itself does not shift measurably. Dynamics are stronger in cells grown on PDL and cluster into hotspot regions, whereas they are more frequent in cells grown on HTlc and do not cluster into large enough regions to be detected with confocal microscopy. Both high potassium and hypotonic stimuli increase the strength of actin dynamics within the boundary region, but high potassium preferentially increases the strength of dynamics within hotspots, which is likely why the relative fraction of dynamics shifts towards the boundary. We find that these dynamics are localized to one or multiple boundary regions characterized by a lack of strong stress fibers, with a spatial scale larger than individual synapses.

While astrocytes do not change shape substantially on the short timescales of our experiments, we see small filopodial and lamellopodial structures near the cell boundary that appear to "idle" by rapidly extending and retracting, effectively sampling their local environment. It is in these regions that we most often observe actin dynamics.

Similar to previous studies, we note that on longer timescales astrocytes are extremely plastic cells. For example, after injury, astrocytes *in vivo* become reactive and highly ramified [34, 35]. Astrocytes cultured *in vitro*, however, appear polygonal and lose their starlike shape when the McCarthy and de Vellis preparation method is used [36-38], but it is possible to induce

differentiation and *in vivo*-like structural and functional properties over the course of a few days using a previously validated approach [31, 32], which consists of growing astrocytes on HTlc nanostructured films.

Surprisingly, actin is more dynamic in polygonal cells grown on flat surfaces (glass coverslips coated with PDL), which also favors the formation "hotspots" of actin dynamics compared to highly differentiated cells grown on nanostructured surfaces (HTlc films). The frequency of activity and the structure of the network is distinct for differentiated cells grown on HTlc, with filaments preferentially oriented perpendicular to the cell boundary.

The presence of a dynamic cytoskeleton during structural remodeling in astrocytes has been hypothesized to support the rapid morphological changes that occur in perisynaptic astrocytes processes (PAPs), seen in organotypic culture, in response to synaptic activity and long-term-potentiation [39]. Our results support this hypothesis, but, unexpectedly, we found that the strength of actin dynamics is lowered in differentiated astrocytes with respect to polygonal cells while the frequency of the movements is higher. Dynamic hotspots in differentiated cells might present as miniature versions of lamellipodia and filopodia, the F-actin-rich subcellular compartments of migrating non-neuronal cells [40].

Our STED data might also provide the key to understanding the conclusion that non-differentiated cells perform more robust cytoskeleton dynamics: a more parallel and dispersed organization of actin fibers into a meshwork underneath the cell membrane is likely to confer mechanical plasticity to the plasma membrane when compared to more differentiated cells on HTLc, where actin fibers are packed into "actin rails" and not only maintain the cell shape (especially in the cellular processes) but also might cause membrane stiffness or resistance to motility. We also hypothesize that this distinct structure will lead to differences in the interaction with neighboring cells. As stellation enables communication with other cell types, perpendicular actin may ensure processes are directed along a specific line of communication. Our finding that almost all cells on HTlc have actin structures perpendicular to the boundary affirms the ability of HTlc to encourage differentiation of astrocytes [31]. This analysis also hints that some cells grown on PDL have actin structures that "look" like the actin structures of stellated cells grown on HTlc, consistent with previous observations that growth of astrocytes on PDL delays but does not fully suppress spontaneous or gliotic differentiation that might occur in standard cell culture [11, 31, 41, 42].

Our previous studies demonstrated that astrocytes grown on HTlc are more efficient in their homeostatic process. In particular, the expression and function of Kir4.1 and AQP4 as well as the functional response to anisotonic challenge are improved in differentiated cells [31, 32]. In this respect, a faster and prompter response to chemophysical challenges might not require a major effort from the dynamic actin network, which might explain the lower magnitude of actin dynamics in differentiated cells. Moreover, the functionally better equipped differentiated astrocytes may also be able to more easily sense changes in the extracellular environment and react more frequently to them via actin dynamics. Thus, our findings are no longer surprising if we consider that astrocytes harness the excitable dynamics of actin to codify and convey information coming from the extracellular milieu.

Our finding that actin dynamics is altered by chemophysical stimuli and topography raises important questions for astrocyte physiology and pathophysiology: Is it possible to control and/or modulate the size of the spatial region where actin dynamically rearranges by activating a Signal Transduction Excitable Network (STEN)? Studies on other cell types suggest that activating STEN would enable traveling waves of varying sizes and may even trigger cell migration [17, 18, 22]. Could extreme conditions strengthen and alter the actin dynamics so much as to drive astrocyte differentiation? These questions remain to be elucidated, and studies in microglia [27] – which demonstrated that actin dynamics is critical for their principal function, surveillance – indicate that actin dynamics also plays an important role *in vivo* in neural cells. We propose that actin dynamics in astrocytes is critical for their principal functions: maintaining homeostasis and modulating neuronal communication. Finally, given that cytoskeletal alterations are reported in a variety of neurological conditions characterized by a gliotic state [43], we expect investigations of cytoskeletal dynamics in defined animal models to be an important area of exploration to validate the pathophysiological relevance [44] of our findings.

## Materials and Methods

### Rat cortical astrocyte culture preparation, maintenance, and plating

*Cell culture:*

Primary astrocytes were obtained from Sprague Dawley rats housed at the University of Maryland (in concordance with the recommendations of and approval by the University of Maryland Institutional Animal Care and Use Committee; protocols R-JAN-18-05 and R-FEB-21-04) or from Wistar rats housed at the University of Bologna (in concordance with the Italian and European law of protection of laboratory animals and the approval of the local bioethical committee, under the supervision of the veterinary commission for animal care and comfort of the University of Bologna and approved protocol from Italian Ministry of Health; ethical protocol number ID 360/2017 PR, released on May 2017, valid for 5 years).

Primary cultures of astrocytes were prepared as described previously, from newborn rat pups between postnatal days 1 and 2 [3, 36, 45]. Briefly, neonatal cerebral cortices devoid of meninges were gently triturated, filtered with a 70 µm cell strainer (cat. no. 22-363-548; Fisher Scientific, MA, USA), and plated in T25 cell culture flasks (cat. no. 229331; CELLTREAT Scientific Products, MA, USA) containing Dulbecco's Modified Eagle Medium (DMEM) with GlutaMAX and high glucose (cat. no. 10-566-024; Fisher Scientific, MA, USA) supplemented with 15% fetal bovine serum (FBS; cat. no. 100-106; Gemini Bio-Products, CA, USA) and penicillin-streptomycin at 100 U/mL and 100 µg/mL, respectively (cat. no. 15070063; Thermo Fisher Scientific, MA, USA). Flasks were maintained in an incubator at 37 °C, 5% $CO_2$, and proper humidity levels for two weeks. During this period, we replaced cell medium every two days, and flasks were gently shaken when necessary to remove undesired microglial cells. When confluence was reached, astrocytes were dispersed using trypsin-EDTA 0.25% (cat. no. 25200056, Thermo Fisher Scientific, MA, USA), and the cell suspension was re-plated on glass coverslips functionalized with Poly-D-lysine hydrobromide (PDL; cat. no. P7886; Sigma-Aldrich, MO, USA) as previously described [31, 45-48] or with HTlc as previously

described [31, 49]. Cells were plated at a density of 5-10×$10^3$ per dish and maintained in culture medium containing 10% FBS.

*PDL and HTlc film preparation:*

Microscope coverslips were functionalized with PDL to serve as a control surface or with Zn-Al hydrotalcite nanoparticles (HTlc) to induce morphological differentiation of astrocytes. For live imaging, PDL was used at a working concentration of 0.1 mg/mL, and cells were cultured for three to seven days after replating prior to imaging. For STED imaging, PDL was used at a working concentration of 0.01 mg/mL, and astrocytes were cultured for five days after replating prior to fixation. In both cases, coverslips were coated with PDL for 20 minutes at room temperature and washed three times with approximately 500 µL of sterile $H_2O$. Coverslips were functionalized with HTlc by adding the HTlc suspension drop by drop on the coverslips and allowed to dry overnight. Once dried, the HTlc coverslips were sterilized by UV for approximately 30 min.

Transduction of cells with actin-GFP

To visualize actin dynamics, astrocytes were transduced with CellLight Actin-GFP, BacMam 2.0 (cat. no. C10506; ThermoFisher Scientific, MA, USA) at a concentration of 100 particles per cell. At 48 hr prior to live imaging, 5-10 µL (depending on the plating density) of the reagent was added to the cell culture media. A full media change was performed 16-20 hr after transduction, and imaging was performed 24-48 hr after the full media change.

Live confocal imaging of transduced astrocytes

Live imaging timelapses were acquired at the University of Maryland CMNS Imaging Core using a PerkinElmer spinning disk confocal microscope with an oil immersion 40x objective (1.30 NA; 0.36 µm/pixel) and under temperature, $CO_2$, and humidity control. The microscope was equipped with a Hamamatsu ImagEM X2 EM-CCD camera (C9100-23B), which recorded 16 bit images. Data acquisition was performed with PerkinElmer's Volocity software (version 6.4.0). A subset of timelapses were taken at the CNR on an inverted confocal microscope (Crisel Instruments) using a 40x water immersion objective (0.16 µm/pixel).

Transduced astrocytes were identified by a positive signal in the 488 nm laser channel. After imaging parameters were set, the media was changed from growth media to standard external solution (control) followed by one of the triggering conditions (high potassium solution or hypotonic solution). Single-plane images were acquired every 2 sec in the 488 channel. A consistent z-plane was assured with Perfect Focus (Nikon PFS).

Immunostaining and superresolution imaging of fixed astrocytes

*Antibodies:*

Mouse monoclonal Anti-Glial Fibrillary Acidic Protein (GFAP) antibody (diluted 1:200; cat. no. G3893; Sigma-Aldrich, MO, USA) and Goat anti-Mouse IgG (H+L) Highly Cross-Adsorbed Secondary Antibody, Alexa Fluor 594 (diluted 1:300; cat. no. A-11032; Thermo Fisher Scientific, MA, USA) were used as primary and secondary antibody, respectively, for GFAP immunostaining. Alexa Fluor 488 Phalloidin (diluted 1:500; cat. no. A12379; Thermo Fisher Scientific, MA, USA) was used for direct labelling of actin.

*STED immunostaining:*

Immunofluorescence for gated STED (gSTED) was performed as indicated in the Quick Guide to the STED Sample Preparation (www.leica-microsystems.com), with some slight adjustments as previously reported [50, 51]. Astrocytes were plated on the PDL and HTlc-treated coverslips and cultured for five days. On the fifth day of culture, cells were fixed with 2% paraformaldehyde (cat. no. P6148; Sigma-Aldrich, MO, USA) in PBS for 10 min, washed with PBS, and permeabilized with 0.3% Triton X-100 (cat. no. T8787; Sigma-Aldrich, MO, USA) for 10 min. After blocking with 0.1% gelatin in PBS, fixed astrocytes were incubated with GFAP-primary antibody for 1 hr at room temperature. Cells were then rinsed with 0.1% gelatin-PBS and co-incubated with Alexa Fluor 488 Phalloidin and Alexa Fluor 594-conjugated secondary antibody for 1 hr at room temperature. After washing with PBS, coverslips were mounted on microscope slides by using the ProLong Glass Antifade Mountant (cat. no. P36980; Thermo Fisher Scientific, MA, USA) without DAPI, as indicated in Leica official guide, and imaged with both confocal and STED microscopy.

*STED imaging:*

Confocal and STED images of fixed astrocytes grown on PDL and HTlc were acquired using a Leica TCS SP8 3X microscope, provided with AOTF and AOBS, white light laser (WLL), Hybrid Detectors (HyD), and two STED lasers (592 nm, 660 nm) [51]. A Leica HC PL APO 100x/1.40 NA Oil STED White objective and Type F Immersion liquid with a refractive index of 1.5 were used. Before starting imaging, the excitation and the doughnut-shaped STED beams were switched on (WLL set laser power= 70%; STED-592 nm set laser power = 98%), aligned, and allowed to reach operating temperature. The beam alignment was repeated whenever necessary. Excitation of the Alexa Fluor 488 dye was achieved using a continuous-wave 488 nm laser line (NKT Photonics supercontinuum laser). For superresolution imaging of actin, g-STED was performed using the continuous wave 592 nm-emitting STED fiber laser. More detailed acquisition settings are reported in **Table 1**. All confocal and STED images were acquired at a set room temperature of 20 °C under constant Acquisition Mode settings (Format scanning resolution: 1024x1024 pixels; Scan Speed: 100 Hz).

*Criteria for acquisitions of ROIs:*

Single or few and well-spaced cells were preferentially chosen for STED imaging to ensure no overlap of actin structure belonging to different cells. Actin and GFAP images of the whole cell were first acquired by confocal microscopy at an original magnification of 100x. Then, multiple random regions of interest (ROIs) (~20x20 µm sized) were selected and imaged using an extra optical zoom (from 5 to 7) by confocal and STED microscopy. Three independent experiments were conducted.

Synthesis of ZnAl-HTlc nanoparticles and film preparation

Colloidal aqueous dispersion of ZnAl-HTlc nanoparticles having the formula $[Zn_{0.72}Al_{0.28}(OH)_2]\,Br_{0.28}\ 0.69\ H_2O$ were prepared by the double-microemulsion technique previously described [31]. For the film preparation, a 125 or 160 µL aliquot of ZnAl-HTlc colloidal dispersion at a concentration of 1.2 mg/mL was dropped onto 15 or 19 mm diameter glass coverslips and successively dried for 4 hr in a sterile hood. The obtained ZnAl-HTlc films were used to culture astrocytes and as substrates for live dynamics imaging and fixed STED

imaging as described above. In this manuscript, the ZnAl-HTlc films are referred to simply as HTlc.

Solutions and chemicals

All salts and chemicals employed for the investigations were of the highest purity grade. For live imaging experiments, the standard external solution ("control") was (mM): 140 NaCl, 4 KCl, 2 $MgCl_2$, 2 $CaCl_2$, 10 HEPES, 5 glucose, pH 7.4 with NaOH and osmolarity adjusted to ~315 mOsm with mannitol. When using external solutions with different ionic compositions, such as the high potassium solution ("high K+", [40 Mm]), salts were replaced equimolarly. The hypotonic extracellular solution ("hypotonic") of 260 mOsm/L was obtained by omitting mannitol in the control solution. When imaging, media was changed carefully to prevent accidental, mechanical stimulation of cells with the pipette. Moreover, we controlled for any effects that changing media might cause by changing media prior to imaging under control conditions (from growth media to the standard external solution) and under triggering conditions (from the standard external solution to high K+ or hypotonic medium).

Analysis of live imaging data

*Pre-processing of timelapses:*

All timelapses were smoothed in time using a Simoncelli smoothing filter [52]. Prior to smoothing, any timelapses that showed noticeable jitter or drift due to thermal gradients were processed through a jitter correction algorithm using discrete Fourier transform (DFT) registration and an upsampling factor of 100 (using the "dftregistration" code package from [53]). For timelapses where drift was inconsistent and unable to be fully corrected with the DFT method, an additional correction using intensity-based image registration (via the MATLAB functions "imregconfig" and "imregister") was applied using the average image of the DFT corrected timelapse as the fixed image.

*Shape analysis and identification of bulk and boundary regions:*

We used shape analysis to identify cell boundaries and subsequently to be able to compare actin dynamics within different regions of astrocytes. Using a snake algorithm from our previous work [16, 29, 30], we analyzed the average fluorescent image of each cell to generate the "true boundary" (**see Figure 1A-B**). Prior to shape analysis, images were smoothed ("imgaussfilt" in MATLAB with a standard deviation of 1.0) and subsequently sharpened ("imsharpen" in MATLAB with a radius of 2.5 and amount of 1.0). Alpha and beta parameters for the snake algorithm (tension and rigidity, respectively) were 0.20 and 0.25, respectively. We found that this true boundary tended to capture the most prominent morphological features of the cell but often excluded regions that were only transiently dynamic. To mitigate this challenge, we eroded or dilated the true boundary using a spherical structural element with a radius of 10 pixels. By subtracting the eroded cell region from the dilated cell region, we identified a boundary region. We considered the eroded cell mask to be the bulk region.

*Optical flow analysis of actin dynamics:*

Optical flow analysis similar to that used in [19] was performed on smoothed and jitter-corrected timelapses in Python 3.8. The optical flow weight matrix was a 19x19 pixel Gaussian with a standard deviation of 3 pixels (1.1 μm) for all timelapses taken at UMD. For a small subset of

HTlc timelapses taken at the CNR, the optical flow weight matrix was a 41x41 pixel Gaussian with a standard deviation of 6.75 pixels (1.1 μm). The truncation value for the Gaussian kernel was consistently set to 3. Because actin dynamics in astrocytes is less prominent than in migrating cells usually studied by our lab [15, 19], we only considered optical flow vectors with the highest 1% of magnitude within the dilated cell boundary that also passed our reliability criteria (at least 33% of the mean reliability value for that timelapse). These strict criteria ensured that we were only considering dynamic actin events that are large and reliable compared to background noise.

*Segmentation of active regions ("hotspots") of actin dynamics:*
To identify regions with the most actin activity, we further analyzed our thresholded data by eroding and dilating in the x, y, and time dimensions using an elongated cube with dimensions of [3,3,2]. To ensure that we were not including regions of low activity, we set an event probability threshold of 0.10, meaning that a region had to be active at least 10% of the time to be considered a "hotspot". Furthermore, we imposed a size constraint of 20 pixels (including the time dimension) to ensure that any active regions did not just barely meet the volume require of 3x3x2. Since the dynamics within HTlc cells are on a smaller scale, the microdomain analysis did not reveal any regions that were clearly active.

Analysis of STED images of fixed astrocytes

*Laplacian of Gaussian (LoG) filtering to segment actin:*
To characterize the organization of the actin meshwork in STED images of fixed cells, as shown in **Figure 4**, we performed several image processing techniques using custom-written algorithms in MATLAB (Mathworks). Prior to processing, all STED images are adjusted using a contrast-limited adaptive histogram equalization ("adjusthisteq" function in MATLAB's proprietary API (https://www.mathworks.com/help/images/adaptive-histogram-equalization.html). The resolution of the STED images is 16.18pix/nm. Next, each image is convolved with an anisotropic, rotating Laplacian of Gaussian (LoG) kernel. The exact kernel parameters were determined through trial and error to approximately match the cylindrical shape of actin as visualized by Phalloidin-488 staining. The number of angles through which the LoG kernel is rotated was chosen to balance computational time and segmentation accuracy. For each pixel, the best match angle is chosen via the maximum value resulting from convolving that pixel with all rotations of the filter, and a threshold is applied to ensure a high-quality match. This processing results in a filtered image that highlights both the actin organization and the angle associated with each filament extracted from kernel (see **Figure 5A1**). The angles associated with the extracted actin are defined in terms of the Cartesian coordinate system, which is not biologically meaningful. To establish the angle at which the actin organizes relative to the cellular boundary, we manually draw a boundary for each cell. The number of pixels per boundary varies on a cell-to-cell basis. For each pixel, we derive the angle of that pixel's actin relative to the closest boundary point. This transformation generates angles in the range of 0 to $\pi/2$. We then apply an additional threshold at an arbitrary value to only segment the longest actin (**Figure 5A2**); doing so greatly reduces the noise in our processed data. We analyzed at least 15 individual cells per nanotopographic surface, and the morphologies of the imaged areas varied from cell to cell. Thus, the boundaries are generated to normalize the distributions of the relative angles across the data sets. We noticed that for the STED images taken of astrocytes grown on HTlc, there is more total boundary per unit-area.

Thus, the boundaries from which the relative angles are calculated are drawn to coincide with only the leading edge of the cell (see **Figure 5B** for representative examples).

*Cluster analysis of relative angles:*

To understand how astrocytic actin organization differs when the cells are grown on different nanotopographies, we use a hierarchical cluster analysis from MATLAB's proprietary API (https://www.mathworks.com/help/stats/cluster-analysis.html). From the relative angle distributions across both PDL and HTlc (22 individual cells and 15 individual cells, respectively), we group the distributions into "parallel" (angles between 0 and $\pi/6$) and "perpendicular" (angles between $\pi/3$ and $\pi/2$), as shown in **Figure 5B**. As inputs to the clustering algorithm, we use the fractions of "parallel" and "perpendicular" actin of the 37 individual cells but do not include information about the corresponding nanotopographic surface. We then use the "pdist," "linkage," "cophenet," and "linkage" functions (while optimizing the cophenetic coefficient of our 'distance' and 'linkage' parameters) to generate predictive clusters of the input data.

Data representation and statistics

All data were plotted and all statistical tests were performed in MATLAB 2021a. For data showing differences between control and triggering or between boundary and bulk regions, paired t-tests were used ("ttest" function in MATLAB). For data comparing PDL to HTlc, unpaired two-sample t-tests were used ("ttest2" function in MATLAB). When analyzing optical flow prevalence vs. distance, ANOVA tests were used: repeated measures ANOVA was used for paired data in Figure 1 ("fitrm" and "ranova" functions in MATLAB), and two-way ANOVA was used to compare PDL and HTlc in Figure 3 ("anovan" function in MATLAB). In both cases, Tukey's multiple comparisons test ("multcompare" function in MATLAB) was used as the post test. All errorbars indicate 95% confidence interval, and the significance level was set at $\alpha$=0.05. Adobe Illustrator (version 25.0.1) was used for final assembly of all figures.

**References**

1. Verkhratsky, A. and M. Nedergaard, *Physiology of Astroglia.* Physiol Rev, 2017. **98**(1): p. 239-389.
2. Rose, C.R. and A. Verkhratsky, *Principles of sodium homeostasis and sodium signalling in astroglia.* Glia, 2016. **64**(10): p. 1611-1627.
3. Benfenati, V. and S. Ferroni, *Water transport between CNS compartments: Functional and molecular interactions between aquaporins and ion channels.* Neuroscience, 2010. **168**(4): p. 926-940.
4. Santello, M., N. Toni, and A. Volterra, *Astrocyte function from information processing to cognition and cognitive impairment.* Nat Neurosci, 2019. **22**(2): p. 154-166.
5. Farhy-Tselnicker, I., et al., *Activity-dependent modulation of synapse-regulating genes in astrocytes.* Elife, 2021. **10**: p. e70514.
6. Bellot-Saez, A., et al., *Astrocytic modulation of neuronal excitability through K+ spatial buffering.* Neurosci Biobehav Rev, 2017. **77**: p. 87-97.
7. Scemes, E. and D.C. Spray, *Extracellular K+ and astrocyte signaling via connexin and pannexin channels.* Neurochem Res, 2012. **37**(11): p. 2310-2306.

8. Spray, D.C., *Molecular physiology of gap junction channels.* Clinical and experimental pharmacology and physiology, 1996. **23**(12): p. 1038-1040.
9. Scemes, E. and D.C. Spray, *Extracellular K+ and astrocyte signaling via connexin and pannexin channels.* Neurochemical research, 2012. **37**(11): p. 2310-2316.
10. Nicchia, G.P., et al., *Actin cytoskeleton remodeling governs aquaporin-4 localization in astrocytes.* Glia, 2008. **56**(16): p. 1755-1766.
11. Benfenati, V., et al., *Functional down-regulation of volume-regulated anion channels in AQP4 knockdown cultured rat cortical astrocytes.* Journal of Neurochemistry, 2007. **100**(1): p. 87-104.
12. Nicchia, G.P., et al., *Different pattern of aquaporin-4 expression in extensor digitorum longus and soleus during early development.* Muscle Nerve, 2007. **35**(5): p. 625-631.
13. Fritzsche, M., et al., *Cytoskeletal actin dynamics shape a ramifying actin network underpinning immunological synapse formation.* Sci Adv, 2017. **3**(6): p. e1603032.
14. Vicker, M.G., *F-actin assembly in Dictyostelium cell locomotion and shape oscillations propagates as a self-organized reaction-diffusion wave.* FEBS Letters, 2002. **510**(1-2): p. 5-9.
15. Sun, X., et al., *Asymmetric nanotopography biases cytoskeletal dynamics and promotes unidirectional cell guidance.* Proc Natl Acad Sci U S A, 2015. **112**(41): p. 12557-12562.
16. Driscoll, M.K., et al., *Cellular contact guidance through dynamic sensing of nanotopography.* ACS Nano, 2014. **8**(4): p. 3546-3555.
17. Edwards, M., et al., *Insight from the maximal activation of the signal transduction excitable network in Dictyostelium discoideum.* Proc Natl Acad Sci U S A, 2018. **115**(16): p. E3722-E3730.
18. Miao, Y., et al., *Wave patterns organize cellular protrusions and control cortical dynamics.* Mol Syst Biol, 2019. **15**(3): p. e8585.
19. Lee, R., et al., *Quantifying topography-guided actin dynamics across scales using optical flow.* Mol Biol Cell, 2020. **mbcE19110614**.
20. Roy, S., *Waves, rings, and trails: The scenic landscape of axonal actin.* J Cell Biol, 2016. **212**(2): p. 131-134.
21. Del Signore, S.J., et al., *An autoinhibitory clamp of actin assembly constrains and directs synaptic endocytosis.* Elife, 2021. **10**: p. e69597.
22. Li, X., et al., *Excitable networks controlling cell migration during development and disease.* Semin Cell Dev Biol, 2020. **100**: p. 133-142.
23. Pal, D.S., et al., *The excitable signal transduction networks: movers and shapers of eukaryotic cell migration.* Int J Dev Biol, 2019. **63**(8-9-10): p. 407-416.
24. Azatov, M., et al., *Topography on a subcellular scale modulates cellular adhesions and actin stress fiber dynamics in tumor associated fibroblasts.* Phys Biol, 2017. **14**(6): p. 065003.
25. Ketchum, C.M., et al., *Subcellular topography modulates actin dynamics and signaling in B-cells.* Mol Biol Cell, 2018. **29**(13): p. 1732-1742.
26. Kumari, S., et al., *Cytoskeletal tension actively sustains the migratory T-cell synaptic contact.* EMBO J, 2020. **39**(5): p. e102783.
27. Bernier, L.-P., et al., *Nanoscale surveillance of the brain by microglia via cAMP-regulated filopodia.* Cell Rep, 2019. **27**(10): p. 2895-2908.e4.

683 28. Lucas, B.D. and T. Kanade. *An iterative image registration technique with an application*
684 *to stereo vision*. in *Proceedings of the 7th International Joint Conference on Artificial*
685 *Intelligence*. 1981. San Francisco, CA, USA: Morgan Kaufmann Publishers Inc.
686 29. Driscoll, M.K., et al., *Spatiotemporal relationships between the cell shape and the*
687 *actomyosin cortex of periodically protruding cells.* Cytoskeleton (Hoboken), 2015 **72**(6):
688 p. 268-281.
689 30. Driscoll, M.K., et al., *Cell shape dynamics: from waves to migration.* PLoS Comput Biol,
690 2012. **8**(3): p. e1002392.
691 31. Posati, T., et al., *A nanoscale interface promoting molecular and functional*
692 *differentiation of neural cells.* Sci Rep, 2016. **6**: p. 31226.
693 32. Mola, M.G., et al., *Cell volume regulation mechanisms in differentiated astrocytes.*
694 Submitted, 2021.
695 33. Campanello, L., et al., *Signaling through polymerization and degradation: Analysis and*
696 *simulations of T cell activation mediated by Bcl10.* PLoS Comput Biol, 2021. **17**(5): p.
697 e1007986.
698 34. Schiweck, J., B.J. Eickholt, and K. Murk, *Important shapeshifter: Mechanisms allowing*
699 *astrocytes to respond to the changing nervous system during development, injury and*
700 *disease.* Front Cell Neurosci, 2018. **12**: p. 261.
701 35. Schiweck, J., et al., *Drebrin controls scar formation and astrocyte reactivity upon*
702 *traumatic brain injury by regulating membrane trafficking.* Nat Commun, 2021. **12**: p.
703 1490.
704 36. Ferroni, S., et al., *Two distinct inwardly rectifying conductances are expressed in long*
705 *term dibutyryl-cyclic-AMP treated rat cultured cortical astrocytes.* FEBS Lett, 1995.
706 **367**(3): p. 319-325.
707 37. Benfenati, V., et al., *Guanosine promotes the up-regulation of inward rectifier potassium*
708 *current mediated by Kir4.1 in cultured rat cortical astrocytes.* J Neurochem, 2006. **98**(2):
709 p. 430-445.
710 38. McCarthy, K.D. and J. de Vellis, *Preparation of separate astroglial and oligodendroglial*
711 *cell cultures from rat cerebral tissue.* J Cell Biol, 1980. **85**(3): p. 890-902.
712 39. Bernardinelli, Y., et al., *Activity-dependent structural plasticity of perisynaptic astrocytic*
713 *domains promotes excitatory synapse stability.* Curr Biol, 2014. **24**(15): p. 1679-1688.
714 40. Hirrlinger, J., S. Hülsmann, and F. Kirchhoff, *Astroglial processes show spontaneous*
715 *motility at active synaptic terminals in situ.* Eur J Neurosci, 2004. **20**(8): p. 2235-2239.
716 41. Ferroni, S., et al., *Characterization of an inwardly rectifying chloride conductance*
717 *expressed by cultured rat cortical astrocytes.* Glia, 1997. **21**(2): p. 217-227.
718 42. Nicchia, G.P., et al., *Aquaporin-4-containing astrocytes sustain a temperature- and*
719 *mercury-insensitive swelling in vitro.* Glia, 2000. **31**(1): p. 29-38.
720 43. Muñoz-Lasso, D.C., et al., *Much more than a scaffold: Cytoskeletal proteins in*
721 *neurological disorders.* Cells, 2020. **9**(2): p. 358.
722 44. Tobe, B.T.D., et al., *Probing the lithium-response pathway in hiPSCs implicates the*
723 *phosphoregulatory set-point for a cytoskeletal modulator in bipolar pathogenesis.* Proc
724 Natl Acad Sci U S A, 2017. **114**(22): p. E4462–E4471.
725 45. Benfenati, V., et al., *A silk platform that enables electrophysiology and targeted drug*
726 *delivery in brain astroglial cells.* Biomaterials, 2010. **31**(31): p. 7883-7891.

46. Saracino, E., et al., *A Glial-Silicon Nanowire Electrode Junction Enabling Differentiation and Noninvasive Recording of Slow Oscillations from Primary Astrocytes.* Adv Biosyst, 2020. **4**(4): p. e1900264.
47. Benfenati, V. and S. Ferroni, *Microdynamics of Water and Ion Homeostasis in the Brain*, in *Homeostatic Control of Brain Function*. 2015, Oxford University Press.
48. Benfenati, V., et al., *Photostimulation of whole-cell conductance in primary rat neocortical astrocytes mediated by organic semiconducting thin films.* Adv Healthc Mater, 2014. **3**(3): p. 392-399.
49. Borrachero-Conejo, A.I., et al., *Stimulation of water and calcium dynamics in astrocytes with pulsed infrared light.* Faseb J, 2020. **34**(5): p. 6539-6553.
50. De Bellis, M., et al., *Translational readthrough generates new astrocyte AQP4 isoforms that modulate supramolecular clustering, glial endfeet localization, and water transport.* Glia, 2017. **65**(5): p. 790-803.
51. de Bellis, M., et al., *Orthogonal arrays of particle assembly are essential for normal aquaporin-4 expression level in the brain.* Glia, 2021. **69**(2): p. 473-488.
52. Simoncelli, E.P., *Design of multi-dimensional derivative filters.* Proceedings of 1st International Conference on Image Processing, 1994. **1**: p. 790-794.
53. Guizar-Sicairos, M., S.T. Thurman, and J.R. Fienup, *Efficient subpixel image registration algorithms.* Opt Lett, 2008. **33**: p. 156-158.



**Acknowledgements**

The authors would like to thank the University of Maryland Imaging Incubator Core Facility for providing and maintaining the systems used in collecting images for this work. They also thank Q. Yang and L. J. Campanello for helpful discussions related to analysis.

**Funding:** This work was supported by the following grants:

US Air Force Office of Scientific Research MURI grant FA9550-16-1-0052 to WL
US Air Force Office of Scientific Research grant FA9550-19-1-0370 (AstroDyn) to WL
VB GPN KMO
US Air Force Office of Scientific Research FA9550-16-1-0502 (AstroMat) to VB
US Air Force Office of Scientific Research FA9550-17-1-0502 (AstroNir) to VB
US Air Force Office of Scientific Research FA9550-18-1-0255 (3D Neuroglia) to VB
COMBINE fellowships to NJM SP


**Author contributions**

Conceptualization: VB WL
Surface preparation: ES TP
Experiments: KMO ES BB MGM
Analysis: KMO NJM SP
Interpretation: KMO ES BB NJM MGM GPN VB WL
Supervision: GPN VB WL
Writing—original draft: KMO ES BB NJM GPN VB WL
Writing—review & editing: KMO ES BB NJM MGM SP TP RZ GPN VB WL

**Competing interests:** The authors have no competing interests to declare.

773 **Data and materials availability:** All data and code will be made available in a repository
774 located in the Losert laboratory's github page.
775

## Figures and Tables

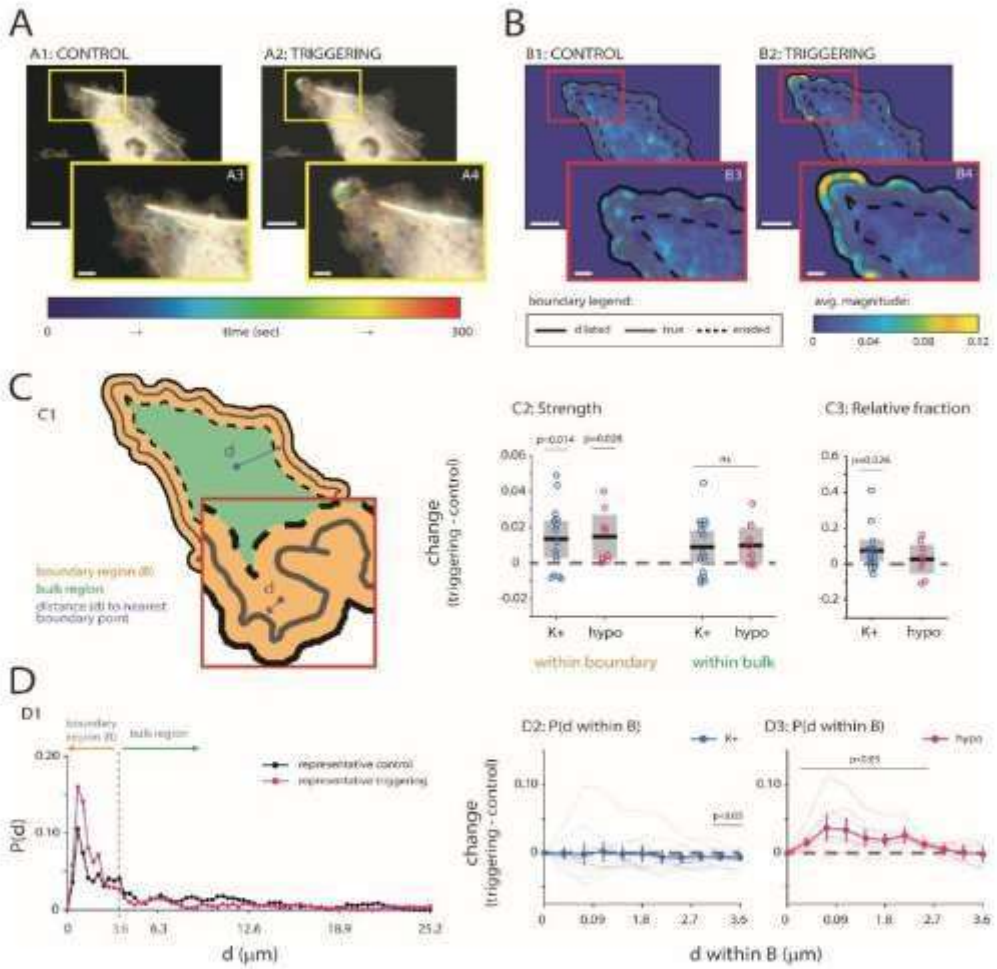


**Figure 1: Optical flow analysis reveals actin dynamics in primary astrocytes.**

**A)** Actin-GFP timelapse for representative cell, control (A1, inset A3) and triggering (A2, inset A4) conditions. Colorbar indicates time. **B)** Optical flow analysis for representative cell from A, control (B1, inset B3) and triggering (B2, inset B4) conditions. Colorbar indicates average optical flow magnitude. **C)** Characterizing actin dynamics. **C1)** Shape analysis [16, 29, 30]

identifies true boundary (solid grey line). Boundary region (orange) is created by dilating (solid black line) and eroding (dashed black line) true boundary by 10 pixels and is distinct from bulk region (green). **C2)** Strength of actin dynamics for control vs. K+ ($p=0.014$ for boundary, $p=0.050$ for bulk) and for control vs. hypo ($p=0.028$ for boundary, $p=0.057$ for bulk). **C3)** Relative fraction of actin dynamics within boundary for control vs. K+ ($p=0.026$) and for control vs. hypo ($p=0.466$). **D)** Distance dependence of actin dynamics. **D1)** Probability *P(d)* vs. distance from boundary *d* for representative data shown in B. **D2-D3)** Probability within boundary region *P(d within B)* vs. distance from true boundary within boundary region *d within B* for all cells for control vs. K+ (D2; $p=0.019$ at 3.24 µm, $p=0.021$ at 3.6 µm) and for control vs. hypo (D3; $p=0.033$, $p=0.032$, $p=0.030$, $p=0.036$, $p=0.025$, $p=0.001$, $p<0.001$ at 0.36-2.52 µm). P-values determined by paired t-test (C) or by repeated measures ANOVA (D). n=15 paired cells for control and K+, and n=8 paired cells for control and hypo. Scalebars indicate 20 µm (A1-A2, B1-B2) or 5 µm (A3-A4, B3-B4). Error bars/boxes indicate 95% confidence intervals. Solid black lines and opaque circles indicate mean. Transparent lines in D2-D3 represent individual distance curves. "Control" indicates cells imaged in standard external medium; "triggering" indicates cells imaged in isotonic high potassium solution ("K+") or hypotonic solution ("hypo").

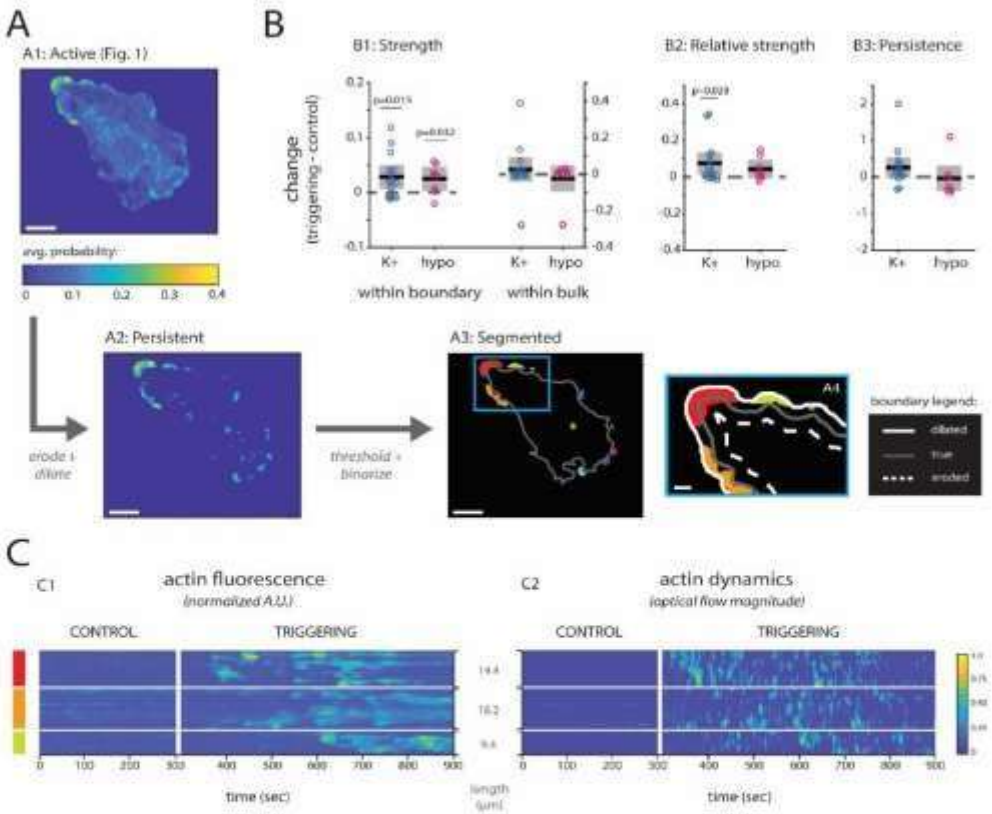


**Figure 2: Persistence analysis of actin dynamics reveal "hotspots" of actin activity.**

**A)** Identification of "hotspot" regions. Optical flow results (A1; from Figure 1) are eroded and dilated in space and in time (A2) to identify the most persistently active regions. Regions that meet criteria are binarized and segmented (A3, inset A4) for comparison between cells and conditions. **B)** Characterization of hotspot dynamics. **B1)** Average strength of actin dynamics for control vs. K+ ($p=0.015$ for boundary, $p=0.464$ for bulk) and for control vs. hypo ($p=0.032$ for boundary, $p=0.527$ for bulk). **B2)** Relative strength of actin dynamics for control vs. K+ ($p=0.028$) and for control vs. hypo ($p=0.087$). **B3)** Average persistence of actin dynamics for control vs. K+ ($p=0.095$) and for control vs. hypo ($p=0.831$). All p-values determined by paired

815 t-test. Solid black lines indicate the mean. Grey regions indicate 95% confidence interval.
816 **C)** Kymographs of normalized actin fluorescence (C1) and of optical flow magnitude (C2) for
817 three largest hotspot regions from A3-A4. Grey labels between kymographs indicate lengths of
818 regions. Colorbar indicates normalized fluorescence (C1) and optical flow magnitude (C2). n=15
819 paired cells for control and K+, and n=8 paired cells for control and hypo.
820

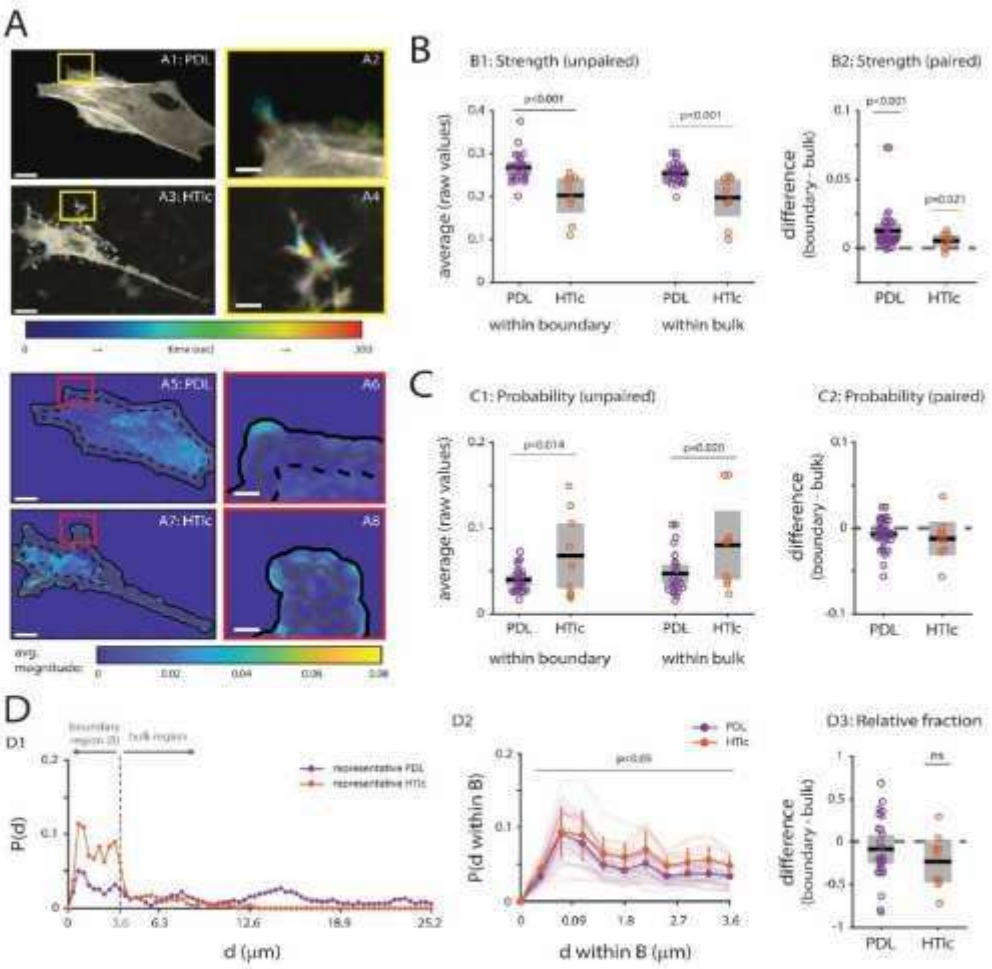


**Figure 3: Actin dynamics differs substantially in undifferentiated astrocytes grown on PDL compared to differentiated astrocytes grown on HTlc.**

**A)** Actin-GFP timelapse for representative cells grown on PDL-coated glass ("PDL"; A1, inset A2) and HTlc films ("HTlc"; A3, inset A4). Colorbar indicates time. Optical flow analysis for representative cells (PDL in A5, inset A6; HTlc in A7, inset A8). Colorbar indicates average optical flow magnitude. **B)** Strength of actin dynamics. **B1)** Strength of actin dynamics within

boundary ($p<0.001$) and within bulk ($p<0.001$) for PDL vs. HTlc cells. **B2)** Strength of actin dynamics in boundary vs. bulk for PDL ($p<0.001$) and for HTlc ($p=0.021$) cells. **C)** Probability of actin dynamics. **C1)** Probability of actin dynamics within boundary ($p=0.014$) and within bulk ($p=0.020$) for PDL vs. HTlc cells. **C2)** Probability of actin dynamics in boundary vs. bulk for PDL ($p=0.072$) and for HTlc ($p=0.184$) cells. **D)** Distance dependence of actin dynamics. **D1)** Probability *P(d)* vs. distance from boundary *d* for representative data shown in A5-A8. **D2)** Probability within boundary region *P(d within B)* vs. distance from true boundary within boundary region *d within B* for all PDL and HTlc cells ($p<0.001$ at 0.36-3.24 μm, $p=0.01$ at 3.6 μm). **D3)** Relative fraction of actin dynamics within boundary ($p=0.287$ for PDL, $p=0.058$ for HTlc). P-values determined by unpaired t-test (B1, C1), paired t-test (B2, C2, D3), or two-way ANOVA (D2). n=24 cells for PDL, and n=9 cells for HTlc. Scalebars indicate 20 μm (A1, A3, A5, A7) or 5 μm (A2, A4, A6, A8). Error bars/boxes indicate 95% confidence intervals. Solid black lines and opaque circles indicate mean. Transparent lines in D2 represent individual distance curves.

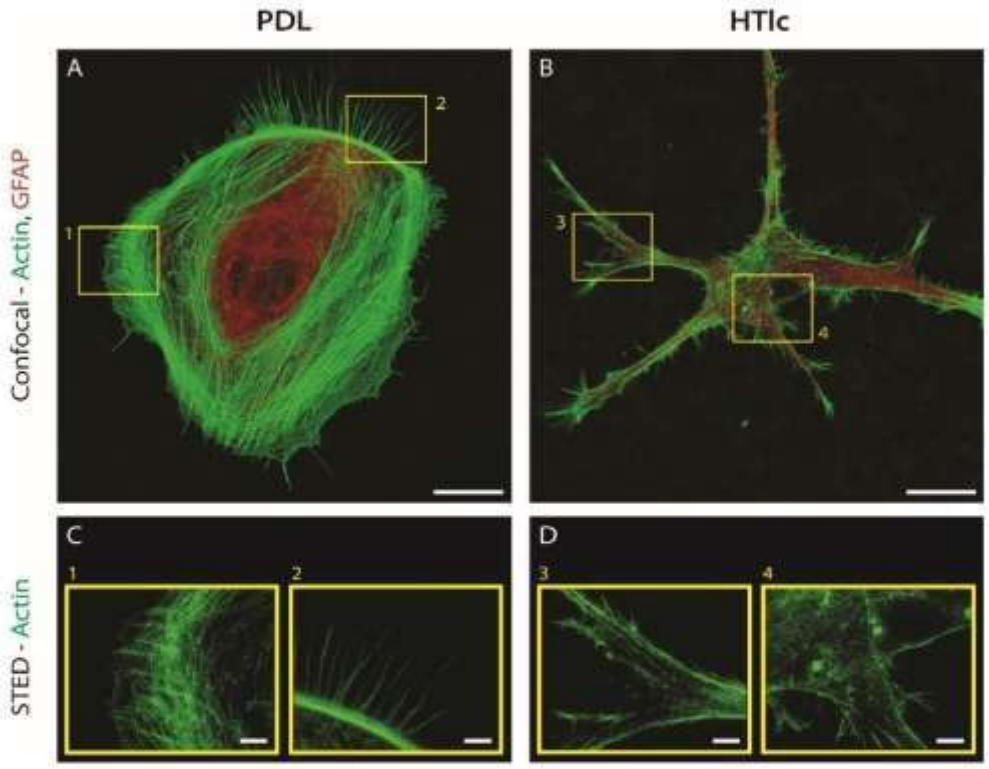


**Figure 4: STED microscopy visualizes nanoscale actin structure within primary astrocytes grown on PDL and on HTlc.**

**A-B)** Confocal microscopy images of representative astrocytes grown on PDL-coated glass (A) or on HTlc films (B) for five days, fixed, and stained for actin (green) and GFAP (red). Scalebars indicate 10 µm. **C-D)** Superresolution images taken via STED microscopy of cells grown on PDL (C) and on HTlc (D) of boxed yellow regions from A and B. Scalebars indicate 2.5 µm.

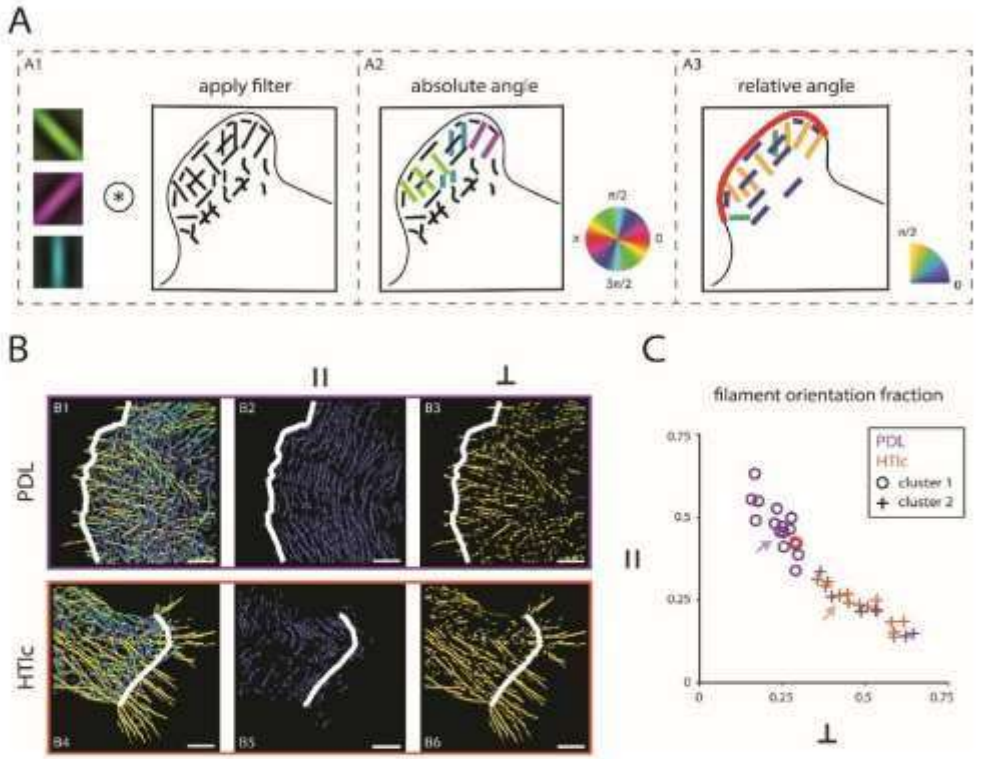


**Figure 5: Filtering STED images with a rotating, anisotropic LoG kernel reveals differences in nanoscale actin structure for astrocytes grown on PDL versus on HTlc.**

**A)** Extraction of relative angle information from actin filaments. **A1)** STED images are convolved with a rotating, anisotropic LoG kernel. **A2)** Filtering extracts actin bundles and a best match angle that is relative to the MATLAB frame ("absolute angle") with a range of $[0, 2\pi]$ (shown as full colorwheel). **A3)** A leading edge boundary (red) is drawn manually and is used to transform actin angles to be relative to the closes boundary point ("relative angle") with a range of $[0, \pi/2]$ (shown as a quarter colorwheel). **B)** Output from A for representative cells (PDL in B1-B3, HTlc in B4-B6). All relative angles, parallel angles only (range of $[0, \pi/6]$), and

867 perpendicular angles only (range of [π/3, π/2]) for representative PDL (B1, B2, B3, respectively)
868 and HTlc (B4, B5, B6, respectively) cells. Solid white lines indicate leading edge boundary.
869 Scalebars indicate 2.5 µm. **C)** Parallel (y-axis) vs. perpendicular (x-axis) fractions of actin
870 detected within PDL (purple) and HTlc (orange) astrocytes. A hierarchical cluster analysis
871 reveals two distinct clusters (cluster 1: open circles, cluster 2: crosses). Arrows indicate
872 representative cells. n=22 cells for PDL, and n=15 cells for HTlc.
873

874

| | Parameter | Actin | GFAP |
|---|---|---|---|
| **Confocal** | WLL (488 nm) intensity, % | 10 | 10 |
| | Gain | 25 | 25 |
| **STED** | WLL (488 nm) intensity, % | 40 | |
| | STED (592 nm) intensity, % | 97 | |
| | Gain | 200 | |

875

876 **Table 1: Imaging parameters.** Parameters used for STED and confocal imaging of fixed
877 astrocytes on PDL and HTlc.
878

**EMBARGO REQUEST- data not yet published**

**Gold Nanocluster impact on astrocytes structure and function**

Evidences over the past 40 years have indicated that astrocytes have a critical role in sensing chemo-physical changes occurring in the brain extracellular environment. Crucial in maintaining thehomeostatic balance of the central nervous system (CNS) *in vivo* are the expression of ion channels and aquaporins at nano-microdomains of astrocytes end-feet. However, how astrocytes modulate their response to different chemo-physical stimuli are still unknown. Herein, we propose ultrasmall size (1-4 nm) metal nanoclusters (NCs) as a new class of nanoprobes useful in understanding the complex chemistry and physics of biological systems. We investigate the effect of gold nanoclusters (AuNCs) on primary rat cortical astrocytes structure and function *in vitro*.

By means of viability assay, time lapse imaging and confocal immunofluorescence, we found that treatment with AuNCs are not toxic for astrocytes and induce a formidable morphological differentiation in astrocytes. The tremendous cytoskeleton rearrangement demonstrates a hugecortical expression of actin in treated cells; data were followed by stimulated emission depletion microscopy (STED) imaging to qualitatively reveal the expression of inward rectifier potassium channels (KIR 4.1) and aquaporin 4 (AQP4), also revealed by western blot (WB) experiments. Moreover, scanning electron microscopy (SEM) was performed to reveal the possible localization ofthe cluster inside the astrocytes. Patch-clamp experiments indicated that differentiation was accompanied by the expression of potassium ($K^+$) currents increase in the whole-cell membrane currents upon photo-stimulation. Calcium Imaging was measured in order to collect $Ca^{2+}$ fluxes across the cell membrane in response to trigger selective activation of transmembrane receptors and channels in treated cells.

Specifically, a category of NCs: NCs-conjugated with Gold (AuNCs), in addition with protein-synthesised bovine serum albumin (BSA, fAuNCs/BSA)[198], endowed with unique and tunable plasmon resonance properties, unique magnetic properties, high signal-to-noise ratio, intense

photoluminescence and high stability, have been analysed in ISOF Laboratories and in collaborationwith ARL Laboratories of Aberdeen by Dr. Shashi Karna, in the context of ASTROGOLD Project (US CCRL-ROP-L Neurophysiology of Cognition Army Research Laboratory W911NF-21-2-0074).Versatility in nano-size, surface and hydrophilic or lipophilic characteristics of fAuNCs *in vitro* allows already the internalisation into cervical, kidney, and fibroblast cell lines without a negative impact on the cell viability; however, the effect of fAuNCs has never been evaluated on brain cells. Here, the effects of 24h treatment of fAuNCs and fAuNCs/BSA on the astrocytes viability, biophysicsproperties, cytoskeleton re-organization and morphology and ion and water channels expressions, arereported. These findings suggest that AuNCs/BSA offer 1) a powerful biocompatible, nanoscale tool to probe and sense astroglial bioelectrical properties and 2) a transformative approach to study astrocytic homeostatic regulation and the glial/neural network involvement in diseased brain physiology.

*AuNCs induce astrocytes morphological differentiation*

In order to determine the impact of fAuNCs on astroglial cell growth, pure rat neocortical astroglial cells were re-plated on glass coverslips coated with poly-D-Lysine (PDL). Single plane fluorescein diacetate (FDA) imaging and morphological observations after 3 div from the re-plating are reportedin Fig. 5.1, revealed viable not treated (NT) and fAuNCs/BSA or fAuNCS treated astrocytes [1 Mm].Polygonal flat shapes, (Fig. 5.1C), resembling the typical phenotype of *in vitro* primary astrocytes grown on polystyrene Petri dishes, were observed in NT cells[268-270], while astrocytes treated for 24h with fAuNCs/BSA displayed a differentiated phenotype, characterised by processes departing from the cell body and projecting their end-feet on distal cells (Fig. 5.1D). To verify astrocyte adhesion and proliferation, images of cells stained with DAPI were taken after 1 div from the fAuNCs/BSA treatment and the cell nuclei in each image were counted. In agreement with the cell viability assay, the histogram plot reports the number/area of DAPI stained cell nuclei, calculated for different fAuNCs/BSA concentrations (Fig. 5.1B). It should be noted that, the survival of astrocytes is not severely compromised by the increasing fAuNCs/BSA concentration, while the morphology of strocytes is strongly influenced by

the higher concentration of fAuNCs/BSA [1mM] treatment, indicating that the cell body size is bigger and that cells look more differentiated when NT or low [fAuNCs/BSA] treated.

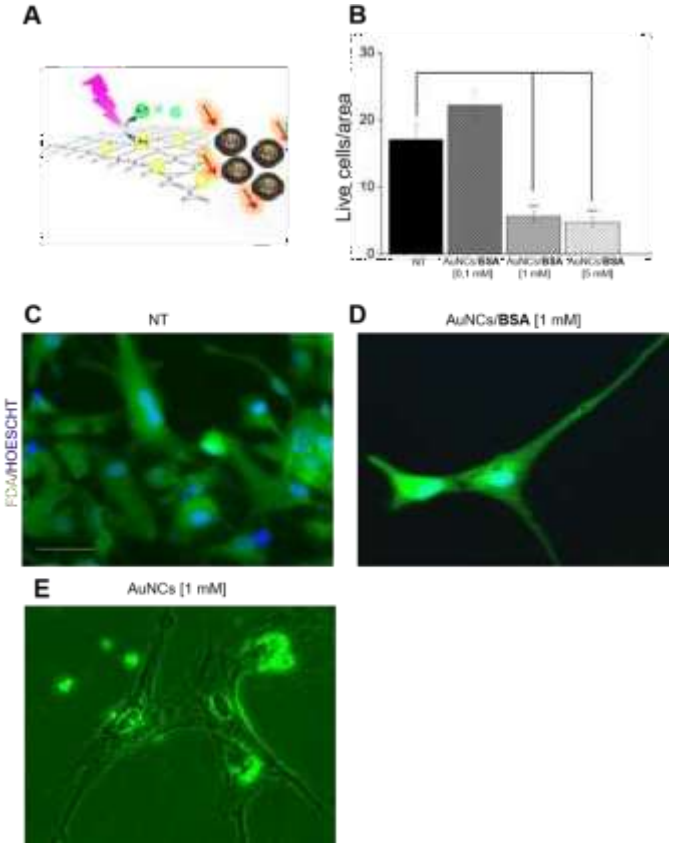


**Fig. 5.1:** Analyses of the effect of AuNCs on astrocytes viability and morphology properties. A) Scheme representing the AuNCs/BSA approach to treat astrocytes. B) Histogram shows the number of live cells/area for each conditions captured after 24h the treatment, C-E) Single plane confocal images of FDA/HOESCHT stained astrocytes: NT cells (C), AuNCs/BSA [1 mM] (D) and AuNCs [1 mM] (E). Scale Bar is 40 μm.

The 24h treatment of astrocytes with no BSA fAuNCs is not toxic for cells, however the quenching of fluorescent, due to the metal, does not allow to properly observe the cell body of astrocytes. The kind of differentiation caused only by fAuNCs seem to have a different impact on the astrocytes morphology treated with fAuNCs/BSA (Fig. 5.1E). In conclusion, fAuNCs are not toxic for the cells after 24h treatment, even the role exercised by BSA protein could be fundamental to increase the biocompatibility of gold nanoclusters, to allow a more *in vivo*-like morphological differentiation, andto be employed as a useful tool for the study of glial cells. The results suggest that, in general the fAuNCs promote morphological phenotype of astrocytes; astroglial cell viability is severely

compromised over the long term when astrocytes are treated with fAuNCs (Fig. 5.1E), demonstratingonce more, the importance of BSA protein blending with fAuNCs in the adhesion and healthy differentiation of cells.

*Functional properties of astrocytes treated with AuNCs*

One of the main goals of this study was to verify the effects of fAuNCs on astroglial ion channels' functions, involved in the physiology and pathophysiology of CNS *in vivo*. To this end, whole-cell patch-clamp measurements were performed 3 days after re-plating, on NT, fAuNCs/BSA andfAuNCs treated astrocytes at low density, (Fig. 5.2), Moreover, the following study is the first reporting the demonstration of functional regulation of ion channels by metal NCs application *in vitro*in astrocytes, without the need of either patterning or chemical functionalization of the plating surface(i.e. glass and cover glasses), in contrast to previous models where different methods have been reported to promote astrocytic functional differentiation via the addition of chemicals to the bath media. Cells were voltage clamped at a holding potential (Vh) of −60 mV, a slow ramp from −120 to60 mV inset in Fig. 5.2A) with intracellular and extracellular saline controls, to evoke whole-cell currents. The current amplitude was recorded and passive membrane properties were calculated as anadditional indication that fAuNCs modify astroglial cell morphology, size and cell phenotype (Table5.1) The resting membrane potentials (Vmem) of NT seeded cells were -30,5 ± 5,1 mV, which is comparable with values previously reported for primary astrocytes grown *in vitro* on different substrates[88,92]. Vmem was more hyperpolarized -22,4 ± 11,3 mV in fAuNCs/BSA treated cells. Accordingly, a significant decrease was observed in the input resistance values (355 ± 47 MΩ in NT-astrocytes, 44 ± 6MΩ in fAuNCs/BSA cells) while the specific conductance (0,14 ± 0,01 ns/pF for NT cells; 1,2 ± 0,2 ns/pF fAuNCs/BSA cells) recorded at −60 mV. The capacitance was notsignificantly different between NT and fAuNCs/BSA treated cells (25 ± 2,7 pF for NT astrocytes; 24 ± 2,4 for fAuNCs/BSA treated cells). The ramp current traces in AuNCs/BSA [1mM] cells (Fig. 5.2B) displayed a strong inward and outward rectification, compared to currents recorded on the same daysin NT-plated cells. Importantly, the huge current density recorded at −120 mV and +60 mV was

significantly higher for fAuNCs/BSA compared to NT-plated cells (--6,2± 0,9 pA/pF at −120 mV and37,7± 17,6 at +60 mV for NT; -112 ± 23 pA/pF at −120 mV and 82± 16 at +60 mV for fAuNCs/BSA-treated cells).

| | C (pF) | Vmem (mV) | I MAX (-120) (pA/pF) | I MAX (+60) (pA/pF) | I R (M Ω) | SG (ns/pF) |
|---|---|---|---|---|---|---|
| **NT** N=11 | 25 ± 2,7 | -30,5 ± 5,1 | -6,2± 0,9 | 37,7± 17,6 | 355 ± 47 | 0,14 ± 0,01 |
| **AuNCS/BSA** N=17 | 24 ± 2,4 | -22,4 ± 11,3 | -112 ± 23 *** | 82± 16 *** | 44 ± 6 *** | 1,2 ± 0,2 *** |
| **AuNCS** N=5 | 17,4 ± 5 | -13 ± 4,2 | -59 ± 25 ** | 32 ± 11 | 197 ± 88 | 0,6 ± 0,2 ** |

**Table 5.1**: Electrophysiological properties of astrocytes NT and treated with AuNCs/BSA and AuNCs. Cp, membrane capacitance; Vmem, resting membrane potential; SG, mean specific conductance; IR, input resistance; I, current density.

Furthermore, in astrocytes differentiated *in vitro* and *in situ*, the potassium Kir 4.1 up-regulation is known to be responsible for a significant increase in cell conductance and modulate the biophysical properties of cells[88,92,268,269].

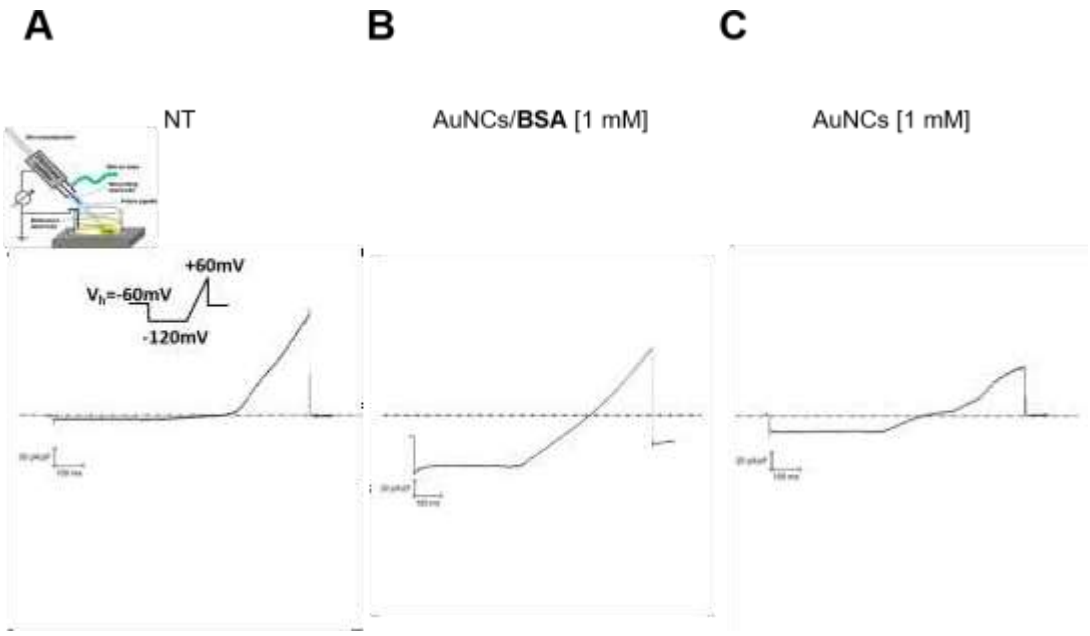


**Fig. 5.2:** Effects of AuNCs/BSA on astrocytes bioelectrical properties. A-C) Current traces recorded stimulating astrocytes with a voltage ramp protocol (inset A) from Vh -120 to +60 mV (500 ms), in NT astrocytes (A) and treated AuNCs/BSA [1 mM], (B), and AuNCs [1 mM], (C). Data are expressed as mean±SE.

In conclusion, the effects of fAuNCs on astrocytes bioelectrical properties seem to be extremely dependent on the presence of BSA protein blended to AuNCs. Indeed, potassium was omitted by intracellular solution to verify the influence of anions on the astrocytes functionality; it was replacedwith cesium (CsCl) to eliminate influence of the $K^+$ currents. As shown in Fig. 5.3A, B, the potassiumseems to be inhibited. Accordingly, astrocytes were clamped at the holding potential (Vh) of 0 mV, next to the astrocyte zero-current potential under our experimental conditions and stimulated with voltage ramps from -80 to 80 mV. Whole-cell membrane conductance was recorded in extracellular saline for both NT and fAuNCs/BS conditions. In order to analyse whether fAuNCs/BSA treatment affects biophysical properties of chloride current, the voltage chloride ramp was analysed in NT and fAuNCs/BSA treated astrocytes (Fig. 5.3C, D). The averaged ratio value for peak current densities

(pA/pF) at -80 mV and +80 mV in NT astrocytes (left panel) and fAuNCs/BSA-[1mM] treated cells(right panel) is reported in the histogram (Fig. 5.3E). Results lead to the conclusion that Au nanoclusters compared to semiconductor quantum-dot emitters for their ultrasmall size, high stability,and nontoxicity of fAuNCs exhibited a high efficiency to be further engineered i.e. in the devices targeting brain disease.

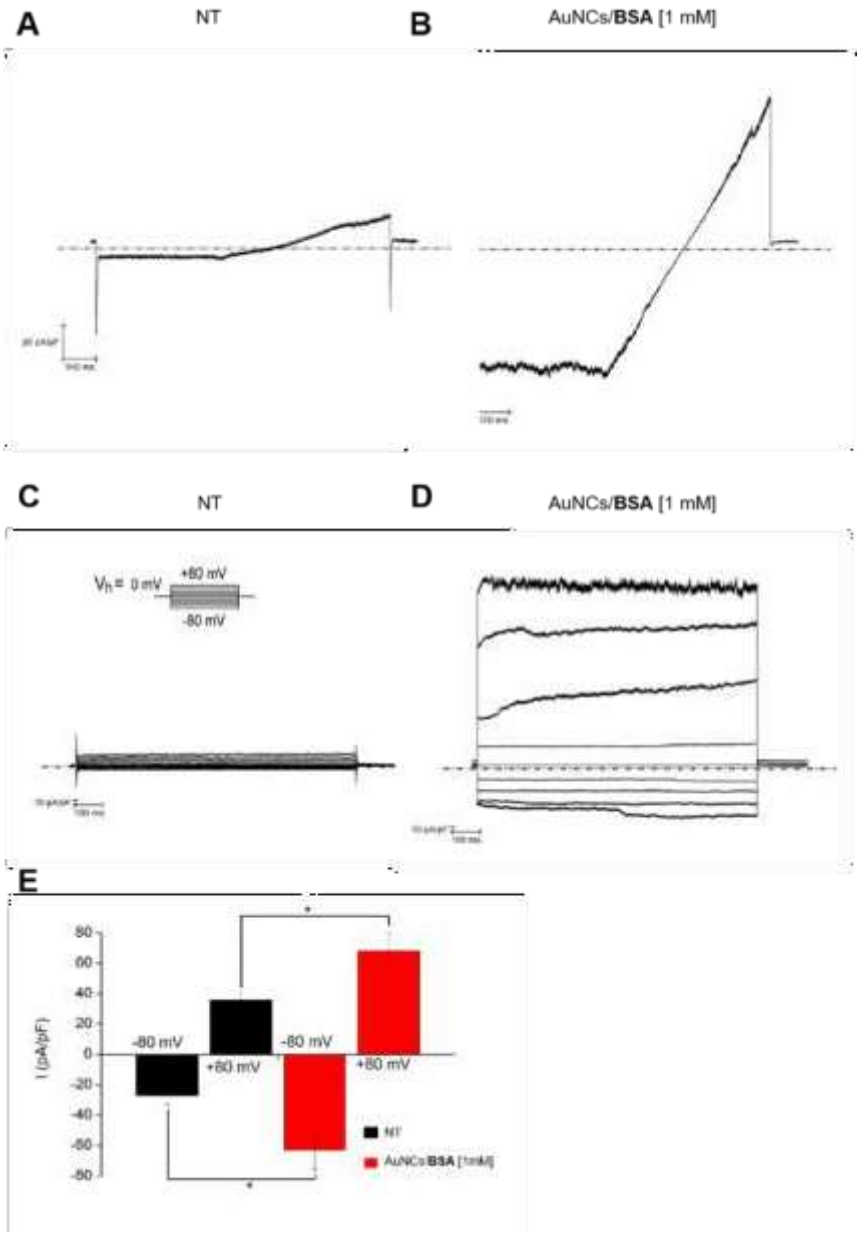


**Fig. 5.3**: Effects of AuNCs/BSA on astrocytes bioelectrical properties when potassium currents were inhibited with internal CsCl solution. A, B) Current traces recorded stimulating astrocytes with a voltage ramp protocol (inset A) from Vh -80 to +80 mV (500 ms), in NT astrocytes (A) and treated AuNCs/BSA [1 mM (B)]. C, D) Representative current traces of activated current recorded in astrocytes plated on PDL (C) and AuNCs/BSA (D) astrocytes in response to family of voltage steps protocol (inset, C). Astrocytes were voltage clamped at the holding potential (Vh) of 0 mV, and families of voltage steps of 20 mV increments were delivered from -80 mV to +80 mV. E) Histogram reports the averaged value for peak current density at -80 mV and +80 mV in NT and AuNCs/BSA treated astrocytes (n=12 for NT, n=9 for AuNCs/BSA [1 mM]). Data are expressed as mean±SE.

In order to investigate the mechanisms underpinning astrocytes and fAuNCs interaction, we performed F-actin staining to mark cytoskeletal fibres. As shown in Fig. 5.4, randomly interweaved F-actin fibres were observed on NT cells (Fig. 5.4A, B). A more ordinary and cortical pattern of actinfibres expression was observed in fAuNCs/BSA treated cells (Fig. 5.4C, D), evident pronounced expression of actin is expressed on lateral endfeet. Collectively these data support the tenet that fAuNCs/BSA treatment induces differentiation in astrocytes by promoting cytoskeleton rearrangement.

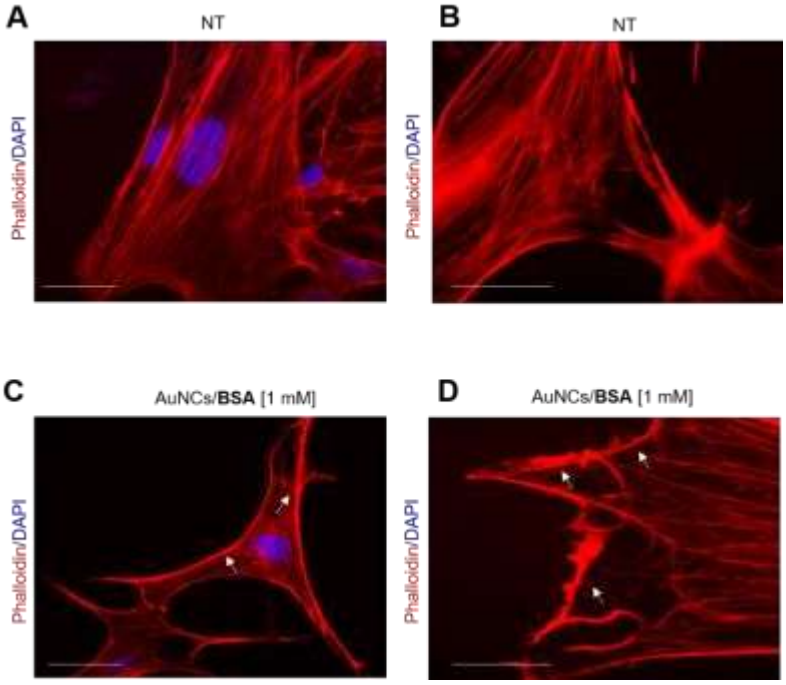


**Fig. 5.4:** Single plane confocal images of primary cortical astrocytes stained with Rhodamine Phalloidin/DAPI in not treated (NT) and AuNCs/BSA treated cells. The graphs show the response of astrocytes morphology and cytoskeleton to AuNCs-24 h treatment: NT cells (A, B) and AuNCs/BSA [1mM] (C, D), treated cells. Scale Bar is 40 μm (A, C) and 100 μm (B, D).

Since morphological alteration occurs upon gliosis, we next evaluated the distribution and expressionlevel of GFAP, a well-known marker of astrogliotic cells *in vivo* and *in vitro*.

Immunoblotting confirmed that the expression levels of GFAP were not different in NT andfAuNCs/BSA treated astrocytes, thereby it indicates that AuNCs do not promote any gliotic reactions*in vitro*. Western blot analyses and relative quantification (Fig. 5.5) revealed that the expression levelsof AQP4 (Fig. 5.5A, B) were not significantly higher in AuNCs/BSA treated cells[271,272].

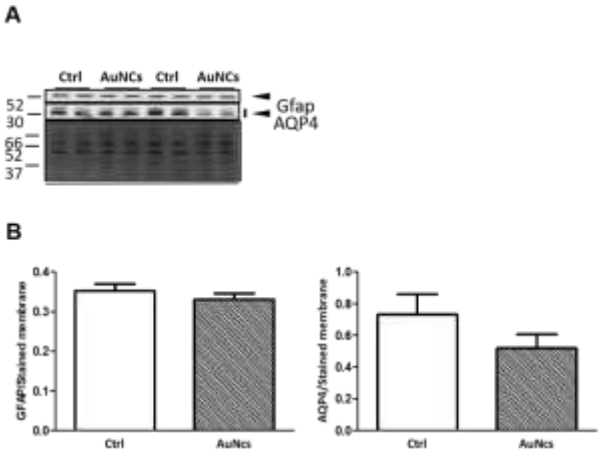


**Fig. 5.5:** A) inset shows the representative western blot analysis of AQP4 and GFAP expression in primary astroglial cultures after 24h of treatment with AuNCs. The immunoblotting and quantification of the expression level of GFAP are used as control for signal normalisation. Note that the expression level of GFAP was not significantly different between NT and AuNCs/BSA treated astrocytes,indicating that AuNCs does not promote gliotic reactions *in vitro*. B) Summary of the densitometric analysis of AQP4 corresponding signals normalised to the No-Stain™ Protein Labelling Reagent-stained membrane.

All the collected results open the way to postulate use of nano-molecules as nanoglial interfaces andfuture sensor technology to catch unknown mechanisms behind the biophysical properties of astrocytes.

*Organic semiconducting polymer pillars for studying structural and functional properties of astroglial cells*

In recent years, it has been investigated on the fabrication of 3D-polymer structures and electrodes interfacing with living cells, expoting specific geometries, such as nanowires, nanopillars, mushrooms. Taking advantage from the use of nanostructured semiconductive polymers that, Tullii et al., fabricated interface made of polythiophene (rr-P3HT), a well-known semiconductive polymer and distinctive

optoelectronic features and biocompatibility processing them in form of nanostructured pillars in the top of the surface. The pillar structure was obtained by pushcoating technique. Tulii et al, demonstrated that interfacing rr-P3HT nanopillars with neurons determined anenhancement of the cell membrane capacitance of neurons, due to the cell membrane thinning in correspondence to the pillars' top. Despite this, any negative effect was identified in the cell proliferation rate of neurons; similar results were obtained with other cell lines (i.e. HEK 293). Withthe perspective of use rr-P3HT pillars as soft interface and taking advantage of conductivity of rr- P3HT, we investigated, in collaboration with the group of Dr. Antognazza, IIT-CNST, on the morphological impact of the architectured pillars of P3HT with astrocytes[262]. Morevorer, ongoing electrophysiological results are defining the functional signal of differentiated astrocytes on rr-P3HTnanopillars interface compared to rr-P3HT FLAT (control, no pillars) interface. Future goal is to establish the role of light-sensitive properties of specific polymers, such as the rr-P3HT and how lightcould be a triggered tool to modulate the functionality of astrocytes.

*Nanopillars Topography of organic semiconducting P3HT polymer allows the differentiation of astrocytes*

As first approach, we evaluated astrocytes cell biocompatibility, growth and proliferation on rr-P3HT pillars and FLAT substrates, used as control (CTRL). The long-lasting biocompatibility was measured by performing bright field imaging at different time points (data not shown) and fluorescentimaging at 5 div from the cells re-plating. The results showed a different response of the cells on different substrates, specifically the morphology of the cells on the flat substrate was more polygonal,while the morphology on the pillar was differentiated. Fig. 5.1.1 shows GFAP immunostaining of astrocytes at 5 div. The GFAP marker was used to evaluate both the morphology and the biocompatibility of the material with cells and no overexpression has been detected, demonstrating that plating cells without the use of standard coating (i.e. PDL) allows the long biocompatibility of the polymer's nanostructure with the astrocytes. The substantial difference of the two system FLAT and P3HT pillars is due to the structured region formed by the hierarchical organization of pillars, that we supposed to be responsible of the response of astrocytes in adhesion and growth. Besides, the health of the cells seeded on the top of the two substrates, fluorescent imaging clearly shows the significant difference in the morphology of cells according to the two different substrates. Both express a phenotype different from PDL standard system, because astrocytes look no polygonal, butthe topography of rr-P3HT pillars leads to a more elongated morphology of the cell body compared to FLAT CTRL. The architecture of FLAT substrate was similar to a 2D system rather than a 3D system as the nanopillars conferred to the rr-P3HT interface. Moreover, fluorescent imaging was ableto quantitatively demonstrate the previous observation by the counting of differentiated and elongatedastrocytes seeded on the top-view surface area of the two substrates. Data (not shown) define a significant increase on rr-P3HT pillars of differentiated phenotype of cells on pillar substrates. The same was confirmed by AB assay and by the determination of proliferation rate. (data not shown). On the basis of the following observation, we speculate that, the topography of the interface remodelsastrocytes cell body expoiting the structure conferred by nanopillars to rr-P3HT interfaces.

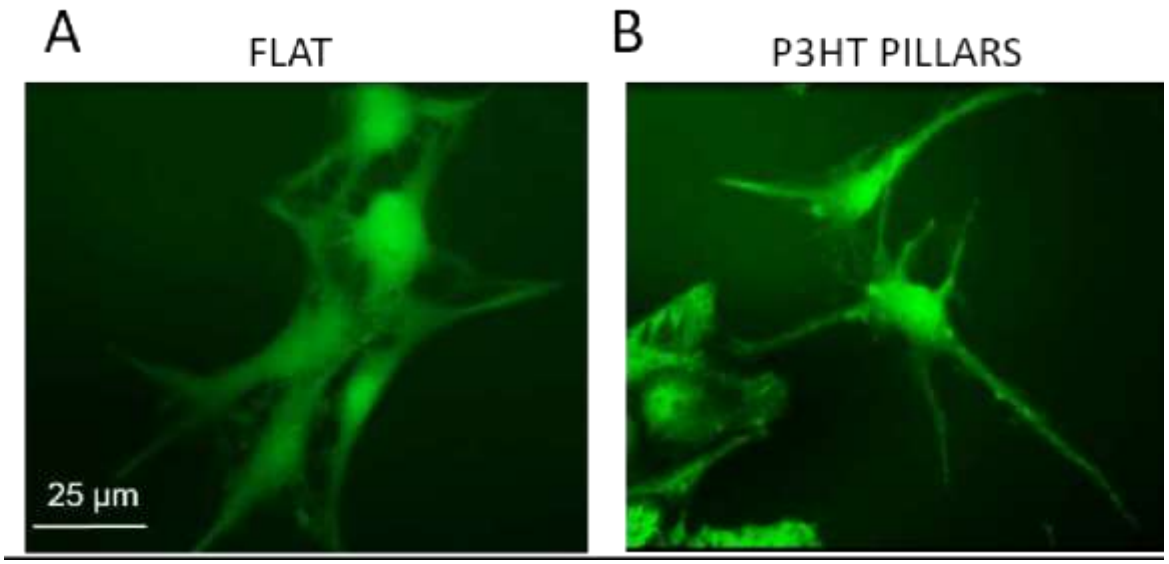


**Fig. 5.1.1:** Analyses of the effect of rr-P3HT nanopillars on astrocytes viability and morphology properties. A) Fluorescent-GFAP image representing the astrocytes phenotype on FLAT substrate B) Fluorescent-GFAP image representing the differentiated astrocytes phenotype on P3HT PILLARS substrate. Scale Bar is 25 µm.

According to these findings, we are investigating the functionality of differentiated astrocytes seededon the rr-P3HT substrates. In particular, the focus is on the modulation of astrocyteselectrophysiological properties exploiting the semiconducting qualities of rr- P3HT (data not shown).Once the role of specific ion channels and mechanisms underpinning the morphological differentiation conferred to astrocytes by the nanostructure has been defined and characterized, we will investigate on the potential of use light (through low-LED stimulation) as possible optical tools to modulate astrocytes functionality. The light sensitivity of rr-P3HT makes it favourable to integratein implantable devices with the aim to become a potential therapeutic approach in case of brain disorders.

# Conclusions and Perspectives

There is an increased demand in Nanoneuroscience for advanced biomedical tools, enabling real-time recording and manipulation of dynamic communication processes between neural cells. In particular, spreading knowledge on the mechanisms underlying brain function are an open issue for neuroscientists, since the advent of neural engineering, when the study of neurons was the main target;however, studies over the past four decades have revealed that astrocytes, which are non-excitable glial cells of the CNS, have a molecular, functional and cellular role in brain physiology. Nonetheless, their role is critical in the homeostasis of the brain, in the synaptogenesis and in the design of the neuronal network and cognitive functions, too. In addition, dysfunctions of astrocytes affect acute and chronic neuropathologies, some of them known as channelopathies. Based on the following assumptions, it is determinant to unravel molecular and cellular mechanisms of astrocytes, targeting selectively specific molecular, functional players expressed by astrocytes (i.e. ion channels, $Ca^{2+}$ signalling, aquaporins) by means of advanced neural interfaces that provide bi-directional communication between electronic devices and neural tissues. The interest of biomaterial science engineering and bioelectronics moved to the "other brain" to overcome the past 50 years' studies in bioelectronics interface targeted the bioelectrical activity of neurons. It revolutionized our understanding of the brain physiology and it introduced innovative procedures for treating pathologies such as AD, Parkinson's disease, epilepsy, depression and psychiatric disorders.

This thesis illustrates how novel approaches can be addressed specifically to target astrocytes' functional, structural and biological mechanisms by proposing glialinterfaces and glioenginnering asan emerging revolution of glioscience. Nanostructured scaffolds have been developed bycollaborators to investigate the astrocytes' complexity at multilevel scale. Several types ofnanostructured materials (inorganic, organic and polymers) were tested to show their suitability forbioelectronic probing and sensing of astrocytes morphological, structural molecular and functionalproperties. The approach of the thesis was to study these materials as active nano*glial interfaces; itwas achieved by results showing the ability of the different approaches to* promoting the structuraldifferentiation of astrocytes accompanied by a mature functional phenotype in *in vivo*-like models. Specifically, the major results are the following:

- Substrates based on electrospun aligned PCL polymers and combined with gelatin allow the adhesion, growth and differentiation of glial cells. The substrates modify astrocytes' structurenot affecting their electrophysiological properties.
- The same electrospun PCL interface, enriched with a conductive polymer (PANi), processedin form of nanoneedles, do not significantly impact on astrocytes' biophysical properties, thus revealing that PCL electrospun fibers are promising platform for potential electrical stimulation of astrocytes with resolution at the nanoscale.
- Au/SiNws promote a favourable nanomaterial-astrocytes interaction over long-term and represent a valid system to obtain *in vitro* a cell culture model of astrocytes with features comparable in terms of molecular morphological differentiation similar to the one expressed*in vivo*. Moreover, it allows insight into astrocytes' function, by unprecedented recording of their bioelectrical slow wave properties. The results set bases for ongoing studies on brain communication and processes through bioelectronics devices that can actively dialogue with astrocytes to record and stimulate their function during disorders that are on the way within the framework of EU-funded.

- Taking advantage from previous results achieved in Benfenati's lab, a nanoscale interface based on hydrotalcite-like compounds was used to study the dynamics underpinning the cellular localization and functionality of channel proteins belonging to astrocytic microdomains. The work done during my PhD demonstrated that the differentiation of astrocytes is associated also with an increased AQP4. Its upregulation influences the sensitivity of the cell to osmotic changes and impact on the RVD and RVI processes. Both TRPV4 and VRAC ion channels are engaged, even though the total protein level of expressionis unaltered.
- As it has been hyhothesized, advanced technologies to probe astrocytes sensing suggest astroglial cells are equipped with their own oscillation and excitability "rhythm" that make them not silent cells. we investigate the physiological response of astrocytes to extracellular environment modifications (increase in ion concentrations or change in nanomechanical features). The results address the role of astrocytes as modulators and targets of the signalling processes in the brain. Advanced tools such as nano-label-free NCs are investigated to modulate astrocytes signalling, revealing a potential as nanoscale sensors or nanoprobes in the neuronal circuit. NCs are able to affect the astroglial cells *in vitro* in an *in vivo*-like phenotype after 24h of exposition and to impact on the functional properties of differentiated astrocytes.
- 3D architectures based on semiconducting rr-P3HT interfaces, endowed with nanosized pillars on the top of the surface and endowed with responsivity to visible light are able to impact on the structural differentiation of astrocytes *in vitro,* resulting in star like phenotype and cell body elongation. The effect is supposed to be dependent on the topography rather than on the chemistry (comparing data with a flat rr-P3HT substrate). Besides, the intrinsic conductivity of the material allows the stimulation of the functional properties of astrocytes. Additionally, the intrinsic responsiveness to light represents novelty and the potential of therr-P3HT interface as photoactive elements for the modulation of cell activity sensing.

All the properties of nanoglial interfaces were considered as “glio-interfacial keys”to drive the design and development of new materials and devices and technologies to define the roleof astrocytes in brain function and to clarify the implication of astrocytes in neuropathology.

The impact and the role of astroglia keys players were investigated in organic and hybrid conductive polymers and organic semiconductor materials that provided recent advances in traditional technologies, such as long-term biocompatibility, mechanical flexibility, stiffness, functionalization, and low-cost fabrication. Instead, natural polymers result in more tuneable and dynamic mechanical properties, flexibility, in addition to intrinsic biocompatibility, biodegradability, and easy processability in different formats (i.e. flat platforms, films, hydrogels, sponges). Materials such as inorganics, metals, metal alloys, employed as semiconductors in bioelectronics devices targeting neurons, show limits in interfacing with living systems, that call for the development and detailed study in the interaction of those materials with glial cells. The first rising problem in facing such devices with brain tissues is biocompatibility. The potential material, recognized as “foreigner body”generates an uncontrollable inflammatory reaction, known as *gliosis*. Gliosis event is mediated by astrocytes and leads to the hyperproliferation of astrocytes surrounding electrodes and implants and compromise its applicability. It demonstrates, that it is obvious, astrocytes can sense material surface properties; however, the molecular mechanisms behind this observation are still unclear. We found that astrocytes sense biomaterials and nanostructured interfaces, influencing water and ion transport,the actin cytoskeleton rearrangement. In addition, we consider new insights regarding the ability of astrocytes to respond directly to electric and photonic stimuli.

In the context of this PhD thesis work, major studies are ongoing *in 3D-in vitro* models through high-resolution dynamic imaging and electrophysiology (Patch-clamp, MEA).

Future outlooks are also targeted to integrate tools, such as drugs, molecules and optical/photonic neural probes into bioelectronic and optoelectronic devices, able to selectively switch “*on* and *off*” the functionality of the astrocytes’ targets.

In conclusion “*Nanoglial Science*” could help either to define new clues in neuroscience but also might

represent a revolutionary approach in designing therapies clinical and advanced diagnostics for brain disorders (fig. 6.1).

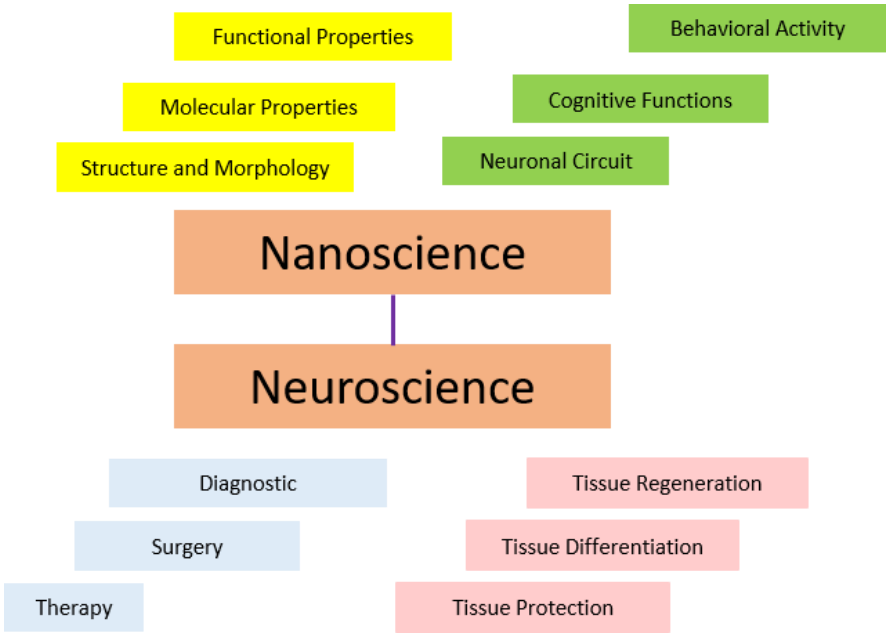


**Fig. 6.1:** Schematic illustration of the relationship between Nanoscience and Neuroscience. The emerging field of crosslinking between these two disciplines aims to improve the knowledge about brain functions at different levels and to address different questions (created by Office PowerPoint ®).

# Acknowledgments

I would like to thank my PI Valentina Benfenati, the Institutions and the Universities that collaborated and supported the work of this thesis: **first of all, the Consiglio Nazionale delle Ricerche, Istituto per la Sintesi Organica e la fotoreattività, that hosted my PhD** and other Institutes where collaborators prepared and sinthethyzed the substrate without whom this work wouldn't be possible, among them: **IPCB,** Naples**, IMM** Rome, **ISMN**, Bologna and. the University of **Bologna**, University of **Bari**, University of **Maryland**, **ARL** Laboratory of Aberdeen, the Italian Institute of Technology **IIT** in Milan.

This work was supported by the following projects- (PI Dr V. Benfenati):

- US Air Force Office of Scientific Research FA9550 16-1-0502 (AstroMat)
- US Air Force Office of Scientific Research FA9550-18-1-0255 (3D Neuroglia)
- US Air Force Office of Scientific Research FA9550-19-1-0370 (AstroDyn)
- US Air Force Office of Scientific Research FA9550-20-1-0386 (AstroLight)
- US Air Force Office of Scientific Research FA9550-17-1-0502 (AstroNir)
- US CCRL-ROP-L Neurophysiology of Cognition Army Research Laboratory W911NF-21-2-0074 (AstroGold)
- Emilia Romagna Region, POR-FESR 2014-2020 (MAT-2-REP)
- IT-ErC- DCM.AD007.085 (LINCE)

## Conflicts of interest

There are no conflicts to declare.

# References


1. Andrews AM, Weiss PS, Nano in the brain: nano-neuroscience. ACS Nano. 2012; 6(10):8463-4.

2. Kobeleva X, López-González A, Kringelbach ML, Deco G. Revealing the Relevant Spatiotemporal Scale Underlying Whole-Brain Dynamics. Front Neurosci. 2021; 15:715861.

3. Buzsaki G, Rhythm of the Brain, Oxford Scholarship 2009.

4. Shepherd, G M, Creating Modern Neuroscience: The Revolutionary 1950s. New York, NY: Oxford University Press.

5. Pampaloni NP, Giugliano M, Scaini D, Ballerini L, Rauti R, Advances in Nano Neuroscience: From Nanomaterials to Nanotools. Front Neurosci. 2019; 12:953.

6. Banati RB, Neuropathological imaging: in vivo detection of glial activation as a measure of disease and adaptive change in the brain. Br Med Bull. 2003; 65:121-31.

7. Fu R, Shen Q, Xu P, Luo JJ, Tang Y, Phagocytosis of microglia in the central nervous system diseases. Mol Neurobiol. 2014; 49(3):1422-34.

8. Miyamoto A, Wake H, Moorhouse A, Nabekura J, Microglia and synapse interactions: fine tuning neural circuits and candidate molecules. Frontiers in Cellular Neuroscience. 2013; 7:70.

9. Loane DJ, Byrnes KR, Role of microglia in neurotrauma. Neurotherapeutics. 2010; 7(4):366-77.

10. Mariani MM, Kielian T, Microglia in infectious diseases of the central nervous system. J Neuroimmune Pharmacol. 2009; 4(4):448-461.

11. Wu Y, Dissing-Olesen L, MacVicar BA, Stevens B, Microglia: Dynamic Mediators of Synapse Development and Plasticity. Trends Immunol. 2015; 36(10):605-613.

12. Chvátal A, Verkhratsky A, An Early History of Neuroglial Research: Personalities. Neuroglia. 2018; 1(1):245–81.

13. Peters A, Oligodendrocytes, their Progenitors and other Neuroglial Cells in the Aging Primate Cerebral Cortex. Cerebral Cortex. 2004; 14(9):995–1007.

14. Ransom BR, Sontheimer H. The neurophysiology of glial cells. J Clin Neurophysiol. 1992; 9(2):224-51.

15. Chi Wang IP, Kroner A, Bendszus M, Leder C, Kobsar I, Fischer S, Windle H, Nave KA, Martini R, Immune Cells Contribute to Myelin Degeneration and Axonopathic Changes in Mice Overexpressing Proteolipid Protein in Oligodendrocytes. Journal of Neuroscience. 2006; 26(31):8206–16.

16. Poskanzer KE, Molofsky AV, Dynamism of an Astrocyte In Vivo: Perspectives on Identity and Function. Annu. Rev. Physiol. 2018; 80, 143–157.

17. Maiolo L, Guarino V, Saracino E, Convertino A, Melucci M, Muccini M, Ambrosio L, Zamboni R, Benfenati V, Glial Interfaces: Advanced Materials and Devices to Uncover the Role of Astroglial Cells in Brain Function and Dysfunction. Adv Healthc Mater. 2021;10(1): e2001268.

18. Hertz L, Possible Role of Neuroglia: A Potassium-Mediated Neuronal – Neuroglial – Neuronal Impulse Transmission System. Nature 1965; 206, 1091–1094.

19. Kandel ER, Schwartz JH, Jessell TM, Principles of Neural Science, New York McGraw-Hill. 2000.

20. Reemst K, Noctor SC, Lucassen PJ, Hol EM, The Indispensable Roles of Microglia and Astrocytes during Brain Development. Front. Hum. Neurosci. 2016; 10, 15983–28.

21. Allen NJ, Astrocyte regulation of synaptic behaviour. Annu. Rev. Cell Dev. Biol. 2014; 30, 439–463.

22. Khakh BS, McCarthy KD, Astrocyte calcium signalling: from observations to functions and the challenges therein. Cold Spring Harbor Perspectives in Biology. 2015; 7, a020404.

23. Araque A, Carmignoto G, Haydon PG, Oliet SH, Robitaille R, Volterra A, Gliotransmitters travel in time and space. Neuron. 2014; 81(4):728-39.

24. Robitaille R, Volterra A, Gliotransmitters travel in time and space. Neuron. 2014; 81(4):728-39.

25. Larsen BR, Assentoft M, Cotrina ML, Hua SZ, Nedergaard M, Kaila K, Voipio J, MacAulay N, Contributions of the $Na^+/K^+$-ATPase, NKCC1, and Kir4.1 to hippocampal $K^+$ clearance and volume responses. Glia. 2014 Apr;62(4):608-22.

26. Daneman R, Prat A, The blood-brain barrier. Cold Spring Harbor Perspectives in Biology. 2015; 7, a020412.

27. Nortley R, Attwell D, Control of brain energy supply by astrocytes. Current Opinion in Neurobiology. 2017; 47, 80–85.

28. Allen NJ, Eroglu C, Cell Biology of Astrocyte-Synapse Interactions. Neuron. 2017; 96, 697–708.

29. Allen NJ, Lyons DA, Glia as Architects of Central Nervous System Formation and Function, Science. 2018; 362(6411): 181–185.

30. Buzsáki G, Draguhn A, Neuronal oscillations in cortical networks. Science. 2004; 304(5679):1926-9.

31. Chebabo SR, Hester MA, Jing J, Aitken PG, Somjen GG, Interstitial space, electrical resistance and ion concentrations during hypotonia of rat hippocampal slices. J Physiol. 1995; 487, 685-97.

32. Woo SK, Kwon MS, Geng Z, Chen Z, Ivanov A, Bhatta S, Gerzanich V, Simard JM, Sequential activation of hypoxia-inducible factor 1 and specificity protein 1 is required for hypoxia-induced transcriptional stimulation of Abcc8. J Cereb Blood Flow Metab. 2012; 32(3):525-36.

33. Simard M, Nedergaard M. The neurobiology of glia in the context of water and ion homeostasis. Neuroscience. 2004;129(4):877-96.

34. Anderson CM, Swanson RA, Astrocyte glutamate transport: review of properties, regulation, and physiological functions. Glia. 2000; 32(1):1-14.

35. Verkhratsky A, Nedergaard M, Physiology of Astroglia. Physiol Rev. 2018; 98:151. Guyton I., Hall J., Textbook of Medical Phisiology, ed. XII, 2011; Elsevier International.

36. Kofuji P, Newman EA, Potassium buffering in the central nervous system. Neurosci. 2004; 129(4):1045-56.

37. Odette LL, Newman EA, Model of Potassium Dynamics in the Central Nervous System, Glia. 1988, 1, 198.

38. Steinhäuser C, Seifert G, Bedner P, Astrocyte dysfunction in temporal lobe epilepsy: $K^+$ channels and gap junction coupling. Glia. 2012; 60(8):1192-202.

39. Hertz L, Chen Y, Importance of astrocytes for potassium ion ($K^+$) homeostasis in brain and glial effects of $K^+$ and its transporters on learning. Neurosci Biobehav Rev. 2016; 71:484-505.

40. Bellot-Saez A, Kékesi O, Morley JW, Buskila Y. Astrocytic modulation of neuronal excitability through $K^+$ spatial buffering. Neurosci Biobehav Rev. 2017; 77:87-97.

41. Walz W, Hertz L, Ouabain-sensitive and ouabain-resistant net uptake of potassium into astrocytes and neurons in primary cultures. J Neurochem. 1982; 39(1):70-7.

42. Li L, Lundkvist A, Andersson D, Wilhelmsson U, Nagai N, Pardo AC, Nodin C, Stahlberg A, Aprico K, Larsson K, Yabe T, Moons L, Fotheringham A, Davies I, Carmeliet P, Schwartz JP, Pekna M, Kubista M, Blomstrand F, Maragakis N, Nilsson M, Pekny Ml Protective role of reactive astrocytes in brain ischemia. J Cereb Blood Flow Metab. 2008; 8:468–481.

43. Levitt P, Rakic Pl Immunoperoxidase localization of glial fibrillary acidic protein in radial glial cells and astrocytes of the developing rhesus monkey brain. J Comp Neurol. 1980; 193:815–840.

44. Lim MC, Maubach G, Zhuo L, Glial fibrillary acidic protein splice variants in hepatic stellate cells–expression and regulation. Mol Cells. 2008; 25:376–384 125.

45. Lin JH, Lou N, Kang N, Takano T, Hu F, Han X, Xu Q, Lovatt D, Torres A, Willecke K, Yang J, Kang J, Nedergaard M, A central role of connexin 43 in hypoxic preconditioning. J Neurosci. 2008; 28:681–695.

46. Liu X, Bolteus AJ, Balkin DM, Henschel O, Bordey A, GFAP-expressing cells in the postnatal subventricular zone display a unique glial phenotype intermediate between radial glia and astrocytes. Glia 2006; 54:394–410.

47. Lutz SE, Zhao Y, Gulinello M, Lee SC, Raine CS, Brosnan CF, Deletion of astrocyte connexins 43 and 30 leads to a dysmyelinating phenotype and hippocampal CA1 vacuolation. J Neurosci. 2009; 29:7743–7752.

48. Maginnis MS, Atwood WJ JC virus: an oncogenic virus in animals and humans? Semin Cancer Biol 2009; 19:261–269.

49. Magnus T, Carmen J, Deleon J, Xue H, Pardo AC, Lepore AC, Mattson MP, Rao MS, Maragakis NJ, Adult glial precursor proliferation in mutant SOD1G93A mice. Glia 2008; 56:200–208.

50. Malatesta P, Hack MA, Hartfuss E, Kettenmann H, Klinkert W, Kirchhoff F, Gotz M, Neuronal or glial progeny: Regional differences in radial glia fate. Neuron. 2003; 37:751–764.

51. Manley GT, Fujimura M, Ma T, Noshita N, Filiz F, Bollen AW, Chan P, Verkman AS, Aquaporin-4 deletion in mice reduces brain edema after acute water intoxication and ischemic stroke. Nat Med. 2000; 6:159–163.

52. Parkerson KA, Sontheimer H, Biophysical and pharmacological characterization of hypotonically activated chloride currents in cortical astrocytes. Glia. 2004; 46(4):419-436.

53. Oberheim NA, Takano T, Han X, He W, Lin JH, Wang F, Xu Q, Wyatt JD, Pilcher W, Ojemann JG, Ransom BR, Goldman SA, Nedergaard M. Uniquely hominid features of adult human astrocytes. J Neurosci. 2009; 29:3276–3287.

54. Occhipinti R, Somersalo E, Calvetti D, Astrocytes as the glucose shunt for glutamatergic neurons at high activity: an in silico study. J Neurophysiol. 2009; 101:2528–2538.

55. Ogata K, Kosaka T, Structural and quantitative analysis of astrocytes in the mouse hippocampus. Neurosci. 2002; 113:221–233.

56. Ohab JJ, Fleming S, Blesch A, Carmichael ST, A neurovascular niche for neurogenesis after stroke. J Neurosci. 2006; 26:13007–13016.

57. Oide T, Yoshida K, Kaneko K, Ohta M, Arima K, Iron overload and antioxidative role of perivascular astrocytes in aceruloplasminemia. Neuropathol Appl Neurobiol, 2006; 32:170–176.

58. Okada S, Nakamura M, Katoh H, Miyao T, Shimazaki T, Ishii K, Yamane J, Yoshimura A, Iwamoto Y, Toyama Y, Okano H, Conditional ablation of Stat3 or Socs3 discloses a dual role for reactive astrocytes after spinal cord injury. Nature Med. 2006; 12:829–834.

59. Omary MB, Lugea A, Lowe AW, Pandol SJ, The pancreatic stellate cell: a star on the rise in pancreatic diseases. J Clin Invest. 2007; 117:50–59.

60. Papadopoulos MC, Manley GT, Krishna S, Verkman AS, Aquaporin-4 facilitates reabsorption of excess fluid in vasogenic brain edema. FASEB J. 2004; 18:1291–1293.

61. Formaggio F, Saracino E, Mola MG, Rao SB, Amiry-Moghaddam M, Muccini M, Zamboni R, Nicchia GP, Caprini M, Benfenati V, LRRC8A is essential for swelling-activated chloride current and for regulatory volume decrease in astrocytes, FASEB J. 2018; 33, 1.

62. Borrachero-Conejo AI, Adams WR, E. Saracino E, Mola MG, Wang M, Posati T, Formaggio F, De Belli M, Frigeri F, Caprini M, Hutchinson M, Muccini M, Zamboni R, Nicchia GP, Mahadevan-Jansen A, Benfenati V, Stimulation of water and calcium dynamics in astrocytes with pulsed infrared light, FASEB J. 2020; 34, 6539.

63. Oberheim NA, Tian GF, Han X, Peng W, Takano T, Ransom B, Nedergaard M. Loss of astrocytic domain organisation in the epileptic brain. J Neurosci 2008; 28:3264–3276.

64. Maragakis NJ, Rothstein JD Mechanisms of Disease: astrocytes in neurodegenerative disease. Nat Clin Pract Neurol. 2006: 2:679–689.

65. Matute C, Melone M, Vallejo-Illarramendi A, Conti F, Increased expression of the astrocytic glutamate transporter GLT-1 in the prefrontal cortex of schizophrenics. Glia, 2005; 49:451–455.

66. Merkle FT, Tramontin AD, García-Verdugo JM, Alvarez-Buylla A, A Radial glia gives rise to adult neural stem cells in the subventricular zone. Proc Natl Acad Sci USA. 2004; 101:17528–17532.

67. Messing A, Head MW, Galles K, Galbreath EJ, Goldman JE, Brenner M, Fatal encephalopathy with astrocyte inclusions in GFAP transgenic mice. Am J Pathol. 1998; 152:391–398.

68. Meyer EM, St Onge E, Crews FT, Effects of ageing on rat cortical presynaptic cholinergic processes. Neurobiol Aging. 1984; 5:315–317.

69. Miguel-Hidalgo JJ, The role of glial cells in drug abuse. Curr Drug Abuse Rev. 2009; 2:72–82.

70. Miguel-Hidalgo JJ, Baucom C, Dilley G, Overholser JC, Meltzer HY, Stockmeier CA, Rajkowska G, Glial fibrillary acidic protein immunoreactivity in the prefrontal cortex distinguishes younger from older adults in major depressive disorder. Biol Psychiatry. 2000; 48:861–873.

71. Milligan ED, Watkins LR, Pathological and protective roles of glia in chronic pain. Nat Rev Neurosci. 2009; 10:23–36.

72. Gu C , KIR4.1: K+ Channel Illusion or Reality in the Autoimmune Pathogenesis of Multiple Sclerosis. Frontiers in Molecular Neurosci. 2016; 9.

73. Min KJ, Yang MS, Kim SU, Jou I, Joe EH, Astrocytes induce heme oxygenase-1 expression in microglia: a feasible mechanism for preventing excessive brain inflammation. J Neurosci. 2006; 26:1880–1887.

74. Mirza B, Hadberg H, Thomsen P, Moos T, The absence of reactive astrocytosis is indicative of a unique inflammatory process in Parkinson's disease. Neurosci. 2000; 95:425–432.

75. Mischel PS, Nguyen LP, Vinters HV, Cerebral cortical dysplasia associated with paediatric epilepsy Review of neuropathologic features and proposal for a grading system. J Neuropathol Exp Neurol. 1995; 54:137–153.

76. Mitterauer B, Nonfunctional glial proteins in tripartite synapses: a pathophysiological model of schizophrenia. Neuroscientist. 2005; 11:192–198.

77. Messing A, Head MW, Galles K, Galbreath EJ, Goldman JE, Brenner M, Fatal encephalopathy with astrocyte inclusions in GFAP transgenic mice. Am J Pathol. 1998; 152:391–398.

78. Meyer EM, St.Onge E, Crews FT, Effects of ageing on rat cortical presynaptic cholinergic processes. Neurobiol Aging. 1984; 5:315–317.

79. Morest DK, Silver J. Precursors of neurons, neuroglia, and ependymal cells in the CNS: what are they? Where are they from? How do they get where they are going? Glia. 2003; 43:6–18.

80. Nag S, Manias JL, Stewart DJ Pathology and new players in the pathogenesis of brain edema. Acta Neuropathol. 2009; 118:197– 217.

81. Oberheim NA, Tian GF, Han X, Peng W, Takano T, Ransom B, Nedergaard M, Loss of astrocytic domain organisation in the epileptic brain. J Neurosci. 2008; 28:3264–3276.

82. Mackie EJ, Neufeld EB, Patel RC, Brady RO, Patel YC, Pentchev PG, Ong WY, Localization of Niemann-Pick C1 protein in astrocytes: implications for neuronal degeneration in Niemann- Pick typeC disease. Proc Natl Acad Sci USA. 1999; 96:1657–1662.

83. Pekny M, Pekna M, Astrocyte intermediate filaments in CNS pathologies and regeneration. J Pathol. 2004; 204:428–437.

84. Pekny M, Leveen P, Pekna M, Eliasson C, Berthold CH, Westermark B, Betsholtz C, Mice lacking glial fibrillary acidic protein display astrocytes devoid of intermediate filaments but develop and reproduce normally. EMBO J. 1995; 4:1590–1598.

85. Pellerin L, Bouzier-Sore AK, Aubert A, Serres S, Merle M, Costalat R, Magistretti PJ, Activity-dependent regulation of energy metabolism by astrocytes: an update. Glia. 2007; 55:1251–1262.

86. de Bellis M, Cibelli A, Mola MG, Pisani F, Barile B, Mastrodonato M, Banitalebi S, Amiry-Moghaddam M, Abbrescia P, Frigeri A, Svelto M, Nicchia GP, Orthogonal arrays of particle assembly are essential for normal aquaporin-4 expression level in the brain. Glia. 2021; 69(2):473-488.

87. Jin BJ, Rossi A., Verkman A. S Model of Aquaporin-4 Supramolecular Assembly in Orthogonal Arrays Based on Heterotetrameric Association of M1-M23 Isoforms Biophy. J, Elsevier Enhanced Reader. 2011; 2936-2945.

88. Posati T, Pistone A, Saracino E, Formaggio F, Mola MG, Troni E, Sagnella A, Nocchetti M, Barbalinardo M, Valle F, Bonetti S, Caprini M, Nicchia GP, Zamboni R, Muccini M, Benfenati V, A Nanoscale Interface Promoting Molecular and Functional Differentiation of Neural Cells. Sci Rep. 2016; 6(1) :31226.

89. Olson JE, Fleischhacker D, Murray WB, Holtzman D, Control of astrocyte volume by intracellular and extracellular $Ca^{2+}$. Glia. 1990;3(5):405-12.

90. Parkerson KA, Sontheimer H, Biophysical and pharmacological characterization of hypotonically activated chloride currents in cortical astrocytes. Glia. 2004;46(4):419-436.

91. Benfenati V, Nicchia GP, Svelto M, Rapisarda C, Frigeri A, Ferroni S, Functional down-regulation of volume-regulated anion channels in AQP4 knockdown cultured rat cortical astrocytes. J Neurochem. 2007;100(1):87-104.

92. Mola MG, Saracino E, Formaggio F, Amerotti AG, Barile B, Posati T, Cibelli A, Frigeri A, Palazzo C, Zamboni R, Caprini M, Nicchia GP, Benfenati V, Cell Volume Regulation Mechanisms in Differentiated Astrocytes. Cell Physiol Biochem. 2021; 55(S1):196–212.

93. Formaggio F, Saracino E, Mola MG, Rao SB, Amiry-Moghaddam M, Muccini M, Zamboni R, Nicchia GP, Caprini M, Benfenati V, LRRC8A is essential for swelling-activated chloride current and for regulatory volume decrease in astrocytes, FASEB. 2018; 33, 1.

94. Rao KV, Panickar KS, Jayakumar AR, Norenberg Astrocytes protect neurons from ammonia toxicity. Neurochem Res. 2005; 30:1311–1318.

95. Rajkowska G, Miguel-Hidalgo JJ, Gliogenesis and glial pathology in depression. CNS Neurol Disord Drug Targets. 2007; 6:219–233.

96. Rajkowska G, Miguel-Hidalgo JJ, Makkos Z, Meltzer H, Overholser J, Stockmeier C, Layer-specific reductions in GFAP-reactive astroglia in the dorsolateral prefrontal cortex in schizophrenia. Schizophr Res. 2002; 57:127–138.

97. Rossi DJ, Brady JD, Mohr C, Astrocyte metabolism and signalling during brain ischemia. Nat Neurosci. 2007; 10:1377–1386.

98. Budara V, Retamal M, Del Rio R, Orellana J, Synaptic Functions of Hemichannels and Pannexons: A Double-Edged Sword. Frontiers in Molecular Neurosci. 2018; 11.

99. Santello M, Calì C, Bezzi P, Gliotransmission and the tripartite synapse. Adv Exp Med Biol. 2012; 970:307-31.

100. Perea G, Navarrete M, Araque A, Tripartite synapses: astrocytes process and control synaptic information. Trends Neurosci. 2009; 32(8):421-31.

101. Araque A, Parpura V, Sanzgiri RP, Haydon PG, Tripartite synapses: glia, the unacknowledged partner. Trends Neurosci. 1999; 22(5):208-15.

102. Egawa K, Yamada J, Furukawa T, Yanagawa Y, Fukuda A, $Cl^-$ homeodynamics in gap junction-coupled astrocytic networks on activation of GABAergic synapses. J Physiol. 2013; 591(16):3901-17.

103. Buzsáki G, Draguhn A, Neuronal oscillations in cortical networks. Science. 2004; 304(5679):1926-9.

104. Engel AK, Fries P, Singer W. Dynamic predictions: oscillations and synchrony in top-down processing. Nat Rev Neurosci. 2001; 2(10):704-16.

105. Steriade M, Impact of network activities on neuronal properties in corticothalamic systems. J Neurophysiol. 2001; 86(1):1-39. Klimesch W. EEG alpha and theta oscillations reflect cognitive and memory performance: a review and analysis. Brain Res Brain Res Rev. 1999; 29(2-3):169-95.

106. Klimesch W, EEG alpha and theta oscillations reflect cognitive and memory performance: a review and analysis. Brain Res Brain Res Rev. 1999; 29(2-3):169-95.

107. Nowack WJ, Neocortical Dynamics and Human EEG Rhythms Neurology 1995; 1793-1793.

108. Steriade M, Timofeev I, Neuronal plasticity in thalamocortical networks during sleep and waking oscillations. Neuron. 2003; 37(4):563-76.

109. Klimesch W, EEG alpha and theta oscillations reflect cognitive and memory performance: a review and analysis. Brain Res Brain Res Rev. 1999; 29(2-3):169-95.

110. Fellin T, Pascual O, Gobbo S, Pozzan T, Haydon PG, Carmignoto G, Neuronal synchrony mediated by astrocytic glutamate through activation of extrasynaptic NMDA receptors. Neuron. 2004; 43(5):729-43.

111. Spray, ES, D, Extracellular $K^+$ and Astrocyte Signalling via Connexin and Pannexin Channels. Neurochem Res., 2012; 37, 2310–2316.

112. Buskila, Y, Crowe SE, Ellis-Davies GCR, Synaptic deficits in layer 5 neurons precede overt structural decay in 5xFAD mice, Neuroscie. 2013; 254, 152–159.

113. David Y, Cacheaux LP, Ivens S, Lapilover E, Heinemann U, Kaufer D, Friedman A, Astrocytic dysfunction in epileptogenesis: consequence of altered potassium and glutamate homeostasis? J Neurosci. 2009; 29(34):10588-99.

114. Leis Ja, Bekar L K & Walz W, Potassium homeostasis in the ischemic brain. Glia. 2005; 50, 407–16.

115. Bazhenov M, Timofeev I, Steriade M, Sejnowski TJ, Potassium Model for Slow (2–3 Hz) In Vivo Neocortical Paroxysmal Oscillations. J Neurophysiol. 2004; 1116–1132.

116. Fröhlich F, Bazhenov M, Timofeev I., Steriade M, Sejnowski TJ, Slow state transitions of sustained neural oscillations by activity-dependent modulation of intrinsic excitability. J. Neurosci, 2006; 26, 6153–62.

117. Ding F, O'Donnell J, Xu Q, Kang N, Goldman N, Nedergaard M, Changes in the composition of brain interstitial ions control the sleep-wake cycle. Science. 2016; 352(6285):550-5.

118. Bellot-Saez A, Cohen G, van Schaik A, Ooi L, W Morley J, Buskila Y, Astrocytic modulation of cortical oscillations. Sci Rep. 2018; 8(1):11565.

119. Jackson FR, You S, Crowe LB, Regulation of rhythmic behaviours by astrocytes. Wiley Interdiscip Rev Dev Biol. 2020; 9(4): e372.

120. Lines J, Martin ED, Kofuji P, Aguilar J, Araque A, Astrocytes modulate sensory-evoked neuronal network activity. Nat Commun. 2020;11(1):3689.

121. Sardinha VM, Guerra-Gomes S, Caetano I, Tavares G, Martins M, Reis JS, Correia JS, Teixeira-Castro A, Pinto L, Sousa N, Oliveira JF, Astrocytic signaling supports hippocampal-prefrontal theta synchronization and cognitive function. Glia, 2017; 65(12):1944-1960.

122. Zerr DM, Hall JC, Rosbash M, Siwicki KK, Circadian fluctuations of period protein immunoreactivity in the CNS and the visual system of Drosophila. J Neurosci.1990; 10(8):2749-62.

123. Patel DC, Tewari BP, Chaunsali L, Sontheimer H, Neuron-glia interactions in the pathophysiology of epilepsy. Nat Rev. Neurosci. 2019; 20(5):282-297.

124. Edell DJ, Toi VV, McNeil VM, Clark LD, Factors influencing the biocompatibility of insertable silicon microshafts in the cerebral cortex. IEEE Trans Biomed Eng. 1992; 39(6):635-43.

125. Salatino JW, Ludwig KA, Kozai TDY, Purcell EK, Glial responses to implanted electrodes in the brain. Nat Biomed Eng. 2017; 1(11):862-877.

126. Chvátal A, Anderová M, Neprasová H, Prajerová I, Benesová J, Butenko O, Verkhratsky A, Pathological potential of astroglia. Physiol Res. 2008; 57.

127. Ji RR, Berta T, Nedergaard M. Glia and pain: is chronic pain a gliopathy? Pain. 2013;154.

128. Borbély É, Payrits M, Hunyady Á, Mező G, Pintér E, Important regulatory function of transient receptor potential ankyrin 1 receptors in age-related learning and memory alterations of mice. Geroscience. 2019; 41(5):643-654.

129. Seifert G, Schilling K, Steinhäuser C, Astrocyte dysfunction in neurological disorders: a molecular perspective. Nat Rev Neurosci. 2006; 7(3):194-206.

130. Kozai TD, Eles JR, Vazquez AL, Cui XT, Two-photon imaging of chronically implanted neural electrodes: Sealing methods and new insights. J Neurosci Methods. 2016; 258:46-55.

131. Zhong Y, Bellamkonda RV, Dexamethasone-coated neural probes elicit attenuated inflammatory response and neuronal loss compared to uncoated neural probes. Brain Res. 2007;7; 1148:15-27.

132. Pekny M, Pekna M, Astrocyte reactivity and reactive astrogliosis: costs and benefits. Physiol Rev. 2014; 94(4):1077-98.

133. Wilhelmsson U, Bushong EA, Price DL, Smarr BL, Phung V, Terada M, Ellisman MH, Pekny M, Redefining the concept of reactive astrocytes as cells that remain within their unique domains upon reaction to injury. Proc Natl Acad Sci USA 2006; 103: 17513–17518.

134. Puschmann TB, Zanden C, De Pablo Y, Kirchhoff F, Pekna M, Liu J, Pekny M, Bioactive 3D cell culture system minimises cellular stress and maintains the in vivo-like morphological complexity of astroglial cells. Glia, 2013; 61: 432–440.

135. Jung JS, Bhat RV, Preston GM, Guggino WB, Baraban JM, Agre P, Molecular characterization of an aquaporin cDNA from brain: candidate osmoreceptor and regulator of water balance. Proc Natl Acad Sci USA. 1994; 91:13052–13056.

136. Pisani F, Simone L, Mola MG, De Bellis M, Frigeri A, Nicchia GP, Svelto M, Regulation of aquaporin-4 expression in the central nervous system investigated using M23-AQP4 null mouse. Glia. 202; 69(9):2235-2251.1.

137. Stokum JA, Kurland DB, Gerzanich V, Simard JM, Mechanisms of Astrocyte-Mediated Cerebral Edema. Neurochem Res. 2015; 40(2):317–28.

138. Zurolo E, de Groot M, Iyer A, Anink J, van Vliet EA, Heimans JJ, Reijneveld JC, Gorter JA, Aronica E, Regulation of Kir4.1 expression in astrocytes and astrocytic tumors: a role for interleukin-1 β. J Neuroinflammation. 2012; 9:280.

139. Bockenhauer D, Feather S, Stanescu HC, Bandulik S, Zdebik AA, Reichold M, Tobin J, Lieberer E, Sterner C, Landoure G, Arora R, Sirimanna T, Thompson D, Cross JH, van't Hoff W, Al Masri O, Tullus K, Yeung S, Anikster Y, Klootwijk E, Hubank M, Dillon MJ, Heitzmann D, Arcos-Burgos M, Knepper MA, Dobbie A, Gahl WA, Warth R, Sheridan E, Kleta R, Epilepsy, ataxia, sensorineural deafness, tubulopathy, and KCNJ10 mutations. N Engl J Med. 2009; 360(19):1960-70.

140. Pan JW, Kuzniecky RI, Utility of magnetic resonance spectroscopic imaging for human epilepsy. Quant Imaging Med Surg. 2015; 5(2):313-322.

141. Coulter DA, Steinhauser C, Role of Astrocytes in Epilepsy. Cold Spring Harbor Perspectives in Medicine. 2015; 5(3): a022434–a022434.

142. Louis DN, Ohgaki H, Wiestler OD, Cavenee WK, Burger PC, Jouvet A, Scheithauer BW, Kleihues P. The 2007 WHO classification of tumours of the central nervous system. Acta Neuropathol. 2007; 114(2):97-109.

143. O'Brien ER, Howarth C, Sibson NR, The role of astrocytes in CNS tumours: pre-clinical models and novel imaging approaches. Front Cell Neurosci. 2013; 7:40.

144. Roslin M, Henriksson R, Bergström P, Ungerstedt U, Bergenheim AT, Baseline levels of glucose metabolites, glutamate and glycerol in malignant glioma assessed by stereotactic microdialysis. J Neurooncol. 2003; 61(2):151-60.

145. Zamanian JL, Xu L, Foo LC, Nouri N, Zhou L, Giffard RG, Barres BA, Genomic analysis of reactive astrogliosis. J Neurosci. 2012; 32(18):6391-410.

146. Brandao M, Simon T, Critchley G, Giamas G, Astrocytes, the rising stars of the glioblastoma microenvironment. Glia. 2019; 67(5):779–90.

147. Turner KL, Sontheimer H, $Cl^-$ and $K^+$ channels and their role in primary brain tumour biology. Philos Trans R Soc Lond B Biol Sci. 2014; 369(1638):20130095.

148. Sontheimer H, An unexpected role for ion channels in brain tumor metastasis. Exp Biol Med (Maywood). 2008; 233(7):779-91.

149. Simone L, Pisani F, Mola MG, De Bellis M, Merla G, Micale L, Frigeri A, Vescovi AL, Svelto M, Nicchia GP, AQP4 Aggregation State Is a Determinant for Glioma Cell Fate. Cancer Res. 2019; 1;79(9):2182-2194.

150. Umans RA, Sontheimer H, Combating malignant astrocytes: Strategies mitigating tumor invasion. Neurosci Res. 2018; 126:22-30.

151. Christopherson KS, Ullian EM, Stokes CC, Mullowney CE, Hell, JW, Agah A, Barres BA, Thrombospondins are astrocyte-secreted proteins that promote CNS synaptogenesis. Cell, 2005; 120(3), 421–433.

152. Guttenplan KA, Liddelow SA, Astrocytes and microglia: Models and tools. Journal of Experimental Medicine, 2019; 216(1), 71–83.

153. Slezak M, Goritz C, Niemiec A, Frisen J, Chambon P, Metzger D, Pfrieger FW, Transgenic mice for conditional gene manipulation in astroglial cells. Glia. 2007; 55(15), 1565–1576.

154. Deverman BE, Ravina BM, Bankiewicz KS, Paul SM, Sah DWY, Gene therapy for neurological disorders: Progress and prospects. Nature Reviews Drug Discovery. 2018; 17, 641–659.

155. Drouet V, Perrin V, Hassig R, Dufour N, Auregan G, Alves S, Deglon N, Sustained effects of non allele specific Huntingtin silencing. Annals of Neurology. 2009; 65(3), 276–285.

156. Mazuel L, Blanc J, Repond C, Bouchaud V, Raffard G, Deglon N, Bouzier-Sore AK, A neuronal MCT2 knockdown in the rat somatosensory cortex reduces both the NMR lactate signal and the BOLD response during whisker stimulation. PLoS One. 12(4), e0174990.

157. Toro Cabrera G, Mueller C, Design of shRNA and miRNA for delivery to the CNS. Methods in Molecular Biology. 2016; 1(382), 67–80.

158. Reeves AM, Shigetomi E, Khakh BS, Bulk loading of calcium indicator dyes to study astrocyte physiology: key limitations and improvements using morphological maps. J Neurosci. 2011; 31(25):9353-9358.

159. Knöpfel T, Genetically encoded optical indicators for the analysis of neuronal circuits. Nat Rev Neurosci. 2012; 13(10):687-700.

160. Fenno L, Yizhar O, Deisseroth K, The development and application of optogenetics. Annual Review of Neurosci, 2011; 34, 389–412.

161. Okada Y, Sasaki T, Oku Y, Takahashi N, Seki M, Ujita S, Ikegaya Y, Preinspiratory calcium rises in putative pre-Botzinger complex astrocytes. J. of Physiol. 2012; 590(19), 4933–4944.

162. Pelluru D, Konadhode RR, Bhat NR, Shiromani PJ, Optogenetic stimulation of astrocytes in the posterior hypothalamus increases sleep at night in C57BL/6J mice. European J. of Neuroscie. 2016; 43(10), 1298–1306.

163. Perea G, Yang A, Boyden ES, Sur M, Optogenetic astrocyte activation modulates response selectivity of visual cortex neurons in vivo. Nature Communications. 2014, 5, 3262.

164. Sasaki T, Beppu K, Tanaka, KF, Fukazawa Y, Shigemoto R, Matsui K, Application of an optogenetic byway for perturbing neuronal activity via glial photostimulation. Proceedings of the National Academy of Sciences of the United States of America, 2012, 109(50), 20720–20725.

165. Sweeney P, Qi Y, Xu Z, Yang Y, Activation of hypothalamic astrocytes suppresses feeding without altering emotional sstates. Glia. 2016; 64(12), 263–2273.

166. Yamashita A, Hamada, A, Suhara, Y, Kawabe, R., Yanase, M., Kuzumaki, N, Okano, H, Astrocytic activation in the anterior cingulate cortex is critical for sleep disorder under neuropathic pain. Synapse. 2014; 68(6), 235–247.

167. Gourine AV, Kasymov V, Marina, N Tang, Figueiredo MF, Lane S, Kasparov S, Astrocytes control breathing through pH-dependent release of ATP. Science. 2010; 329(5991), 571–575.

168. Gradinaru V, Mogri M, Thompson KR, Henderson JM, Deisseroth K, Optical deconstruction of parkinsonian neural circuitry. Science. 2009; 24(5925), 354–359.

169. Poskanzer KE, Yuste R, Astrocytes regulate cortical state switching in vivo. Proceedings of the National Academy of Sciences of USA. 2016; 113(19), 2675–2684.

170. Hirbec H, Déglon N, Foo LC, Goshen I, Grutzendler J, Hangen E, Kreisel T, Linck N, Muffat J, Regio S, Rion S, Escartin C, Emerging technologies to study glial cells. Glia. 2020; 68(9):1692-1728.

171. Renz A F, Reichmuth A M, Stauffer F, Thompson-Steckel G, Vörös J, A guide towards long-term functional electrodes interfacing neuronal tissue. J Neural Eng. 2018; 15(6).

172. Fattahi G, Yang G, Kim MR, Abidian A, Review of Organic and Inorganic Biomaterials for Neural Interfaces Adv. Mater. 2014; 26, 1846.

173. S. Bonetti, A. Pistone, M. Brucale, S. Karges, L. Favaretto, M. Zambianchi, T. Posati, A. Sagnella, M. Caprini, S. Toffanin, Zamboni R, Camaioni N, Muccini M, Melucci M, Benfenati V, A Lysinated Thiophene-Based Semiconductor as a Multifunctional Neural Bioorganic Interface, Adv. Healthc. Mater. 2015; 4, 1190.

174. S. Bonetti, M. Prosa, A. Pistone, L. Favaretto, A. Sagnella, I. Grisin, M. Zambianchi, S. Karges, A. Lorenzoni, T. Posati, Zamboni R, Camaioni N, Mercuri F, Melucci M, Benfenati V, A self-assembled lysinated perylene diimide film as a multifunctional material for neural interfacing, J. Mater. Chem. B 2016; 4, 2921.

175. Dodla MC, Bellamkonda RV, Differences between the effect of anisotropic and isotropic laminin and nerve growth factor presenting scaffolds on nerve regeneration across long peripheral nerve gaps. Biomaterials. 2008; 29, 33.Y.

176. Zhong Y, Bellamkonda RV, Dexamethasone-coated neural probes elicit attenuated inflammatory response and neuronal loss compared to uncoated neural probes. Brain Res. 2007; 1148, 15.

177. Hai A, Shappir J, Spira ME, In-cell recordings by extracellular microelectrodes. Nat Methods. 2010; 7(3):200-2.

178. Alivisatos AP, Chun M, Church GM, Greenspan RJ, Roukes ML, Yuste R, The brain activity map project and the challenge of functional connectomics. Neuron. 2012; 74(6):970-4.

179. Bekyarova E, Ni Y, Malarkey EB, Montana V, McWilliams JL, Haddon RC, Parpura V, Applications of Carbon Nanotubes in Biotechnology and Biomedicine. J Biomed Nanotechnol. 2005 Mar 1;1(1):3-17.

180. de Boer AG, Gaillard PJ, Drug targeting to the brain. Annu Rev Pharmacol Toxicol. 2007; 47:323-55.

181. Saraiva C, Praça C, Ferreira R, Santos T, Ferreira L, Bernardino L, Nanoparticle-mediated brain drug delivery: Overcoming blood-brain barrier to treat neurodegenerative diseases. J Control Release. 2016; 235:34-47.

182. Taniguchi N, "On the basic concept of 'nano-technology'", presented at Proc. Int. Conf. Prod. Eng. Tokyo, Part II, Tokyo, 1974.

183. Maurer N, Fenske DB, Cullis PR, Developments in liposomal drug delivery systems, Expert Opin. Biol. Th 2001; 1, 923.

184. Spillane J, Kullmann DM, Hanna MG, Genetic neurological channelopathies: molecular genetics and clinical phenotypes. J Neurol Neurosurg Psychiatry. 2016; 87(1):37-48.

185. Kim JB, Channelopathies. Korean J Pediatr. 2014; 57(1):1-18.

186. Seymour JP, Wu F, Wise KD, Yoon E, State-of-the-art MEMS and microsystem tools for brain research Microsys. Nanoeng 2017; 3, 16066.

187. Huang H, Delikanli S, Zeng H, Ferkey DM, Pralle A, Remote control of ion channels and neurons through magnetic-field heating of nanoparticles. Nat Nanotechnol. 2010; 5(8):602-6.

188. Kumar A, Tan A, Wong J, Spagnoli JC, Lam J, Blevins BD, G N, Thorne L, Ashkan K, Xie J, Liu H., Nanotechnology for Neuroscience: Promising Approaches for Diagnostics, Therapeutics and Brain Activity Mapping. Adv Funct Mater. 2017; 27(39):1700489.

189. Chevrier DM, Chatt A, Zhang, Properties and Applications of Protein-Stabilized Fluorescent Gold Nanoclusters: Short Review. J. Nanophotonics, 2012; 6.

190. Venkatesh, V, Shukla A, Sivakumar S, Verma S, Purine Stabilized Green Fluorescent Gold Nanoclusters for Cell Nuclei Imaging Applications. ACS Appl. Mater. Interfaces. 2014; 6, 3, 2185–2191.

191. Sivakumar, S.; Verma, S, Purine Stabilized Green Fluorescent Gold Nanoclusters for Cell Nuclei Imaging Applications. ACS Appl. Mater. Interfaces 2014; 6, 2185−2191.

192. West AL, Griep MH, Cole DP, Karna SP, DNase 1 Retains Endodeoxyribonuclease Activity Following Gold Nanocluster Synthesis. Anal. Chem. 2014; 86, 7377−7382.

193. Su MN, Ye J, Li QW, Li SH, Ge W, Chen X, Jiang H, Wang XM, Novel in situ Biosynthesized Fluorescent Zinc Nanoclusters for Specific Cellular Bio-Imaging. Chin. Chem. Lett. 2015; 26, 1400.

194. Wang, JL, Zhang, G, Li, QW, Jiang H, Liu CY, Amatore C, Wang XM, in vivo Self-Bio-Imaging of Tumors Through in situ Biosynthesized Fluorescent Gold Nanoclusters. Sci. Rep. 2013; 3.

195. Gao, S. P.; Chen, D. H.; Li, Q. W.; Ye, J.; Jiang, H.; Amatore, C.; Wang, X. M. Near-Infrared Fluorescence Imaging of Cancer Cells and Tumors Through Specific Biosynthesis of Silver Nanoclusters. Sci. Rep. 2014, 4.

196. Chen D, Zhao C, Ye J, Li Q, Liu X, Su M, Jiang H, Amatore C, Selke M, Wang X, In Situ Biosynthesis of Fluorescent Platinum Nanoclusters: Toward Self-Bioimaging-Guided Cancer Theranostics. ACS Appl. Mater. Interfaces. 2015; 7, 18163−18169.

197. West AL, Schaeublin NM, Griep MH, Maurer-Gardner EI, Cole DP, Fakner AM, Hussain SM, Karna SP, In situ Synthesis of Fluorescent Gold Nanoclusters by Nontumorigenic Microglial Cells. ACS Appl Mater Interfaces. 2016; 8(33):21221.

198. Agans RT, Dymond CE, Jimenez RE, Bunce NJ, Perry KJ, Salisbury RL, Hussain SM, Gupta RK, Karna SP Human Nontumorigenic Microglia Synthesize Strongly Fluorescent Au/Fe Nanoclusters, Retaining Bioavailability. ACS Omega. 2020; 5(33):20983-20990.

199. Nagelhus EA, Mathiisen TM, Ottersen OP, Aquaporin-4 in the central nervous system: cellular and subcellular distribution and coexpression with KIR4.1. Neurosci. 2004;129(4):905-13.

200. Amiry-Moghaddam M, Ottersen OP, The molecular basis of water transport in the brain. Nat Rev Neurosci. 2003; 4(12):991-1001.

201. Green R, Abidian MR, Conducting Polymers for Neural Prosthetic and Neural Interface Applications. Adv Mater. 2015; 27(46):7620-37.

202. Cellot G, Lagonegro P, Tarabella G, Scaini D, Fabbri F, Iannotta S, Prato M, Salviati G, Ballerini L, PEDOT:PSS Interfaces Support the Development of Neuronal Synaptic Networks with Reduced Neuroglia Response In vitro. Front Neurosci. 2016; 9:521.
203. Prasad A, Sanchez JC, Quantifying long-term microelectrode array functionality using chronic in vivo impedance testing. J Neural Eng. 2012 Apr;9(2):026028.

204. Ghezzi D, Antognazza MR, Dal Maschio M, Lanzarini E, Benfenati F, Lanzani G, A hybrid bioorganic interface for neuronal photoactivation. Nat Commun. 2011; 2:166.

205. Maya-Vetencourt JF, Ghezzi D, Antognazza MR, Colombo E, Mete M, Feyen P, Desii A, Buschiazzo A, Di Paolo M, Di Marco S, Ticconi F, Emionite L, Shmal D, Marini C, Donelli I, Freddi G, Maccarone R, Bisti S, Sambuceti G, Pertile G, Lanzani G, Benfenati F, A fully organic retinal prosthesis restores vision in a rat model of degenerative blindness. Nat Mater. 2017;16(6):681-689.

206. Antognazza MR, Di Paolo M, Ghezzi D, Mete M, Di Marco S. Maya-Vetencourt JF, R. Maccarone R, Desii A, Di Fonzo F, Bramini M, Russo A, Laudato L, Donelli I, Cilli M, Freddi G, Pertile G, Lanzani G, Bisti S, Benfenati F, aracterization of a Polymer-Based, Fully Organic Prosthesis for Implantation into the Subretinal Space of the Rat. Adv. Healthcare Mater. 2016; 5, 2271.

207. Benfenati V, Martino N, Antognazza MR, Pistone A, Toffanin S, Ferroni S, Lanzani, G Muccini M, Photostimulation of Whole-Cell Conductance in Primary Rat Neocortical Astrocytes Mediated by Organic Semiconducting Thin Films, Adv. Healthcare Mater. 2014; 3,392.

208. Borrachero-Conejo AI, Saracino E, Natali M, Prescimone F, Karges S, Bonetti S, Nicchia GP, Formaggio F, Caprini M, Zamboni R, Mercuri F, Toffanin S, Muccini M, Benfenati V, Electrical Stimulation by an Organic Transistor Architecture Induces Calcium Signaling in Nonexcitable Brain Cells. Adv Healthc Mater. 2019; 8(3): e1801139.

209. Benfenati V, Toffanin S, Bonetti S, Turatti G, Pistone A, Chiappalone M, Sagnella A, Stefani A, Generali G, Ruani G, Saguatti D, Zamboni R, Muccini M, A transparent organic transistor structure for bidirectional stimulation and recording of primary neurons. Nat Mater. 2013; 12(7):672-80.

210. Lee C, Wei X, Kysar JW, Hone J, Measurement of the elastic properties and intrinsic strength of monolayer graphene. Science. 2008; 321(5887):385-8.

211. Balandin AA, Ghosh S, Bao W, Calizo I, Teweldebrhan D, Miao F, Lau CN, Superior Thermal Conductivity of Single-Layer Graphene, Nano Lett., 2008; 8, 902.

212. Melucci M, Treossi E, Ortolani L, Giambastiani G, Morandi V, Klar P, Casiraghi C, Samorì P, Palermo V, Facile covalent functionalization of graphene oxide using microwaves: bottom-up development of functional graphitic materials. J. Mater. Chem., 2010; 20, 9052.

213. Georgakilas V, Otyepka M, Bourlinos AB, Chandra V, Kim N, Kemp KC, Hobza P, Zboril R, Kim KS, Functionalization of graphene: covalent and non-covalent approaches, derivatives and applications. Chem Rev. 2012; 112(11):6156-214.

214. Palermo V, Kinloch I, Ligi S, Pugno NM, Nanoscale Mechanics of Graphene and Graphene Oxide in Composites: A Scientific and Technological Perspective. Adv. Mater., 2016; 28, 6232.

215. Goenka S, Sant V, Sant S, Graphene-based nanomaterials for drug delivery and tissue engineering. J Control Release. 2014; 173:75-88.

216. Wick P, Louw-Gaume AE, Kucki M, Krug HF, Kostarelos K, Fadeel B, Dawson KA, Salvati A, Vázquez E, Ballerini L, Tretiach M, Benfenati F, Flahaut E, Gauthier L, Prato M, Bianco A, Classification framework for graphene-based materials. Angew Chem Int Ed Engl. 2014; 53(30):7714-8.

217. Durso M, Borrachero-Conejo AI, Bettini C, Treossi E, Scidà A, Saracino E, Gazzano M, Christian M, Morandi V, Tuci V, Giambastiani G, Ottaviano L, Perrozzi F, Benfenati V, Melucci M, Palermo V, Biomimetic graphene for enhanced interaction with the external membrane of astrocytes, J. Mater. Chem. B, 2018; 6, 5335.

218. Chiacchiaretta M, Bramini M, Rocchi A, Armirotti A, Giordano E, Vázquez E, Bandiera T, Ferroni S, Cesca F, Benfenati F, Graphene Oxide Upregulates the Homeostatic Functions of Primary Astrocytes and Modulates Astrocyte-to-Neuron Communication. Nano Lett. 2018; 18(9):5827-5838.

219. Fabbri R, Saracino E, Treossi E, Roberto Zamboni R, Palermo V, Benfenati V, Graphene glial-interfaces: challenges and perspectives. Nanoscale. 2021; 13, 4390.

220. Maccaferri G, Terzi F, Xia Z, Vulcano F, Liscio A, V. PalermoV, Zanardi C, Highly sensitive amperometric sensor for morphine detection based on electrochemically exfoliated graphene oxide. Application in screening tests of urine samples Sens. Actuators B. 2019; 281, 739.4407.

221. Hutzler M, Lambacher A, Eversmann B, Jenkner M, Thewes R, Fromherz P, High-resolution multi transistor array recording of electrical field potentials in cultured brain slices. J Neurophysiol. 2006; 96(3):1638-45.

222. Blanche TJ, Spacek MA, Hetke JF, Swindale NV, Polytrodes: high-density silicon electrode arrays for large-scale multiunit recording. J Neurophysiol. 2005; 93(5):2987-3000.

223. Robinson JT, Jorgolli M, Shalek AK, Yoon MH, Gertner RS, Park H, Vertical nanowire electrode arrays as a scalable platform for intracellular interfacing to neuronal circuits. Nat Nanotechnol. 2012; 7(3):180-4.

224. Hai A, Shappir J, Spira ME, Long-term, multisite, parallel, in-cell recording and stimulation by an array of extracellular microelectrodes. J Neurophysiol. 2010; 104(1):559-68.

225. Saracino E, Maiolo L, Polese D, Semprini M, Borrachero-Conejo AI, Gasparetto J, Murtagh S, Sola M, Tomasi L, Valle F, Pazzini L, Formaggio F, Chiappalone M, Hussain S, Caprini M, Muccini M, Ambrosio L, Fortunato G, Zamboni R, Convertino A, Benfenati V, A Glial-Silicon Nanowire Electrode Junction Enabling Differentiation and Noninvasive Recording of Slow Oscillations from Primary Astrocytes. Adv Biosyst. 2020;4 (4):e1900264.

226. Convertino A, Mussi V, Maiolo L, Ledda M, Lolli, MG Bovino FA, Fortunato G, Rocchia M, Lisi A, Array of disordered silicon nanowires coated by a gold film for combined NIR photothermal treatment of cancer cells and Raman monitoring of the process evolution. Nanotech. 2018; 29, 415102.

227. Mestre ALG, Cerquido M, Inácio PMC, Asgarifar S, Lourenço AS, Cristiano MLS, Aguiar P, Medeiros MCR, Araújo IM, Ventura J, Gomes HL, Ultrasensitive gold micro-structured electrodes enabling the detection of extra-cellular long-lasting potentials in astrocytes populations. Sci Rep. 2017;7(1):14284.
228. Strasser P, Teasdale I, Main-Chain Phosphorus-Containing Polymers for Therapeutic Applications. Molecules. 2020; 25(7):1716.

229. Fattahi P, Yang G, Kim G, Abidian MR. A review of organic and inorganic biomaterials for neural interfaces. Adv Mater. 2014 26; 26(12):1846-85.

230. Viventi J, Kim DH, Vigeland L, Frechette ES, Blanco JA, Kim YS, Avrin AE, Tiruvadi VR, Hwang SW, Vanleer AC, Wulsin DF, Davis K, Gelber CE, Palmer L, Van der Spiegel J, Wu J, Xiao J, Huang Y, Contreras D, Rogers JA, Litt B, Flexible, foldable, actively multiplexed, high-density electrode array for mapping brain activity in vivo. Nat Neurosci. 2011; 14(12):1599-605.

231. Tao H, Kaplan DL, Omenetto FG, Silk Materials a Road to Sustainable High Technology. Adv. Mater. 2012; 24, 2824.

232. Fernández-García L, Marí-Buyé N, Barios JA, Madurga R, Elices M, Pérez-Rigueiro J, Ramos M, Guinea GV, González-Nieto D, Safety and tolerability of silk fibroin hydrogels implanted into the mouse brain. Acta Biomater. 2016; 45:262-275.

233. Capelli R, Amsden JJ, Generali G, Toffanin S, Benfenati V, Muccini M, Kaplan DL, Omenetto FG, Zamboni R, Integration of silk protein in organic and light-emitting transistors. Org Electron. 2011; 12(7):1146-1151.

234. Guarino V, Benfenati V, Cruz-Maya I, Saracino E, Zamboni R, Ambrosio L, 2 - Instructive proteins for tissue regeneration. In: Deng Y, Kuiper J, curatori, Functional 3D Tissue Engineering Scaffolds. Woodhead Publishing. 2018; 23–49.

235. Sagnella A, Chieco C, Di Virgilio N, Toffanin S, Cavallini S, Posati T, Pistone A, Varchi G, Muccini M, Ruani G, Benfenati V, Zamboni R, Rossi F, SILK.IT project: Silk Italian Technology for industrial biomanufacturing J. Composite B 2015; 68, 281.

236. Prosa M, Sagnella A, Posati T, Tessarolo M, Bolognesi M, Posati T, Toffanin S, Cavallini S, Benfenati V, Seri M, Ruani G, Muccini M, Zamboni R, Integration of a silk fibroin based film as a luminescent down-shifting layer in ITO-free organic solar cells. RSC Adv. 2014; 4, 44815.

237. Lam J, Carmichael ST, Lowry WE, Segura T, Hydrogel design of experiments methodology to optimize hydrogel for iPSC-NPC culture. Adv Healthc Mater. 2015; 4(4):534-9.

238. East E, Golding JP, Phillips JB, Engineering an integrated cellular interface in three-dimensional hydrogel cultures permits monitoring of reciprocal astrocyte and neuronal responses. Tissue Eng Part C Methods. 2012; 18(7):526-36.

239. Guarino V, Ambrosio L, Electro Fluid Dynamics: exploring a new toolbox to design biomaterials for tissue regeneration and degeneration. Nanomedicine (Lond), 2016; 11(12):1515-8.

240. Thompson R, Sakiyama-Elbert S, Using biomaterials to promote pro-regenerative glial phenotypes after nervous system injuries. Biomed Mater. 2018; 13(2):024104.

241. Zuidema JM, Gilbert RJ, Gottipati MK, Biomaterial Approaches to Modulate Reactive Astroglial Response. Cells Tissues Organs. 2018; 205(5-6):372-395.

242. Kaushik A, Jayant RD, Bhardwaj V, Nair M, Personalized nanomedicine for CNS diseases. Drug Discov Today. 2018; 23(5):1007-1015.

243. da Silva D, Kaduri M, Poley M, Adir O, Krinsky N, Shainsky-Roitman J, Schroeder A, Biocompatibility, biodegradation and excretion of polylactic acid (PLA) in medical implants and theranostic systems. Chem Eng J. 2018; 340:9-14.

244. Mir M, Ahmed N, Rehman AU, Recent applications of PLGA based nanostructures in drug delivery. Colloids Surf B Biointerfaces. 2017; 159:217-231.

245. Lau CL, Kovacevic M, Tingleff TS, Forsythe JS, Cate HS, Merlo D, Cederfur C, Maclean FL, Parish CL, Horne MK, Nisbet DR, Beart PM, 3D Electrospun scaffolds promote a cytotrophic phenotype of cultured primary astrocytes. J Neurochem. 2014; 130(2):215-26

246. Puschmann TB, Zandén C, De Pablo Y, Kirchhoff F, Pekna M, Liu J, Pekny M, Bioactive 3D cell the culture system minimizes cellular stress and maintains the in vivo-like morphological complexity of astroglial cells. Glia. 2013; 61(3):432-40.

247. Guarino V, Zuppolini S, Borriello A, Ambrosio L, Electro-Active Polymers (EAPs): A Promising Route to Design Bio-Organic/Bioinspired Platforms with on Demand Functionalities, Polymers 2016; 8, 185.

248. Saracino E, Cirillo V, Marrese M, Guarino V, Benfenati V, Zamboni R, Ambrosio L, Structural and functional properties of astrocytes on PCL based electrospun fibres. Mater Sci Eng C Mater Biol Appl. 2021; 118:111363.

249. Saracino E, Zuppolini S, Guarino V, Benfenati V, Borriello A, Zamboni R, Ambrosio L, Polyaniline nano-needles into electrospun bio active fibres support in vitro astrocyte response. RSC Adv. 2021;11(19):11347–55.

250. Bjugstad KB, Redmond DE Jr, Lampe KJ, Kern DS, Sladek JR, Mahoney MJ, Biocompatibility of PEG-based hydrogels in the primate brain. Cell Transplant. 2008;17(4):409-15.

251. Hadler C, Aliuos P, Brandes G, Warnecke A, Bohlmann J, Dempwolf W, Menzel H, Lenarz T, Reuter G, Wissel K, Polymer Coatings of Cochlear Implant Electrode Surface - An Option for Improving Electrode-Nerve-Interface by Blocking Fibroblast Overgrowth. PLoS One. 2016; 11(7):e0157710.

252. Furlani F., Montanari M., Sangiorgi N., Saracino E., Campodoni E., Sanson A., Benfenati V., Tampieri A., Panseri S., Sandri M., Electroconductive and injectable hydrogels based on gelatin and PEDOT:PSS for mini-invasive approaches in nervous tissue regeneration. Biomat. Science, submitted.

253. Pires F, Ferreira Q, Rodrigues CAV, Morgado J, Ferreira FC. Neural stem cell differentiation by electrical stimulation using a cross-linked PEDOT substrate: Expanding the use of biocompatible conjugated conductive polymers for neural tissue engineering. Biochimica et Biophysica Acta (BBA)- General Subjects. 2015; 1850(6):1158–68.

254. Hirase H, Nikolenko V, Goldberg JH, Yuste R, Multiphoton stimulation of neurons. J Neurobiol. 2002; 51(3):237-47.

255. Rapozzi V, Ragno D, Guerrini A, Ferroni C, della Pietra E, Cesselli D, Castoria G, Di Donato M, Saracino E, Benfenati V, Varchi G, Androgen Receptor Targeted Conjugate for Bimodal Photodynamic Therapy of Prostate Cancer in Vitro. Bioconjug Chem. 2015; 26(8):1662-71.

256. Peplow PV, Neuroimmunomodulatory effects of transcranial laser therapy combined with intravenous tPA administration for acute cerebral ischemic injury. Neural Regen Res. 2015; 10(8):1186-1190.

257. Lee HI, Lee SW, Kim NG, Park KJ, Choi BT, Shin YI, Shin HK, Low-level light emitting diode (LED) therapy suppresses inflammasome-mediated brain damage in experimental ischemic stroke. J Biophotonics. 2017;10(11):1502-1513.

258. Khuman J, Zhang J, Park J, Carroll JD, Donahue C, Whalen MJ, Low-level laser light therapy improves cognitive deficits and inhibits microglial activation after controlled cortical impact in mice. J Neurotrauma. 2012; 29(2):408-417.

259. Song S, Zhou F, Chen WR, Low-level laser therapy regulates microglial function through Src-mediated signaling pathways: implications for neurodegenerative diseases. J Neuroinflammation. 2012; 9, 219.

260. Zhao Y, Zhang Y, Liu X, Lv, X Zhou W, Luo Q, Zeng S, Photostimulation of astrocytes with femtosecond laser pulses, Opt. Express. 2009; 17, 1291-1298.

261. Cayce JM, Friedman RM, Chen G, Jansen ED, Mahadevan-Jansen A, Roe AW, Infrared neural stimulation of primary visual cortex in non-human primates. Neuroimage. 2014; 84:181-90.

262. Tulii G, Giona, F, Lodola F, Bonfadini S, Bossio C, Varo S, Desii A, Criante L, Sala C, Pasini M, Verpelli C, Galeotti F, Antognazza MR, High-Aspect-Ratio Semiconducting Polymer Pillars for 3D Cell Cultures. ACS Appl Mater Interfaces. 2019; 11(31):28125-28137.

263. Verkhratsky A, Krishtal OA, Petersen OH, From Galvani to patch clamp: the development of electrophysiology. Pflugers Arch - Eur J Physiol. 2006;453(3):233–47.

264. Sakaba T, Hazama A, Maruyama Y, Patch-Clamp Capacitance Measurements. In: Okada Y, Patch Clamp Techniques: From Beginning to Advanced Protocols, Tokyo: Springer Japan; 2012, 277–86. (Springer Protocols Handbooks).

265. Bootman MD, Rietdorf K, Collins T, Walker S, Sanderson M, Ca2+-Sensitive Fluorescent Dyes and Intracellular Ca2+ Imaging. Cold Spring Harb Protoc. 2013; 2013; (2):pdb.top 066050.

266. Buzsáki, G. & Draguhn, A, Neuronal oscillations in cortical networks. Science, 2004; 304, 1926–9.

267. Steriade, M., McCormick, D. A. & Sejnowski, T. J, Thalamocortical Oscillations in the Sleeping and Aroused Brain. Science,1993; 262, 679–685. Steriade, M. & McCarley, R. W. Brain Control of Wakefulness and Sleep. Springer, 2005.

268. Ferroni, S., Marchini, C., Schubert, P. & Rapisarda, C, Two distinct inwardly rectifying conductances are expressed in long term dibutyryl-cyclic-AMP treated rat cultured cortical astrocytes. FEBS Lett. 1995; 367, 319–325.

269. Benfenati V, Caprini M., Nobile M., Rapisarda C, Ferroni S, Guanosine promotes the up-regulation of inward rectifier potassium current mediated by Kir4.1 in cultured rat cortical astrocytes. J Neurochem. 2006; 98, 430–345;

270. Nicchia GP, Rossi A, Mola MG, Procino G, Frigeri A, Svelto M, Actin cytoskeleton remodeling governs aquaporin-4 localization in astrocytes. Glia. 2008;56(16):1755–66.

271. McConnell GC, Rees HD, Levey AI, Gutekunst C-A, Gross RE, Bellamkonda RV, Implanted neural electrodes cause chronic, local inflammation that is correlated with local neurodegeneration. J Neural Eng. 2009; 6(5):056003.

272. Kam L, Shain W, Turner JN, Bizios R, Selective adhesion of astrocytes to surfaces modified with immobilized peptides. Biomaterials. 2002; 23(2):511–5.